Astrocytes & neural network synchronization:

in vivo two-photon Calcium imaging and field recording

Astrocytes & neural network synchronization:

in vivo two-photon Calcium imaging and field recording of neocortical activity

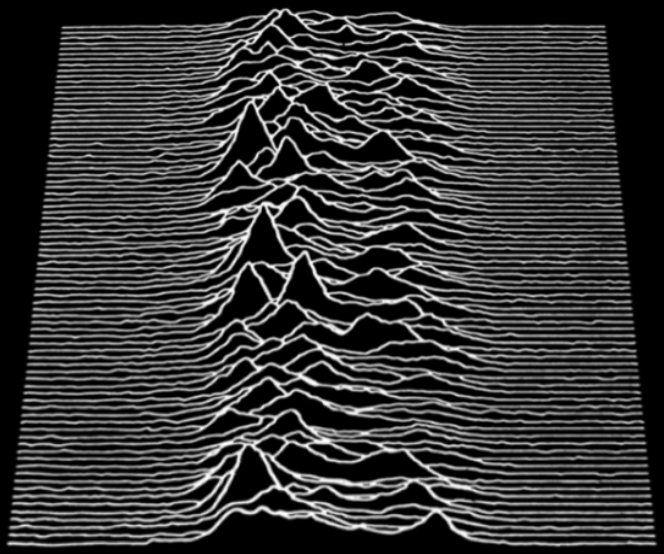

Marco Brondi

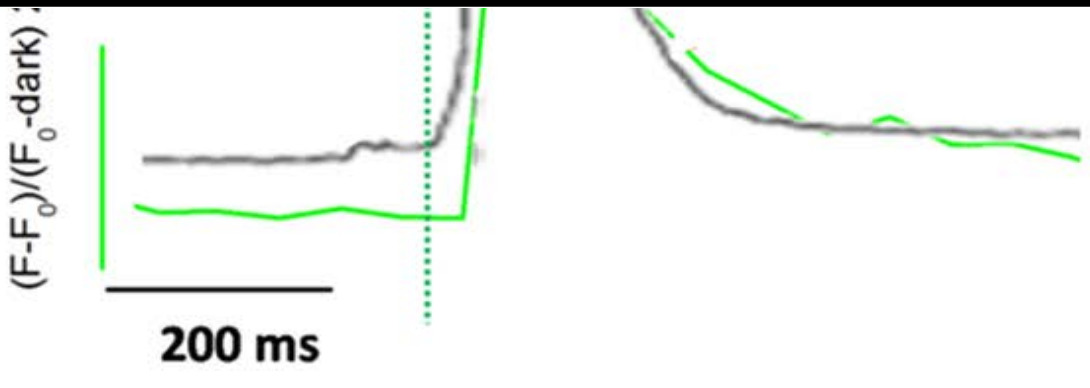

ABSTRACT

“the brain’s ability to generate coherent thoughts derives from the spatiotemporal orchestration of neuronal activity” (Hebb, 1949). Oscillation in the degree of synchronization among neural cohorts, appears to be the epiphenomenon of a yet poorly understood process, through which information is computed in the central nervous system (Buzsàki G. ; 2013). Although considerable efforts have been made in order to shed light upon the basic mechanisms regulating neural network synchronization, several scenarios remain to be further explored. In the last 15 years the hypothesis that astrocytes, the “dark side of glia” (Miller G.; 2005), are involved in the fine modulation of neural activity, rapidly gained remarkable interest in the scientific community. These non classically excitable cells are organized in a circuit in parallel to that of neurons, operating on wider space and time scales, integrating and interacting with the excitable cell network (Navarrete M. and Araque A.; 2011). Nowadays a plethora of works demonstrate how their functions are deeply interwoven with the neural network physiology (Fellin T., *et al*.; 2004. Agulhon C. *et al*.; 2008) and how strongly astrocyte dysfunctions correlate with different neurologic disorders, such as epilepsy (Kimelberg and Nedergaard 2010). Epilepsy is an extremely complex and widespread neurological condition (Engel *et al*.; 2013). Epileptiform activity is characterized by peculiar patterns of neural activity, ranging from hyper-synchronous events to almost completely uncorrelated phases (Traub and Wong, 1982; Trevelyan *et al*., 2006; Menendez de la Prida and Trevelyan, 2011). If astrocytes are actually involved in the modulation of neural activity, then spontaneous, pathological or induced variations in the coordination of neurons shall be mirrored in correlated alterations in astrocytes behavior. Both neurons and astrocytes behavior can indeed be probed employing intra-vital fluorescent Calcium sensitive dyes while ensemble electrical activity is recorded with extracellular field electrodes. These joined approaches allow observations with tunable spatial and temporal resolution, ranging from large populations to single cells with millisecond precision. However, a mandatory requirement in order to investigate on such a topic is to keep both physiological and anatomical cues as preserved as possible. Minimally invasive *in vivo* two-photon imaging and local field recotrding techniques enable the endeavor. Target of the work presented here is to characterize how astrocytes Calcium dynamics change accordingly to a variety of different patterns of neural population activity. Employing the isolated guinea pig brain preparation it is possible, with the appropriate pharmacological treatment, to elicit recurrent epileptiform episodes in the entorhinal cortex (Uva L. *et al*.; 2005). Some of the data we collected from this model are published (Gómez-Gonzalo M. *et al*.; 2011. Gómez-Gonzalo *et al*.; 2010.) and summarized here as follows:

1) Epileptiform activity summons large coordinated Calcium transients in cortical astrocytes in the transition from ictal phase to synchronous activity.

2) Triggering Calcium elevation in astrocytes, induces phase transition in neural coordination.

3) During neural hyper-synchronous interictal phase, astrocytes remain silent.

4) Astrocytes endfeet, show Calcium transients during ictal phase.

We then moved to the anesthetized mouse model in order to further investigate on the behavior of astrocyte in the context of spontaneous physiological activity and in visual processing. Moreover using transgenic mice, it is possible to discern between different neural cell types, here we used animals expressing green fluorescent protein in a subclass of inhibitory neurons considered involved in the synchronization of electrical activity and epilepsy (Fujiwara-Tsukamoto Y. *et a*l.; 2010. Sohal *et al*.; 2009). Furthermore, pharmacological dishinibition induces a steady-state interictal phase that lasts for hours with highly synchronized electrographic events. The list that follows resumes some results obtained:

1) Spontaneous slow wave activity is associated with weak astrocyte activation.

2) Calcium activity of excitatory and inhibitory neurons, are phase locked in each interictal event.

3) Physiological processing of visual stimulation is abolished during interictal activity.

4) After each interictal event an “absolute refractory period” prevents neural firing.

5) Calcium transients in astrocytes are rare during interictal activity.

6) In long lasting interictal phase spontaneous de-synchronization is observed to be correlated with astrocytes Calcium elevation.

7) Astrocytes display Calcium oscillations preceding the manifestation of electrical coherence at the onset of hyper-synchronous phase.

8) Pharmacological tools reducing the synchronization of neural population events produce considerable increase in the astrocytes Calcium transients frequency.

Track list:

1---Introduction:

1.1---The color and the shape / Basic structure of the neocortex.

1.2---A fairytale of slavery / Interneurons govern cortical function.

1.3---Automatic for the people/ self-organized rhytmogenesis in the cortex.

1.4---Ghost in the machine / Oscillators.

1.5---Through the looking glass / Astrocytes process information.

1.6---Unknown pleasures / Epilepsy as cortical dysrhytmia.

1.7---The serpent's egg / Role of astrocytes in epileptogenesis.

1.8---The head on the door / Why investigating on astrocytes?

2---Materials and Methods.

3---Results // *Cavia porcellum*.

3.1--- Dishinibition triggers recurrent epileptiform activity in medial enthorhinal cortex.

3.2--- Two-photon Calcium imaging during ictal phase reveals massive activity in astrocytes.

3.3--- Synchronization of astrocyte is maximal during ictal activity.

3.4--- Activation of astrocyte Calcium elevation triggers ictal events.

3.5--- Astrocytes are (almost) silent during hypersynchronous events in epileptic medial enthorhynal cortex.

3.6--- A-synchronous ictal events trigger intense endfeet activity.

3---Results // *Mus musculus*.

3.7--- Low activation of astrocyes during up/down states.

3.8--- Photic stimulation increase astrocyte activity.

3.9--- Reduction of inhibition in V1 induces sustained interictal activity.

3.10--- Astrocytes are (almost) silent during hypersynchronous events in V1.

3.11---"Low-synch" interictal events trigger massive responses in astrocytes.

3.12--- Photic stimulation unmasks the existence of an absolute refractory period between interictal spikes.

3.13--- Calcium in neurons remains higher than baseline levels during interictal activity.

3.14--- Astrocytes show strong activation at the onset of hypersynchronous activity.

3.15--- Collapse of absolute refractory period leads to micro-ictal activity.

3.16--- Astrocytes are massively activated during micro-ictal events.

4---Conclusions.

5---Bibliography.

6---Acknowledgments.

Chapter 1 / INTRODUCTION:

1.1---The color and the shape/basic structure of the neocortex.

In architecture the term "*tensegrity"* (tension+integrity as developed by R. B. Fuller in the '40s) refers to a building concept based on the stabilization between counteracting forces: a discrete *compression* and continuous *tension*. The whole structure sustains itself with the modular *compressing* elements floating in the web weaved with *tensile* structures (Fig. 1.1). Tensegrity favors the top-down approach to stability problems mirroring the Gestalt psychology paradigm (R. B. Fuller, 1975-1979): the *whole* is decomposed in fundamental elements and a meshing network. Tensegrity solution is an economic and simple one, based on robust and scalable geodesic design. Convergence provided by tension is counterbalanced by discrete compressing elements, the relative distance among which is imposed by the converging network itself (for a more evocative "vision" see C. Castaneda, 1972). These structures display an isotropic stability, independence from gravity pull and display no weakest points, thus faults do not propagate. Tensegrity structures deal with no intrinsic limitation on the size, C_{60} Buckminsterfullerene one of the most stable molecule, obeys the same principles (Kroto et al., 1985). During the cold war P. Baran (1964) designed a communication network capable to withstand a conspicuous number of braking points. He developed a distributed tensegrity structure: in case of failure in a random chosen point the network should reassemble itself learning how to use the residual operative path in order to propagate information with the shortest delay. Evolutionary biologist D'arcy Thompson (1917) expressed similar ideas: the *shape* is a mathematical problem while the process of *growing* is a physical transformation acting upon it (see for example Thompson's geometric transformation of baboon's skull into other primate skulls). The *Bauplan* provided by genetic information is actually subjected to the forging physical processes that shape the organism depending on its *scale*. The brain cortex is actually a solid and scalable geodesic structure, more properly named neocortex. All mammals share the same blueprint: modular elements adjacent and recurrent interconnected in a layered structure. The isocortex is the predominant design, with 5 thick layers populated by cells bodies and a 1^{st} top layer of cabling elements, while the allocortex or heterotypical cortex displays a variable layering. The number of unitary modules building up different animal's cortices, grows linearly with the scale-up process increasing the magnitude of the brain along evolution, with a scale factor > 10^4 from mice to humans estimated by Hubel and Wiesel (1974) in a single piece of visual cortex. Local organization of neocortex remains fairly constant across evolution though, and, with the remarkable exception of visual cortex, it is also homogeneous in different brains areas: 1 mm^3 of cortex contains around 10^4 neurons (Rock et al., 1980). Unitary modules are often difficult to tell apart in small brains while easily bordered in others (mini/macro columns, stripes, blobs, barrels, interblobs are some of the name given to elementary modules in different areas). Theoretically, each module should comprise all cell classes found in neocortex, modules shall

propagate across the cortex and connect each other with a stereotyped array of cables. This is actually the case except for a widespread set of local, intermediate and long-range connections that pops out with increasing complexity along phylogenesis. Processing capability is not confined within *in parallel* stand alone modules; rather it is a flexible property originating from regulated degree of interaction among modules. Yet the conserved paradigm in brain evolution is the predominantly local wiring, as in the tensegrity structures (Fig 1.2). This is deducible even on a macroscopic scale: the surface of large brains is folded to keep local neighborhood modules close together. Van Essen (Van Essen and Drury, 1997) proposed a model for the shaping of large brains surface taking into account hydrostatic compressure of the tissue and the mechanical tension of axons, predicting that strongly interconnected modules were invariably separated by a gyrus and weakly interconnected ones by a sulcus. Neurons prefer to connect with a path length proportional to the "strenght" of the connection. Most of the information a chosen neuron receives, come from the closest neighbor (Fig 1.2). On the other hand, transmission via cable over long distances is metabolically expensive. Recent speculations suggests that any neuron contact the nearest without any bias (Glickfeld et al., 2013; Kalisman et al., 2005; Fino et al., 2013) and there could potentially be more synaptic contacts per volume than those observed. The observed density of synaptic switches oscillates between 10% and 90% of the theoretical value (Markram et al., 1997; Thomson and Bannister, 2003). This topography of neural connection has several consequences. First is the redundancy: neuron "A" has a probability to connect to the same neuron with which "B" is connected a probability that increases with decreasing A---B distance. Connected layer II/III pyramidal neurons are more likely to receive same input from layer IV and through cortico-cortical connections, from L II/III (Yoshimura et al., 2005). Adjacent skeletal muscles are much better coordinated in a movement than distant ones and the map of motor sub-areas in the motor cortex, display a stunning somatotopia. The same is true for somatosensory areas or for the organization of auditory cortex. The same is particularly true in all levels of visual processing: two neighboring neurons are much more likely to combine information concerning adjacent pieces of space in the visual environment (Cowey, 1979; Allman, Hasenstaub; 1999). This organization is conserved in spite of a dedicated area mismatches the actual extent of the peripheral structure (eyes) (Allman, 1999). Retinotopic representation is distributed along ever higher visual "stations" of increasing dedicated areas, split and folded for wiring optimization (Cherniak, 1995; Chklovskii and Koulakov, 2004). Another important consequence of cortical organization resides in the representation capability, a sort of "meaningfulness filter". If an observer, for instance, is presented with a screen of on-off pixels flickering in a sequence spanning all possible configuration, only very few dispositions will have a "meaning" for the subject: the shape is in the eyes of the beholder and is wired *a priori* though updatable to some extent (the Rorschach test mechanism is an example). Bèla Julesz (1995) hypothesis was that the "meaning" of flickering dots shall be extracted analyzing each dot's neighbor position and coherence in temporal distribution and motion. If the brain was capable to extract meaning from all possible dispositions of say "n" dots in the visual space, the number of connection required will be many orders of magnitude greater than the observed. But the brain rejects most configurations as noise instead of meaning. The visualized meaning is supposed to be selected as evolutionary advantageous, the rest would required an expensive and useless (in the best case) computation. In between are sensory illusions. Remarkably even in

higher cortices, like those involved in human or Primate intellectual faculty, connectivity remains the same, what changes between different species is the amount of cortex allocated for a certain sensorial modality or, in this case, associative function. The statistical correlation between features in perceived world is indeed the driving force for the generation of cortical neural wiring into the tensegrity structure. Neurons in retina, LGN and V1 respond more intensely and more sparsely when excited with an image with a fractal structure which is the most frequent in natural landscapes (Bell and Sejnowski, 1997; Yu et al., 2005). In the ferret for example, recorded neural activity in V1 was significantly more intense and coherent in sessions of "natural scenes" presentation instead of equiluminant-equicontrast "random noise" (Weliky et al., 2003; Fiser et al. 2004). The tensegrity structures allow for little negligence in the construction process, which leads to a third consequence: accuracy. Suppose we could build a copy of a human brain neuron by neuron and shuffle their position in order to use 10% more wiring to obtain the original computational capabilities. The new metabolic yield will dramatically rise, extensive rearrangement of vasculature will be needed and the cumulative delay upon synaptic transmission will impair the proper coordination of a simple movement. These effects are observed in MS patients, where myelinated fibers are damaged and axonal conduction, in an otherwise normally wired brain, slows down (Keegan and Noseworthty 2002). Enlarged brains must cope with the delay in propagating synaptic communication along networks with increasing number of basic modules. Mammalian brain innovation consists in the development of global computation capabilities maintaining ancestral local modular organization. Mammalian neurons are endowed with longer and thicker axons as well as more complex dendritic arborizations with increased number of post synaptic spine terminals. From mice to humans the average pyramidal dendritic tree diameter grows approximately from 200 μm to 1 mm. This also led to increased overlap probability between synaptic contacts in neighboring cells. The mean path length for an afferent axonal projection between consecutive post synaptic potential targets shortens with increasing brain size (Braitemberg; 2001; Buzsáki et al., 2013) far from being a random assembly, network generated with a "scale free" geometry in connection density, are indeed more complex then random ones (Chklovskii and Koulakov, 2004; Sporns et al., 2004). A scale free statistic in connection probability is also the local connectivity strategy (Binzegger et al., 2005). In order to obtain an effective global communication capability, the average synaptic path length shall be kept constant aver all ranges. In growing brains, white matter volume increases with a 4/3 power over the gray matter volume: increasing the number of fundamental modules implies an increase in long range wiring. Small brained animals require fewer long range connections: small insectivores white to gray matter ratio is around 0.06 while in humans is 0.4 (Swadlow, 2000). Only taking into account brain volume thus, may lead to inappropriate conclusions on the global computation capability, e.g. giraffe's brain is quite as big as human's yet its long range connections are a great deal fewer. Furthermore brain expansion across species is not homogeneous in all cortical areas, for example V1 cortices only doubles in human compared with macaques and parietal and frontal areas is 10 an 40 times bigger respectively. Somatosensory areas also follow a scale-free expansion

rule since processing in these areas deal with the environmental regularity to which all species are exposed. On the other hand in associative areas, wiring and cellular tiling could obey yet unknown rules boosting functions so far poorly understood. Neural Darwinism supports the idea that evolution of cortical complexity is the consequence of adaptation to the statistical structure of sensory inputs, thus brains shall be

most sensitive to those environmental perturbations displaying cortical-like statistical organizations (Sporns et al., 2000). Another consequence of "inflated" brains is the problem of conduction speed. Myelinated fibers have characteristic conduction speeds linearly proportional with axon diameter while in unmyelinated ones goes with diameter square root. The vast majority of axonal collaterals remain local (Braitemberg, 2001). Mammalian brains are presented with another fundamental problem descending from the relatively low density of long range connection: the bandwidth. One strategy evolved to compensate for the poor bandwidth is the "acceleration" of communication via heavily myelinated thick fibers. Conduction speed in these long range fast fibers is 100 fold that of local unmyelinated collaterals (typically 0.3 meters/sec in local 0.1-0.5 µm fibers). 50 meters/sec fibers connect primary sensory areas in mammalians brains. Greater myelination and thickness allow for both increasing speed and signal transmission rate but also protect against signal contamination and conduction failure. Fast and reliable conduction is achieved at the expense of available space: thick myelinated fibers may occupy 10000 times the volume accessible by thin local projections. Van Essen and Felleman (1991) observed that 30 visual associated domains in the cortex are connected by > 300 intermediate and long range connections in a hierarchical structure (see Salthe 2008 for discussion on the emergence of hierarchical organization from complex structures). Disposition of processing units in the cortex appear to be chosen in order to minimize the wiring and communication delay between them, also, connection probability peaks between areas involved in the same processing system (e.g. visual areas or motor cortices). Wiring complexity in the neocortex is the product of local tensegrity with scale free long range connection probability. Given the fractal geometry of brain organization at both the meso and macro scale together with the almost random micro circuitry in each module, neocortical connectivity stands in peculiar configuration: complexity. Tononi et al., (1994, 1996) applied stochastic processes and information theory in order to estimate complexity in modeled brain structures. Entropy in this context is associated with the degree of randomness in the signal propagated, being $\mathbf{I}(x|y)$ the difference in entropy content upon variable x produced by the fact that another variable y is known. Different neural networks were modeled and their statistical independence estimated. Minimum level of statistical independence is associated both with complete integrated (dependent, deterministic) circuits and complete segregated (independent, chaotic) ones. Complexity manifest itself in the transition from order to chaos, where $\mathbf{I}(x|y)$ is halfway and statistical independence reaches the maximum. In this regimen, several local segregated microcircuits stands inside a dispersed interconnecting deterministic network in a scale-free fashion as observed in real mammalian brains. Using artificial Darwinian selection algorithms they further showed that high complexity was subtended by a scale free power law distribution of connections Real world data will further increase the spectrum of possibilities in neural assembly architecture, but the overall statistical properties would probably remain the

same. Like in Prigogine's non-equilibrium thermodynamics: complex systems near equilibrium minimize their entropy production rate, or rephrased from Darwin: "**order emerges from disorder without an external agent**", neural networks structure and dynamics will be constantly "pumped" just about equilibrium.

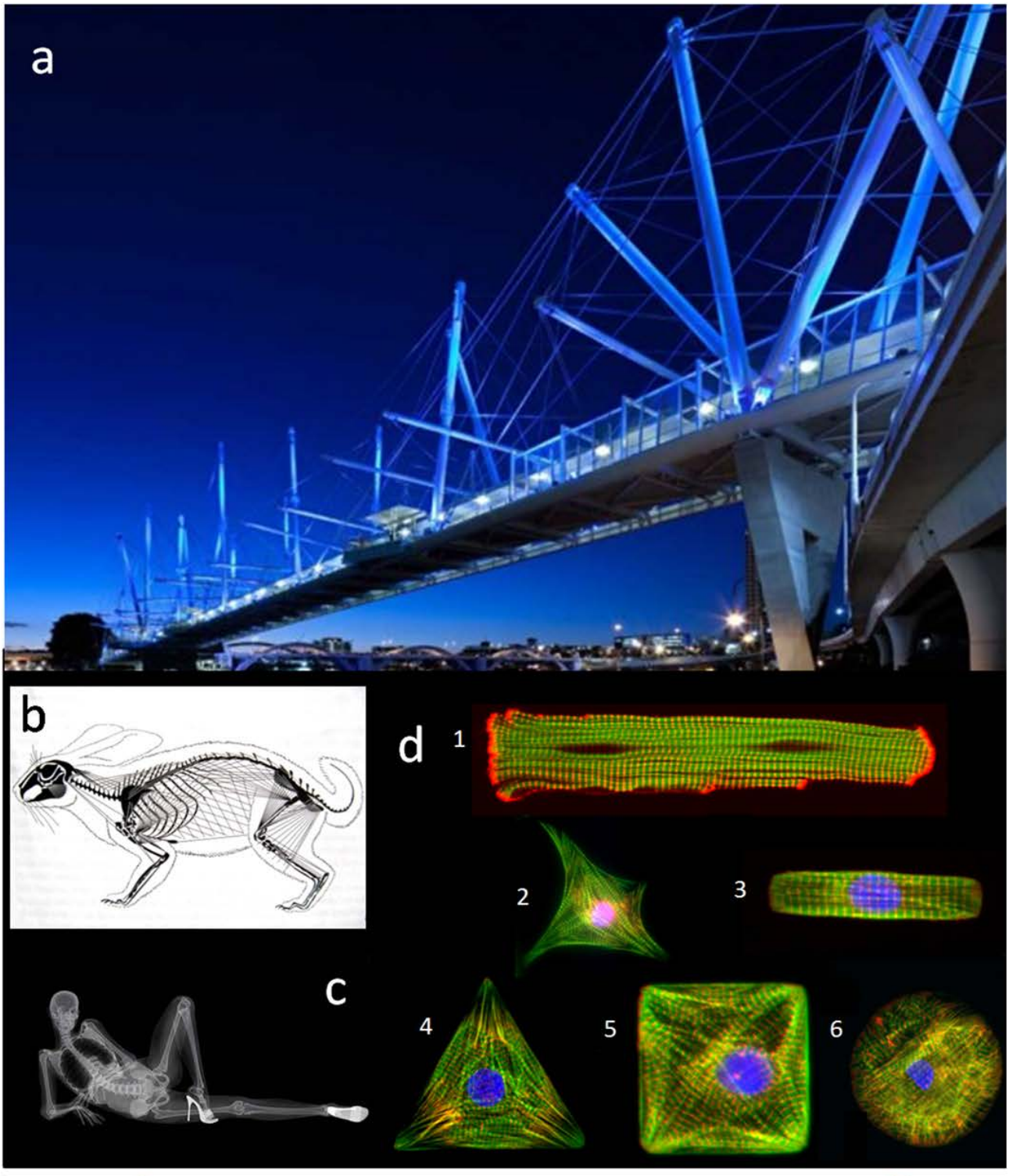
a
b
c
d
1
2
3
4
5
6

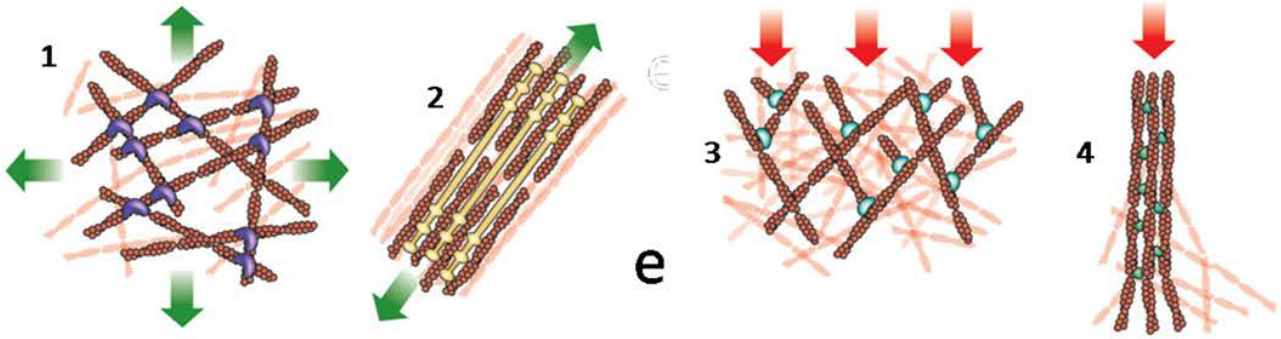
1
2
3
4
e

Figure 1,1 *Tensegrity across dimensions. a) Kurilpa bridge in Brisbaine, Australia, projected and realized by Cox Rayner Architects and Arup Engineers, an example of tensegrity-based architectonic structure. b) Tensegrity model of a rabbit skeleton with tendons. c) Human body plan is organized on the basis of compression and tension balance, bones are arranged to minimize supportive structures and allowing ease of movements. d) Tensegrity at the cellular level. 1) Cardiomycyte stained green against actin cytoskeleton, the nucleus is blue, 2-6) cardiomyocytes differentiated on micropatterned surface, organize cytoskeleton in order to best-fit imposed constraints. (source: http://diseasebiophysics.seas.harvard.edu/research/mechanotransduction/) Compressive and tensile elements of cytoskeleton. 1) cortical Filamin network carry away tensile forces across cytoplasm, 2) stress fibers emerges from actin bundles and associates with myosin to generate tension against cell adhesion, 3) outward-protruding actin mesh cope with external compressive force and 4) filaments arrays in filopodia experience a similar compressive force (from Fletcher and Mullins, 2010).*

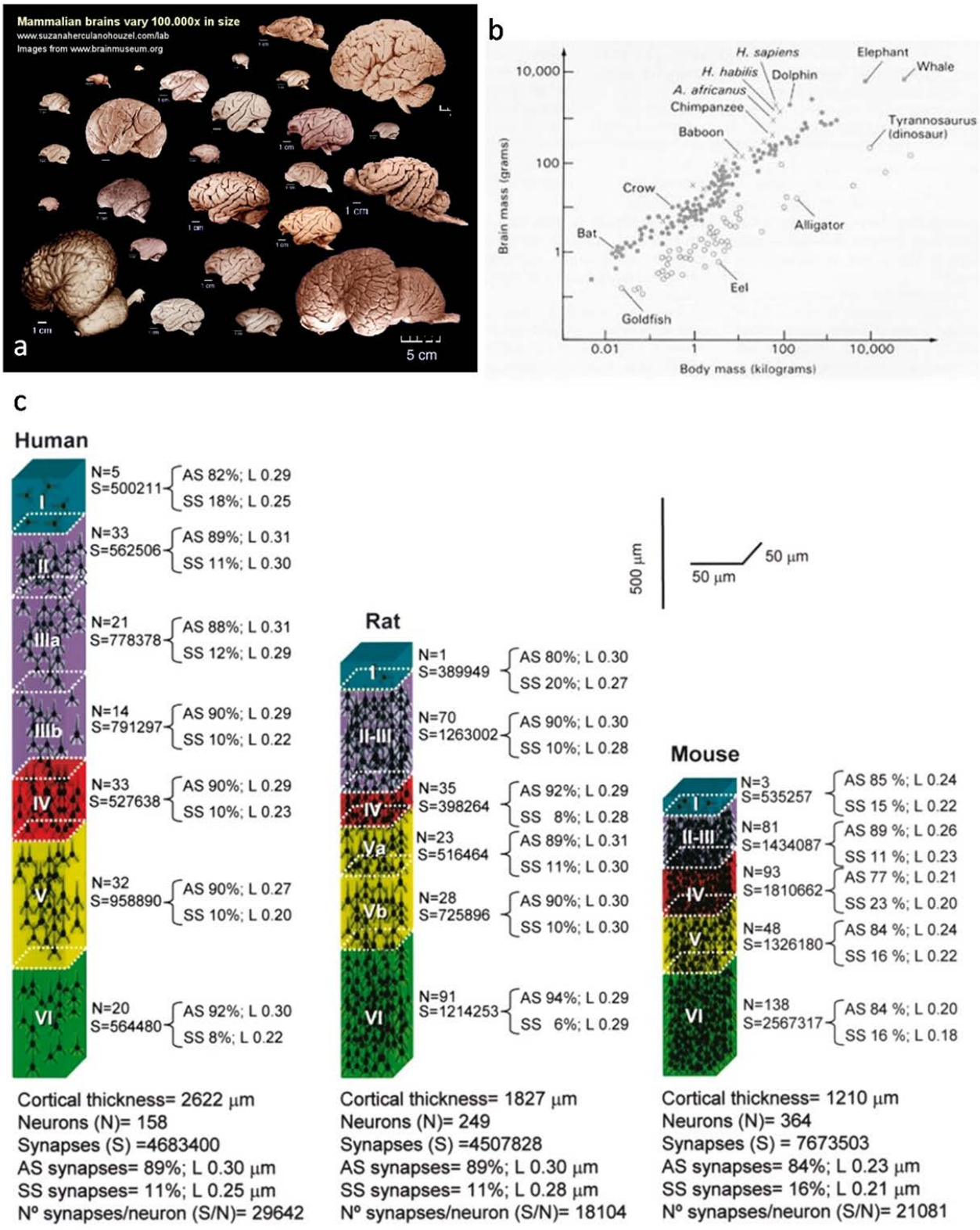

Figure 1.2 *Neocortex cellular organization is conserved across mammalian evolution. a) Brain specimens from different Mammalia species compared. Brain size may vary by 4 order of magnitude (Mota and Herculano-Houzel, 2012). Metabolic cost associated with normal brain function is estimated around 25% of total body caloric consumption (irrespective of brain size, at an average cost of 6 kCal per billion neurons per day). b) Brain to body mass index is used to estimate how cephalization index develops troughout evolution. Larger species tend to exhibit larger brains.*

c) Neocortical neuronal density is inversely related to brain size. Neuronal density turns out not to be predicted by cortical surface, being considerably variable across cortical areas (Herculano-Houzel et al., 2008). Nevertheless, both gross architecture and fine morphology appear to be strictly conserved among neocortices even of different species (Ventura-Antunes et al., 2013).

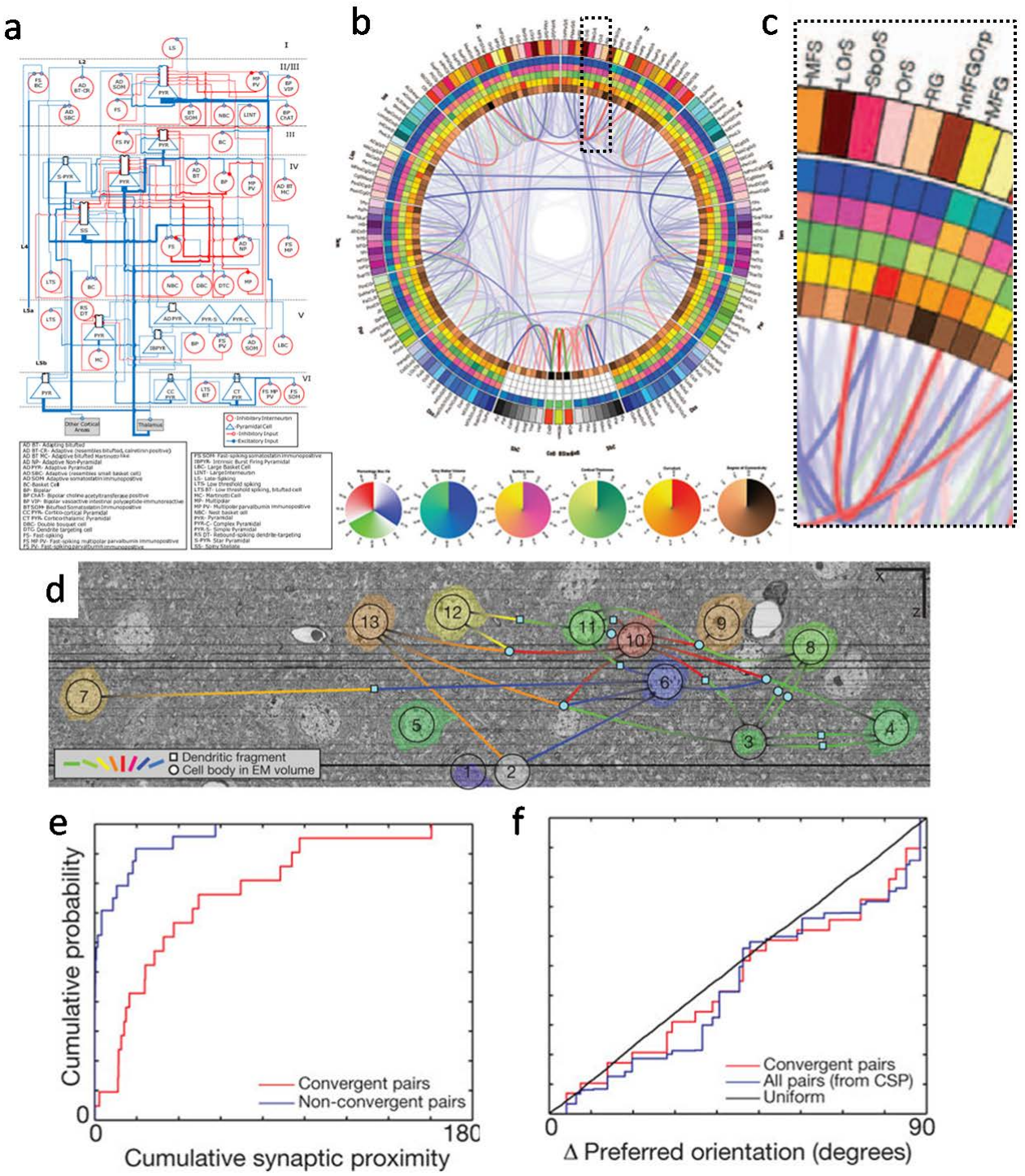

Figure 1.3 *Global and local connectivity. a) Wiring scheme of a canonical module in the mouse neocortex (from http://www.columbia.edu/cu/biology/faculty/yuste/databases.html). b) Whole-brain connectivity in average human brain (right handed, 25-36 years old) obtained from functional and structural data (Van Horn et al., 2012). Outermost ring: cortical areas named according to lobular position, first colored ring: cortical parcellation according to MRI mapping and BOLD signals (color coded scales are reported in the six small circles below), consecutive 5 colored rings (outer to inner): connectivity average, regional volume, cortical thickness, surface area, cortical curvature. Average connectivity of each parcellation with respect to white matter emanating from them is*

color coded in the trajectories interconnecting different parcellations, displayed in the central area of the plot. 12'-6' vertical line divides right-left hemispheres up to brainstem parcellations displayed at position 6'. c) Magnification of boxed region in b). Few parcellations in the frontal lobe are highlighted with relative dense connectivity trajectories. d) A region in mouse V1 was two-photon imaged in order to characterize single cell responsivity to visual stimuli. The very same region is then serial-sectioned and imaged in electron microscopy. Consecutive planes are reconstructed to retrieve exact location and identity of imaged neurons. Same pseudocolored cells displayed a similar orientation selectivity to visual stimulation during two-photon Calcium imaging sessions. Colored lines points to real synapses connecting cells either to soma or dendritic fragment of an inhibitory interneuron (tracked in serial EM sections) indicated with cyan circles or squares respectively. e,f) Coupling visual response properties to local wiring, the cumulative synaptic proximity and convergence index was then calculated for several cells (Bock et al., 2011).

1.2---A fairytale of slavery/interneurons govern cortical function.

Brain's code is hard to crack probably due to its nested complexities: macroscopic features are complex functions of meso and microscopic complex structures living in 4D. A common bottom-up approach considers the "canonical module" (Szentagothai, 1978). Consecutive canonical module will connect each other and propagate a signal in a chain of clustered neurons. Abeles' "synfire chain" (1982, 2004) is a simple connectivity model in which all knots are excitatory pyramidal neurons generating a unidirectional wave of activity in the chain with a feedforeward mechanism. In real brains, synfire chains are rare, being utterly inefficient. In such a flimsy network, errors will propagate amplificate and reverberate along knots, Furthermore the whole message itself will take too long from one end to the other due to the delayed imposed by feedforewrd hierarchical dynamic. Hierarchy indeed forbids the possibility for other chains to interact until the synfire is completed. Simple synfire chains improves their performance without implementation of inhibitory interneurons, some degree of feedback excitation is just required to produce a recurrent network: an autoassociator (Naudé et al., 2013). Neocortex is composed mostly of excitatory neuron (80%) displaying a large variability in their biophysical properties. These enable estimated 5 degrees of freedom in the computational capability among different neurons, to be expanded by connectivity. The plausibility of canonical module as an evolutionary conserved feature has some observational clues in cortical mapping of somatosensation, visual and auditory inputs processing. Of course cellular elements are highly conserved (with the remarkable exception of V.E.N. neurons or spindle cells only found in big brained animals like *Mysticeti, Loxodonta* and *Hominidae,* see Butti et al., 2013) and the same is true for connectivity rules . In this perspective the characterization of neural dynamics in small brained mammals is of great value in order to extrapolate a scale-up function capable to fit same properties in larger brains. Regardless connectivity or intrinsic properties of excitatory neurons a synfire chain is no more than a low pass inaccurate amplificator propagating signals in a "rolling snowball" fashion. Without a control system excitation will build up, spreading along the network and eventually cross the entire extent of the net or fade away in an exhausted loop. Inhibitory interneurons provide control. Classical thermodynamic, contemplate only one kind of interaction between elements namely collisions=excitation, system relying on "collision" dynamics are doomed to increasing entropy. Inhibitory neurons shift the system toward complexity. From the tensegrity viewpoint, interneurons provide the tensile force. Without inhibition, different input will eventually lead to a global excitation with more or less the same kinetic, the brain become a binary operator: either silent or massively excited. Just few interneurons embedded in a synfire chain are enough to diminish predictability in the firing pattern of each downstream neuron. In a distributed networks (i.e. intermixed excitatory and inhibitory neurons) the firing pattern of each cell is highly dependent upon contribution from excitatory and inhibitory neurons, their intrinsic characteristics and most importantly, the condition prior the broadcast of the next signal ("history" of the network activity). Small changes in the parameters produce large effects on the propagation dynamics in a "butterfly-effect" dynamic. This strong dependence from initial conditions, a.k.a. nonlinearities, affects both interneurons and principal cells. Distributed networks are able to converge toward predictability or diverge in chaos, thus are capable of self-organized complexity. The most sensible parameter in such a network is actually the wiring between excitatory and inhibitory neurons. three major classes of connectivity schemes are classified as: 1) feedforward

inhibition (excitation activate an interneuron that inhibits downstream) acting like a filter, 2) feedback inhibition (excitation activate an interneuron that inhibits upstream) stabilizing the tone of excitation and 3) lateral inhibition (divergent excitation activate an interneuron that inhibits all co-activated neurons downstream), a “winner takes all” mechanism (Buzsaki and Eidelberg, 1981, 1982; Alger and Nicoll, 1982; Buzsaki, 1984; Swadlow, 2002). Feedback inhibition modulates excitatory drive and typically manifests itself with peculiar oscillating patterns. Feedforward inhibition compresses the time window of discharge probability downstream, increasing the precision of excitatory coupling. Combining excitation and inhibition properly in feedforward inhibited network shrink the spike timing precision down to sub-milliseconds scale, forbidding signal out of frame altogether (Pouille and Scanziani, 2001). When two strains of synfire chains are coupled by lateral inhibition, initial different gain is enhanced nonlinearly which otherwise would wane to a common value sooner or later. The same effect is achieved even if there is no difference in the strength activating one synfire chain with respect to the other provided that a difference in timing although the slightest, is present. This is one of the basis of a widespread mechanism known as “gain control” deployed mostly in sensory processing principal areas, allowing for a modulation of the output in response to the input features. On this very mechanism is computed the recognition of a figure sliding over a background, a highly adaptative property (think about predatory behavior of mimetic preys, Heimel et al., 2010). Complexity burst out when multiple interneurons are recruited even in a simple feedback/forward circuit: the effect on signal propagation depend upon the interaction between interneurons involved. Other major sources of modulation of avalanche synfire chains consist in subcortical diffuse projections (noradrenaline, acetylcholine, serotonine, histamine among others) some of which are mediated by interneurons nonetheless (Steriade et al., 1990; McCormick et al., 1993; Freund, 2003). Also intrinsic membrane properties of principal cells are important modulators, such as Potassium conductances of which I will discuss later. Collectively interneurons provide the force either toward convergence (lateral inhibition), divergence (feedforward inhibition) or entrainment of distant modules (feedback inhibition). Segregation and entrainment effect of inhibitory network keeps the brain safe from falling into self sustained excitatory spreading fire and relieve from the “silence” of the cortex collectively engaged in feed-forward excitation. The brain is physiologically maintained near the transition phase between unresponsivity and hyperresponsivity. External forces might well be enough to trigger the transition and the input calibration has been extensively shaped by natural selection. Brain is always in a metastable state, awaiting the proper perturbation igniting the transition. Bak (Bak and Paczuski, 1995) refers to a “self-organized criticality” talking about physical systems. The phase transition threshold is so finely set that, although evolved to exhibit fast massive reaction to the slightest stimulus, brains are not overwhelmed by the constant bombardment of inputs. This is true as far as the physiological integrity is granted. Another important feature associated with neural network is obviously the degrees of freedom with which single cells are endowed. Although several classes of principal neurons exist with different properties, interneuron population is an astonishing heterogeneous class (Figure 1.4). Molecular

repertoire, morphology, location, connectivity and firing patterns are only useful when considered in a combinatorial approach. Structures other than the neocortex developed relatively simple interneuron-principal cells network, these are endowed with simple computational tasks (consider cerebellar, basal ganglia, thalamus structures). Neocortex evolved 5 types of principal cells and an enormous array of different interneuron types some of which are still elusive to classification (almost monthly a new class of interneuron emerges, for the most widely accepted taxonomy concerning inhibitory neurons consult the “Petilla Interneuron Nomenclature Group” PING Barrionuevo et al., 2008). An useful criterion could be deployed in order to categorize different interneurons: the effect each class has on pyramidal processing. Four major groups arise in this view: the largest one comprising these interneurons that control the output from pyramids by means of perisomatic inhibition (basket cells projects to the soma and chandelier cells to the axon initial segment, for example). Chandelier cells are shows to be capable even to bypass the pyramid, taking control over the axon by a depolarizing effect of GABA, entraining targets despite the computation processed above (Szabadics et al., 2006). The second heterogeneous group encompasses these interneurons controlling dendritic domains; the third group contains the so called “long-range interneuron” projecting axonal collaterals across layers, travels to the other hemisphere or contact subcortical regions. This last class is mostly peculiar and least characterized so far, these interneurons are thought to be responsible for synchronization across different cortical areas or between symmetric hemispheric domains (Peters et al., 1990; McDonald and Burkhalter 1993; Sik et al., 1994), most of them are Soamtostatin, Neuropeptide Y and Nitric oxide synthase positive as described in Tomioca et al, 2005, some of Martinotti cells display axonal collaterals entering the white matter. The fourth group collects interneurons that avoid any contact with principal cells and project only to other interneuron of every class (Gulyas et al., 1996; Freund and Gulyas, 1997). This feature seems to be interneuron-specific since no pyramidal cell have ever been observed to project only to pyramids or interneurons. Furthermore, this interneuron-interneuron class also displays long-range projections. What seem clear is that different interneurons are devoted to different functions in the network, multiplying the available degrees of freedom of the system. A given stimulus replicated in time, for instance, will seldom produce the same effect in the network. What is an absolute common feature of inhibitory projection is the release of γ-aminobutirric acid (some vesicles also contain glycine). On average each pyramidal cell receives 5-10 boutons from each interneuron associated. Different interneurons select peculiar subcellular targets in order to deploy specific functions. A clear example is given by the projection of basket cells-fast spiking-parvalbumin containing nterneuorons. These cells present axonal terminals clustered on the hillock of principal cells, where AP pattern is generated. Here EPSPs summate to build up depolarization beyond threshold. Chloride conductance in this district is obviously critical for the behavior of the whole cell. Furthermore on the initial axonal segment of principal cells, the symporter KCC2 is highly localized granting a stable ECl potential below membrane potential which is often more depolarized then the resting value here. Considering that the threshold for AP generation in interneurons is lower than in pyramidal cells (Gulyas et al., 1993; Csicsvari et al., 1998), a small excitatory drive (EPSP in fast spiking interneurons can be detected following a single release event after a single spike from a single presynaptic site, Barthò

et al., 2004; Silberberg et al., 2004) on basket cells is enough to start a GABA barrage on some pyramidal hillock.

Moreover, fast spiking interneurons owe their name to the peculiar high frequency of AP firing rate they deliver when excited. This is probably due to fast kinetics of NaV and Kv channels but also to the abundance of Calcium-binding protein Parvalbumin (Kd in the lower micromolar range) that clamps back Calcium levels after each AP. This allow the almost perfect match of incoming EPSPs frequency on the pyramidal hillock with GABA tonic firing rate. PV+ cells impose an insurmountable barrier to pyramidal AP firing (also taking into account shunting effects, massive Chloride flux will bolt hillock Vm to ECl for any EPSP combination observed), shaping a narrow window of possibility for action potential generation between consecutive inhibitory trains. Vesicular release of GABA is also observed to be spontaneous, giving rise to the so called “minis” manifesting as small and short-lived hyperpolarizing fluctuations in pyramidal cell that serve to keep principal neurons away from threshold when interneuron firing is idling (Nusser and Mody, 2002; Mody and Pearce, 2004). GABAergic conductance is wider in amplitude and faster in kinetic compared with EPSP, two characteristic that turns interneurons apt to the role of peacekeepers. This is mirrored by LFP high frequency oscillation recorded at the level of pyramidal cell bodies compared to the lower frequencies at the dendrites where EPSPs dominates. A scenario emerges in which excitation and inhibition are counterbalanced in an homeostatic fashion among large cortical territories, not precluding the capability of transient focal increases of excitation inside precisely time-restricted “windows of opportunity” required for signal broadcast and connection rearrangement. Morphological features of principal cells add up to complexity shaping inhibition efficiency and excitatory output. Pyramidal cells display large computational capacity harbored in the vast dendritic trees, the topology of which is sculptured by both genetic cues and neural activity. Channel distribution is associated with structural features (Mainen and Sejnowski, 1996) e.g. two hypothetical pyramidal neurons with same dendritic geometry but even slightly different channel distribution generate different outputs to the same input, the converse is also true keeping channel distribution equal between the two and altering the shape of dendritic tree in one. The large computational capability of each pyramidal neuron is never achieved ad once, instead subcellular domains are dedicated to segregated subroutines that can be switched and or integrated at need. Shunting junctions in the pyramidal circuitry are interneuron-operated: bunch of spines can be silenced, a whole dendritic compartment can be easily switched-off from the computation, the firing rate of the pyramid can be modulated or abolished and the axon can be segregated from the soma. These operations are effectively equivalent to the replacement of a pyramid with another one with same channel distribution but different geometry, increasing greatly the complexity in a flexible way. Each subdomain in every pyramidal cell is under control of an interneuron. Furthermore, hierarchic organization exists in which each layer in the cortex is dominated by the effect of a particular interneuron class. Computational complexity is linear with the density of interneuron of a specific type so the extreme variety in inhibitory neuron population allows an impressive divergence toward supralinear combinatorial properties as described for

evolving systems by Alvarez de Lorenzana and Ward (1987). This expensive design is accomplished mostly through local inhibitory connections, saving space and time. As a consequence of the specialization of projective territories, different interneural subclasses display peculiar firing patterns adapted to match pyramidal needs. This is actually even more striking when the time domain is taken into account. It is to be kept in mind that interneurons are generally triggered in a feedforeward fashion by principal cells yet their biophysical properties are also as variable as their morphology, thus different interneuron classes could be recruited at peculiar “triggering frequencies” of principal cells. Parvalbumin containing interneurons for example, are highly responsive to low frequency pyramidal input but show a decreasing firing probability as the pyramidal input increase in frequency. On the other hand, several dendrite-targeting interneurons are more prone to fire when the input is high in frequency or require prolonged presynaptic activity to start firing due to slow facilitating synapses, acting like an high pass filter or a capacitor. When the pyramidal branch of the network is in low-frequency firing mode, perisomatic interneurons are engaged the most. Given the fact that these classes are predominantly short ranged projective, in most of the cases a negative feedback is looping on. While in high frequency pyramidal discharge, dendritic targeting interneurons are preferentially activated. In this case it is more likely that a negative feedforeward is operating on short range. Interneuron-interneuron communication relies not only upon GABA: same class interneurons also arrange gap-junction electrical synapses (Katsumaru et al., 1988; Connors and Long 2004; Hestrin and Galarreta, 2005). In addition to GABA release, most interneuron also secrete hormones (Cholecistokinine, Somatostatine, Neuropeptide Y, Vaso Intestinal Peptide among others) exerting pleiotropic functions on glucose homeostasis, blood flows, feeding behavior etc. adding on complexity to the system. Efficiency is routinely enhanced by keeping principal cells just below threshold for AP generation: this decrease the energy and the time required to discharge but is also a double edged blade because little fluctuation in resting membrane potential could be enough to set the cell in firing mode. Noise is such a source of membrane potential fluctuation and a pervasive one. Both physical conditions (i.e. temperature, extracellular milieu, pH) and the high chance for stochastic resonance in such a dense synaptic space as that experienced by pyramidal cells, are conspicuous noise sources. If cells were to be kept in a narrow regimen of resting membrane potential, below the threshold all the time until selective stimulus is received, the metabolic cost should be unaffordable and the noise will dominate. On the other hand if cells were massively hyperpolarized to avoid noisy processing, efficiency will be reduced to ineffectiveness. The evolved solution is to shift membrane potential closer and below threshold rhythmically in a coordinated fashion across the cortex. An obvious drawback associated to this solution is that if for example the same stimulus is repeatedly administered, each time the output will depend on the “internal status “of coordinated oscillation. Processing with high selectivity and efficiency will be only possible inside pulsating “windows of opportunity” when pyramidal membrane potential is just about threshold. Between these windows a stimulus of fixed magnitude shall be overlooked or could only elicit subthreshold responses when membrane potential lies far beneath threshold. Fluctuating membrane potential is low cost compared with a membrane constant clamping and evolved in a great variety of contexts. Temporal sampling rate of reality obviously is to be matched with the expectancy rate of feature changing. Vertebrates inhale proper quantity of odors during

explorative behavior and insect fidget their sensilla in similar rhythmic way until an “interesting” molecule is sniffed, at this point oscillation frequency is increased (Stopfer and Laurent, 1999). Oscillations built up only on principal cells are also possible as observed when GABAergic drive is removed. Hypersynchronous epileptiform activity ensues and pyramids oscillate due to their bistable behavior generated by intrinsic biophysical properties such as the kinetics of neurotransmitters turnover. In physiological conditions rhythm city is imposed by inhibitory interneurons. Not just a single pacing pattern is actually imposed by interneurons, a wide repertoire of rhythms are instead set in existence, resulting in a beguiling interplay. Interneurons per-se won’t be able to generate oscillation, which is an emergent property of excitatory-inhibitory networks. Even in the case of a single rhythm of oscillation, forces external to the network are needed. Single kick in the circuit will determine oscillation that eventually will fade away in silence: there must be some sort of excitation drive in the network to sustain oscillation. This is provided indeed by subcortical structures that in turn oscillate intrinsically and are apart from the computation taking place in the cortex. Another source of tonic excitation is the glutamate spillover and basal transmission. Structures such as the cerebellum that lack recurrent excitation loops, fail to generate oscillatory activity. One way to generate oscillations in targets is the ability of interneuron of several classes that intrinsically oscillate in response to stimulation. Otherwise non-oscillating interneurons can still generate oscillation in targets: this is another observed patter generator process. Non-oscillating interneurons may fire stochastically inside the network, when two or more interneurons fire together by chance; their targets are inhibited at the same time starting entrainment. Given the high convergence factor of interneuron projection over pyramids, synchronous discharging interneurons also silence synchronously the same targets with high probability. Time required to regain “normal” membrane potential in these synchronously inhibited pyramids shall increase, segregating them from the rest of stochastically inhibited ones. Because of the high divergence of pyramidal projections to interneurons, some further inhibitory neurons shall be entrained in the next cycle generating a seed of synchronicity that could expand collecting stochastically available cells until another seed is reached (Figure 1.5). Synchronous seeds will wax and wane rhythmically. In each seed not all interneurons are required to be discharging at each cycle and a minimum fraction of them will sustain the rhythm. Inside a synchronous oscillating territory, any two cells fire with zero time lag. This is observed for long range oscillations coupling between functionally connected regions in the cortex while other rhythmic patterns are controlled by other specialized interneuron-pyramids interactions. Gamma clock is a wide distributed one, in each cycle no same neuron is responsible for an initiation but all synchronous ones participates. Connectivity is not an enabling factor for gamma oscillation, defining only the mean extent of each synchronous seed, what endows the network with gamma clock is the degree of convergence and divergence of interneuron-pyramids and pyramids-interneurons. When a particular rhythm is engaged, individual firing freedom in compressed inside a shared window of opportunity. The emergent probability of oscillation was tested in theoretical networks: pyramidal-only, generate only hypersynchronous patter in few cycles of firing sessions,

interneurons-only networks never generate oscillations and a mixture of mostly pyramids and about 20% interneurons with a power law distribution probability in function of the distance (as described for real networks), generates robust oscillation with the highest probability without hypersynchronous events (Buzsaki et al., 2004). Gamma oscillations are typically short lived because of their sensibility to external drive and because of superimposed rhythms. 20-100 Hz oscillation is frequently observed especially associated with higher computational processes. Gamma band activity is also an hallmark of epilepsy and appears compromised in some pathologies associated to the autism spectrum. Long-range synchronization is also sensible to conductance delay at least in the genesis and extent of initial seed. Larger brains thus evolved strategies to compensate for dealing processes, in agreement with the idea that synchronization mechanisms are of high evolutive significance. Coordinating firing activity of neurons located far apart as in the case of large brains, is a difficult task: the same population behavior observed say in a small rodent, is conserved in large mammals. Synaptic length increases in bigger brains and distances are short-cut increasing the percentage of long range interneurons. Nevertheless, there should be a critical brain volume above which synchronization between distant regions become unfeasible: exceptionally large mammalian brains like *Loxodonta* or *Cetacea*, display poor synchronization capability between hemispheres or distant cortical areas. Human brain seems to be placed to the edge and synchronization is allowed virtually across the entire cortex which is a human distinctive trait. Some authors speculate that the more the cortex is capable of synchronization over increasing distances, the more probable is the emergence of “consciousness”. Human long range synchronization seems to be the best achievable in mammalian brains equipped with the same interneuron array. Poorer synchronization capability in smaller brains seems to be a byproduct of the smaller percentage of long range interneurons or, conversely, “consciousness” might be interpreted as a byproduct of increasing need for long range inhibitory connections growing with brain size up to a maximum observable in humans.

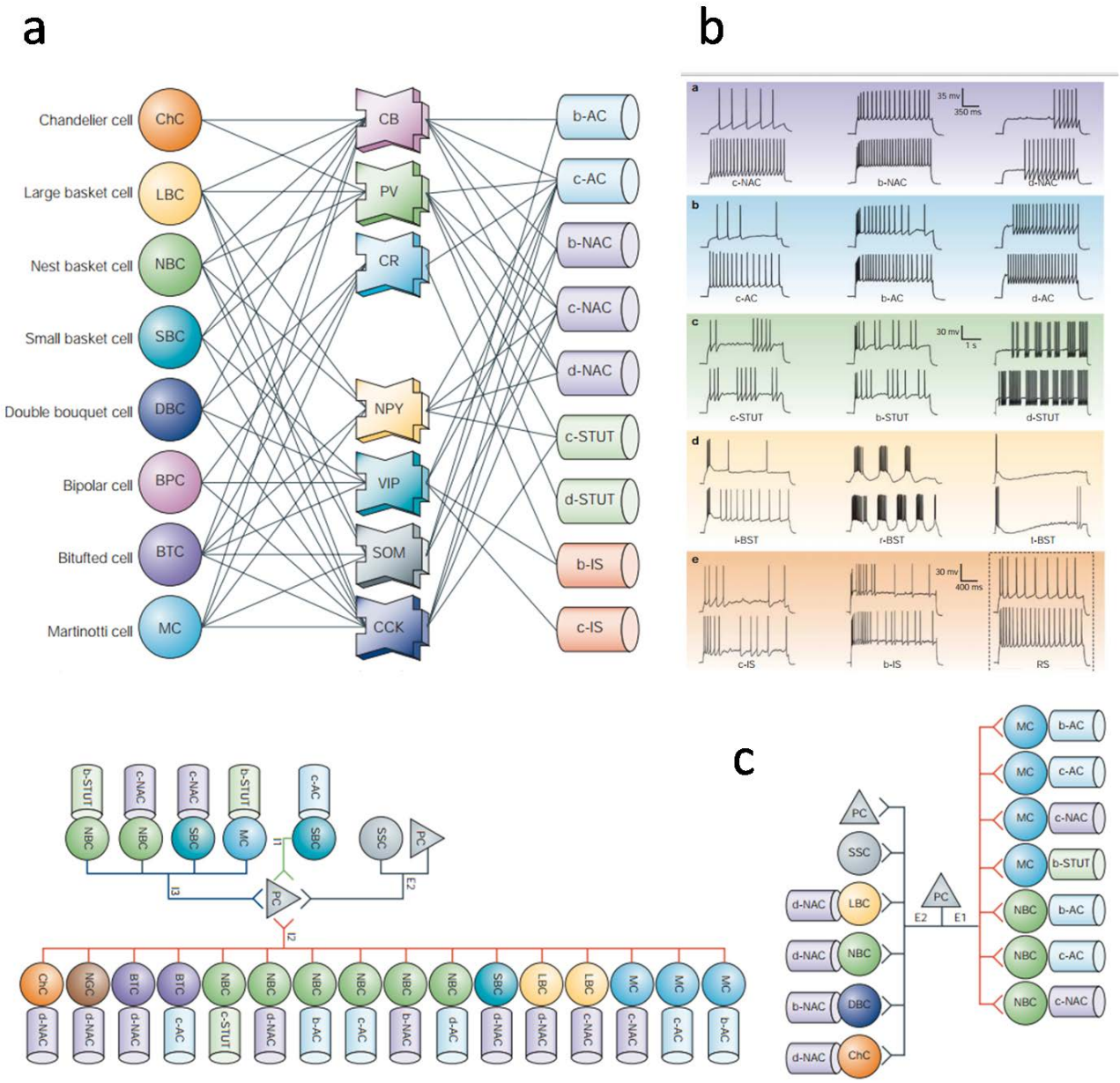

Figure 1.4 *Interneuron diversity. a) Interneurons are classified according to their morphology in the left row, central row lists key molecules found to be expressed exclusively in inhibitory cells while the right row summarize their typical firing pattern. Combination of these properties define the identity of interneuron classes, visualized here by tangled connections. b) Firing patterns of interneuron in response to depolarizing current injection. c) Interneurons convergence onto a pyramidal cell (left) and connectivity of pyramidal cell with interneuron classes (right). A wide spectrum of categories, still poorly characterized, define the nature of inhibitory interneurons (Markram et al., 2004).*

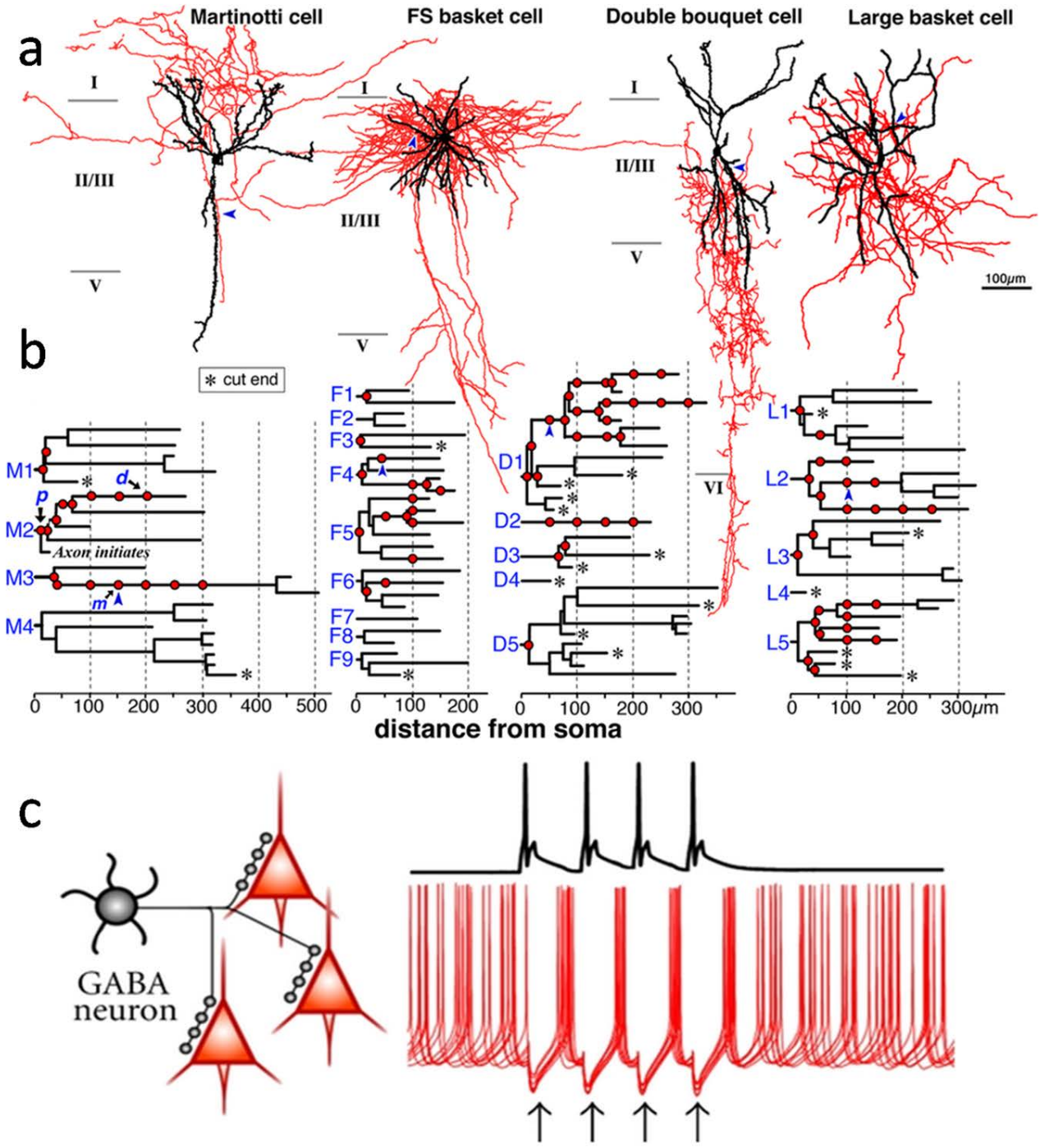

Figure 1.5 *interneurons control of network function a) Representation of the dendritic arborization (black) and axonal projections (red) of four interneurons. b) Dendrogram relative to neurons in a) representing the extension of dendritic structures (Kubota et al., 2011). c) Representation of the effect of impulsive firing of a fast spiking interneuron upon phase relation among three principal cells. Black firing pattern impose the peace in unrelated (red) firing pyramids. IPSC (black arrows) is the hallmark of phase resetting (Gonzalez-Burgos et al, 2011).*

1.3---Automatic for the people/self-organized rhythmogenesis in the cortex.

In absence of external forces (inputs), cortical network generates oscillatory patterns of activity. At any given moment not all the "synaptic space" is engaged with spontaneous (or stimulus-triggered) activity, quite the other way around, only a tiny percentage of possible configurations are explored. Local seeds of synchronizations quickly expand, propagate and fade away leaving space to others. Brain activity constantly oscillates from complexity to predictability. As Friston (2000) put it: network dynamic shifts from stable incoherence, through dynamic instability, to complete entrainment, yet high-complex and high-entropy behaviors require, theoretically, radically different structures (Sporns et al., 2000; 2002). Complexity is actually highly sensible to interferences while predictable oscillations resist divergence. This bi-stable organization seems to be the most efficient solution in order to detect modifications concerning surrounding physical world and internal parameters. From their first EEG characterization in 1929 by Berger, several types of oscillatory behavior have been described is numerous mammals. Distinctive trait is the frequency ranging from infraslow, with periods of minutes, to ultrafast rhythms oscillating at 600 Hz (Cracco, 1971). The common classification includes: δ 0.5-4 Hz, θ 4-8 Hz, α 8-12 Hz, β 12-30 Hz, γ>30 Hz; the typical EEG bands characterized first in humans. Band separation is arbitrary and affected by the sensibility of outdated recording devices. Each oscillator is indeed the result of an independent physiological process: rhythms are non overlapping (Komisaruck 1970 suggests an integer phase-locked relationship). Starting from hippocampal θ, γ and fast oscillations, Tanskanen (Tanskanen et al., 2006) extrapolated a law that best fit all other known rhythms: discrete oscillation power bands are arranged on a geometric progression when frequency is linearly scaled up (or a linear progression on a natural log frequency scale, Figure 1.6). Although non-overlapping, the progression is continuous from 0.02-600 Hz. 10 different mechanisms are postulated to be necessary to generate the complete spectrum. But not all the rhythm are persistent is one structure alone, thus different brain areas must interact to generate emerging rhythms, conversely different mechanism in different areas may give birth to the same oscillation. Each known band mean frequency divided by the previous one on a linear frequency scale, result in a constant Neperian ratio (***e***=2.17……). Since ***e*** is an irrational number, the phase-lock relationship between different oscillators in the various bands won't be the same at any given cycle shifting from a rhythm to the next: the oscillation between different rhythms is non-repeating, quasi-periodic, weakly-chaotic. Sampling of reality relies upon these rhythms but could be as accurate just with one fast oscillator for every purpose. Probably the simultaneous existence of diverse rhythms is a remnant of evolutionary history of mammals selecting ever faster sampling capability. Multiplicity in rhythmicity could also be the product of wiring evolution: several circuits deploy fast and thick axons while other save space shrinking the size and slowing down conduction speed. As the number of available computational processes increases neuronal loops number required shall increase as well and further information extraction result in hierarchic engagement of consecutive loops. Stimulus triggers activation of different rhythms one after the other or the first activated summons the follower and so on (McClelland et al., 1995). In some cases such as in the visual

stream of mammal cortex, features of the stimulus are extracted in parallel: different information contents are split in segregated areas soon after V1 (Figure 1.6), these starts to oscillate at different characteristic frequencies in order to convey output into superior areas merging computation in time and space regardless differences in the distances. This seems to be a solution to the "binding problem" i.e. coalescence of information analyzed by different areas into a single percept associated to a physical stimulus. Not surprisingly, superior areas pyramids are discharged by converging afferents while remain silent when only a path is activated (complex versus simple stimuli). Short lived artificial stimulation on somatosensory cortex only triggers unconscious sensations/responses, while longer trains of stimulation (200-500 msec) elicit a conscious percept (Libet, 2004). Oscillation in a neural loop equals a time window of computation or broadcast of signals: the brain processes information split in quanta. Because of the axon conductance delay, only slow oscillations travel far. Low pass filtering explains propagation of noise in the network: spatial correlation of noise at given frequency **F**, increases as **F** decreases (Vogels and Abbott, 2005, Vogels et al., 2005). The "wavelength" of each oscillation restricts the capability of the rhythm itself to propagate due to the filtering properties of the tissue. Thus, high frequencies shall be the hallmark of local computation while slow ones could be associated to broadcast or biding. Exposing a subject to increasing density of "black bars" drifting on a gray background on a monitor, increases the power of the gamma band (low gamma 24-32 Hz) only in the visual cortex, while asking the subjects to associate "names" to presented images, augment the power in the beta band (13-18 Hz) across temporal e occipital areas. The size of neural pool engaged in synchronous activity inversely correlates with frequency of oscillation (Von Stein et al., 1999; Sarnthein et al., 1998). Amplitude ***A*** of EEG signal is inversely related to the frequency f of ongoing predominant oscillation: $\boldsymbol{A} \sim 1/f^{\alpha}$ where α is between 1 and 2, typical of the power spectrum of "pink noise" (Linkenkaher-Hansen et al., 2001). Different oscillatory patters only transiently phase lock each other because of the Neperian ratio between consecutive rhythms, what is observed is a constant fluctuation between phase synchrony and instability. The phase of different oscillators has no common attractor; they attract and repel each other in turn (Bressler and Kelso, 2001). A local oscillator is continually attracted and repelled by more global oscillatory activity until it succumb or shut the other oscillator. In principle this should produce a global EEG random noise, but inside chaotic behavior, transient phase coupling is allowed: $\boldsymbol{A} \sim 1/f^{\alpha}$ indicates that a temporal relation between different oscillatory frequencies exists. This is a critical feature in brain oscillation: transient phase coupling also means that a perturbation in a say "alpha wave band" propagates to all subsequent oscillatory activity explored, and reverberates to the next alpha rhythm. The "speed" at which amplitude decreases at increasing frequency, indicates how long is the persistency of propagation of a perturbation in a given frequency to the next ones. In pink noise, power density decreases 3 dB per octave at increasing frequency, or $\alpha \sim$ 1-2, amidst from highest informative/highest chaotic "white noise", where power density is constant at all frequencies (α=0) and highly predictable/low informational "brown noise" (α=2) (Gilden, 2001). Brain is able to self organize large-scale and long-term patterns generated by sub-routines of neural groups and, conversely, these very pattern direct the behavior of their generators: an example of "circular causality" (Kelso ad Fuchs, 1995). Activity recorded in each cell depends not only upon incoming inputs but also on the recent history of the cell in the context of the whole network. Given the $\boldsymbol{A} \sim$

$1/f^{1.5}$ relation in the power spectrum of oscillatory brain activity, one could predict that brains are more apt to detect stimuli with same power density distribution. Such is the case of cortical responses to white audio-noise versus music: the latter bearing the same $\boldsymbol{A} \sim 1/f^{1.5}$ structure (probably because generated by brains). If one computes a large scale/long time power distribution over frequencies in, say, Ravel's Bolero and Cure's album "disintegration", least expected, the two profile will be almost identical ($\boldsymbol{A} \sim 1/f^{\alpha}$). The very same appear to be true for visual "naturalistic" stimuli regardless the scene depicted. What is interesting is that in dedicated sensorial areas, $\boldsymbol{A} \sim 1/f^{\alpha}$ stimuli are able to discharge "better" a larger neural population. The chance whit which a random chosen neuron, in the suitable sensorial modality, is observed to generate APs during presentation of optimal stimulation, is greater for $\boldsymbol{A} \sim 1/f^{1.5}$ contents compared with "white statistics" or "brown statistics". This is true with all mammals studied so far. Even small brained mice exhibits a robust $\boldsymbol{A} \sim 1/f^{1.5}$ power density distribution of brain waves. $\boldsymbol{A} \sim 1/f^{1.5}$ distribution is typical even for human speech but importantly not for bird's songs as recently observed where neocortex is almost neglected in favor of pallium archeocortex. $\boldsymbol{A} \sim 1/f^{\alpha}$ is also the best fit for other complex time-related behavior (such as forgetting, habituation, coordination in motion, reinforcement effects and rate sensitivity) observed in all mammals tested. The magnitude of subjective sensation reported by subjects, increases with the log of the physical intensity of the stimulus itself, a property known as the Weber's law. This law is proposed to underlie the octave structure of music as well as visual sensitivity to luminance. In Weber's laws also is stated that: fraction by which a stimulus is to be increased in intensity to produce an unitary increment in reported subjective sensation, is not fixed in time but, notably, depends strongly by the magnitude of the previous stimulus perceived, underling the dependence of computation capabilities from history of the network. Some authors push the border even further stating that the elusive "qualia" derive from electrical architectures embedded in neural circuitry capable of such logarithmic order (LLinas and Steriade, 2006). Errors in behavioral tasks timing distributes with different coefficient of variation (σ/μ) in dependence of the time scale measured. The distribution, again follows $\boldsymbol{A} \sim 1/f^{1}$ law (interval magnitude in relation to interval generating error), thus internal "mind clock" merge with real time only in the millisecond to second range. The existence of multiple oscillators operating with different characteristic frequency covering the whole timescale, may explain the absence of a characteristic timescale in time perception. $\boldsymbol{A} \sim 1/f^{1.5}$ distributions observed in all cortical areas measured are scale invariant, reminiscent of fractal architecture. Although the fascinating simple $\boldsymbol{A} \sim 1/f^{\alpha}$ distribution, cracking the neural code is quite hard to accomplish. Consider for example 100 independent neurons characterized by binary states: firing/non firing, one can calculate 10^{30} different firing combination, yet those observed are just a tiny fraction. First: neurons are not independent and, second, complex networks have memory, the firing patterns employable are restricted by past activity. As a consequence of $\boldsymbol{A} \sim 1/f^{1.5}$ statistic is the fact that neocortex lives in a perpetual state of "self organized criticality". This allow for quick and flexible responses to stimuli. Metastability enables the cortex to reorganize its internal dynamics to the smallest efficient stimulation. Self organized criticality emerge in systems

characterized by an ***A***~ 1/f temporal dynamics and fractal geometry (Beggs and Plenz, 2003; Poil et al., 2012; Friedman and Landsberg, 2013; Park and Friston, 2013; Pu et al., 2013) which do not need any external tuning for transition. Spontaneously the system experiences the loss of characteristic spatiotemporal scale and episodes of correlations manifests at all scales. Thus a complex system is such if assembled on 1/f statistic and has fractal geometry (like avalanches, earthquakes, forest fires, power lines blackouts, airport traffic and mass extinctions). EEG dynamics seems to be best described by means of self organized criticality (Linkenkaen-Hansen et al., 2001; Le Van Quyen, 2003; Stam and de Bruin, 2004). This adaptative behavior comes at a cost. First: in restricted timeframes the network is only intermittently capable of processing inputs and second: rare extremely large events of hypersynchronicity may happen. The first drawback is damped by the relatively high frequency of reality sampling calibrated by evolution upon expected changes in environment. The second one might be under control of fast inhibitory local activity that might be able to smash global synchrony into segregated independent domains (see gamma rhythms that rides on slow prolonged activity). When this emergence exit fails to operate properly, hypersynchronous events may arise like in epileptiform interictal activity. On the other hand, containment of extended synchrony cannot be too stringent otherwise large scale processing may be impeded. In the absence of external perturbation the complex system behave on the basis of pink noise statistic as a result of coexisting oscillators with different frequencies and wiring geometry but when a stimulus ensues, a transition is triggered. Classical Fourier power spectrum analysis on long epochs of EEG recordings may be blind to transition shifts being forgetful of time-locked transient events. Stimulus-timed analysis or FFT/wavelets calculations allow uncovering hidden phase transitions. When the stimulus hit the network, predictability emerges: characteristic temporal scales (oscillations) manifests. Though short lived, these periods of stability may be helpful for example in storing information in the circuit for an appropriate time. The tonic pink noise dynamic allow the system to be ready for an unpredictable alteration of the environment. When the perturbation is detected the pink noise system coalesce instantaneously (a stimulus triggered EEG feature in humans presented with visual stimulation is the so called ***Bereitschaftspotenzial*** (Walter et a., 1964, Figure 1.6) and later interpreted as the first transition toward oscillation to be observed in visual processing) to a set of linear variables in a predictable oscillatory pattern of activity: the hallmark of processing and output broadcast. This condition must be as short as possible because an overlapping stimulus might interfere with the ongoing computation/transmission and might be neglected as a whole. To circumvent this possibility, hierarchical stages are employed: first encoding stations are first to be entrained but quickly disperd information downstream to second order stations and become ready to process the following stimulus (Figure 1.6). As observed in primary visual cortex of mice, a simple stimulus (sliding grids) is readily decomposed in band of spatial frequencies and sent to MT and LT areas. While extracting orientation features, each hierarchic level perform fast and light computation to avoid overflow. Eventually, information is somehow bound to the same percept in higher areas. When the perturbation ceases, the system goes back in the “default” idle state of readiness: pink noise multiple oscillating loops (Friston, 2000; Gilden, 2001). Because of its dependence upon past history, stimulus-locked network analysis might produce more information about internal state of the “observer” rather than on the nature of the stimulus itself. The determinants of complexity are

not yet understood. Surely enough the number of participants is not a critical one: small brains or short networks are able to perform complex computation still out of the reach of the most sophisticated robot. *In silico* models are so far able to generate extra-stable oscillations that never fade away or silent networks that overreact to each stimulus like in epileptic discharges even though neural class proportion, wiring, synaptic strength and intrinsic oscillation are simulated on the basis of what observed *in vivo*. Actually a piece of cortex disconnected from the whole network behaves much like an in *silico* model: large epileptiform population discharges emerge separated by periods of silence. Even 2000000 neurons in the hippocampus when taken apart from underlying connected structures, just remain silent until a large network epileptiform event ensues (Traub and Wang, 1982; Bragin and Vinogradova, 1983; Timofeev et al., 2002). Noise level is obviously a parameter to accurately tune in order to grant metastability, yet in all *in silico* models the power of noise must be severalfold increased compared to natural one in order to generate irregular patterns but in this context the system is resilient to stimuli unless of extremely high magnitude. Furthermore such a noisy model is anti-economic considering that often more than 10% of the neurons are “spent” to generate noise. Energy consumption evaluation in the brain though, indicates that doubling the firing rate will lead to complete exhaustion in few minutes (Laughlin and Sejnowski, 2003) not taking into account that spike generated noise shall intermingle with signal processing deteriorating it.

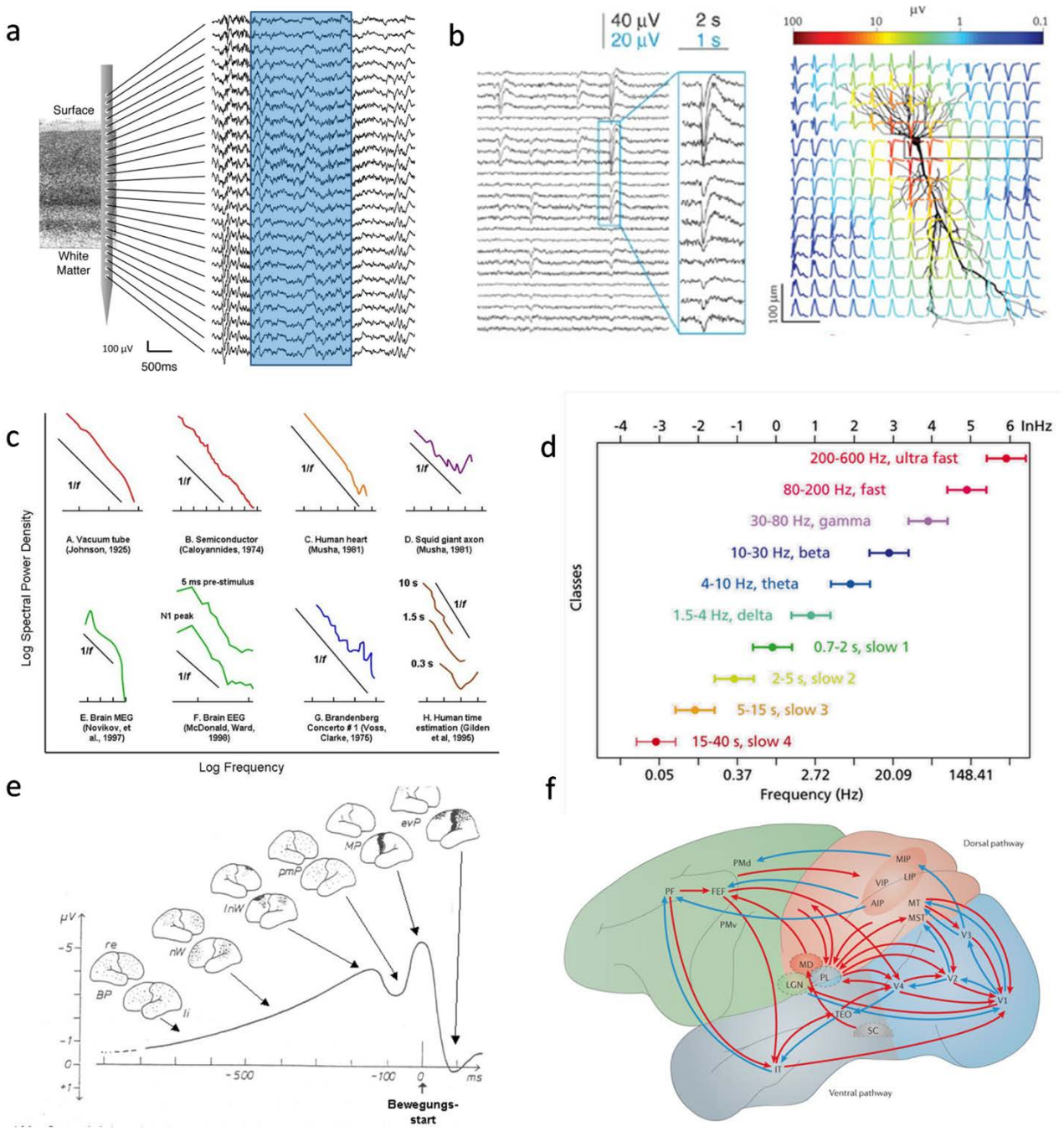

Figure 1.6 *frequency domain of cortical activity. a) Macaque visual cortex LFP recorded with depth multichannel electrode while the animal is subjected to visual stimulation (blue shade). Each line report the electrical behavior sampled at specific position in neocortical layering. Visual task entrains a conspicuous amount of neurons across layers (Maier et al., 2010). b) left: LFP depth profile obtained from rat neocortical acute slice preparation. Spontaneous activity is disseminated with sporadic episodes of transient synchronization (neuronal avalanches) readily damped. These sudden bursts of coherence emerges with a fractal geometry in a scale-free fashion across neocortical structures (Plenz and Thiagarajan, 2007). Right: extracellular electrical signature of an action potential. The spike picked up by LFP recording at different distance from the actual surface of the spiking neuron are depicted as variation of voltage in time. The amplitude of each LFP spike*

is color coded and normalized while the shape is normalized across all dataset. Polarity is preserved across the pyramidal layer (black box) and appear reversed along axo-dendritic axis. As the electrode-neuron distance increases the amplitude of extracellular spikes rapidly falls (Buzsaki et al., 2012). c) Examples of pink noise distributions of representative freequencies in different systems. d) The same power-law arrangement of brain frequencies is constantly observed in necortical structures. Frequency bands typical of classical electroencephalographic recordings are non-overlapping and continuous on a linear progression in a logarhytmic frequency scale (Buzsaki and Draguhn, 2004). e) The bereitschaftspotential observed in anticipation of a recorded motor cortex activation in response to a motor task (recorded from monkey). Dark shade reported on the schematic representation of the brain indicates peak location and field intensity progression in time. The motor output is indicated in time by the black arrow (Kornhuberi and Deeke, 1965; Shibasaki et al., 1980). f) Hierarchical organization of visual input decoding process in primates. Visual "raw" data are processed is steps, each stage is a further station of visual features extraction. Cortical areas downhill in the flow are engaged by the preceding one and signals back once date are locally processed (Gilbert and Li, 2013).

1.4---Ghost in the machine/oscillators.

Biological oscillators are classified as “limit cycle” or weakly chaotic oscillators (Mackey and Glass, 1977).The limit cycle is an attractor to which the trajectories in the phase-space explored by the oscillator are drawn back after a perturbation after a suitable amount of time (Figure 1.7). Harmonic oscillators are limit-cycle ones. In an harmonic oscillator a physical parameter varies above and below a mean value with a constant frequency and fixed rate. Harmonic oscillators are excellent time keepers and predictors. When the rate at which the physical parameter rise and fall is not constant yet the frequency is kept, the oscillator becomes non-harmonic. Most biological limit cycle oscillators are non-harmonic, characterized by a slow accrual phase and a fast discharge or relaxation phase conferring the typical pulsate behavior (heartbeats, respiration, walking, hormone secretion). Minimum requirement for an oscillator to be set in motion are two opposing forces provided with a proper feedback. Relaxation oscillators are described by: X=y-f(x); Y=-**e**x where “e” is a parameter that modulates coupling between the slow accrual phase and the fast relaxation phase in each cycle: when **e**→0 time spent in accrual phase →0. Low values for **e** are typical of low frequency rhythmic neurons displaying highly nonlinear behavior. When low-**e** relaxation oscillators are wired, synchronization develops in few cycles and is greatly stable. Increasing **e** decrease accrual time and time spent “charging” becomes comparable to that spent in “discharging” (Figure 1.7). High **e** values allow for high frequencies *e.g.* 500 Hz firing in neurons, and low **e** oscillators might turn into fast ones when discharging probability increases. The accrual phase for relaxation oscillators like in neurons, is associated to “energy accumulation” to a threshold that trigger the transition to discharging phase (rising of membrane potential toward AP threshold would be the slow phase and the genesis of AP the fast one). A dripping faucet or a van der Pol circuit are simple examples of relaxing oscillators. In the van der Pol oscillator, energy accumulates on the plates of the capacitive element (with an **e** value determined by C and R) until an adequate ΔV builds up, enough to shift neon tube to conductive state. Once threshold is reached, electrons transverse the neon tube glaring. This event is fast and consumes the ΔV that stats again to builds up but threshold is now distant and the tube is off: another cycle starts. In an harmonic oscillator, short time behavior and long term ones are the same, one can determine the “position” in the cycle just calculating the derivative of the oscillating parameter in an arbitrary short time window (provided that the limit cycle and frequency are known). A perturbation on an harmonic oscillator exerts the same effect on the orbit in phase-space regardless the position in the cycle at which the perturbation is delivered. After the perturbation, the limit cycle attract the orbit back again to the characteristic frequency of the oscillator. Determining the position inside the limit cycle of a relaxation oscillator is not as easy and confronting with a perturbation, non-harmonic oscillators display 3 different responses: 1) excitable state in which the accrual phase is almost complete and a slight external perturbation may precipitate toward threshold (tapping the dripping faucet when the drop is almost of the critical size), 2) the duty cycle, which is the discharge phase itself and 3) early step in accrual phase or refractory period in which no perturbations will ever be enough to precipitate toward the duty cycle. Triggering transition in relaxation oscillator responsive phase, produce a “smaller” duty cycle, but unlike harmonic oscillators, the next cycle is readily a typical one. Neuron behaves almost entirely like relaxation

oscillators: the accrual phase correspond to the integrating interspike phase and the duty cycle to the firing activity. If set free, a neuron shall oscillates at its typical frequency in a non-harmonic fashion. When coupled, neurons may perturb each other only in the ready phase. Because of the ability to restore normal limit cycle oscillation after a perturbation, relaxation oscillators have excellent phase resetting properties: they can “learn” and “remember” patterns. Also extended to coupled neurons, phase resetting may only happen in discrete windows of chance, elsewhere the coupling is ignored altogether. Generation of oscillating behavior may rely on phase controlled energy supply and a simple damping mechanism: energy is injected in the system in phase with natural frequency of the oscillator that dissipates it at regular peace (like a swing). But energy source might be uncoupled to the natural frequency of the oscillator that becomes now a forced oscillator. Depending on the phase relation between energy supply and oscillation frequency oscillator phase changes in time, oscillators are started or even could die away. Actually, neuronal assemblies, oscillate transiently. When a sudden burst of energy is fed into a quiescent oscillator, it starts to “swing” and the amplitude is dampened at each cycle until it stops. When energy is fed into the oscillator with a frequency that is an integer multiple of the natural frequency of the oscillator, this starts to resonate. Amplitude of the oscillation increases with cycles in resonating oscillators. Since resonation is best achieved when fixed proportion between energy input frequency and natural oscillator frequency are met, resonators are also frequency filters, and N same-frequency oscillators may resonate (Figure 1.7). Population behavior complicates the scenario adding resonance, noise and unpredictability. Due to the molecular arsenal of channels and modulators with which is armed, a neuron self generate its own oscillation pattern: the power spectrum of intrinsic rhythm is best approximated by $\boldsymbol{A} \sim 1/f$ relation (Diba et al., 2004). The plethora of channels and their distribution on the membrane are the molecular face of opposing forces governing membrane potential. Threshold for duty cycle is a complex property of neuronal membrane defining the sensitivity to selected inputs. When a “strong” (high in intensity and precise in space-time distribution) comes in, the neuron typically respond with transient damped oscillation with its own natural frequency. Eigenfrequency is the result of competitive forces acting on membrane potential: the leak conductance and membrane capacitance. Due to the low pass filtering of capacitive elements and slow gated conductancies, neural oscillators resonate worse or respond with less reliability, when input frequency is increased. On the other hand several conductances are activated in proximity of resting membrane potential *i.e.* any little displacement from the resting state will operate these channels. These confer an high pass filtering property to the neuron. Neurons endowed with a great density of such conductances are more precise in propagating AP at fast rates and loses reliability for lower frequencies. Hippocampal pyramids resonate at θ frequencies (2-7 Hz) while basket cells at beta-low gamma frequencies (10-50 Hz) (Pike et al., 2000). Depending on the combination (even on a subcellular scale) of slow conductances ,capacitive properties and fast conductances, a neuron can operate in basically 5 different modes: low pass filters, high pass filters, band pass filter, notch filters and sub threshold oscillators. Inputs are thus selected by receiving neurons on the basis of their frequency content.

An input composed of multiple frequencies content is fed into the network and readily decomposed in “resonant bands” each pertaining to a local group of neurons. These in turn, given the connectivity rule of neocortex and the shared natural frequency of intrinsic oscillation, are highly prone to couple in an entrained population oscillator. Input frequency bands thus tend to segregate. Interference with ongoing spontaneous population oscillations and connectivity eventually merges the outputs. A neuron is also provided with a vast repertoire of eigenfrequencies: the frequency filtering algorithm is a complex one and also appears to be dynamic and history dependant. Among ion channels contributing the most to the filtering ability are the great variety of K channels. These are mainly responsible for setting the interspike interval and the accrual phase duration. K channels display the highest density compared with other channels and the wider gating kinetics range spanning several order of magnitude. Furthermore gating itself and regulation could be simple (voltage gated or Calcium gated for example) or complex (second messengers or mixed gating by voltage-Calcium and second messenger). Some neuromodulators released to control wakefulness, acts just on some classes of K channel regulating their “readiness”. During sleep low concentration of Ach for example, correlates with low kinetic in some K channels in the cortex (or a low reliability in computing high frequency signals, those typical of waking life). This modality is altered at arousal and in awakening processes, when Histamine, Noradrenaline and Ach increases, as a result K gating becomes faster and the high pass filtering capability of “awake” neurons increases (D’angelo et al., 2001). I_{KS} current (slow Potassium current) increases spike timing, tuning it to the eigenfrequency of the neuron while I_{NaP} (persistent Sodium current) has the opposite effect, contributing to divergence (Rabert et al., 1998). Increasing I_{KS} current *in vivo*, augment neural tuning to gamma frequency range (Penttonen et al., 1998). On a subcellular resolution, every single patch of neuronal membrane is a resonator tuned to a natural frequency, all that is least required is the presence of opposing conductances with different kinetics. Composition of elementary resonators is dependent upon their density and location, giving rise to the complex resonator at the cellular level. In a pyramidal neuron, slow kinetic conductancies are homogenously distributed along the whole cell, while fast activated ones are clustered and fewer. As a result top firing rate in a principal cell is around few hundred Hz. Network elements regulate the contribution of elementary oscillators to the whole neural one (Steriade, 2004). Despite the highly predictability of isolated single neuron oscillation, *in vivo* average single unit activity, appears stochastic. On the other hand the same single unit activity is phase locked and predictable when activity is recorded upon stimulation in short time windows (Shadlen and Movshon,1999; Singer, 1999; Engel et al., 2001). Network effects are evident when pharmacological manipulation of conductances is performed. Removing contribution of excitation in a single neuron embedded in the hippocampal network for example, result in decreasing single unit firing rate, the converse is observed removing inhibitory drive. Combining both treatments result in a dramatic increase of firing rate well above dishinibition with emerging rhythmicity and predictability. The default modality of neocortical neurons appears to be firing instead of silence (Cohen and Miles, 2000). In the network environment though, each neuron has a very low probability of spiking when spontaneous activity is allowed. This is to be interpreted as a tonic inhibition. Such inhibition lowers noise amplitude increasing S/N ratio when a stimulus is presented. Output “gain” is also modulated by intensity in inhibitory inputs. Collective neural

behavior is required and observed in signal processing and information extraction. From a relativistic point of view, concomitant events are discerned by two observers only if they share a common temporal reference array. Most commonly, a time window of arbitrary amplitude is to be defined inside which all events are considered synchronous. A neuron receiving from two peers located at two different wiring distances, should be capable to tell apart individual messages when "asynchronous", *i.e.* an integration time window of finite size shall be operating. When a moving image change color at phase locked frequency of 2 Hz, that is simultaneously, human observer tells that change in color precedes change in direction. Color and motion are processed separately and bound to the same percept downstream. Furthermore, color is processed faster than motion. Events are synchronous when perceived together rather than happening together (Moutoussis and Zeki, 1997). The time window of integration might be defined by the "retention" time of past inputs: how long an input effect is able to alter the next incoming one. PSPs for example, although short lived (milliseconds to hundreds of milliseconds, depending, in case of EPSPs upon gating of AMPA or NMDA receptors, for example) and space restricted (few microns according to the cable constant of thin postsynaptic spine neck, for example), are typically integrated over time. Cronassia or time constant is the time at which the ΔV, produced by received input, is reduced to 37% (1/e) of the peak value. Time constant is a function of input resistance, because ΔV charged across membrane dissipate slower when membrane is less leaky (higher input resistance, which is also slower charge) and membrane capacitance, since a ΔV is slower discharged the higher is the capability of membrane to allocate charges (high capacitance, which is also ability to develop higher ΔV). Typical time constant at rest is 10-50 milliseconds for a 10-20 mV ΔV. Yet neurons embedded in active networks are constantly subjected to conductance gating, or, its input resistance falls compared to resting isolate state. Furthermore, awake brains have even lower input resistances because of subcortical modulators increasing gating probability of K channels. Thus integrating time windows are variable depending upon activity mode of the receiving neuron: synchrony is relative from neuron's point of view (Borg-Graham et al., 1998; Kamondi et al., 1998; Destexe et al., 2003; Steriade and Timofeev, 2003). From the population point of view, synchrony depends upon duration of ready state in the limit cycle of coupled oscillators. This can be much wider then each single cell integration capability: slower rhythms allow wider windows of chance for synchronization. This also implies that the slower the peace of oscillation the wider the pool of synchronous participants may be. This is also allowed by conductance delay which obviously affects more distant members. Thus the extent (or numerosity) of synchronous events is extended for slow rhythmical activity. If all oscillators participating to the population rhythm were harmonic ones, of the same eigenfrequency, the synchronizing event shall fall within half the period to be effective. Otherwise subset of oscillators will emerge that have a phase space trajectory non-overlapping with the others and the coupled population oscillator soon disaggregates. In gamma bands coupling for example, an excitatory drive must be received from all participants within 10 msec (half the gamma period) in order to increase coupling resonance and recruit more participants. This is also the reason why gamma bands are not quite wide oscillators: conductance

delay forbids synchronous triggering beyond a certain distance (10 milliseconds correspond on average to 1mm volume). In relaxation oscillators time windows for integration could be larger. This also depends on the effect the synchronizing stimulus have on the limit cycle *e.g.* in gamma coupling, inhibitory drive have effect on the large accrual phase (long integration) and to be synchronous must enter the cycle within 16 milliseconds, while excitatory inputs are effective on the readiness period, the window of which is about 4 milliseconds only. Thus synchronization by discharging peers is less effective. Neural network synchronization depends on time constants and may vary from submilliseconds to tens of seconds, the slower the rhythm the weaker the dependence upon long range connection the larger the population entrained. Excitatory feedbacks and feedforeward circuit allow efficient recruitment of large populations yet refractoriness and inhibition reduce the probability of synchrony triggering events, enlarging the accrual phase possibly entraining the phase of simultaneously targeted neurons. Shunting inhibition on the other hand, reduce both input resistance and EPSP ΔV amplitude with the net effect of reducing time constant. Synchronization among interneurons is provided both by interneuron-interneuron projection and by gap junctions mediated electrical coupling. This latter synchronizing mechanism impose another low pass filter due to the slow “propagation” of depolarization through electrical synapses which is a consequence of capacitive behavior of membranes and of “space clamp” effects. Another mechanism, arise from ephaptic coupling. Extracellular field intensity decay with $1/l^2$ from the source or sink location, but, given the high density of processes in the neuropile (free space *in vivo* is poorly characterized and is a highly dynamic parameter ranging in porosity from angstrom to micrometers in an highly tortuous configuration), there is chance for the propagating field to depolarize juxtaposed membranes. Even this path rely on low pass filtering properties because it depends upon ion diffusion which do not follow neither a free walk Brownian statistic nor a deterministic one (Vorisek and Sykova 2009). From an informatic point of view, both synchronous and asynchronous patterns are plausible coding alternatives. It is not clear although how repetitive loops of neural populations might be discharged by asynchronous incoming inputs since time constants forbid summation beyond integration time and single excitatory inputs are almost 100% subthreshold (Friston, 2000). Synchronization is not exclusively generated by external driving forces. In hippocampal neurons at rest, single cell firing statistic is dominated by Poissonian distribution in time and different cells are often uncoupled. With unpredictable occurrence rate (long time averaging produce a mean value of 80-150 msec), 20% of hippocampal pyramids cooperate synchronously producing a single spike or a short train: the sleep associated “fast ripples” at 140-200 Hz in CA1 region, one of the most synchronous event in physiological conditions. (Csicsvari et al., 1998, 1999). Similar fast rhythms are observed in sleeping somatosensory cortex (Kandel and Buzsaki, 1997). At the population level thus, explicit temporal dimension manifests that are completely absent at the single cell level (emergent property) and population events (strongly affecting downstream targets) may arise without any alteration of intrinsic firing statistic of single members. Local field potential (LFP, or more properly: local extracellular averaged measure of electrical field intensity) is a measure of coherence across neural population, the higher the synchronicity, the wider the recorded deflection in LFP and the greater the effect on targets. Even the ephaptic coupling effect increases with synchrony because extracellular field is the sum of each sink/source in a given time window defined by extracellular

time constant and across a finite space defined by extracellular electrical permissivity. Recording from couples of not directly connected neurons in monkey neocortex during meaningful visual stimulation, resulted in observed coordination of firing activity of these cells, without any change in average firing rate (Vaadia et al., 1995). This suggests that information about the stimulus is encoded in dynamic change in synchrony across the network, instead of spiking frequency coding (Figure 1.7). Encoding through transient coordination is energy saving: no increase in cellular activity is required. Probably this is a wide employed coding strategy in sensory cortices and might be overlooked in fMRI observations because no BOLD increase is needed. Poisson firing statistic in visual cortex is observed for stimulation with images moving at a constant speed, with no evidences of oscillations while time pattern clearly showed up when the image accelerated. Acceleration of the image motion was mirrored by a single neuron spiking precision within 3 msec. theoretic calculation suggests an information flow of about 1 bit/sec for constant velocity stimulation and a 39 bit/sec in accelerated images (Buracas et al., 1998). It is a well established concept that single neuronal responses or population activity may vary considerably from stimulation trial to the next and usually all the variability is traditionally accounted for “noise” and averaged out. Spike trains generation in reiterated sensory stimulation trials, present a coefficient of variation around 1 which is a sign of Poisson statistic (Softky and Koch, 1993; Csicsvari et al., 1999). This noisy behavior is instead best explained by interaction of network generated synchronization events and stimulus triggered ones. Single cell responsiveness depends upon its past history and that of the network in which it is embedded. Even for invariant stimulation, brain activity result highly variable. In the absence of noise sources, a silent neuron might display subthreshold oscillations and never fires or it is isolated from downstream targets. Adding a congruous amount of white noise, which alone won’t be enough to discharge the neuron, might turn the neuron into a firing one by stochastic resonance. Firing rate will be random because there is no relation between stochastic noise and underlying subthreshold rhythmicity. It is not possible to forecast the timing of the next spike at least on restricted time scales. The problem with stochastic resonance mechanism resides in the genesis of noise. Some authors discard the “noise problem” as a mere epiphenomenon generated by misfiring neurons. In this perspective an oscillating population may contain some “less efficient” participants that resist the entrainment and randomly generates ectopic AP. These should be recycled in the network end fed back as random noise. Some others suggest the existence of dedicated subset of “constantly” firing neurons that are disengaged from oscillatory patterns. Both cases would be energy consuming solutions probably not affordable. In the last decade, in a number of works the view of “energy saving brain” is brought back: APs are actually used sparingly; their faithfulness to stimuli is indeed greater than previously thought (Mainen and Sejnowski, 1995; Wehr and Zador, 2003; Fellous et al., 2004). Reliability of single neuron firing upon stimulation is increased when factors as recent history and network neighbors are taken into account and precise timing is observed even in the context of complex circuitry (Henze and Buzsaki, 2001). After all a sparse coding strategy presents

several advantages (Levy and Baxter, 1996) and is actually observed in most recent works employing in vivo Calcium imaging (Ko et al., 2013; Harris and Mrsic-Flogel 2013).

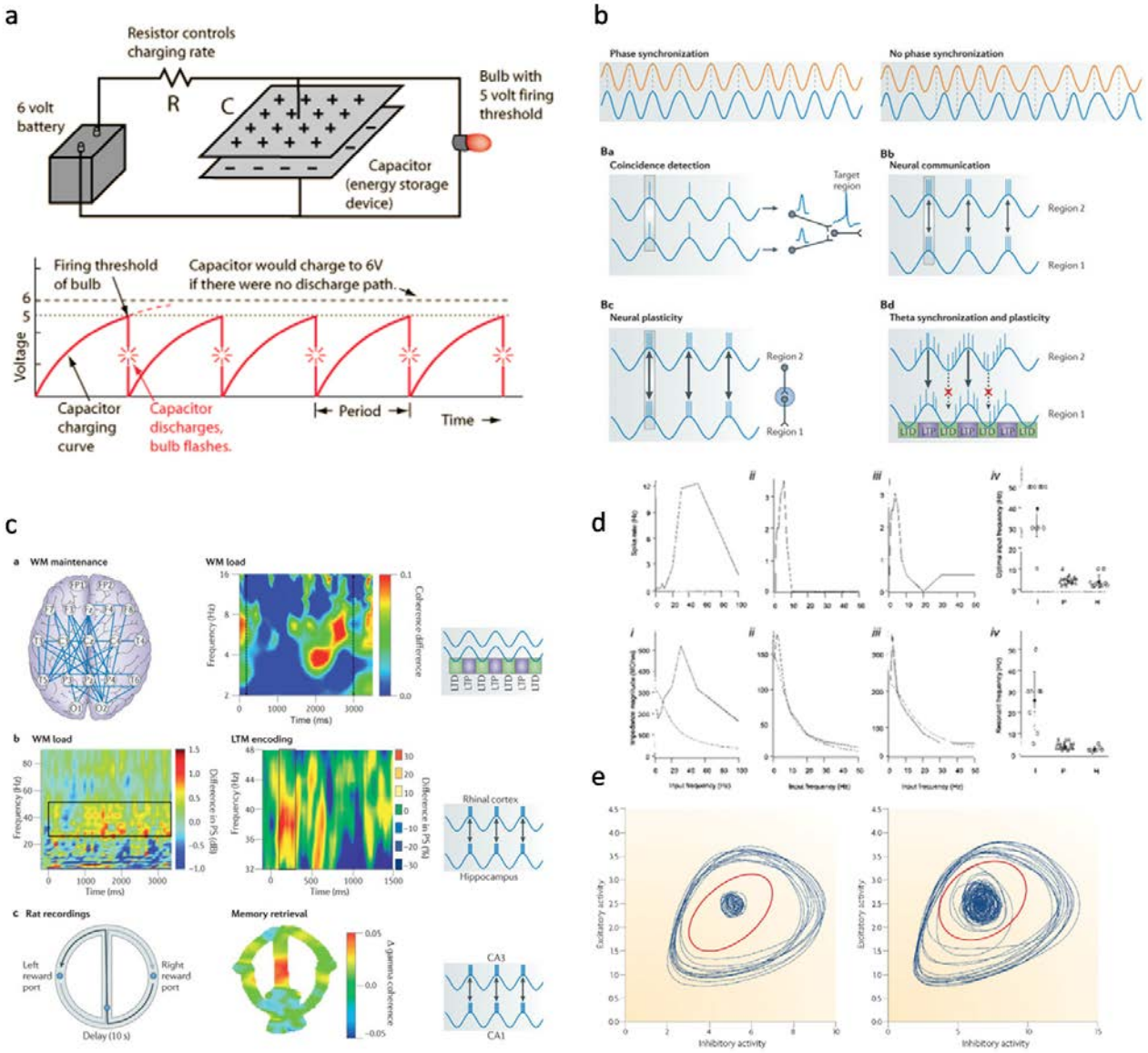

Figure 1.7 *osciilating neural activity. a) a relaxation oscillator exemplified by a Van der Pol circuit. a battery repeatedly charges a capacitor to the firing threshold of a bulb, so that the bulb flashes at a steady rate. After the flash, the battery begins charging the capacitor again. Capacitor recharge time and resistor impedence determine the flashing rate. The flashing rate. Neurons recharge like a capacitor, but then wait for some kind of stimulus to fire. In some cases, firing threshold is lowered enough to "self fire" and the neuron act as a relaxation oscillator. b) Neuronal membrane potentials may oscillate showing phase synchronizations (top left) or could display no signg of phase coupling (top right). Ba, two neuronal assemblies project to a third region. Phase synchronization of projecting assemblies coordinates the timing of synaptic broadcast to the third region. A coincident bombardment, most likely increases the chance of discharging the target. Bb, Phase synchronization allow for efficient information transfer between connected regions. Bc,*

Coincidence of incoming inputs, facilitated by phase synchronization, enhances the efficacy of spike timing dependent plasticity, further facilitating communication. Putative function of theta phase synchronization between two regions. Theta oscillating region 2 sends APs onto region 1 also oscillating with theta frequency. Generation of APs in region 2 is most probable when the assembly is a the peak of theta cycle. The probability with which region 2 APs discharge region 1 is maximal when region 1 is at the peak ot theta cycle (here LTP is more likely). When region 1 and region 2 theta rhythm are entrained, most of the region 2 APs are efficient in discharging region 1. Communication between region 1 and region 2 is thus reinforced. Before entrainment, incoming APs could be responsible for a driving input toward phase synchrony (Fell and Axmacher, 2011). c) top right: Working memory tasks enhance coherence in EEG between brain regions (differences in coherence manifest between connected region tested against a control task). Top middle: differences in coherence are increased in fronto-temporal EEG when working memory load is increased (stimulus presentation between dotted lines). Precise timing and frequency bands are engaged in the coherence shift. Top right: theta band increment in EEG coherence may indicate a role in theta phase synchronization in working memory tasks (frontal cortex would be the analog of region 2 and temporal lobe the analog of region 1 as described in the previous figure). Increments in theta phase synchronization are observed in intracranial recording between rhinal and ippocampal regions during multi item working memory and long term memory formation (center left and center middle panels respectively). increase in theta synchrony could be instrumental to increased communication between frontal and temporal cortex as well as facilitatory of spike timing dependent plasticity (center right panel). In a spatial memory task (bottom left panel: a rat is given a reward in a circular t-maze alternating position of the reward), gamma phase synchronization is enhanced between CA1 and CA3 just at the decision point (bottom middle panel). Gamma synchronization may help retrieval of consolidated memories through enhanced communication enabled by phase entrainment (bottom right panel. Fell and Axmacher, 2011). d) top row: firing frequency against input frequency for 3 types of ippocampal neurons (I, ii, iii). Most pyramidal neurons as well as horizontal interneurons resonate better with inputs in the 3-10 Hz band, while fast spiking interneurons prefere 30-50 Hz (scatterplot on the right.). bottom row: impedence magnitude against input frequencies of the same tre neural classes (dotted line represent the theoretical impedence curve).Inpedence resonate best at 30 Hz for fast spiking interneuron, while pyramidal neurons and horizontal interneurons resonate below 10 Hz. Impedence Vs. input frequency scatter plot is reported on the bottom right (Pike et al., 2000). e) Two-dimentiona slices of state space relative to modeled normal (left) and epileptic (right) networks. Trajectories define changes in two state variables: excitation and inhibition. A red circle define the border between two attractors in both cases: the inner one is relative to normal network behavior, the outer one represent epileptic seizure condition. In normal networks, trajectories define well-separated attractors the border between them is hardly crossed. In the case of an epileptic network instead the border between the two attractors is much more labile and trajectories are much more disperded so that slight perturbation could allow for attractor shift (Lytton, 2008).

1.5---Through the looking glass/astrocytes process information.

Contemporary neuroscience stems out from the acrimonious controversy among reticularism and neuronism of late 19th century. At the reticularist corner were supporters like Golgi, KÖlliker and Gerlach (Mazzarello, 2007), at the opposite corner were people like Waldeyer and Cajal. Golgi postulated the existence of a vastly interconnected lattice of neural elements, communicating through inter-cellular diffusion via anastomoses: a sort of functional syncitium. Waldeyer instead coined the term "neurone" to be attributed to discrete cellular elements which would be responsible for cerebral function. The impressive insights of Cajal soon contributed to strengthen the "neuronal doctrine". In 1906 Golgi and Cajal were awarded with the Nobel prize with explicit dedication to the neural Vs reticular controversy (Figure 1.8). The neuronal doctrine quickly gained popularity in the scientific community, meanwhile Golgi was hindered and misguided by technical limitations. Sherrington (1906) produced the first evidences for the existence of synapses, conclusively nailing the coffin in which reticularism would have rest in peace for almost 100 years. The importance of glial cells, although already characterized by Virchow in 1858, was utterly underestimated, overshadowed by the bursting interest in neurons. Four main classes of glial cells populate the CNS: NG2 glia, oligodendroglia, microglia and astroglia (Ransom, 2003; Verkhratsky and Kirchoff, 2007). Glia cells evolved together with the first neuronal aggregates (for studies on invertebrates: Abbott and Pichon, 1987; Coles and Abbott, 1996) and the density of glial cells clearly increases along with the enlargement of neural network size according with the increasing requirement of nutrients supply and waste scavenging. From a molecular point of view, few proteins are recognized as astrocytic markers, GFAP is most often cited although quite inappropriately being a specific marker of reactive gliosis rather than "healthy" astrocytes. GFAP-KO mice have normal astrocyte albeit resistant to reactivity and impaired in "glial-scar" formation (Pekny et al., 1995; Pekny and Pekna, 2004). Furthermore GFAP-IHC only stains big caliber processes and appears undetectable in fine process as well as in somata. Fine processes moreover, harbor no cytoskeletal formation (no GFAP, no Vimentin) neither in activated glia (Theodosis et al., 1981; Kosaka and Hama, 1986). Other "specific" markers such as Glutamine synthetase and S100β, proved to be not that "specific" (Norenberg, 1979). Beside many other putative markers (racemase, Synaptotagmin II, Inositol 3-phosphate receptor 2, Protease activated receptor 1, Glutamate Aspartate transporter, Connexin 43, Aquaporin 4….) for which there is still poor consensus on specificity or exhibit subcellular compartmentalization, Aldh1L1 protein seems to be a good candidate (Barres, 2008) (Image 13). Each protoplasmic astrocyte develops a network of thin processes that do not overlap with nearby astrocyte (Bushong et al., 2002; Ogata and Kosaka, 2002; Nedergaard et al., 2003; Halassa et al., 2007). Astrocytes that happen to share a border, establish gap junctions. Dye coupling reveal extensive conjugation only inside a radius of on average 300 μm, beyond this distance the network seems to be abruptly interrupted and a contiguous one emerges (Seifert et al., 2010) Noteworthy this complex organization is quickly lost in many cases of chronical alteration of CNS physiology (Oberheim et al., 2006). Connexin coupling is also drastically restricted in case of intracellular acidification or large Calcium increases even

when such events are short lived and sporadic, pointing in the direction of a fine regulation of transcellular communication (Figure 1.9). With experimental evidences progressively accumulating, astrocytes were gradually promoted from merely scaffolding cells to more active roles until in recent years when a true reappraisal of reticulismo is witnessed. Astrocytes are produced during development, shortly after the genesis of the first committed neurons, most likely from a common progenitor (Figure 1.8). Notably, neurons could be obtained in vitro retrodifferentiating cortical astrocytes (driving expression of Neurog2 or Mash1+Dlx2) into neural fate, producing both glutamatergic and GABA-ergic neurons that integrate in the network once implanted (Heinrich et al., 2012). Some authors also suggest that adult neurogenesis might rely upon similar mechanism that could also be employed for therapeutic purposes (Chouchan and Costa, 2012). During development, radial glia provides molecular cues for both axonal guidance and neuronal migration, while astrocytes modulates synaptogenesis through secretion of adhesive ECM molecules like Trombospondin (Christopherson et al., 2005; Ullian et al., 2001) or promoting pruning inducing C1q complement factor expression to be recognized by microglia (Stevens, 2003). Astrocitic processes are enriched with surface glycoproteins, most commonly, polysialated Ig motifs. PSA-NCAM is a neural cell adhesion molecule, due to its hydratation and negative charge, restrain cell-to-ECM adhesion. PSA also promote differential expression of receptors and transporters regulating glia and neuronal function (Muller et al., 1996; 2002; Vutskits et al., 2001; Bonfanti, 2006). In addition astrocytes release most of the ECM proteins, like Tenascine and CSPGs in the ECS, this also seems to be a highly regulated process, probably susceptible to activity dependent control (Berardi et al., 2004; de Vivo et al., 2013). ECM glycoproteins properly shape extracellular space and allow for cell-to-cell recognition through integrin and RAS-family GTPases (Dityatev and Schachner, 2003; Kleene and Schachner, 2004) (Image 14). As often seen in biology, the same morphogenetic mechanisms are well recapitulated in case of repair or in dynamic remodeling like in structural plasticity where both astrocyte physiology and ECM architecture are critical (Deller et al., 1997; Joester and Faissner, 2003; Theodosis et al., 2004). An early divergence in the differentiation of glial cell line appears between central glia, interfacing with neural somata and dendrites (early example is the giant glia in Hyrudo) and peripheral glial, devoted to the homeostasis of neural fibers (later in phylogenies). Glial cell count in CNS increases from 2-10% in invertebrates to 50% in mice reaching the highest value in humans: 90%. Astrocytes alone counts 0.3:1 with respect to neurons in rodents and 1.65:1 in Homo (Oberheim et al., 2006). Complexity of glial shape also scales up with increasing brain dimension: human astrocytes are 2.7 times larger than those in mice, also having less processes and much lower ramification. Every human protoplasmatic astrocyte contact on average 1 million synapses from different neurons while in mice the number is around 100000 (Oberheim et al., 2006; Giaume et al., 2006; Houades et al., 2006). Human astrocytes display a characteristic complexity and are the largest observed in nature. Humans also have peculiar specialization in astrocitic shape that is not observed elsewhere: human SON, contains at least two classes of human-specific astrocytes namely the radial and the polarized ones beside the “classical” protoplasmatic astroglia (Oberheim et al., 2006). In mammals astrocytes have been classically divided in two major sub-groups: protoplasmatic and fibrous (Figure 1.8), the former residing in gray matter displaying a bushy-globular appearance, the latter present in white matter and equipped with long processes. Protoplasmic astrocyte fine processes

(30-40 μm in length) enwrap synapses (like thin veils of submicrometer thickness) while fibrous projections contact Ranvier nodes. In both groups gap junctions exist between adjacent cells. Protoplasmic astrocyte projections extend toward vessel, pial surface, synapses and neuronal somata. The whole vascular bed in the CNS is continuously ensheathed with endfeet while virtually every synapse is surrounded by astrocitic membrane. It is estimated that almost 80% of total membrane surface in CNS is provided by astrocytes and perisynaptic ones is devoided of any organelle. Certain variability is observed in the degree of synaptic coverage: in cortex glutamatergic terminals boutons and spines are not uniformly "shielded" by astrocitic processes as instead is the case for cerebellar synapses (Ventura and Harris, 1999; Grosche et al., 2013). Even within cortex there is variability, V1 for instance present the brain's least extensive coverage per synapse in L I and the highest in L II/III (Jones and Greenough, 1996). 4 days of enriched environment is enough to detect in parallel with increased dendritic arborizations, a similar increase in GFAP positive processes. 30 days of visual enriched environment exposure, increases astrocyte spine coverage in L IV and, although to a lesser extent, in L II/III of V1 (Jones et al., 1996). On the other hand dark rearing in the cat inhibits astrocytes maturation and drastically reduces the count of astrocitic processes in V1 neuropile (Mueller, 1990). AntiGFAP-invisible fine processes are actually even more motile. Hyppocampal LTP induce tighter coupling between astrocytes lamellae and synaptic counterparts within 8h from potentiation, as observed in ultrastructural analysis on Dentate Gyrus (Wenzel et al., 1991). In situ analysis on acute hippocampal slices, revealed that a "basal" motility activity exist in fine processes and emergence of filopodia-like protrusion is frequent (Benediktsson et al., 2005; Haber et al., 2006; Nestor et al., 2007). Neighboring spines undergo more striking "maturation" when in close contact with motile astrocitic process (Nishida and Okabe, 2007; Murai et al., 2011). 24h whisker stimulation produces an increase in synaptic ensheathment of spines in contralateral barrel cortex with conserved topia while the entire estimated membrane area remains unchanged (Genoud et al., 2006). BDNF, which is released in activity dependent fashion, have a great effect on astrocytes remodeling: in neocortex this neurotrophine induce elongation of thin processes up to 15 μm (Hirrlinger et al., 2004). Another paradigmatic example concerns lactating rodent's SON. Using real time TMA assay, authors were able to test changes in tortuosity, volume fraction and other diffusion-related parameters in ECS. In virgin animals tortuosity present strong anisotropy in dorsoventral axis and diffuse across is strongly hindered, in lactating animal such obstacle to diffusion is completely removed and diffusion result isotropic (Theodosis and Poulain, 1993). No detectable alteration was found in neural structures but a massive remodeling was evident in astrocyte processes. Astrocitic motility is not to be confused with a byproduct of spine head motility at least for three simple reasons: processes transformation precedes spine remodeling, astrocytes filopodia are directed toward dendrites and oscillation frequency is much higher than that of postsynaptic terminals. In order to operate properly, neural aggregates must be submerged in a peculiar extracellular environment, substantially different from the fluid penetrating the rest of the body's parenchyma. Of great importance is the neurotransmitters (Glutamate, GABA and Glycine mainly) scavenging function of astrocytes that avoid excitotoxicity

and increase synaptic efficiency (Figure 1.9). Excitatory presynaptic vesicles are filled with Glutamate which is only partly of neural synthesis in fact glutamate spilled from synaptic release, is transported in astrocytes, converted in Glutamine and shuttled back to neurons. Astrocitic Glutamine synthetase is located predominantly around glutamatergic synapses, while neuronal Glutaminase is concentrated in synaptosomal mitochondria and convert back Glutamine into Glutamate. Yet not all Glutamate released is recycled: some diffuse away and some other enters TCA cycle in astrocytes to be converted in α-KG. In some although dated papers, authors envisage the possibility for a dynamic regulation of the availability of Glutamate with respect to some hypothesized homeostatic regulation of excitatory tone. In this perspective, astrocytes would be capable to shift between Glutamate-Glutamine shuttling and TCA cycle in response to "measured" excitatory input (Stobart and Anderson, 2013). Glutamate uptaken by astrocytes is also involved in the Pyruvate-Lactate-Glycogen cycle regulation. Neurons do not accumulate Glycogen which seems to be a peculiar ability of astrocytes inside CNS, thus they depend strictly upon a steady Glucose supply. Moreover neurons do not extract Glucose directly from blood stream but delegate completely their energy fueling to astrocytes which endfeet are enriched with GLUT-1. Glutamate in astrocytes is a potent activator of Glycolysis: Glucose uptake and Lactate production. The more Glutamate is released from presynaptic terminal the more Glycolysis is triggered, presumably under regulation of GLAST itself (Pellerin and Magistretti, 1994). LDH5, an enzyme associated with lactate production, is expressed in astrocytes, while LDH1, the lactate utilization counterpart, in neurons. MCT mediate the shuttling of Lactate into neurons with two isoforms distinctively expressed in anstrocytes (MTC1-export) and neurons (MCT2-import) (Broer et al., 1997; Pellerin et al., 1998). Glutamate and Lactate shuttling are thus coupled to neural activity in a supportive loop. Metabolic coupling would then be responsible for an "average", "long timescale" regulation of neuronal firing and excitatory tone: no evidences support independent activity of individual processes and the overall process might result time expensive. But rapidly increasing number of evidences support for a more complex and far better resolute astrocitic regulation of neuronal activity. Glutamate clearance of synaptic cleft has also a couple of extremely important consequences: reduction of excitotoxicity and reduction of spillover. Glutamate reverberating onto presynaptic terminal will cause a decrease in vesicular release which could impair the capability for high firing rates, on the other hand, spillover might "intermix" synaptic inputs compromising propagation and information analysis (Oliet et al., 2004). Astrocyte processes are rich in AQP4 and Potassium transporters as well as a large artillery of Proton exchanger (Na^+/H^+, $HCO3^-$ transporter, monocarboxylic acid transporter, vacuolar type proton ATPase). Extracellular osmotic pressure, ion content and pH are under control of astrocytes both on a local scale, around synapses, and on a global scale, resulting from interaction with ependima and blood vessels (Seifert et al., 2006; Zador et al., 2009). Resting membrane potential in astrocytes is largely affected by huge Potassium conductance, keeping them hyperpolarized around -85 mV. Kir4.1 is the major Potassium channel expressed in astrocyes that also exhibits marked inward rectifying properties. These channels are actually voltage sensitive and open below -80 mV, thus operating at resting membrane potential (Ransom and Sontheimer, 1992). Other "more neural" voltage gated ion channels are also expressed in astrocytes yet to a far lesser extent forbidding regenerative action potential generation (Bordey and Sontheimer, 2000). The large allowance for inward K^+ current, predispose

astrocytes to be particularly sensitive to $[K^+]_e$ oscillations. Extracellular $[K^+]$ is homeostatically regulated (Figure 1.9) but AP firing pushes toward an increase of concentration which is the stimulus for astrocyte K^+ channel gating. Astrocytes then depolarize and accumulate Potassium restoring the $[K^+]_e$ set-point. For example, when $[K^+]_e$ is increased from 4 mM (the typical resting value measured in extracellular medium) to 20 mM, astrocytes depolarize by 25 mV (by contrast, neurons will only depolarize by 5 mV). At the same time astrocytes forbid $[K^+]_e$ accumulation otherwise easily pushed above neuronal tolerance. The more intense the neural firing the more $[K^+]_e$ accumulates and the more astrocytes are activated. Visual stimulation for instance (gratings presentation) is observed to be sufficient to depolarize local V1 astrocytes by 10 mV. One of the observed responses to increased $[K^+]_i$ is Glycogen breakdown which produce Glucose with which neuron are fed. Teleologically, an increase in neural firing will require more Glucose to be sustained and $[K^+]_e$ increase will serve as the signal for astrocyte to release more fuel. Each action potential is enough to increase local instantaneous $[K^+]_e$ by 0.75 mM, while a linear relation exist between AP frequency and $[K^+]_e$ accumulation only until a "ceiling" level of about 20 mM beyond which pathological conditions may ensues (Adelman and Fitzhugh, 1975; Kofuji and Connors et al., 2003). If $[K^+]_e$ would be left to re-normalize by only passive diffusion, the ceiling level would be trespassed easily even in low neural activity whereas, although in intense AP firing rate, $[K^+]_e$ increases only below 3mM due to highly efficient astrocytes Potassium homeostasis. Impairing control over $[K^+]_e$ leads to positive feedback on neural excitability, increases in neurotransmitter release, alteration in CNS blood flow, disregulation of ECS volume and Glucose metabolism. Potassium loaded into the syncitium is then passively diffused in the network until diluted and secreted back in low $[K^+]_e$ regions (spatial buffering) or inside vessels (siphoning). These mechanisms allow for the proper modulation of neural excitability and are among the most sensible functions easily compromised in a wide variety of neural conditions. Due to an uneven distribution of Potassium channel favoring endfeet, siphoning process may prevail until a great $[K^+]_e$ increase require spatial buffering to intervene yet this might prove detrimental since Potassium spread in other region could in principle drive neuron toward hyperexcitability (Image 16). Sodium ECS homeostasis is also balanced by astrocytes. This function is of particular importance in brain region dedicated to water-salt intake control, like the subfornical organ and the organum vasculosum of the lamina terminalis (Watanabe et al., 2005; Liu et al., 2009). Confinement of neural extracellular landscape is provided by glial cells: blood brain barrier is organized by glia in all invertebrates and in lower vertebrates (up to Ichtis and Amfibia, Bundgaard and Abbott, 2008), while, more recently in evolution, endothelial cells replaced glial (Figure 1.8, 1.9) although under the control of the latter. Astrocytes endfeet were shown to be capable of inducing BBB-like feature in endothelial layers and are involved in the maintenance and induction of BBB in vivo through BMP-GSNO reciprocal signaling (Savidge et al., 2007; Araya et al., 2008). In neurohemal structures like neurohypophysis and the external layer of medial eminence, specialized glial cells (pituicytes and tanycytes respectively) hinder neurosecretion to gain free access to blood flow: specialized astrocytes modulates the rate of hormonal release in the stream (Tweedle and Hatton, 1980; Hatton et al.,

1984; Theodosis and Mac Vicar, 1996). Individual neuro-vascular units in the cortex are composed by a single astrocyte, a section of a capillary and pre and post synaptic processes from several different neurons. Neurovascular coupling allow astrocytes to modulate blood supply in order to meet neural requirements, sensing local neural activity and releasing vasoactive substances (Zonta et al., 2003; Mulligan and Mac Vicar, 2004). Astrocytes release PGE, NO and AA all released in coordinate fashion with neural activity (Gordon et al., 2007; Iadecola and Nedergaard, 2007). BOLD fMRI signal in response to visual stimuli in V1 was demonstrated to depend upon astrocyte function (Wolf and Kirchhhoff, 2008). Both vasoconstriction and vasodilatation was observed following Calcium elevation in astrocytes triggered by neural activity (Zonta et al., 2003; Mulligan and Mac Vicar, 2004; Filosa et al., 2004; Metea and Newman, 2006; Takano et al., 2006). Calcium activates PLA2, increasing the production of AA which is then converted to PGE, a class of potent vasodilatant, by COX-1, highly expressed in endfeet (Takano et al., 2006). When AA is released instead of or in excess with respect to PGE, smooth muscles cells in the vessel tonaca, are induced in the production of vasoconstrictor 20-HETE (Mulligan and Mac Vicar, 2004). NO is another astrocyte-derived modulator of blood flow: NOS inhibitors completely abolishes vasoconstriction (Metea and Newman, 2006) (Image 17). Very early in phylogenesis, astrocyte function started to be based on receptor mediated signal transduction: Cephalopoda for instance, developed a feedback mechanism in which axonal AP activates glial mGLUR (Figure 1.10) triggering Ach release that increases Schwann cAMP gated K^+ influx (Coles and Abbott, 1996). Natural selection favored long ago the development of a “reverberating” circuit between neurons and astrocytes operating through neuro and glio transmitters. In 1970s astrocytes were first observed to express a wide number of receptor for most neuro-active molecules (reviewed in Porter and McCarthy, 1997). Soon it was demonstrated that local application of Glutamate to cultured cells increased intracellular Calcium concentration propagating as a wave throughout the syncytium with a speed of 19μm/s (Cornell-Bell et al., 1990). Soon after was demonstrated that standard Schaffer collaterals stimulation caused Calcium elevation in Stratum Radiatum astrocytes in acute mouse slice preparations (Porter and McCarthy 1996). Schaffer mediated Calcium rise was blocked by metabotropic Glutamate receptor inhibitor or by SER Calcium release inhibitor. Elevation in astrocyte Calcium often triggers the release of neuroactive molecule: Bradykinin was first observed to induce both Calcium increment in cultured astrocytes and release of glutamate in the medium which in turn started Calcium elevation in co-cultured neurons (Parpura et al., 1994). Most interestingly this first evidence was supported by the fact that co cultured neurons did not display any Calcium responses to Bradykinin and neuronal Calcium elevation was demonstrated to be of NMDA origin. The first evidence of an astrocitic activity on electrical physiology of neurons came recording patched neuron co-cultured with mechanically stimulated astrocytes: SICs and increased synaptic activity were observed (Araque et al., 1998). Muller glia was observed to increase Calcium in response to physiological stimulation (flashes of light in the retina) via an ATP dependent mechanism started by increased neural activity (Newman and Reichenbach, 1996; Newman, 2001). Not only astrocytes signal back to neuron when triggered by neurotransmitters: astroglia also display intrinsic, spontaneous Calcium oscillation in the absence of neurotransmitter release or electrical activity (Parri and Crunelli, 2003; Nett et al., 2002). These intrinsic oscillations are only restricted to microdomains within thin processes, while neuronal-triggered ones might well

propagate to the soma and eventually spread through connected cells. Astrocytes “measure” neural activity by means of receptors for most of known neurotransmitters: different cells from different brain areas are observed to express different receptors (Verkhrastky and Kettenmann, 1996; Porter and McCarthy, 1997; Verkhartsky et al., 1998). NMDA receptors are expressed by cortical and spinal cord astrocytes, P2X receptor in cortex alone, while dopamine receptors only in basal ganglia and glycine receptor only in spinal cord (Kirchhoff et al., 1996; Seifert and Steinhauser, 2001; Jabs et al., 2007; Verkhratsky and Kirchhoff, 2007). Hyppocampal astrocytes are subdivided in GluR cells expressing AMPA receptor but lack any Glutamate transporter and GluT, expressing Glutamate transporter but no Glutamate receptor. Interestingly, gap junctions are formed exclusively between GluT cells (Matthias et al., 2003; Wallraff et al., 2004). In Cerebellum, Bergmann’s glia co-express α_1 adrenoreceptor, H1 histaminereceptor, AMPA, mGluR5, P2Y and $GABA_a$: most peculiarly, each process expresses the same receptor as the nearest Purkinje cell, which is also congruent to the neurosecretion in the immediate surroundings. The local neurotransmitter repertoire seems to match astrocyte receptor expression. Notably, although, most astrocytes express mGluR1/5 and P2Y regardless their proximal neural counterpart (Pocock and Kettenmann, 2007). Fine astrocytic processes, are mostly dedicated to the constitution of the tripartite synapse (Araque et al., 1999), providing fundamental “services” to the neural structure: isolation and specificity, neurovascular coupling, astroglia-neuron lactate shuttle, regulation of synaptic plasticity (Parpura et al., 2004; Newman, 2003; Haydon and Carmignoto, 2006; Magistretti, 2006; Verkhratsky and Toescu, 2006; Iadecola and Nedergaard, 2007) (Image 17). It is well established now that both neural evoked (Porter and McCarthy, 1996; Araque et al., 1998; Newmann and Zahs, 1998; Kirischuk et al., 1999; Jeremic et al., 2001; Newmann, 2005) as well as spontaneous Calcium transients in astrocytes (Parri et al., 2001; Aguado et al., 2002; Nett et al., 2002; Parri and Crunelli, 2003) originates from intracellular stores. Signal propagation within individual cells and across the syncytium is delegated to endomembranes and volume transmission respectively, less clear is the autocrine and paracrine route. Endomembranes assembled in the SER, are equipped with a variety of Calcium channels (InsP3R, Ryanodine, ligand gated channels like the NAADH) and Calcium pumps, sensitive to and regulated by Calcium gradient across ER itself (Wuytack et al., 2002; Bezprozvanny, 2005; Galione and Ruas, 2005). Whatever the induction signal shall be there seems to be agreement on the transduction cascade that follows: Gq proteins are recruited, PLC is activated and IP2 is phosphorilated into IP3 which in turn binds to InsP3R2 on SER, triggering Calcium efflux. Neural evoked Calcium transients always goes through a metabotropic receptor on astrocyte and are independent from either ionotropic or VGCCs (Carmignoto et al., 1998). Also intrinsic spontaneous Calcium oscillation are blocked by CPA, Thapsigargin or InsP3R2 antagonists, yet the starting stimulus is yet to be elucidated: some authors suggest an active role of VGCCs or the so called “Calcium induced Calcium release” mechanisms since frequency of spontaneous events is attenuated by Nifedipine or Cobalt (Parri and Crunelli, 2003). SER Calcium channels display indeed a great rise in open probability when exposed to cytoplasmatic $[Ca^{++}]_i$ increase. The sensitivity to CICR occurrence expose astrocytes to “natural”

oscillation provided a “tonic” activation of both metabotropic and VGCCs (Parri and Crunelli, 2003). This suggestive hypothesis opens yet unexplored landscapes over the possibility of two coupled oscillators in the brain, operating on very dissimilar timescales. Alternative hypothesis is that astrocytes release some quantal glutamate which might starts spontaneous oscillations. Another interesting observation is that spontaneous Calcium activity increases in frequency after either exogenous or neural stimulation: when IP3 photouncaging or Schaffer collateral stimulation is suppressed, targeted astrocytes continue spontaneous Calcium transients. Suprathresholod focal stimulation of a Calcium channel (i.e. long enough and with the appropriate conductance) might be responsible for a local increase in $[Ca^{++}]_i$ propagating along SER. Calcium channel density is actually much higher than the least expected to be supportive for regenerative Calcium events. Moreover Calcium efflux has been shown to easily propagate across connexons and start a regenerative Calcium event in a connected resting cell (Berridge and Irvine, 1989; Matyash et al., 2002; Solovyova et al., 2002; Berridge et al., 2003). SER Calcium efflux result from a variety of upstream signaling cascade pivoting around InsP3R2, the astrocyte specific isoform. Calcium events come in several forms either from the temporal and the spatial perspective. Most commonly, neural secretion starts $[Ca^{++}]_i$ increase in perisynaptic processes that might evolve in different ways. Some transients remain local, confined in short lived microdomains, others from local, propagate in a wider domain or seems to start abruptly in the whole branch, Calcium transients extended to the soma are less frequent and are believed to follow incoming processes propagation while syncytium Calcium travelling wave is seldom observed in vivo (sometimes associated with non physiological conditions) (Bezzi et al., 2001). Distance at which Calcium transients are observed to propagate might depend upon the initiation events, being it neural evoked or spontaneous: exogenous stimulation (photouncaging of glioactive compounds, mechanical stimulation, extracellular administration of agonists or afferent stimulation) is often associated with long range propagation of Calcium transients which are rarely observed in neural evoked paradigms or never at all in spontaneous transients. Massive travelling waves seem to require concomitant individual increase in $[Ca^{++}]_i$ and a focal stimulation of IP3 production. Large activation of InsP3R2 will ensues and both Calcium and IP3 levels could allow for transcellular diffusion. Calcium diffusion in nearby “subthreshold” astrocytes will increase both PLC activity and InsP3R2 activation and so on and so forth in the next coupled astrocyte (Davis and Bezprozvanny et al., 2001; Miyakawa et al., 2001; Tu et al., 2005) (Image 18). Of great interest is the observation that while spontaneous transients remain confined and are rarely coordinated among >2 astrocyes, in presence of normal neural activity the degree of coherence in Calcium events is significantly higher (Aguado et al., 2002). Some authors only observed significative increase in astrocytes coordination only in abnormally elevated excitatory regimen (GABAa blockade) while in control condition only a weak bias toward synchronization is observed (Hirase et al., 2004). When IP3 photouncaging release is performed in acute slices (neural activity in control regimen), only propagation throughout all processes are observed with no involvement of transcellular communication (Fiacco and McCarthy, 2004). Furthermore, Calcium wave propagation seems to require an ATP-dependent paracrine mechanism beside that of Cx-mediate transcellular communication. The former is Calcium dependent and the second needs Calcium to regenerate or propagate (Nedergaard et al., 2003; Haydon and Carmignoto, 2006). Whatever the route of

Calcium oscillations is explored, one end seems the most likely: induction of gliotransmitter release by Calcium dependent vesicle exocytosis. Vesicular machinery homologous to those observed in neurons (Figure 1.10), have been discovered in astrocytes (Bezzi et al., 2004; Barclay et al., 2005; Volterra and Meldolesy, 2005) among other yet poorly characterized non canonical excretion mechanism (reversed pumps, connexin hemychannels, lysosomes fusion). Calcium dependent vesicular release of neuroactive gliotransmitters, close the loop of information flow inside this complex neuro-astro network. Astrocytic vesicles are equipped with transporters and Calcium sensitive release complex homologous to those characterized in neurons. Calcium increase in astrocytes have been associated with vesicular release of Glutamate, ATP, D-Serine, Cytokines, vasoactive compounds and GABA (Parpura et al., 2004; Bezzi et al., 2001; Coco et al., 2002; Zonta et al., 2002; Mothet et al., 2005; Wang and Bordey, 2008). Glutamate release is blocked by BAPTA and forbidden by previous incubation with CPA (Araque et al., 1998). Glutamate release independent of Calcium elevation was also observed but only in culture or in pathological conditions, possibly depending upon reversal of Glutamate transporter, Cx-hemichannels, P2X7 receptors, VRACs (Aanderson and Swanson, 2003; Duan et al., 2003; Yu et al., 2003; Takano et al., 2005; Fellin et al., 2006; Suadicani et al., 2006). Vesicular machinery in astrocytes comprises: Syb2-3, Syntaxin, VGLUT-I/II, Syt2-4, but the arsenal is under continuous update (Parpura et al., 1995; Araque et al., 2000; Montana et al., 2004; Crippa et al., 2006). Strong evidences support the Calcium regulate secretion at least for Glutamate, D-Serine and presumably GABA (Araque et al. 2000; Jourdain et al., 2007; Pascual et al., 2005). Ultrastructural analysis, TIRF imaging and impedenzometric measure all converge to the fact that glutamate release is of vesicular origin (different pools of vesicle were also observed possibly containing different glutamate “companions”) although several other possible ways could operate in a minority of cases (Nedergaard et al., 2003; Mothet et al., 2005; Montana et al., 2006). Calcium dependent astrocyte control of neural activity was observed in several models, both in slices and in vivo (Araque et al.; 2002). Dominant negative for Syt2 (observed in acute hippocampal slices) have altered phenotype: reduction in both synaptic transmission and LTP (Pascual et al., 2005). Mice with dnSNARE complex have gross alteration of behavior: they sleep less and are more prone active exploration while awake (Halassa et al., 2010) Few observations also advocate for a “less critical” role of astrocytes in “neural affairs”. InsP3R2 KO mice (Petravicz et al.; 2008) appear normal albeit Calcium activity in astrocyte strongly reduced. Heterotopic MrgA1 expression in hippocampal astrocytes was employed to circumvent co-activation of neurons when gliotransmitters were administered with little effect on LTP when Calcium was raised through proper agonist (Fiacco et al., 2007). These controversial results could be the product of undesired transgene expression/silencing patterns or compensation by redundant vicarious pathways (Halassa et al., 2010). In order to investigate on the impact of astrocyte signaling back to neurons, selective stimulation of glial cells should be attained which is seldom the case when pharmacological agonists/antagonists are used. Most of neural and astrocitic receptor are actually common to both lines. When ACPD is administered to astrocytes, a rise in Calcium is observed that precedes depolarizing currents in neurons, mediated

by iGLURs and mirrored by Calcium elevation (Pasti et al., 1997). Selectively increased Calcium in a single astrocyte in culture induces large SICs in nearby pyramidal neurons abolished by iGLURs blockers and prevented by Calcium chelators in astrocytes. Increase in neuronal frequency of miniature EPSPs and IPSPs was also observed to follow Calcium increase in astrocytes: again only those neurons adjacent to the stimulated astrocyte were “activated” (Araque et al., 1998). It was then postulated that Glutamate from astrocytes might target synaptic loci both on pre and post synaptic terminals, as well as extrasynaptic ones. In immature thalamic slices, large Calcium events are spontaneously observed propagating through the syncytium. Although interpreted as developmental “oddity”, these intense oscillations produces SICs of great amplitude (200-300 pA) which results to be activated with a time constant of 145 ms and decayed with a time constant of 158 ms (Parri et al., 2002). These results were confirmed in mature hippocampal slices were spontaneous large Calcium waves are never to be observed. Here selective stimulation of single or few astrocytes, triggers SICs in nearby neurons (within hundred microns) mirrored by Calcium increase (Agulon et al., 2004; Fellin et al., 2004; Kang et al., 2005; Perea and Araque, 2005). Notably, astrocitic activation is associated with both coherent neural Calcium oscillation and synchronous SICs. Also a period of entrainment of subthreshold Vm oscillations or overt firing is observed following astrocyte challenge (Agulon et al., 2004; Fellin et al., 2004, Shigetomi et al., 2004). Slow kinetics of SICs and TBOA sensitivity strongly indicate their extrasynaptic origin depending upon NR2B containing NMDA receptor, in contrast to NR1/NR2A. Evidences for a synaptic effect of astrocyte Glutamate release, comes from IP3 photouncaging of pipette loaded IP3-caged astrocytes in hippocampal slices (Fiacco and McCarthy, 2004). AMPA EPSPs were recorded in neighboring neurons when Calcium was activated in single astrocytes which were blocked by bath application of mGLUR1. These observations were interpreted as the effect of astrocitic Glutamate on presynaptic metabotropic glutamate receptors that mediate bouton Calcium increase and vesicular release probability increase (Emptage et al., 2001) which, in turn, will exert activation of AMPA postsynaptically. SICs were more frequently observed when many astrocytes were triggered. Glutamate released from several synchronous astrocytes might survive dilution effects and activate extrasynaptic NMDAs. The amount of glutamate secreted by a single cell could also be proportional to intensity and/or duration of Calcium increase: the stimulus delivered to astrocytes might have different neural outcome. Astrocitic glutamate containing vesicles, are pushed to a kiss-and-run release modality when the cell is activated by 0.5 mM glutamate while the whole vesicle fusion and massive Glutamate release is observed under mechanical stimulation (Chen et al., 2005). SICs induction might well be operating in physiological condition although developmental effect and NR2B/NR2A ratio shall be taken into account. The overall effect of astrocyte glutamate release on neural activity seems to impinge on NMDA receptors, probably because of co-release of D-Serine (Halassa et al., 2007) on a network of active neurons. Presynaptic NMDA activation will promote vesicular release, postsynaptic ones will contribute to depolarization while NR2B would promote synchronization (Oliet et al., 2001; Fellin et al., 2004; Jaurdain et al., 2007). Together with Glutamate, per-se, vesicular release of D-Serine was often reported. Hypothalamus, hippocampus and retina only employ D-Serine instead of Glycine as glutamate co-agonist on NMDA, in other brain region both molecule might coexist and while Glycine is of neural competence, D-Serine is only astrocitarian (only astrocytes seem to

express Racemase) (Stevens et al., 2003; Yang et al. 2003; Mothet et al., 2005; Panatier et al., 2011). Calcium dependent release of glutamate also was observed to trigger LTP via presynaptic AMPA activation or LTD through mGLUR II/III postsynaptic binding on inhibitory synapses (Pasti, 1997; Liu et al., 2004). Same gliotransmitter, glutamate, may thus have different effects possibly because of co-release of other gliotransmitters or because different cells are targeted with different molecules (Zhang et al., 2003; Pascual et al., 2005; Kozlov et al., 2006; Panatier et al., 2006; Serrano et al., 2006; Martin et al., 2007). ATP is another potent neuroactive substance secreted via Calcium dependent vesicular release (Coco et al., 2003; Zhang et al., 2007; Pryazhnikov et al., 2008). P2Y on astrocyte might serve as paracrine/autocrine feedback loop which increases intracellular Calcium leading both to Glutamate release and to CICR-wave propagation (Guthrie et al., 1999; Fields and Burnstock, 1997). Neuronal presynaptic P2Y leads to tonic reduction of glutamate release in hippocampal pyramids, P2X on the contrary, exert a tonic yet moderate excitatory effect on postsynaptic terminals (Alvarez and Sabatini, 2007). P2X in hypothalamus promotes the translocation of AMPA in the membrane of magnocellular neuron leading to the maturation of Vasopressine and Oxytocine releasing path (Syed et al., 2007; Wang and Hamilton, 2009). ATP is also quickly converted in ADP and adenosine in ECS: If a slight 1% of secreted ATP goes to Adenosine, ECS pool is hundredfold increased. Adenosine suppress neural firing binding purinergic A1 receptor which is coupled to hyperpolarizing Potassium channels and/or activating purinergic A2 receptor that is negatively coupled to depolarizing Calcium channels (Dunwiddie and Masino, 2001). GABAb activation through Schaffer collateral stimulation was observed to trigger Calcium dependent release of vesicular ATP from CA1 astrocytes, which determines heterosynaptic LTD (Zhang et al. 2003; Pascual et al., 2005; Serrano et al., 2006). These are compelling evidences of gliotransmission operating at long range, far beyond local synapses and probably further than a single astrocitic domain. Endocannabinoids are another class of compounds released by neurons and astrocytes. 2AA seems to be the most abundant endocannabinoid secreted through Calcium dependent pathway (Min and Nevian, 2012). Endocannabinoids released by astrocytes in response to glutamate, are observed to modulate firing rate of neurons not connected with those responsible for astrocyte activation and seems to be able to start EPSPs in neurons as far as 200 mm from exogenously activated astrocyte (Navarrete and Araque, 2008, Min and Nevian, 2012). Experimental isolation of single tripartite synapse by means of calcium imaging and neural patch clamp techniques, allowed to investigate on the effect of astrocyte activation at the level of single synapse. Inward excitatory currents and increased synaptic transmission was observed following artificial elevation of intracellular Calcium in a single astrocyte: the effect was SNARE dependent and relied on presynaptic mGLUR I (Perea and Araque, 2007). Besides other cytokines (Bonanno et al., 2007; Ida et al. 2008), astrocytes release TNFα which act on neuron promoting postsynaptic insertion of AMPA receptors via TNF-1 and PI-3K (Schroeter and Jander, 2005; Stellwagen and Malenka, 2006). Removal of TNFa from slices reduce synaptic strength (image 19). Most compelling evidences of astrocyte function inside the neural network, come from recent in vivo experiments. Data from culture and from ex vivo

experiments long awaited the required technical developments to test a physiological activity of astrocytes in preserved and alive CNS. Two major breakthroughs enabled in vivo imaging of astrocitic functions: two-photon microscopy and the incidental discovery that SR 101 is an excellent, “ready-to-use”, intravital astrocyte marker (Nimmerjahn et al., 2004). Calcium transients in vivo are both spontaneous (under TTX), concomitant with neural activity or evoked by neurotransmission (Hirase et al., 2004; Wang et al., 2006; Dombeck et al., 2007; Bekar et al., 2008; Schummers et al., 2008). Repetitive whisker stimulation elicit repetitive and pretty well stereotyped Calcium oscillations in astrocyte somata in barrel cortex of both anesthetized and awake animals (Wang et al., 2003) as well as in the somatosensory map of the hind limbs when congruent stimulation was delivered (Chuquet et al., 2010). In each case, no evidences for a bulk Calcium wave was ever reported, a rather dispersed “astrocitic map” tended to emerge instead. In V1 tuned sesponses were observed in astrocites when the animal was presented with drifting gratings of different orientations, a property previously (and yet not replicated) only appointed to a subset of neurons (Schummers et al., 2008). Running behavior was also observed in awake mice, to trigger astrocytes Calcium transients that faithfully mirrors and with some jitter, precedes neural output in L II/III motor cortex (Kampa et al., 2011; Dombeck et al. 2007). Arousal inducing stimulation of locus coeruleus or nuclei basalis also determine a striking increase in cortical astrocytes Calcium that precedes the neural one and could be obtained even in absence of cortical neural activity (Bekar et al., 2008). Astrocytes from different cortical layers seem to deploy different Calcium codes (Takata and Hirase, 2008). and different brain region, associated with different modality or functions, display peculiar astrocitic Calcium dynamics. Strong evidences in this respect comes from the observation that hippocampal astrocytes discriminate between different synapses that release different neutransmitters and, at least in the barrel cortex, between different rutes of glutamatergic inputs selectively discerning among synaptic inputs (Parry et al., 2004; Perea and Araque, 2005; Schipke et al, 2008). Astrocyte Calcium transients are not consequence of generic spillover. Ventrobasal thalamic astrocytes respond either to afferent sensorial or corticothalamic input but few to both. L II/III barrelloid astrocytes distinguish from glutammatergic inputs incoming from same barrel L IV to which they respond (triggered by whisker stimulation) while remaining silent to converging L II/III signals from adjacent barrel. CA1 stratum oriens astrocytes response to alveus stimulation which is both glutamatergic and cholinergic, but Calcium elevations are only blocked by Atropine. On the other hand, Schaffer collateral stimulation, which produces glutammatergic output in stratum oriens, do triggers Calcium elevation in the same astrocytes not responding to glutamate from alveolus. Furthermore, and more strikingly, co-stimulation of Schaffer collateral and alveus, sums up nonlinearly in a context of low (10 Hz) stimulation, to elicit Calcium transients of an amplitude greater than the sum of isolated inputs. Moreover, when Schaffer and alveolus inputs are simultaneously impinging on astrocytes, Calcium responses amplitude is sublinear when a high level (30-50 Hz) of combined synaptic activity is maintained. Nonlinearity is also observed with exogenous co-application of synthetic Calcium oscillation agonists (Morita et al., 2003). When Ach and GABA was administered exogenously in absence of Schaffer or alveus stimulation, only a linear summation is abserved (Perea and Araque, 2005; Le Meur et al., 2012; Yoon et al., 2012). This last evidence support the idea that integration of neural activity might operate at different multiple levels: Glutamate and

Ach inputs seems to be integrated and computed at least one step above GABAergic ones. Molecular cues further strengthen this hypothesis: mGLURs and muscarinic receptors signaling converge on PLC, upstream to Calcium release and both pathways are susceptible to CICR, whereas GABAb require adenylate cyclase activation which is PLC independent and CIbCR insensible (Perea and Araque, 2006). What remains to be clarified, among other things, is whether astrocyte Calcium oscillation resonate best with peculiar patterns of neural activity and if astrocyte output is actually "digitalized" in all-or-none fashion or different gliotransmitters are chosen to be released in response to different inputs and to serve what purpose. A nonlinear input-output curve will emerge for astrocytes Calcium elevation as well as for gliotrasmission if the previous assumption is true. The effect of single astrocyte activation on the neural physiology remains a debated question: many authors support the idea that in vivo, anesthesia or bad choice of stimulation paradigms, may occlude an otherwise overt effect (Volterra and Meldolesi, 2005; Haydon and Carmignoto, 2006), while others advocate either for a less significative role as whole or for the requirement of some sort of supra-threshold stimulation of astrocytes (Fiacco et al., 2007). It is also possible that the majority of Calcium transients triggered by neural activity remains confined in fine processes and is then fed back to individual synapses with no detectable effect at the level of neuronal or astrocitic somata (Halassa et al., 2007).

Figure 1.8 central astrocytes. a) top: early development of neocortical mantle. (A) Neuroepithelial *cell (red) serves as common progenitor of both neurons (blue) and radial glia (gold). (B) A newly differentiated neuron migrates along radial glia cues. Intermediate progenitor cells (yellow) segregate from neuroepithelial progenitors while neurons keep migrating (C). intermediate progenitor cells spawn neurons (D). radial glia differentiates into astrocytes (E). interneurons are generated elsewhere and populate the cortical plate (CP) migrating tangentially (IZ: intermediate*

zone, VZ: ventricular zone) (Poduri et al., 2013). Bottom: protoplasmatic astrocytes and neurons share a common embryologic brancing point. In green and red are indicated respectively, growth factor promoting and inhibiting the differentiation step marked by the black arrow. Factors maintaining proliferation and cell fate are indicated in blue. Early in the commitment process, glia restricted cells diverge from the fatemap of neurons dividing further in astrocytes and oligodendrocytes. A final divergence is described as type 1 and 2 astrocytes segregates according

both to cytoarchitecture and markers expression (Holland, 2001). b,c) Golgi staining performed on Cornu Ammonis Stratum Radiatum preparation showing astrocytes engaging contacts with blood vessels and enwrapping neurons (Legado Cajal - in: GarcÃa-Segura, 2002). d.e) contemporary staining techniques allow for a detailed descrition of fine morphological features of intricate astrocitic processes. Immunohistochemichal white staining (GFAP) highlights endfeet protrusions enwrapping blood vessels (in blue, DAPI staining for nuclear localization) the yellow box is further

magnified below (scale bar 20 μm). Endfeet tessellate the whole surface of capillaries contributing to the formation of blood-brain barrier (Oberheim et al., 2009). f) Gap junctions between adjacent astrocytes allow for transcellular communication. Here the fine ardorization of several astrocytes are rendered from confocal acquisition. Individual astrocytes form independent territories patrolled by non-overlapping processes, here red and green astrocytes never intersects, the yellow border marks the extent of the green astrocyte territory. Loss of this fine architecture is often described in

neurodegenerative disorders (Volterra and Meldolesi, 2005). g) immunihistological staining for cytoskeletal components in astrocytes (Actin: red in the inserts, green in the larger image). Actin meshwork extends beyond the reach of GFAP fibrils (blue). h) staining against Cx43 showing a dense marcature across the whole terminal surface of fine processes (red). A sparse staining is observed also at the level of the soma (blue) and along principal processes (GFAP green) (Haseleu et al., 2013). i) human astrocytes present peculiar cellular features among mammals. Across the

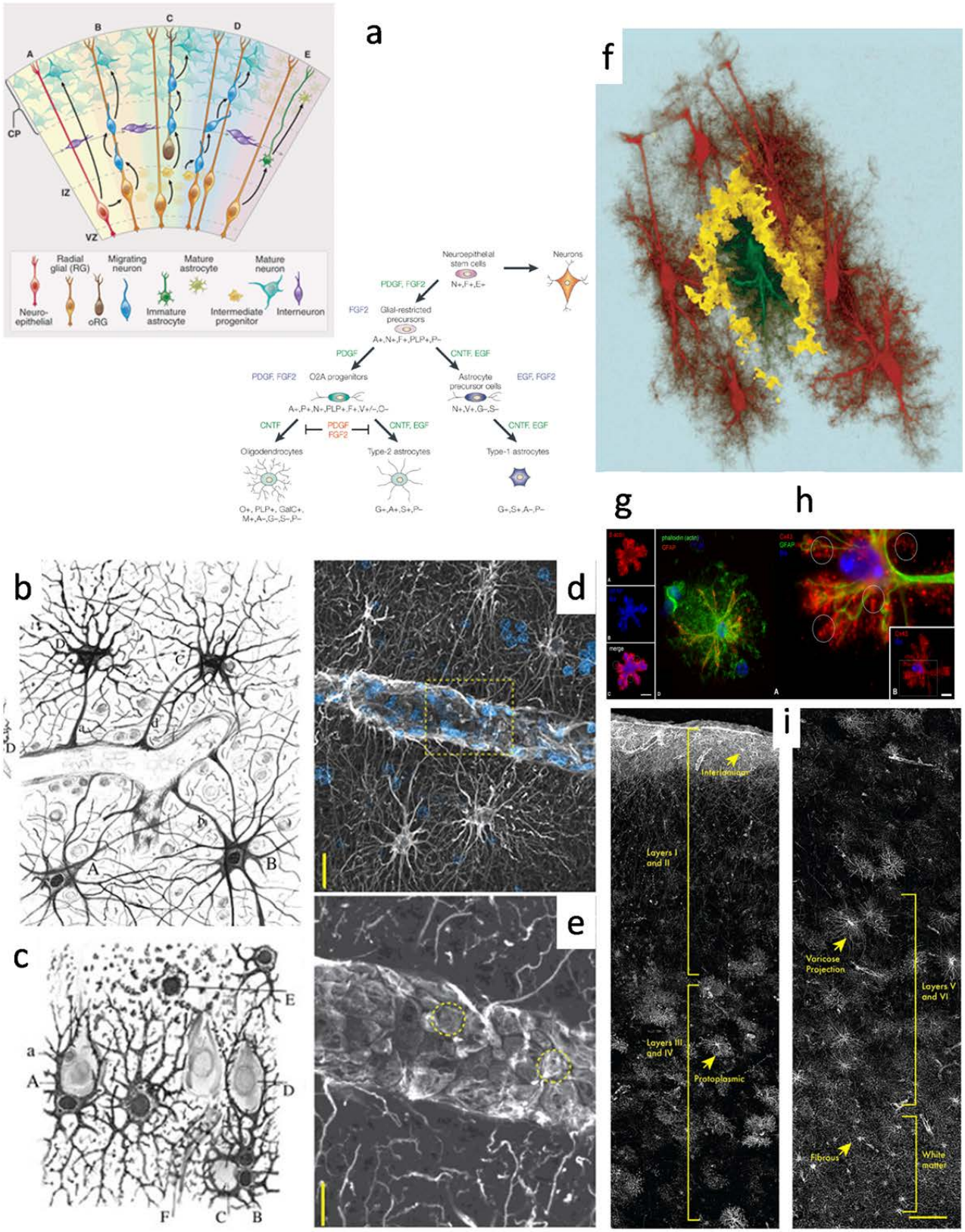

whole extent of neocortical mantle, human astrocytes display laminar specializations such as varicose and fibrous projections. Also the complexity of process arborization result drasticaslly increased in primates compared with other mammals (Oberheim et al., 2009).

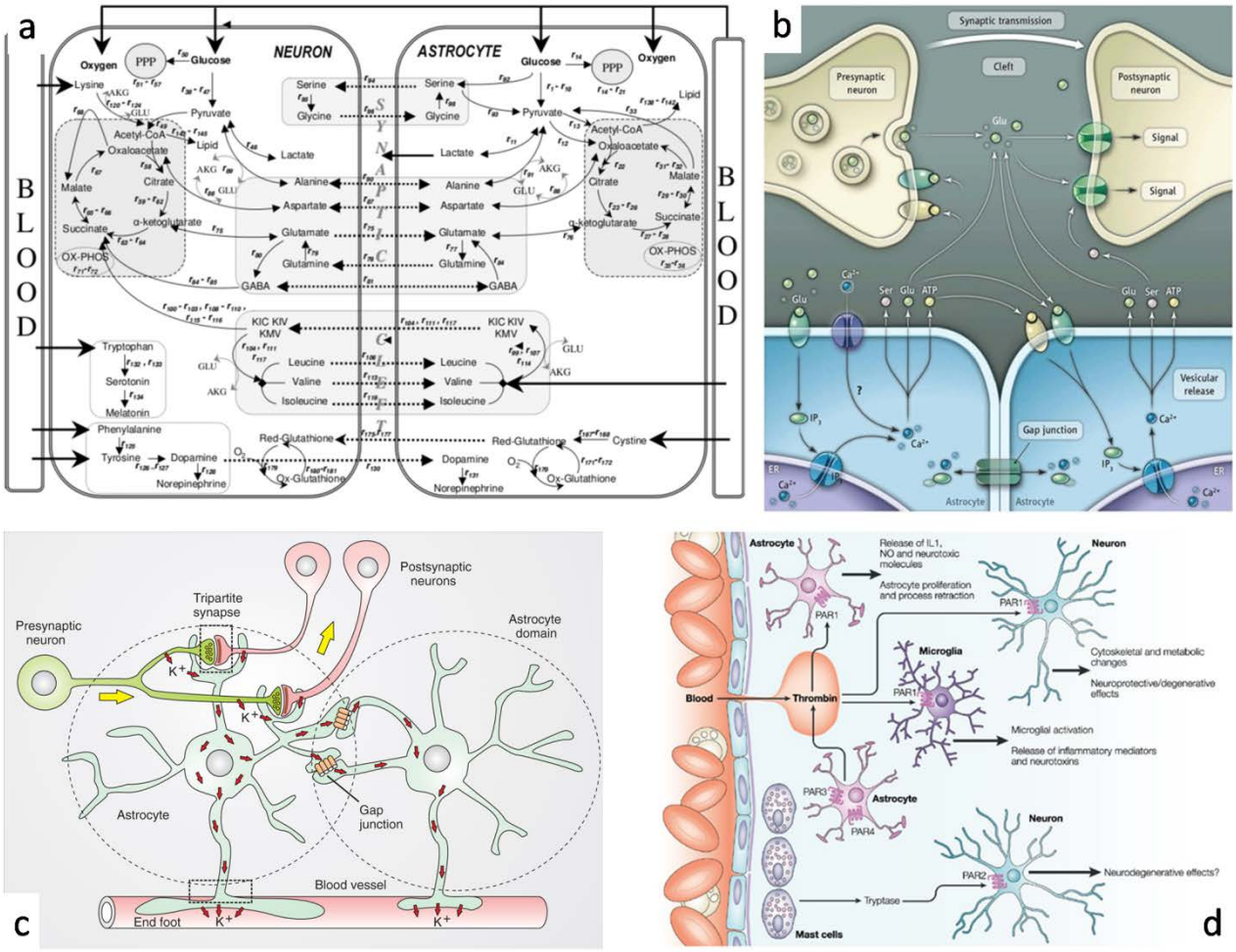

Figure 1.9 *astrocyte control of critical brain functions a) major shuttling mechanism (dashed lines) and uptake processes supported by astrocytes. neurons depend completely from astrocytes both from a metabolical and a functional point of view (Cakir et al., 2007). b) the tripartite synapse. Spillover of neurotransmitters from the synaptic cleft (glutamate here) is sniffed by a large array of receptors and transporters juxtaposed on the surface of termina astrocyte processes. The astrocyte envelope around synapses is both the releasing site of gliotransmitters and the spot of neural activity monitoring. At this location, neural signals are translated in astrocyte intracellular signaling. Morphology, physiology and homeostatic regulation of synapses are finely regulated by astrocytes endfeet (D'Ascenzo et al., 2007). c) Potassium extruded as a consequence of neural AP firing needs to be re-normalized in the extracellular space. Astrocytes perform two major homeostatic control over Potassium concentrations: spatial buffering and siphoning. High Potassium regions are readily clamped by the spatial buffering process: Kir 4.1 (large conductance inward rectifier Potassium channel) mediated uptake ends in the intracellular re-distribution of Potassium through the astrocitic syncitium. Concentration of Potassium is thus buffered and eventually K^+ are extruded far away in regions of lower concentrations. When Potassium keeps increasing in extracellular space, re-normalization through spatial buffering is not enough and re-distribution in plasma sink is required. Siphoning depends upon Calcium signaling and engages endfeet and BBB interactions (Berridge 2012). d) modulation of neuroinflammation depends upon astrocytes. breeching BBB triggers a rapid increase of IL1-β secretion from astrocytes together with*

increased COXa-2 activation and NO production. Interleukin in turn, modulates downhill inflammatory responses in microglia and other astrocytes in a yet poorly characterized way. A direct effect of astrocyte secretions on neurons in response to BBB alteration is also reported. Astrocyte response to BBB disruption is fast relying upon protease activated receptors (PAR-1) expressed mostly on the surface of endfeet (Noorbakhsh et al., 2003).

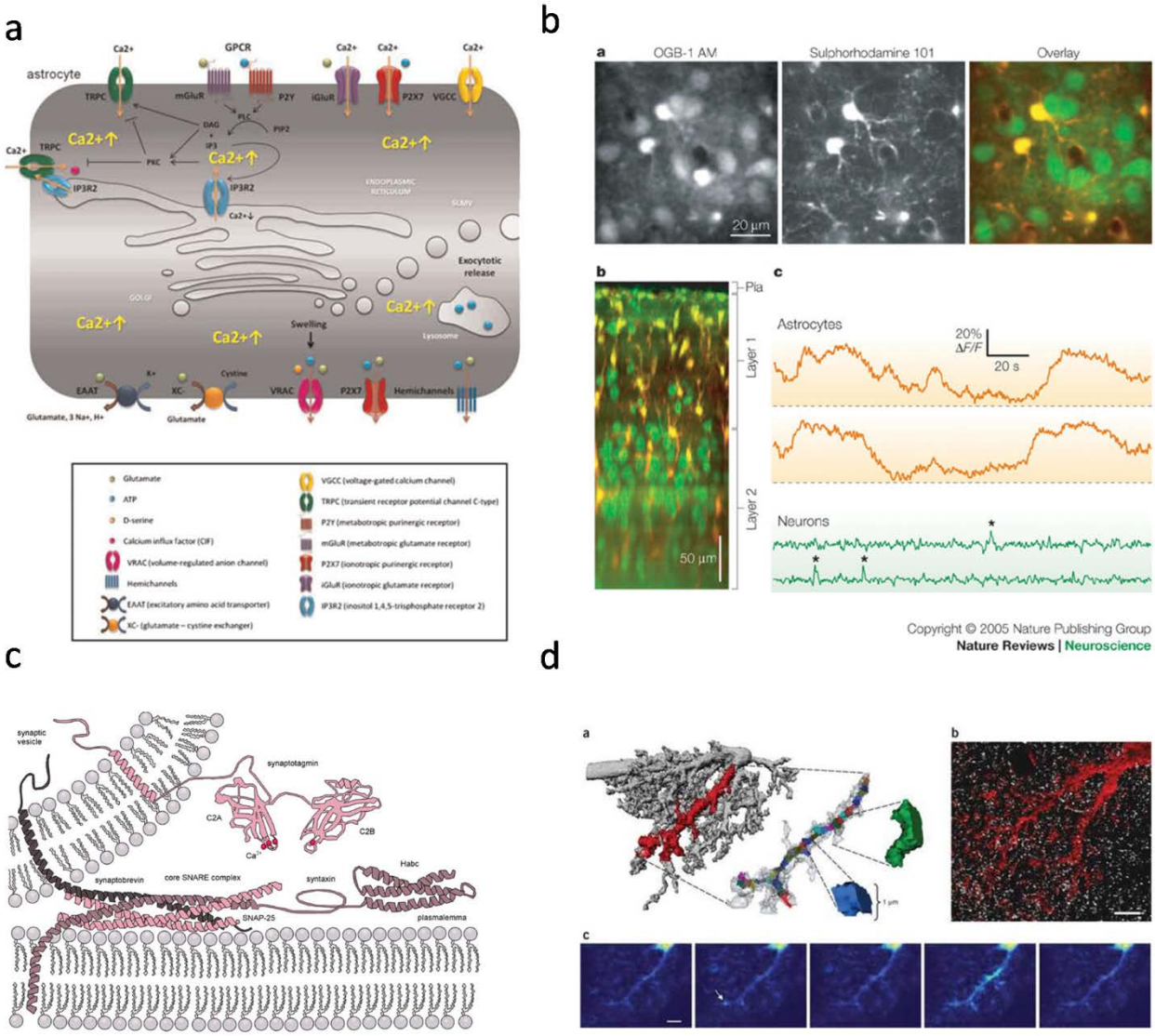

Figure 1.10 *Calcium in astrocytes a) principal intracellular signaling pathways leading to* $[Ca^{2+}]_I$ *increment in astrocytes. According to recent literature, G-coupled metabotropic receptors for glutamate and GABA are the main triggers of Calcium elevation released from SER stores via IP3R2 receptors. Interaction between EAAT, GAT transporters and NCX exchanger is another interesting yet poorly characterized route of Calcium oscillations at least in terminal processes (Haydon, 2001). b) two photon in vivo Calcium imaging of cortical astrocytes reveals intermirttent Calcium oscillations measured at the level of somata during spontaneous cortical activity. Top row reports typical intravital staining of neurons and astrocytes using pressure injected Calcium sensitive dye OGB 1-AM (left) and astrocyte-specific sulforhodamin 101 (center). Discrimination of Calcium signals generated by neurons and astrocite is enabled by spatial segregation of sulforhodamin fluorescence (overlaid with Calcium dependent fluorescence in the right panel). A coronal reconstruction of sequential transverse optical sections is represented in the bottom left panel. Calcium signal can be retrieved with subcellular resolution down to 400 μm in the cortex. Dynamic Calcium-dependent fluorescence acquisitions disclose the typical time course of Calcium transients in astrocyte somata compared with that of neurons. Fast scanning also allow the superposition in time of neural and astrocyte Calcium oscillations for correlative analysis (Volterra and Meldolesi,*

2005). c) Calcium elevation recorded at the level of the soma in astrocytes (as well as in neurons) is believed to lead to vesicular release of gliotransmitters (Synaptotagmin-4, Synaptobrevin-2, Syntaxin-1, SNAP-23). Astrocytes are endowed with molecular machinery homologous to neural one, dedicated to Calcium dependent vesicular fusion and exocytosis although lacking an organized pool of store vesicles. Several mechanisms of gliotransmitter release other than exocytosis are also characterized many of which appear to be Calcium dependent (Haydon, 2001). d) Calcium oscillations are frequent at the level of astrocyte processes during spontaneous activity. Top left panel depicts the rendering of a thin astrocyte process loaded with Calcium sensitive dye acquired with two photon imaging in an ippocampal slice preparation. Main trunk of the process presents sparkling Calcium activity in segregated domains (colored strips indicate uncorrelated Calcium activity). The plot in the middle is relative to each strip and reports Calcium oscillations as variations in fluorescence intensity over time. Note that most of the Calcium transients remain segregated inside a strip while few coalesce along contiguous domains. During spontaneous activity only seldom Calcium transients are observed to flow across the whole extent of an individual process and rarely gain access to the soma. Puncta depicted in top right panel are relative to immunohistochemistry staining against Synaptophysin while red signal is relative to cytosolic EGFP conditionally expressed in adtrocytes (scale bar 5 μm). Territories defined by bushy arborizations of principal processes are entirely disseminatyed with neuronal synapses. Bottom panel depicts isolated frames from a longer time series of two-photon calcium imaging. Isolated, enlarged and widespread calcium events are visible along the same process as increments in fluorescence intensity (Di Castro et al., 2011).

1.6---Unknown pleasures/epilepsy as cortical dysrhytmia.

Epilepsy is a syndromic condition defined by spontaneous occurrence of “seizures” characterized by peculiar alterations in the electroencephalic activity the causes of which are the most heterogeneous and the mechanisms through which epileptic activity is generated still remain utterly elusive after almost 200 years of scientific investigation. According to O.M.S. 2012 estimate, around 43 milion of people worldwide suffer from “epilepsy”. Early works by Bouchet and Cazauvieihl (1825), first demonstrated post mortem gross brain anatomical alteration in people affected. With the development of EEG recording techniques (although first conceived for “mental reading”) by Berger in 1924, an astonishingly complex pattern rapidly emerged linking disparate phenotypical manifestation to a somehow common “electrical brain disorder”. Causative factors soon revealed to be the most disparate: from infection to concussions, from sporadic to inheritable. Nevertheless a wide consensus among scientists was built around the idea that some kind of “equilibrium” between opposing forces in brain activity, i.e. excitation and inhibition, must be out of balance in epileptic manifestations. One common feature in every manifestation: epileptic activity is a pathology of synchrony of cortical circuits (Sullivan et al., , 2011). Generally speking, epileptiform activity is best described as the consecutive or intermittent presentation of at least one of the following EEG phases (Figure 1.11): 1) interictal phase: hypersincronous firing of large ensemble of neurons, intense stereotyped population events with characteristic frequency and variable duration intermittent with prolonged silenced periods. 2) tonic phase: a.k.a. seizure or ictal activity, increased firing rate and marked desynchronization, typically lasting 3 or more seconds. 3) clonic phase: also dubbed afterdischarge phase, increased synchronization and decreased firing rate, of variable duration evolving toward “baseline condition” or interictal phase. People affected may present with one, two or three of them, a single condition might be characterized by a peculiar recurrence or scrambled sequence of manifestations. Mysteriously, there is no way to predict the next crisis nor the duration of each phase although mean frequencies and extent are sometimes, in seemingly random way, recurrent (a clinical description is beyond my intent yet extensive literature is available and far too copious to be cited in any useful way, for a recent comprehensive yet concise review consult Jefferys et al., 2012). Most frequent manifestations falls in one out of three classes: Partial or Focal seizures, Generalized seizures, Atypical seizures. Focal seizures are those which EEG readout remains localized in a small cerebral region. Seizure onset is associated with alteration in the modality related to region containing the focus (e.g. visual allucinations, emotional alterations, motor convulsions, loss of consciousness…). Occasionally multiple foci are observed concomitantly or focal spots appear to be migrating. Generalized seizures starts as focal ones in early onsets but shortly after develope as a whole encephalic seizure. Atypical ones is a generic category comprising all other intermediate cases. Further categorization comes from the pathogenic history: idiopathic, sintomatic and cryptogenic epilepsies are thus recognizable. Idiopathic epilepsies are those for which a priori condition leading to manifestation of epileptiform activity is not to be described. In these cases no prodromic pathological process is recognized. Most epilepsies with familiar inheritable patterns or sporadic mutations falls under this category. Sub categories are divided according to onset age, severity and EEG characteristics. Sintomatic epilepsies are those in which a pregressive condition

led to epileptiform activity, such is the case of injury to the CNS, neoplastic formations, disgenesys or infecdtions for instance. Cryptogenic epilepsies are instead the cases in which an unknown prodromic condition started the seizures and no apparent genetic background is described. A single seizure in a lifetime do not identify an epileptic patient: recurrent manifestations are required to define status epilepticus (Sander, 2003). Frequent are the cases of infants with a single o few episodes of epileptiform activity that fades away aging into puberty. In epileptic patient the frequency of seizures are extremely variable both in single pathologies and across different ones. Some epilepsies sporadically degenerate in seizures (even once in years) in other cases patients barely have time to recover from one that suddenly the next ensues. In some forms is the clonic phase that dominates or the interictal one with drastically less invasive effects. Although a single event might not be prognostic in most cases, almost unnoticed alteration of the normal “brain waves” creeps in during a “silent period” in which a full blown status might develop. The extent of time required to develop the status is also highly variable and as yet unpredictable. From an EEG point of view, micro epileptic events are indeed very common in the population (de-ja vù are now interpreted as miniature hippocampal seizures) and the pathological conditions could be the result of aggravated but common substrate. The high frequency of insurgence could be interpreted as a maladaptative divergence of a widespread phenotype which could have been favorably selected in humans. Nontheless epilepsy is naturally observed in all mammals (Thomas, 2010) and experimentally inducible in virtually all CNSs. Most common are channelopathies even in humans but in the rest of the animal kingdom, epilepsy as a whole is far more rare. Selective pressure, not surprisingly, would have cast away any minimum maladaptation, yet the conservation of the trait and the demographic boom in human, suggests that at the basis of the phenomenon might hide some valuable attribute maybe deeply associated with brain complexity. Probably epilepsy is the price that humans pay the most for our unmatched brain complexity. The possibility that observed frequency of epileptic patients in humans derive from the settlement of the genus in a brand new evolutive niche in a brief time, is also feasible but still speculative. Other neurological disorders are most abundant in humans compared with other animals and surely enough this is not solely due to the increased lifespan or “unnatural” lifestyle. Using clinical considerations it is possible to distinguish among 40 different types of epilepsy, some of the most common are briefely described below (Fisher et al., 2005; Engel, 2006).

Rolandic Benign Epilepsy or Partial epilepsy: is an infancy common idiopathic pathology starting as focal but frequently generalized. Rolandic scissure is the focal origin: patients lose transiently control of facial mimic and speech. When generalized, the stereotyped convulsive manifestation is produced (tonic-clonic seizure). Seizures tend to happen in night hours and, as a constant, the child experience retrograde amnesia in the morning. Between seizures the patient is completely normal and no major alteration of cognitive development have been ever described. In 95% of cases, rolandic epilepsy recedes spontaneously before adulthood and do not require treatments.

Picnolessy or petite-mal or absence seizure: non convulsive idiopatic infantile epilepsy. Seizures are associated invariably with loss of consciousness without loss of muscular tone or pressure drop, sometimes associated with typical facial contractions. These are short lived seizure events that comport no signs of mental distress in the aftermath, unfortunately the frequency may be very high (up to two in an hour for the waking period).

Janz epilepsy or juvenile myoclonic epilepsy: typical of puberty, is an idiopathic generalize epilepsy characterize by stereotyped motor automatisms of arms with manifestation at the transition from sleep to wakefulness.

Temporal lobe epilepsy: the most frequent partial epilepsy. Onset is focalized in the hippocampal-parahippocampal formation but frequently generalizes to one or both hemispheres. Most frequent symptoms are psychic, like fear, owe, wrath but also blissfulness and body detachment (interestingly, most patients describe a profound sense of “sacred” or transcendental communion with nature often accompanied with mystical apparitions or “infernal” visualization, regret, guilt and anxiety). Patients are often capable of “sensing” the incoming seizure approaching, the so called “aura”. The origin resides in misfire of enthorhynal, subiculum and or perirhynal cortices with quick migration to hippocampus CA3 and re-entering enthorhynal path through CA1 iside other limbic structures and also involvement of subcortical nuclei. Typically cognitive impairment follow a crisis and serius consequences are frequent: neurodegenration, alteration of personality, autonomic disfunctions. Some authors also indicate a personality trait that, although controversial, could be diagnostic: hyprgraphy, self exaltation, strong religiosity, depression, compulsive behavior, humorlessness, altered sexuality, aggressiveness, hypermoralism (under the name “interictal personality disorder” or “Geschwind syndrome” see: Bear and Fedio, 1977; Waxman and Geschwind, 1975; Devinsky and Najjar, 1999; Harris et al., 2009). It has been speculated that many mystic characters were TLE patients and some great writers, composers were diagnosed or suspected (beside Fyodor Dostoyevsky and Ian Curtis, for an appointed list consult: http://en.wikipedia.org/wiki/List_of_people_with_epilepsy). TLE seizures are often associated with loss of consciousness, fainting, transient retrograde and anterograde amnesia and slow recovery of motor and mental functions. Congenital hippocampal sclerosis is among the most common causes. Cases of sudden death (SUDE) was described in TLE probably associated with therapeutics, but most common outcome are of cognitive pertinence and loss of consciousness (Hesdorffer et al., 2012).

West syndrome: severe first infancy cryptogenic epilepsy. Children aged 6-12 are more prone to develop this syndrome which is associated with a diagnostic triad: infant muscular spasms, psychomotor arrested development and EEG “ipsarhytmia”

Lennox-Gastaut syndrome: severe infatile cryptogenic syndrome. Peculiarity of this condition is the manifestation of different types of seizures comprising absence seizures, atonic seizures and generalized tonic-clonic seizures. A severe mental retardation is always present and an altered EEG pattern is always present even in periods between seizures. Often Lennox-Gastaut syndrome follows up from West syndrome.

Reflex epilepsy: in this case no spontaneous seizure is observed, a sensorial stimulation of peculiar modalities are the triggering events. Photosensitive epilepsy is the most common but auditory, olfactive, tactile ones are described (see Arthur Sacks books: “the man who mistook his wife for a hat” and “an anthropologist on mars”). Oftentimes reflex epilepsy develops in childhood and is associated with absence seizures.

Cluster seizures: rapid succession of seizures events with little or no time for recovery. This is an emergency instance leading easily to death. Clustered seizures may arise in generalized epilepsy of different kind although rarely.

Grand-mal: continuous seizure. The patient enter a state of constant convulsion with no hope for spontaneous remission. If not treated immediately leads invariably to death. May evolve from cluster seizure conditions.

Febrile seizure: tonic-clonic seizures triggered by infections, inflammation and hyperthermia. Probably due to pro-inflammatory cytokines release in response to LPS and transient BBB breeching. An inheritable component is described and insurgence is typical in infancy. Most of the times do not evolve in status.

Focal epilepsies are postulated to be generated by local increased excitability. Different phenotypes observed in EEG tracks during progression through seizures are epiphenomena of wax and waining transient synchronization in clusters of neurons. Epileptic patients present between electrographic seizures, a peculiar interictal activity including “spikes” (less than 50 ms duration) and “sharp waves” (50-200 ms) (Chatrian et al., 1970; Avanzini, 2010). Characterization of interictal activity location and features is absolutely crucial to diagnosis and to treatment planning. Interictal activity in experimental models as well as in human patients of focal epilepsy, are characterized by strong depolarizations transients followed by a slow wave lasting some milliseconds. Interictal events are stereotyped and highly periodic (Avoli et al., 2013) although sporadically clustered in brief trains that might remain localized in space as “normal” spikes or diffuse rapidly to the whole cortex. It is clear that ictal discharges are not merely the result of time clustering of individual interictal deflections being instead associated to a completely different population activity also characterized by a different synchronization profile also mediated at least partly, by very different mechanisms. As deducible from the short lived EEG deflection and the great amplitude, each IS is the result of large scale network synchronization producing few APs per each cell. Data from intracellular recording performed in several animal models of focal epilepsy, show indeed that every single IS is composed by brief sequence of APs thus ISs are the mean effect of single cell synchronous firing as recorded in ECS. Some rather inconspicuous cells show a markedly different firing profile while still being entrained in ISs: they fire at high frequency (200-500 Hz) a short burst of tightly packed AP that rides upon a slow depolarizing potential. This very pattern is repeated during the whole interictal period and is dubbed paroxysmal depolarizing shift, shortly, PDS. All acute models of focal epilepsy both in case of disrupted GABAergic signaling (bicuculline, for

example) and in models with preserved inhibition (low Magnesium, high potassium, low calcium, 4-AP for instance), exhibits ISs (Matsumoto and Ajmone-Marsan, 1964; Dichter and Spencer, 1969; Zuckerman and Glaser, 1970; Wong and Traub, 1983; Haas and Jefferys, 1984; Rutecki et al., 1985; Mody and Heinemann, 1987; Szente and Baranyi, 1987; Swartzwelder et al., 1987). Beside acute models, also chronic one such as intracortical metal ion administration, kindling, GABA withdrowal, cortical freeze and cortical isolation, Kainic acid, Cholera toxin, present ISs (Echlin and Battista, 1963; Wada et al., 1974; Ben-Ari et al., 1980; Cavalheiro et al., 1982; Ashwood et al., 1986; McIntyre and Racine, 1986; Stinger and Lothman, 1989; Bertram and Lothman, 1990; Silva-Barrat et al., 1992). Finally, recordings from human specimens of patients with drug resistant epilepsy also display ISs (Avoli and Williamson, 1996). PDS consist of a very short high frequency trains of discharges lasting around 100 ms and by a slower depolarizing component, fueled by recurrent excitatory loop incoming from synchronized neural pool. The very start of PDS is triggered by intrinsic oscillation of membrane voltage reaching AP threshold that is utterly independent from any synaptic input. It is well established that subpopulations of pyramidal neurons across the cortex are able to self generate intrinsic bursting activity under “basal” excitability. CA1, CA3 hippocampal pyramidal neurons as well as L V neocortical ones, are intrinsically bursting (Kandel and Spencer, 1961; Connors et al., 1982, Tseng and Haberly, 1989), while bursting activity become evident in case of reduced inhibition and mild excitation for other more superficial layered neurons in somatosensory and visual cortex (Jones and Heinemann, 1988; Fountain et al., 1998). This behavior is nothing special or strictly correlated to epilepsy since is occasionally observed under physiological condition in hippocampus (Buzsaki et al., 1983). The point is that during epileptiform activity a far larger ensamble os such neurons are collectively brought into intrinsic firing mode and also collectively entrained. These intrinsic burstin neurons are a small fraction of cortical population and current sustaining this behavior are different in different regions. Pyramidal neurons posses large conductance/high density Calcium channels that could be responsible for bursting activity in neocortex, enthorhynal and pyriform cortices (Magistretti and deCurtis, 1998; Magistretti et al., 2000). 4-AP model ISs are abolished in single neurons when Vm is depolarized above -30 mV in enthorhynal cortex (Lapanstev and Avoli 1998). L-type Ccalcium channels blockers did not affect 4-AP ISs while R-type blockers greately decreases the occurrence and amplitude of interictal PDS (Magistretti and Alonso, 1999). In neocortical neurons the situation is quite different: no Calcium conductances are able to trigger a PDS while a persistent Sodium conductance starts intrinsic bursting activity instead. Neocortical ISs gains amplitude as inhibition is reduced. Interestingly some wide used antiepileptic drugs like carbamazepine, phenytoin, valporate and topiramate, have strong inpact on persisten Sodium current (Segal et al., 1994; Segal and Douglas, 1997; Taverna et al., 1998; Ragsdale and Avoli, 1998). Furthermore, anemonetoxin or veratridine which releave partially the inactivation of Sodium current, thus incrementing persistence, increase burstin behavior in cortical pyramidal cells (Garber and Miller 1987; Mantegazza et al., 1998). Veratridine alone is sufficient to start ISs and ictal-like events in cortical slices in absence of synaptic transmission (Otoom et al., 1998). Still a satisfactory mechanism describing how large ISs builds up in the face of a low percentage of intrinsically bursting neurons is lacking. A critical point is actually the generation of the first complete PDS i.e. bursting activity followed by sustained depolarization. The starting point in any case should be the increase of mean excitatory firing

compared with baseline. In acute model of focal epilepsy, the first PDS in a single neuron can be attained by gradual summation of excitatory inputs provided they are of appropriate frequency (Hoffman and Haberly, 1991). Once a PDS is generated in “nucleus” of intrinsically bursting neurons, surrounding ones shall be entrained: PDS neurons are the “epileptic pace makers”. PDS modality activation has been demonstrated to be sufficient to entrain population discharge (Miles and Wong, 1983). The point is that in order to create a IS a brain only need few intrinsic bursting neurons producing PDSs and the other neurons will discharge, without the need for intrinsic bursting. Recording from several neurons simmultanously during a IS will result in a vast majority of cells releasing single AP and quite few a PDS. Entrained second order neurons (i.e. those activated by intrinsic bursting first order ones) will in turn entrain more neurons in feedforeward synfire cascade. No need for direct connectivity is required between n^{th} order neurons and intrinsically bursting ones, quite the contrary, the more scattered are the pace makers, the larger the population entraind after sufficient number of synaptic stations. PDS cells act like a Van der Pol relaxation oscillators and Sodium persisten current would perform like the capacitor. ISs is the spatially averaged out contribution of many pyramidal cells firing in a synchronous manner: there is no cleare cues in the shape of ISs indicating a propagating “wave of synaptic activity” rather, once entrained, all neurons oscillate in-synch. So PDS is the manifestation at singular cell level of IS in those intrinsic bursting cells that repete their firing mode at each IS. Other cells, the majority of pyramids, display no PDS but one-two, occasionally three classical AP in coincidence of the 200 ms interictal spike. Since PDS is time keeper and generator of coordinated cortical oscillation, some efforts were devoted to its pharmacological dissection. Sodium persistent current or R-type Calcium channels only could account for regerative trigging depolarizations and for high frequency bursting but nor for prolonged consecutive depolarization current. The late phase of PDS is actually mediated by excitatory currents of AMPA first and NMDA origin. An intermediate Calcium conductance is also present in between (Ayala et al., 1973; Johnston and Brown, 1981; Traub and Wong, 1982; Hablitz, 1984; Miles et al., 1988; swann et al., 1993; Traub et al., 1993;). The role of inhibition could also be critical: several evidences indicate that cortical pyramids could be synchronized through a rebound depolarization induced by GABAa mediated hyperpolarization (Surges et al., 2012). Interneurons recorded intracellularly together with field recordings, show high degree of synchronization with physiological gamma activity (Buzsaki and Chrobak, 1995). The contribution of gabaergic neurons to the genesis of fast activity is also demonstrated by gamma depletion when bicuculline is administered (deCurtis et al., 1996). Fast activity in the gamma range is recorded prior to onset of IS, just after bicuculline administration and never observed in slice preparation unperturbeb (Ylinen et al., 1995). On these basis it is possible to suspect that in slice preparation treated with bicuculline, early increase of excitation but prior to first IS appearance, might hyperactivate gabaergic interneuron in a feedforeward fashion. This will result in high frequency GABA firing, which, as stated before, is believed to have a “phase resetting” action on resonating pyramidal neurons, entraining them and starting gamma low coherence activity. Increasing blockade of diffusing GABAa antagonist pushes further the mechanism but also would

be eventually enough to recruit “low chance” intrinsic bursting neuron (i.e. those activated by depolarization above -30 mV and most common in cortex in contrast to hippocampal ones). As soon as intrinsic bursting neurons are activated, entrainment by GABAergic neurons competes with entrainment by hyperfast intrinsic bursting. Concomitantly GABA effect decreases due to increasing blockade and at the end, intrinsic bursting neuron prevail on the rest of the population. At this moments recurrent excitation activates AMPA, Calcium and NMDA currents developing PDS in rhythmic neurons. The first IS is now ready to be served to the “first order” network and accumulating synchrony ensues. Astrocytes could be a crucial player in this game: they could operate in early stages supporting inteneurons with gabaergic signaling before the IS onset or they could precipitate PDS development through glutamate release. Also the synchronizing effect via NR2B-mediated SICs could be critical. What remains to be clarified is also the periodism of ISs which, on these basis should be far quicker. Another tantalizing question is whether IS are protective against ictal discharges or rather precipate or enable seizure onset. Focal application of bicuculline have been for ages the principal manipulation aimed to recreate full epileptiform activity in simplified systems or in vivo approaches. Unfortunately the strong effect of bicuculline seems to reduce the chance of ictal onset in all tested models. A more fruitful approach is to replace bicuculline with pycrotoxyn (non anthagonist inhibitor of GABAa) or shifting to 4-AP, pilocarpine or high $[K^+]$, zero $[Mg^+]$ (Avoli and deCurtis, 2011;). In 4-AP treatment of extended hippocampal-parahippocampal slice preparation the full epileptiform spectrum in observed where ictal discharge is demonstrated to depend upon NMDA, nonNMDA and GABAa activation (Avoli and deCurtis, 2011). In bicuculline treated slices one critical feature of interictal activity disapper which is on the other hand well represented in 4-AP model: slow interictal discharges, appearing with 1-4 sec frequency an lasting several seconds. Same pattern is observed in the isolated guinea pig brain in both low bicuculline or 4-AP administration (Uva et al., 2009; Carriero et al., 2010). These slow interictals events are not to be confused with aforementioned ones with higher frequency and faster kinetic and are shown to be originating from proper hippacampal structure instead of the fast ones emanating from enthorinal cortex (Uva et al., 2009; Avoli and deCurtis, 2011). Slow interictals are insensitive to glutammatergic input blockade but vanish with GABAa antagonists (Capogna et al., 2003). Both milder GABAa inhibition or even GABAa potentiation increase the chance for ictal generation and slow interictal as well. Each ictal events are preceded by a large slow interictal event both in 4-AP and low bicuculline models (in ex vivo slice preparations and in the isolated guinea pig brain). This triggering slow interictal is associated with GABAa current driving a strong synchronous hyperpolarization (Avoli and deCurtis, 2011). Potassium selective microelectrode analisis shows that with slow interictals a strong increase in $[K^+]_e$ is observed that is even larger in the slow interictal preceding ictal onset: isolated slow interictals pushes $[K^+]_e$ to 4.4 mM while “big slow waves” to 6 mM (Avoli et al., 1996). These values are below the ceiling levels described latear yet might be enough to trigger astocyte $[K^+]$ buffering with associated swelling (Waltz, 1987; Olson et al., 1997) , intracellular Calcium increase and gliotransmission via PLC (also described later). Furthermore, glutamate signaling blockade do not interfere with $[K^+]$ elevation that is completely abolished with GABAa (but not GABAb) antagonists (Avoli et al., 1996). Similar $[K^+]$ elevation was observed when GABAa (and not GABAb) agonists was administered in the presence of TTX (Barolet and Morris, 1991) ruling out definitively the

possibility that [K^+] elevation might result from “paroxystic” firing of GABAergic interneurons. Abolition of recurrent slow intarictal events and pre-ictal ones were obtaind using μ-opioid receptor agonists that reduce GABA relese from vesicular presynaptic pools. Pre-ictal GABA-ergic slow activity is also described in neocortex where is observed to support a strong “inhibitory veto” on firing, in regions circumventing ictal focus thus opposing seizure propagation (Trevelyan et al., 2006; Trevelyan, 2009). Increase of [K^+] might produce a significative kick toward excitation synchronizing neural population until ictal start (Figure 1.11). Similar results are observed in isolated hippocampal slices fron juvenile rats where GABA reversal won’t be complete or even shifted the other way around compared with aged animals, strongly arguing against a Chloride flow inversion triggered by [K^+] elevation and Chloride intracellular pre-ictal accumulation (Avoli et al., 1996). In the isolated guinea pig brain preparation, low bicuculline perfusion (estimated 40% blockage of GABAa) triggers slow interictals preceding ictal onset which are associated with huge GABAa-mediated hyperpolarization of enthorinal pyramidal cells and are mirrored with intracellular recordings of intense bursting discharges from local interneuros (Gnatkovsky et al. 2008). At seizure onset, fast (gamma) GABAa-mediated oscillations are typically observed in fiels recordings (Gnatkovsky et al., 2008). Also in the low Magnesium model, fast GABAa-mediated oscillation are observed just about ictal onset in CA3 fields from hippocampal slices (Kohling et al., 2000). Slow interictal activity in absence of complete block of GABAa signaling, increased excitability or inhibition, is crucial to ictal onset although the source of [K^+] remains to be elucidated. A completely opposite scenario emerges considering the role of “fast” interictal activity. Back in 1987 a negative correlation between fast interictal frequency and ictal onset probability was described in slice Magnesium-free hippocampal model (interictal and ictal events generats from CA3). The relation still holds when fast interictals are reduced in frequency by GABAb agonist added to the bath (Swartzwelder et al., 1987) and confirmed in fully connected hippocampal-parahippocampal slice preparation (ictal activity generats in enthoirinal cortex and interictal one starts in CA3). Preparation showed typical ictal generation in enthorinal cortex under “fast interictal waves” absence, yet, when interictal fast activity was started by 4-AP or low Magnesium, ictal discharges readily disappeard. In this sustained fast interictal activity, schaffer collateral cut (abolishing CA3-to-EC propagation of fast interictals) restore ictal generation in EC (Barboise and Avoli, 1997). Many hypothesis was previousely formulated to explain how fast interictal activity from CA3 hinders ictal start in EC including synaptic activity, pH changes, Potassium alterations and Cx coupling (deCurtis et al., 1998). 4-AP model suggests that the main effect resides in the dampening of [K^+] raise in EC performed by incoming fast interictal activity Vs slow interictal events that, conversely, promote Ptassium extracellular accumulation. Notably, slow interictal activity persist unaltered in EC after Schaffer resection, while fast waves do not and ictal onset is unrestrained. A logical consequence one can drow from these premises, is that fast CA3 interictal activity somehow downregulates EC GABAergic Potassium, increasing slow interictal waves. “Artificial” electrical stimulation of EC at frequencies comparable to those observed in incoming CA3 fast interictal events (0.5-1 Hz) in Schaffer collateral resected hippocampal-

parahippocampal preparation, depress ictal generation. In the presence of EC ionotropic glutamate blockade, low frequency stimulation (mimicking fast CA3 interictal waves), elicits a much lower increase in [K^+] than that observed in lower frequency stimulation (< 0.1 Hz) simulating local GABAergic presynaptic AP firing triggering slow wave interictal events. In conclusion, fast interictal waves from CA3 into EC comes with a frequency that seems able to distructively interfere with synchrony building local slow wave/slower frequency interictal events. Most notably, patients presenting with TLE, subjected to low frequency (1-0.5 Hz) magnetic transcranial stimulation witness reduction of seizure generation even in drug resistance scenario (Tergau et al., 1999; Vonck et al., 2002;Theodore and Fisher, 2004; Yamamoto et al., 2006). In TLE patients, hippocampal cell damage might exacerbate ictal generation in parahippocampal structures due to increasingly inefficient CA3 fast interictal barrage and recurrent seizures entering Schaffer collaterals will in turn progressively destroy hippocampal structure. Data collected from longitudinal chronic EEG animal recordings in time windows extended from silent period to complete status induction, demonstrate that slow interictal activity in EC is scanty during induction when compared to chronic period and CA3 interictals diminishes as seizure recurrency increases (Bortel et al., 2010).

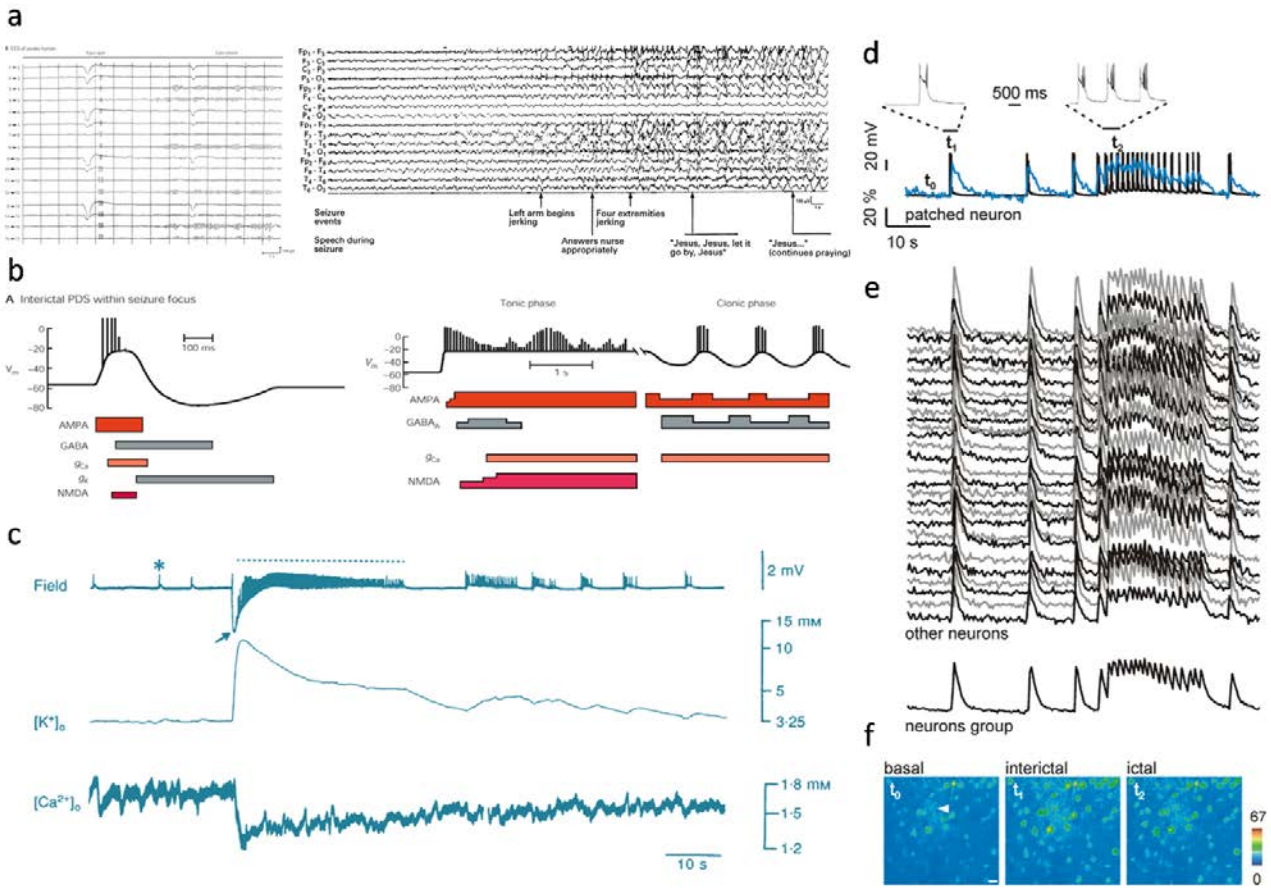

Figure 1.11 *seizures a) human normal (left) scalp EEG compared with a recorded electrographic seizure (right) without loss of consciousness. Comments on the state of vigilance and behavior of the patient during seizure are reported below the track. Note the appearance of typical spiked transients preceding the behavioral alterations increasing in frequency as the severity of the clinical manifestations increases (Kandell et al., 2000; Bell et al., 1997). b) epileptiform activity in the context of tonic-clonic seizures and experimental acute models, presents frequently with 3 typical phases represented in the scheme depicting intracellular behavior: interictal (left), ictal (middle), afterdischarges (right). Interictal events are hypersynchronous at the level of neuronal network with individual cells experiencing few AP overriding the so called paroxysmal depolarizing shift. Below the picture of membrane potential oscillation the progression in time of channels gating is represented as horizontal bars. AMPA, NMDA and Calcium conductances build up the PDS which is damped and extinguished when Potassium and GABA channels are gated. These are short lived population events repeating in a stereotyped fashion and observed in conditions other than epilepsy (e.g. migraine). Ictal phase is characterized by prolonged high frequency firing of most*

principal cells in the focus (with reduced network coherence compared with interictal events). failure of GABA brake seems to be at least in part responsible for the extended duration and sustained firing rates. Also abortive Potassium conductances forbids the spacing of AP bursts as observed in interictal phase. Afterdischarge phase, following an ictal one, presents a rhythmic GABA-ergic activity inbetween trains of population bursting events. NMDA gating is impaired possibly as a consequence of waxing and waining AMPA conductance (Lothman and Bertram 1993). c) Potassium concentration in the extracellular fluid changes dramatically at seizure onset. An extracellular field recording (top) performed in rat hippocampal slice preparation subjected to 4-AP treatment is simultaneously acquired with $[K^+]_o$ (middle) and $[Ca2+]_o$ (bottom) monitoring. The 3 phases of epileptiform activity previously described are evident. Concomitant with a slow downward transient in the field, a large surge of Potassium is observed associated with a decrease of Calcium. Potassium peaks just at start of ictal phase. Estimated Potassium levels are far above ceiling values for astrocyte buffering capability (Avoli et al., 1996). d) Calcium imaging in experimental models of focal epileptiform activity, allows analysis of population behavior with individual cell resolution. Here a patched principal cell performs transition from interictal phase into a complete ictal discharge. Oscillations of membrane potentials (enlarged for an interictal event and 500 ms inside ictal phase) are superimposed with Calcium behavior. e) Calcium traces extracted from nearby un-patched neurons showing the coherent network activity. f) individual frames representative of interictal, ictal and baseline Calcium dependent fluorescence intensity. Note the larger Calcium increase during short-lived interictal events (Gomez-Gonzalo et al., 2011).

1.7---The serpent's egg/role of astrocytes in epileptogenesis.

Physiological activation of astrocytes remains controversial to some extent, but, as in the case of genetics, the role of a particular component of a complex system might be best elucidated in a context in which its activity is abolished or radically alterated. Neurological disorders presents as a whole, a high degree of comorbidity with astrocyte disfunctions of sorts (Seifert et al., 2006). Epileptiform activity may burst out as a consequence of impaired $[K^+]_e$ homeostasis: increased neural firing rate could be both the cause of $[K^+]_e$ increase, the consequence or a link in a perverse loop (Nicholson and Sykova, 1998). Na/K ATPase and Na-K-Cl cotransporters in astrocytes presides $[K^+]_e$ uptake and siphoning in astrocytes is associated with cell swelling and Vm depolarization (Kofuji and Newmann, 2004). Na/K ATPase is a major candidate in maintaining $[K^+]_e$ levels below the ceiling and is upregulated after status epilepticus induction although a malfunction in epileptogenesis is yet to be elucidated (D'Ambrosio et al., 2002). Redistribution of $[K^+]_e$ through region of normal concentration via astrocitic syncytium (i.e. spacial buffering), rely upon astrocytes AQP4, Cx43, Vm and several potassium channels (Kofuji and Newmann, 2004) although "indirect coupling" might help (Wallraf et al., 2006). Sclerotic human hippocampi shows altered homeostasis of $[K^+]_e$ due to astrocitic Kir altered expression. MTLE-HS differs from other non sclerotic MTLE in their incapacity to re-equlibrate $[K^+]_e$ in the presence of Ba+, a Kir 4.1 blocker as confirmed by patch clamp analysis on astrocytes, lacking Kir currents in MTLE-HS (Bordey and Sontheimer, 1998; Hinterkeuser et al., 2000). Genetic linkage analysis also couple Kir downregulation to high susceptibility to epilepsy in familiar screening in case of SeSAME or EAST syndrome (Bockenhauer et al., 2009). Mice with deleted Kir 4.1 develop seizure as well as traumatic brain injuries model in which a rapid decrease of Kir 4.1 expression is reported (D'ambrosio et al., 1999; Djukic et al., 2007). Brain injuries are associated with neurodegeneration and vascular lesions and inflammatory responses but seizure phenotype develops after the "acute phase" when Kir 4.1 starts to disappear from astrocytes processes, possibly as a response of serum extravasation (Yang et al., 2005). Transient BBB breeching is sufficient to induce focal epileptogenesis while BBB lesion is a primary event in human MTLE proigression (Seifert et al., 2004; Marchi et al., 2007; Van Vliet et al., 2007). Extravasation is believed to be a major epileptogenic event. Albumin is uptaken by astrocytes through TGF-β receptor leading to downregulation of Kir 4.1 and massive Calcium increase with consequent NMDA excitoxicity and hyperexcitability (Choi and Friedman, 2009). Blood-borne proteases also trigger activation of PAR-1 receptors which appear to be expressed mainly on astroglia endfeet producing increase of intracellular Calcium and release of gliotransmitters. PAR-1 signaling induce vasoconstriction, local hypoperfusion and, when protracted, neural hyperexcitability (Carmignoto and Gomez-Gonzalo, 2010; Gomez-Gonzalo et al., 2010). Ultrastructure analysis demonstrates close association of Kir 4.1 to AQP4 in capillary associated endfeet, supporting the notion that $[K^+]_e$ clearance depends upon water flow across the cell membrane in order to compensate for osmotic challenge produced by ion dislocation (Higashi et al., 2001). Astrocyte swelling is actually observed when parenchyma in loaded with Potassium and swelling itself is reported to be linked to activation of VRAC-mediated gliotransmission (Akita et al.,

2011). when AQP4 is downregulated maintaining Kir4.1 expression in the physiological range, $[K^+]_e$ clearance is impaired and hyperexcitability ensues leading to epileptiform activity and status epilecticus in most cases (Binder et al., 2010) supported by longer seizure duration in AQP4 null mice (Binder et al., 2006) although pre-status astrocyte coupling result higher compared with control and spatial buffering increased in efficiency (Benfenati et al., 2011; Strohschein et al., 2011). Human polymorphisms of AQP4 strongly links with chronic migraine and epilepsy and mouse models carrying human mutations are highly epilepsy-prone. Human MTLE-HS specimens show ablation of AQP4 from astrocyte endfeet (Eid et al., 2005) and patients with FCD type IIIB manifest increased AQP4 expression around dysplasic neuron but marked reduction in endfeet (Medici et al., 2011). Kir 4.1 and AQP4 functional and structural association depend on Dystrophin complex anchorage and $[K^+]_e$ homeostasis impairment in epileptic patients might result in supramolecular disorder at this level (Sheen et al., 2011). Multivariate analysis highlighted correlation between human SNPs polymorphism in AQP4 and Kir 4.1 associated with idiopatic febrile seizure and MTLE-HS: one of the rare case of candidate gene for still elusive sporadic epilepsy and a most peculiar one since the two SNPs correlated best when together (Ngomba et al., 2004; Lenzen et al., 2005; Heuser et al., 2010). AQP4 and Kir 4.1 are tightly associated even in a developmental point of view with the two protein traduced concomitantly in the same postnatal time window. Together with induction of status epilecticus in hippocampus with means other than downregulation of AQP4 and Kir 4.1, a reduction in ECS volume and IHC staining for these two key protein is observed in parallel with prolongation and increased frequency of ictal activity (Hsu et al., 2007; Seifert et al., 2009). Connexine have been the long sought-for target for magic bullet in antiepileptic drugs research and it was not until recently, recognized as poor candidate for its dualistic role. Lattate and Glutamine shuttle effect is strongly reduced in Cx43/Cx30 (both of astrocyte origin) downregulation. In epileptiform activity mean probability of neural firing is grately increased compared with resting states and with explorative/processing tasks in mouse models, thus metabolic support from astrocytes is believed to be charged with extra load to sustain hyperexcitability (Giaume et al., 2010). From this standpoint, extensive Cx-coupling in astrocytes would turn adverse in the sense that it might sustain the increased firing rate precipitating ictogenesys and excitotoxicity. Conversely, well established gap junctions are believed to allow proper $[K^+]_e$ spatial buffering dampening vicious loops of recurrent excitation/tonic depolarization. Cx43 knocked down mice exhibits spontaneous epileptiform activity and reduced threshold for ictal ignition as well as extensive $[K^+]_e$ clearance impairments (Wallraf et al., 2006). At least transientely, BBB disruption also downregulate Cx43/30 transcription prior to epileptiform manifestation (Cacheaux et al., 2009). On the other hand, gap junction disruption (Carbenoxolone, Glycirrhytin, octanol), leads to “neural starvation” and decreased frequency of spontaneous epileptifor events although available Cx blockers are not as astro-specific as required (Steinhauser and Seifert, 2002). In resected specimens from FCD type IIIB patients with short epilepsy history, a surprising upregulation of Cx43 is observed surrounding neoplastic tissue and ballon cells (Naus et al., 1999; Fonseca et al., 2002; Garbelli et al., 2011), presumably indicating an early stage of tentative compensatory response of neighboring astrocytes facing increased $[K^+]_e$. This very mechanism could also precipitate ictogenesys since more coupling also means neural fueling with more ease sustaining hyperexcitability secondary to neoplastic progression. Cx43 transcript and

phosphorilated protein is increased in experimental models: this upregulation follows first ictal episodes in a hyperactivity dependent modality abolished by neural silencing with TTX (Mylvaganam et al., 2010). In a bicuculline slice model of acute epileptiform activity, incubation with Cx43-mimetic peptide disrupted astrocyte coupling but, surprisingly, strongly contained propagation of ictal activity triggered focally (notably not interictal one) and produced dose-dependent neuroprotection (Yoon et al., 2010). Kainate induced status epilepticus is accompanied with increase dye coupling among astrocytes and increased expression of Cx43 (Takahashi et al., 2010). Alteration of astrocitic glutamate uptake function is quite a common feature in many neurological disorder including epilepsy, EAAT1/2 are the major transporters scavenging synaptic cleft from prolonged exposure to glutamate (Seifert et al., 2006). Retention of diffusing glutamate in ECS is a well established risk factor prodromic of ictogenesis and facilitating recurrent seizures (Glass and Dragunow, 1995). As in the case of Cx42, both increased expression and downregulation of EAAT is reported in human temporal lobe epilepsy. An early overexpression might serve as compensative process to cope with otherwise increased excitatory tone that is successively, somehow, dropped down or downregulation might indeed be a causative phenomenon leading to increased glutamate extracellular concentration (Ramirez-Munguia et al., 2003). EAAT expression is actually activity dependent, i.e. the more glutamate released the more EAAT is produced, conversely, nerve resection or neurodegeneration (like in ALS mouse models) causes a decrement in EAAT levels. FCD patients with prolonged history of recurrent seizures present decreased EAAT expression, while idiopatic epileptic ones with short progressions are indistinguishable from controls. Interestingly, beta lactam antibiotics trigger EAAT transcription and exert some neuroprotective a antiepileptic effect (Maragakis and Rothstein, 2005). In excess glutamate generated by focal pharmacological blockade of EAAT, operate onto NMDA receptors, both synaptic and, through spillover, extrasynaptic ones leading to recurrent depolarizations, increased firing rate and excitotoxicity. The increased excitatory tone than propagate to “normal” residual circuits, recruiting increasing number of neurons in feedforeward progression decreasing the threshold for seizure susceptibility (Jorge et al., 2011). Enhanced NMDA activity is also related to a negative shift in Kv channels voltage dependent activation that further enhance excitatory tone). Low Magnesium (facilitation on NMDA signaling) slice model of epilepsy in wt animals present recurrent seizure which result magnificated and more frequent when EAAT is anthagonized (Nyitrai et al., 2010). Also loss of glutamine sintase is associated with epileptic phenotype: altered glutamine shuttle decrease glutamate gradient toward astreocytes hindering its removal. Upregulation of GS is described in the latent phase os status epilepticus induction (first spontaneous overt seizure is yet to be presented) addressing the possibility of an increasing release of glutamate that builds up until a certain threshold is reached, beyond which seizures starts. GS downregulation in this period shorten the latent phase (Hammer et al. 2008) and could well be a causative factor when blocked in not induced wt animal where susceptibility to epileptiform is thus increased (Eid et al., 2008). Glutamine shuttle is also accessible to interneurons: a decrease in GS activity leads to decreased GABA availability in GABAergic

presynaptic terminals while glutamate in excitatory synapses do not seems to be minimally affected (Ortinski et al., 2010). Sample from resected patients with TLE and FCD showed marked increase of mGLUR2/3/4/8 expression in reactive astrocytes (Aronica et al., 2003). Since activation of mGLURs (see ACPD effects on slice preparation discussed in Halassa and Haydon, 2010) in astrocytes was clearly linked to augmented intracellular Calcium concentration leading to glutamate release, the possibility of a positive feedback loop between increased synaptic glutamate release in developing status and increased astrocytes gliotransmission is proposed. In concert with impairment of glutamine shuttling and EAAT function, neural hyperactivation via gliotransmission seems a plausible mechanism exacerbating hyperexcitability. In acute seizure models, Calcium oscillation frequency, amplitude and astrocytes enrolment are clearly magnificated and damped by antiepileptic drugs: neuronal hyperexcitability begets astrocyte hyperexcitability. Moreover, due to the progressive propagation of Calcium raise in “far from focal” astrocytes, local seizures, once barraged by short range inhibitory firing (Trevelyan and Schevon, 2013; Trevelyan, 2013) could encounter a more permissive territory in the surrounding area already bombarded with astrocytes secretionand propagate (Gomez-Gonzalo et al., 2010). Ictal phase generatated in low Magnesium slice model by exogenous application of NMDA, manifest itself as increase focal firing of asynchronous neural population that propagates in the tissue (not interested in NMDA direct action) in a “step by step” jacksonian march (Traub and Wong, 1982; Pinto et al., 2005; Trevelyan et al., 2006). Neurons already driven close to seizure threshold by NMDA application signals to astrocytes thet, in turn, respond with Calcium increase and augmented gliosecretion feeding back into hyperexcited focus and kicking into action neighboring neurons. Excitatory long and intermediate connections also converge on the periphery of focal stimulation contributing to depolarization while entraining local interneuron. Short range inhibitory projections fires back to cope with increased glutamate release (in an homeostatic negative feedback loop) but lack the capability to match either long range excitatory connections and astrocytes transcellular communication in reaching periphery. The slow time integration of glutamate sensing and the extensive convergence of excitatory synaptic space into astrocytes domains, contribute to piling up Calcium increment in a synchronous fashion in astroglya while asynchronous neural hyperexcited local network goes on increasing firing rate pushed by reverberating gliotrasmission triggered by Calcium elevation itself. Possibly NMDA NR2B contribute to synchronization of focal firing meanwhile Calcium propagation to more distal processes ensheathing “resting” synaptic territories, triggers “out of focus” gliotrasmission favoring hyperexcitation and synchronization. At this point threshold for paroxysmal depolarizing shift in pyramidal neurons is attained and excitatory firing is no longer restrained by GABAergic inputs (Trevelyan et al., 2006; Schevon et al., 2012): seizure threshold is achieved. A massive synchronous release of glutamate floods astrocytes that return excitatory inputs back to the focus sustaining ictal activity and drive toward threshold nearby neurons helped by direct pyramidal projections. A recurrent neuro-astrocyte excitatory loop is activated and propagates ictal activity away from focus. Subsequent seizures propagate with ease since astrocytes are already entrained and neural network has been brushed with intense excitatory activity (Fellin et al., 2004; Angulo et al., 2004; Kozlov et al., 2006; Ding et al., 2007; Gomez-Gonzalo et al., 2010). All observed astrocyte activity was abolished with TTX indicating that neural hyperexcitation is the “primum movens” , yet,

blocking Calcium elevation in astrocytes before NMDA administration, disrupt recurrent loop initiation resulting in abortive seizure. Beside glutamate, the release or co-release of D-Serine might add fuel to the fire inpinging on both NMDA depolarization, neural Calcium increase and synchronization. Moreover, sub-optimal NMDA stimulation i.e. inefficient to ictal generation, can be “aided” to threshold co-stimulating with TFLLR PAR-1 agonist: in this case the number of neurons activated is in fact larger than that obtained with NMDA alone. When a critical number of neuron is engaged with hyperexcitation, gliotransmission further increase the cohort and if this second ensamble is large enough, seizure threshold is reached. Efficient NMDA pulse could be split in two concomitant administration delivered at increasing distance apart: seizure is triggered when a single astrocyte territory is activated in the overlapping region of NMDA propagation.

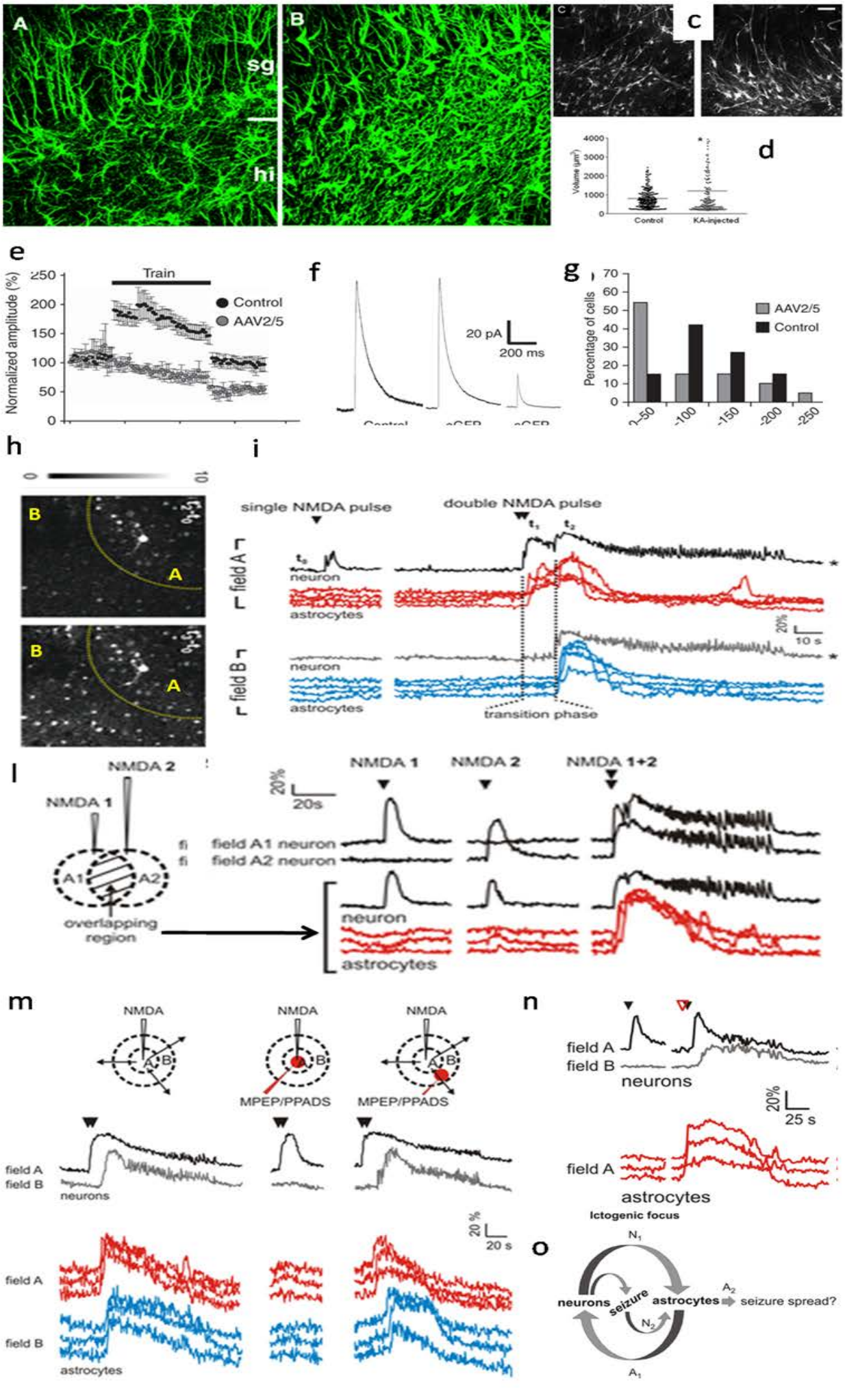
A
sg
hi
B
c
c
d
Volume (µm³)
Control
KA-injected
e
Train
Normalized amplitude (%)
Control
AAV2/5
f
20 pA
200 ms
g
Percentage of cells
AAV2/5
Control
h
i
single NMDA pulse
double NMDA pulse
field A
field B
neuron
astrocytes
transition phase
l
NMDA 2
NMDA 1
A1
A2
overlapping region
NMDA 1
NMDA 2
NMDA 1+2
field A1 neuron
field A2 neuron
neuron
astrocytes
m
NMDA
MPEP/PPADS
field A
field B
neurons
astrocytes
n
field A
field B
neurons
field A
astrocytes
Ictogenic focus
o
neurons
seizure
astrocytes
seizure spread?

Figure 1.12 *astrocytes and epilepsy a) immunostaining against GFAP in a control healthy rat hippocampal Dentate gyrus. b) Kainic acid triggered status epilepticus causes massive gliosis in the injected Dentate gyrus surveyed here after a complete status was induced. astrocytes display increased protoplasmic volume with larger processes and no signs of astrogenesis are reported (Fedele et al., 2005). c) Sulforhodamin 101 staining of contralateral (left) and ipsilateral (right) KA unilateral injected hippocampus. Status epilepticus correlate with a massive enlargement of astrocyte somata as reported in the scatterplot in d) (Appaix et al., 2012). e) AAV2/5 in vivo transduction of an high titer /high yield eGFP expression construct leads to astrogliosis without status epilepticus. The resulting downregulation of glutamine synthetase in gliotic astrocytes leads to the reduction of recorded eIPSC in otherwise normal neurons. A protocol of hippocampal LTD fails indeed to increase the eIPSC in transduced mice. f) eIPSC measured in control mice or in neurons from transduced ones located further than a critical distance from a eGFP positive astrocyte do not differ at all. On the other hand, eIPSC recorded from a neuron neighboring a eGFP positive astrocyte, result drastically decreased compared with the others. g) Frequency distribution of eIPSC amplitudues recorded in hippocampus from control (black) and tranduced (gray) mice. Skeweness of the two distributions indicates a reduction in average eIPSC amplitude in gliotic hippocampi. This also may suggest that astrocyte disfunction might drive toward an unbalance of inhibition Vs. excitation, favouring the latter and precipitating epileptogenesis (Ortinski et al., 2010). h) In the 0 Magnesium model of focal epilepsy in hippocampal slice preparation, a double pulse of NMDA is enough to trigger an ictal discharge in neurons in a region around the pipette tip (A) and a subsequent propagation of ictal activity further away (B). Top image represents the difference in Calcium-dependent fluorescence between the time of NMDA double pulse (t1 i.e. the activation of field A) and baseline (t0), while the bottom image depicts the difference between field B invasion (t3) and baseline. i) A single pulse of NMDA is not enough to start an ictal discharge in this model although capable of increasing neuronal Calcium. Astrocytes remains indifferent to a single NMDA pulse. Furthermore, no spontaneous ictal activity is recorded without manipulation. A double pulse of NMDA in field A readily recruits both astrocytes and neurons into an ictal discharge. Field A leads but after a transition phase Field B starts ictal activity. t2 is the position in time when both Field A and Field B are entrained in a synchronous ictal discharge. At t1 (pulse) no sign of either propagation or local generation of Calcium oscillations are to be observed in Field B. l) when the double NMDA pulse is split in two pipettes few microns apart, obviously agonist concentration sums in the region amidst. When a single pulse is administered in either two regions, no sign of ictal discharge are detected and only local neurons respond with a short-lived Calcium elevation. When two pipettes puff together, both regions are recruited into synchronized ictal activity. Notably, astrocytes in the overlap region experience strong Calcium increase as well as neighboring neurons. m) When NMDA is delivered in a double pulse together with MPEP and PPADS only a short Calcium increase is observed exclusively in Field A neurons. Astrocytes from both fields remain silent and ictal activity is not started as if a single NMDA pulse was puffed. When PPADS and MPEP are puffed in Field B while a double NMDA pulse is administered in Field A,*

ictal activity is generated as usual in the NMDA site and surprisingly, spreads into Field B with concomitant activation of local astrocytes. n) TFLLR (red triangle) together with a single NMDA puff surrogates the NMDA double pulse. Without concomitant activation of astrocytes, a single NMDA pulse is ineffective in the genesis of ictal activity. Ictal activity triggered by TFLLR+NMDA spreads into field B as in the case of double NMDA puff. Astrocytes from Field A align their Calcium transients on those of neurons. o) Proposed model for ictal generation in mild pro-excitatory context ([0 $Mg^{2+}]_o$). A threshold of excitation is set below which ictal activity is forbidden. Crossing the threshold would require massive neuronal activation (double NMDA puff) or concurrent activation of neurons (single NMDA puff) and astrocytes (TFLLR) each receiving an excitatory drive of a lesser magnitude. When seizure is attained, neural firing bombards astrocyes that reinforce neural activity and keeps ictal threshold far below. Activated astrocytes also signal in the periphery of local neural activation, increasing excitation in resting neurons toward ictal threshold (Gomez-Gonzalo et al., 2010).

1.8---The head on the door / Why investigating astrocytes?

Astrocytes increases substantially the D.O.F. in CNS computations and are strongly implicated in the process of decoding reality (Fellin and Carmignoto, 2006; Perea and Araque, 2006). Calcium increases in astrocites appear to manifest with a highly nonlinear behavior reguardless estimated neurotransmitter release. Astrocytes seem to be entangled with neurons in the very information processing machinery. Like neurons, where a nonlinear response greatly diverge from converging inputs, astrocytes produces all sorts of Calcium oscillations with an as yet undisclosed relation with neural activity. Information processing in the neural network are believed to rely upon two principal properties: selectivity of responses to diversificated inputs and intrinsic resonance properties of Vm. The highly non-linear input-output curve calculated from neurons is the hallmark of neural integrative properties (Llinas and Sugimori, 1980; Kandel and Squire 2000). Since Calcium "excitability" is demonstrated for astrocytes in the context on neural network activity (Perea and Araque, 2005), two possible scenarios might be envisaged: either astrocytes are linear reader of synaptic bombardment or they are integrative elements. In the first case, gliotrasmitter release should be proportional to incoming imput amplitude and the very same shall be for Calcium levels. In the second case, a nonlinear response or several ones should be observed in terms of Calcium oscillation and gliosecretion in response to different patterns of neuronal activity. So far is still unknown whether the different observed $[Ca^{++}]_i$ oscillations are mere epiphenomena of astrocyte's Calcium homeostasis perturbed by intermittent neurotransmitters release or, more intriguingly, they reflect a plethora of different encoding system allowing for a complex neural-to-astrocyte "transfer function". in this latter perspective one could envisage some sort of floating threshold mechanism enabling the selection of one among several possible Calcium events. in other words, neural activity could be clustered not just according to the "intensity" or "modality", conversely astrocytes could operate some sort of time integration of neural activity. When neural inputs remains below a certain threshold, only local transients are observed that could operate in some reinforcement feedback loop. Exceeding a lower level of "flux of neural activity", Calcium propagation to the soma might be engaged: here other processes once resting might be invaded with Calcium waves and release gliotransmitters. Thirdly, an even more sustained neural activity could trigger CICRs mechanism to allow for transcellular Calcium wave propagation. This could be responsible for activation of astrocytes distant from a focal region of intense neural activity, with possibly devastating effects on local circuitry. Most strikingly, this latter manifestation is only observed in vivo during ictal propagation, spreading depression or great intensity stimuli administration (Schipke et al., 2002; Peters, et al., 2003). Evidences in support for a non linear transfer function regulating neuro-astro-neuro processing are still poor, one being the existence of at least two Synaptotagmine in astrocytes SNARE complexes with fairly different Calcium Kd (Agulhon et al., 2010). Each $[Ca^{++}]_i$ elevation odality, on the other hand could be associated with different functional outcome on the network, in dependence on which vescicle array is triggered (Which synaptotagmin is activated). So far there are no evidences that different gliotransmitters are stored in vesicles associated with different Syt, but there are strong evidences for the co-

segregation of different compounds in different vesicles (Halassa et al., 2008). Astrocyte signaling to neuron operates on timescales order of magnitudes larger (seconds or tens of seconds) than those observed in neurons (milliseconds). Modulatory effects on synaptic strength may be intermittent within a range of seconds or last considerably longer as observed in the case of LTP/LTD. A tonic secretion of ATP/adenosine have been related to a steady suppression of of synaptic transmission in hippocampal slices resulting in the increase of LTP dynamic range (Pascual et al., 2005). A faster mechanism emerges in the case of CA1 LTP in which phasic gliosecretion operate in an hebbian fashion when coincidence with presynaptic release is granted (Perea and Araque, 2007). All these results together do not account for an estimated 60% of synapses which seem to be insensitive to astrocyte signaling (percentage extrapolated from LTP hippocampal experiments and ultrastructural data from cortex). A substantial underestimation of the impact of astrocyte activity might result from a poor optical resolution in Calcium imaging experiments (for high resolution data see DiCastro et al., 2011) or from the poorly understood complexity of neuro-astrocyte “connectome”. A scenario in which tripartite synapses in hippocampus are around 40% might be consistent with the possibility that these very synapses are indeed the potentiable ones or, in other words, the plastic ones. Again these considerations are supportive for a highly regulated connectivity between astrocytes and neurons in contrast with a generic “spillover effect”. Beside the obvious interest for the basic mechanism promoting/terminating epileptiform acxtivity, our efforts were dedicated to a broader target which is also the main theme I’m trying to expose in this work: HOW ASTROCYTES BEHAVES IN DIFFERENT CONTEXT OF ELECTRICAL NEURAL ACTIVITY. Epileptiform activity is a particularly useful model of alterated electrical activity spanning from hypersinchronous to totally de-synchronized. These two extreme behavior are not observed within physiological range of electrica activity and proved useful to challenge astrocyte function.

Thesys: DIFFERENT PATTERNS OF NEURAL POPULATION ACTIVITY CORRESPOND TO DIFFERENT PATTERNS OF ASTROCYTE CALCIUM BEHAVIOUR.

Hypothesys: SHIFT IN NEURAL POPULATION ACTIVITY COHERENCE DISCRIMINATES DIFFERENT ASTROCYTE CALCIUM BEHAVIOUR.

Null hypothesys: ASTROCYTE CALCIUM BEHAVIOUR FLUCTUATIONS DO NOT CORRELATE WITH CHANGES IN COHERENCE IN NEURAL POPULATION ACTIVITY.

Chapter 2/Materials and Methods:

Isolated *Cavia porcellum* brain preparation.

Experiments were performed on brains isolated from young adult guinea pigs (females, 150–200 g weight; Charles River Laboratories, Calco, Italy). Animals are sacrificed with an intraperitoneal dose of sodium thiopental (125 mg/kg; Farmotal, Pharmacia, Milan, Italy). Three minutes after the paw pinch reflex was extinguished, an intracardiac perfusion with cold saline solution (composition below) is executed to cool brain temperature and to remove blood cells. The head is cut and the brain is then isolated according to the protocol described in Muhlethaler et al., 1993; de Curtis et al., 199 . Isolated brain is readily transferred into the recording chamber filled with cool saline solution (Figure 2.1). A polyethylene cannula was inserted in the basilar artery within 2 min to restore brain perfusion via a peristaltic pump (Minipulse 3; Gilson Middleton, WI, U.S.A.). The composition of the perfused carboxygenated (95% O2 / 5% CO2) solution was: 126 mM NaCl, 3 mM KCl, 1.2 mM KH2 PO4, 1.3 mM MgSO4, 2.4 mM CaCl2, 26 mM NaHCO3, 15 mM glucose, 2.1 mM HEPES and 3% dextran MW 70,000 pH 7.3). The above procedure was performed at 15°C and brain temperature was slowly raised to 32°C via a temperature controller (PTC 10; NPI, Tamm, Germany) before starting the experiment. Guinea pigs are suitable models for this peculiar preparation due to their brain perfusion apparatus which predominantly rely upon basilar artery instead of carotids artery (de Curtis et al. 2012), which alleviate perfusion and surgical cumbersome procedures encountered in other mammals (see also Figure 2.1). *Cavia porcellum* also display a fast E-GABA switch compared with other mammals and the well characterized sexual dimorphism also encouraged the choice of female animals (White and Platt, 2000). Beside a well conserved limbic structure architecture, Guinea pigs unfortunately present a myelinated “capsule” below 300 μm in the mEC which is less prominent in other mammals. This resulted in a major inconvenience when trying to record Calcium dependent fluorescence from neurons as described further in the text.

Visual cortex *Mus musculus* craniotomy

C57BL/6j (both sexes, Jackson Laboratory, Bar Harbor, Maine) and Gad67-EGFP knocked in transgenic (Tamamaki et al, 2003) adult (p30-40) animals, were anesthetized with 0.6 gr/Kg of urethane (SIGMA) dissolved 20% in 0.9% NaCl/water. Paw pinch and pupil reflexes were used to evaluate anesthesia depth. Eyes were moisturized with eye ointment (Lacrigel, Bracco) and covered with round coverglass (8 mm diameter) to prevent damages. Eyes were blindfolded with tinfoil patches applied over the coverslip, to avoid desensitization. Scalp was trimmed and strewn with lidocaine (2.5%, Luan, Molteni). Skin flap was removed and connective tissue tore apart. Custom made metal frame (Figure 2.6) was glued with cyanoacrilate over V1 region (Bregma from -2.18 to 5.20) then sealed with ink-powder blackened dental cement (Paladur, Pala, Heraeus). The frame is then screwed to a custom made support and a 2 X 3 mm oval shape is drilled (Silfradent)

in the skull, the procedure is performed under a dissection microscope (Olympus SZX10). Frequent superfusion with aCSF soluition (composition below) during drilling is suggested in order to cool the tissue. Bone speck was gently removed without damaging dural surface. Meningeal surface was kept constantly irrorated in aCSF. Mouse was placed under the microscope objective and brain surface focused with X10 objective (LMPlanApo, Olympus) using epi-illumination (Ultima multiphoton microscopy system, Prairie Technologies Inc. Bruker corp.). a thermic blanked (Harvard apparatus) is placed on the animal's back, recording body temperature through an anal probe, reference temperature is set at 36° and respiration aid is provided with low flowing O_2 enriched air (NewLife elite Oxygen concentrator, Airsep). aCSF composition is as follows: 126 mM NaCl, 3 mM KCl, 1.2 mM KH_2PO_4, 1.3 mM $MgSO_4$, 26 mM $NaHCO_3$, 2.4 mM $CaCl_2$, 15 mM Glucose, 1.2 mM HEPES in distilled H_2O, pH 7.4.

Bulk loading

According to the protocol described in Stoisek et al., 2003 and Garaschuk and Konnerth, 2010, dye solution was prepared from Oregon Green BAPTA 1-AM (Invitrogen) powder redissolved in Pluronic acid F-127 (Invitrogen) 5 μg/4.5 μl. aCSF solution was added 1:10 and 1 mM Sulforhodamin 101 (Invitrogen) 2.7 μl added at last. Prolonged pipetting of the solution, precedes sonication (Ultrasonic clearer cp104) at 37°C for 15-20'. Solution is transferred to a insulin syringe and a 0.22 μm filter (Millipore) is placed on top. An Hamilton needle is mounted to the filter. Glass pipette (Boro-silicate glass, Sutter instruments, with filament, O.D. 1mm, I.D. 0.58) is pulled (Sutter instruments p-97 Flaming-Brown micropipette puller) and the tip smashed under control of a calibrated microscope (Olympus CX-41 X50 objective), to obtain a tip diameter of 3 μm. the pipette is filled with the dye solution carefully avoiding bubble formation. Injection pipette is plugged in the pipette holder (EH-01 electrode holder, npi) and moved in the proximity of the craniotomy. Micromanipulator (Sutter instruments, ROE-200) is set into 45° diagonal modality and brief puffs (0.2 p.s.i. PDES-029, npi) are delivered while descending. Pipette position with respect to the cortex is monitored through the microscope using fluorescent lamp (SR-101 signal excited in blu light, X-lite series 120Q, EXFO). Red puffs helps detecting the 0 depth landing point. Here slow progression modality is set in the micromanipulator and a depth of 180-200 μm is reached slowly. 0.5 p.s.i. pressure is then delivered to the pipette and dye solution is allow to diffuse for 5'. A green bolus is readily visible in blue light fluorescent illumination. The pipette is kept in place and the brain allowed to load dyes for at least 1h. The injecting pipette is then removed and the surface of the exposed brain is covered with a thin layer of molten Agarose in aCSF (0.1% low melting point Agarose, Promega) once temperature has reached approximately 36°C. Agarose is readily covered with a round coverslip (8 mm diameter) which is exceeding in surface the underneath craniotomy , allowing fixation with dental cement directly on the skull. A region between glass and skull is left unglued to provide entry for the extracellular pipette. The animal is then positioned under the microscope and loaded cortex is explored for a nice field to be imaged. A second pipette (4 mm tip) filled with aCSF is inserted in the cortex in order to approach the region imaged.

Calcium imaging and local field recordings

After loading the cortex is imaged with X40 or X60 objective (Olympus LumPlanFL, mounted on Ultima multiphoton microscopy system, Prairie Technologies Inc. Bruker corp.). *In vitro* two-photon excitation spectra of OGB (hydrolyzed in 2mM Ca) and SR 101 (procedure described in Brondi et al., 2012) are reported in Figure 2.1. We chose 820 nm for Calcium imaging, given the relatively higher laser efficiency (Chameleon, Coherent, 80 MHz pulses) and the comparable SR 101-OGB fluorescence yield at this wavelength (a large disproportion would have led to an increase in excitation power in order to ameliorate S/N, with undesirable increment in phototoxicity). 820 nm excitation result in an homogenous green signal from neurons and a yellow to red one from astrocytes. In Figure 2.2,6,7 are depicted examples of good loading procedures. To distinguish EGFP positive cells in the context of a pan-neural green staining, excitation wavelength is shifted to 890 nm to acquire fields in which interneurons result brighter than EGFP-negative cells (Albota and Webb, 1998; Brondi et al., 2012). Relative position of fields acquired are tracked between successive Calcium imaging sessions and position of EGFP+ cells is reconstructed according to maps realized from images acquired at 890 nm (Figure 2.7). LFP recordings are performed with a 4μm tip glass pipette filled with aCSF, positioned in the imaged field or in close proximity (Figure 2.2,6,7). Ground reference is placed on the skull in a dorsal location. Amplifier (EXT-02F-extracellular amplifier, npi) bandpass is set at 0.1-1000 Hz, 1KHz gain recording in AC configuration. Line scan acquisition are performed selecting regions of the field imaged in which few well loaded cells are contiguous. Scanning mirrors are rotated to allow for a straight horizontal line to connect chosen cells. scanning line is extended through the software across the selected cells and a loop of line acquisitions is started (usually 1024 lines in each acquisition, reiterated 10-20 times). Each acquisition is usually about 1.5 s long with millisecond resolution (Figure 2.5).

Analysis

LFP signals are acquired (Axon Digidata 1440a, Molecular devices, Sunnyvale, CA) together with duplicated “end of frame” and “galvo” signals. End of frame signal is generated by the at the end of each scanned frame while the galvo one is a sawtooth output the duration of which is equal to that of each frame. Since LFP and microscope-generated signals, are acquired on a common time reference, it is thus possible to precisely align in time, electrical events with fluorescence outputs. Imaging series are then analyzed with ImageJ software (http://rsbweb.nih.gov/ij/), while LFP with pClamp 10.0 (Molecular devices). Using end of frame and galvo signals as reference, fluorescence and LFP data are time-aligned and processed with Origin pro 7 (OriginLab). In each imaging time series, a set or ROI is drawn for somata and neuropile, (ImageJ ROI analysis tool) absolute fluorescence in each ROI is converted in $\Delta F/F=(F-F_0)/(F_0\text{-dark})$ where F is the fluorescence value at frame “i”, F_0 is the average fluorescence value across the whole series and “dark” is the estimated value of electrical PMT “pedestal” calculated in a series acquired with laser off. LFP tracks are cropped according to reference signals and plotted mV over seconds. $\Delta F/F$ is then plotted against

time together with LFP. Motion artifacts possibly present in imaging time series, are corrected using Iris software (AstroSurf, http://www.astrosurf.com/buil/us/iris/iris.htm). As described in Figure 2.3 this procedure allow to manually translate ROIs in each frames in case of drifting series, without distorting $\Delta F/F$ signal. Imaging series with defocusing artifacts or manifest z-axis oscillations, are altogether discarded. Cross-Correlation analysis (see Figure 2.4) is performed using a custom build software.

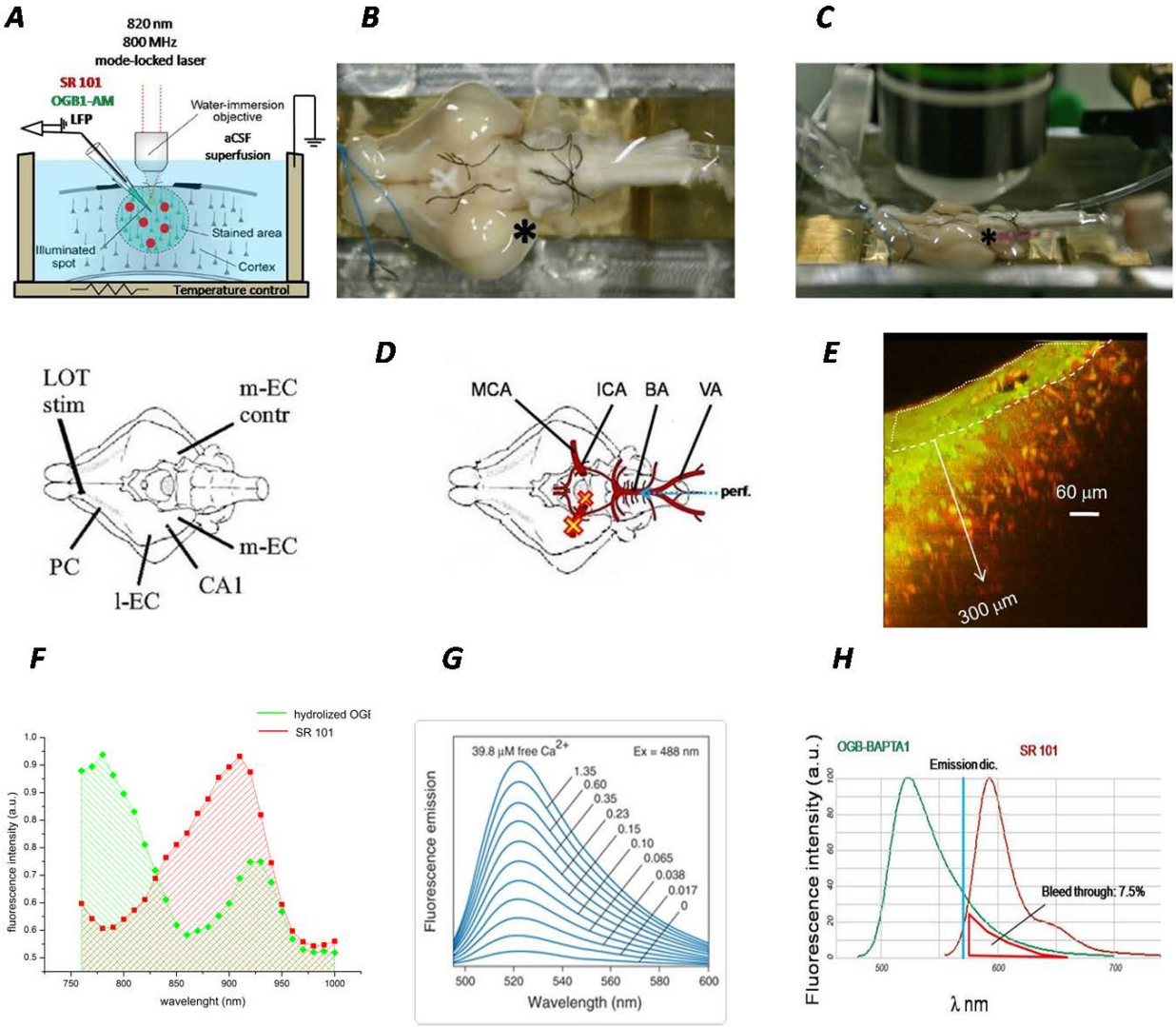

Figure 2.1: Imaging/electrophysiology set-up: the ex-vivo isolated Cavia porcellum brain. A) Scheme of the set-up. The brain, once explanted, is artery-perfused and submerged in aCSF. Temperature inside the perfusion chamber is kept low before bulk loading then gradually raised to physiological levels (38 °C). B) Ventral view of isolated and prfused isolated brain. Asterisk * indicate the enthorinal cortex (EC). Stitches occlude MCA and ICA. Dorsal cortex is glued to a custom made pyrex wedge to allow for a horizontal positioning of EC. To prevent gross motion artifacts most of the perfusion chamber is filled with small (0.5 mm) polished glass beads (Sigma). C) Lateral view of the set-up. Arterial perfusion cannula is visible on the right together with the glass pipiette for extracellular recording and bulk loading the red tip of which is positioned on the EC (*). An extracellular stimulation electrode, placed on the lateral olfactory tract (LOT), is visible on the left. D) Left: schematic depiction of the main neocortical ventral limbic structures in the guinea pig brain. LOT: lateral olfactory tract, PC: pyriform cortex, L-EC: lateral enthorinal cortex, CA-1: cornu

ammonis region 1 in the hippocampus (beneath the cortex), m-EC: medial enthorinal cortex, m-EC contr: contralateral medial enthorinal cortex. Right: scheme of the Willis' polygon. In red the artheries supplying the brain. MCA: medial cerebral artery, ICA: internal carotid artery, BA: basilar arthery used for perfusion (perf.), VA: ventral artery. E) Digital 3D coronal reconstruction of a low magnification two-photon progressive transverse optical sections acquired in EC after bulk loading with SR 101 and OGB 1. Optical sectioning extends to a depth of 300 μm in the cortex, below this level a "capsule" of myelinated fibers greatly increases scattering degradating the imaging acquisition. Dashed line indicates the surface level, the pipette entry site is visibile in the center. Neurons and astrocytes are stained Green, red dye only stains astrocytes. F) In vitro Two-photon excitation specra of Oregon green BAPTA 1-AM (green) and Sulforhodamine 101 (red). OGB 1-AM and SR 101 were dissolved in aCSF containing 15 mM Ca^{++}. actexymetylesther groups of OGB 1-AM hydrolyze in solution overnight at 45°C. Spectra are obtained keeping the number of photon constant while changing wavelength in steps of 10 nm. Red and green slopes are normalized. F) 0.1 mM OGB 1 solution emission intensity (Ex. 488) increases as [Ca^{++}] increases, as reported by Invitrogen (www REF ???). OGB 1-AM producers report a Kd of 175 nm ??? for BAPTA 1. G) Emission spectra of OGB 1 and SR 101 as reported by Molecular Probes (http://www.lifetechnologies.com/it/en/home/references/molecular-probes-the-handbook/indicators-for-ca2-mg2-zn2-and-other-metal-ions/fluorescent-ca2-indicators-excited-with-visible-light.html#head4). Upper badpass value for the detection dichroic mirror mounted on our set up is indicated as a vertical line in the graph (bandpass: ??? , estimated green-to-red bleedthrough: 7.5%).

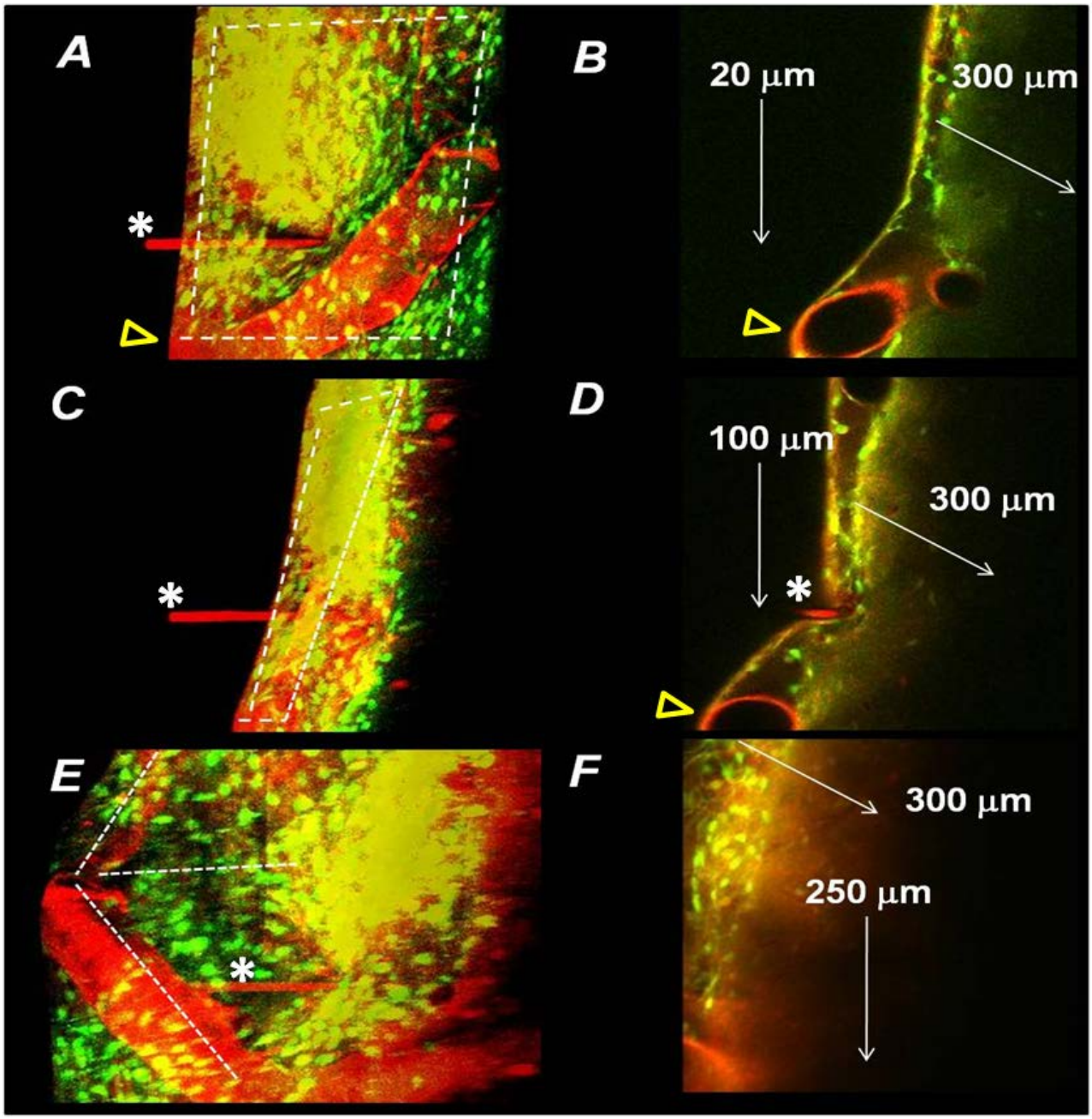

Figure 2.2: Two-photon in vivo imaging in Cavia porcellus EC. A,C,E) Digital 3D coronal reconstruction from transverse optical sectioning of increasing depth along dorso-ventral axis in EC: A) 0-20 μm, C) 0-100 μm D) 0-300 μm. the red shaft on the left is the dyes-filled pipette. Tangential thick blood vessels are visible in red. B,D,F) sigle frames from z series on the left relative to different depths: B) 20 μm, D) 100 μm F) 250 μm. Being spheroidal, EC bulges out from each optical sectioning plane, thus as the scanning proceeds deeper superficial layers in the cortex are progressively more distant from the center of the image. Upper L II/III portion is visible in each frame as a belt of green cells in the proximity of the surface (take the red electrode shaft for reference). The position of any given cell along dorso-ventral axis (vertical arrows) is not the actual depth of the cell in the cortex which has to be calculated from the surface (transverse arrow). The deeper the acquisition the fainter the signal also due to the decurrence of a thick myelinated bundle of fibers around 300 μm.

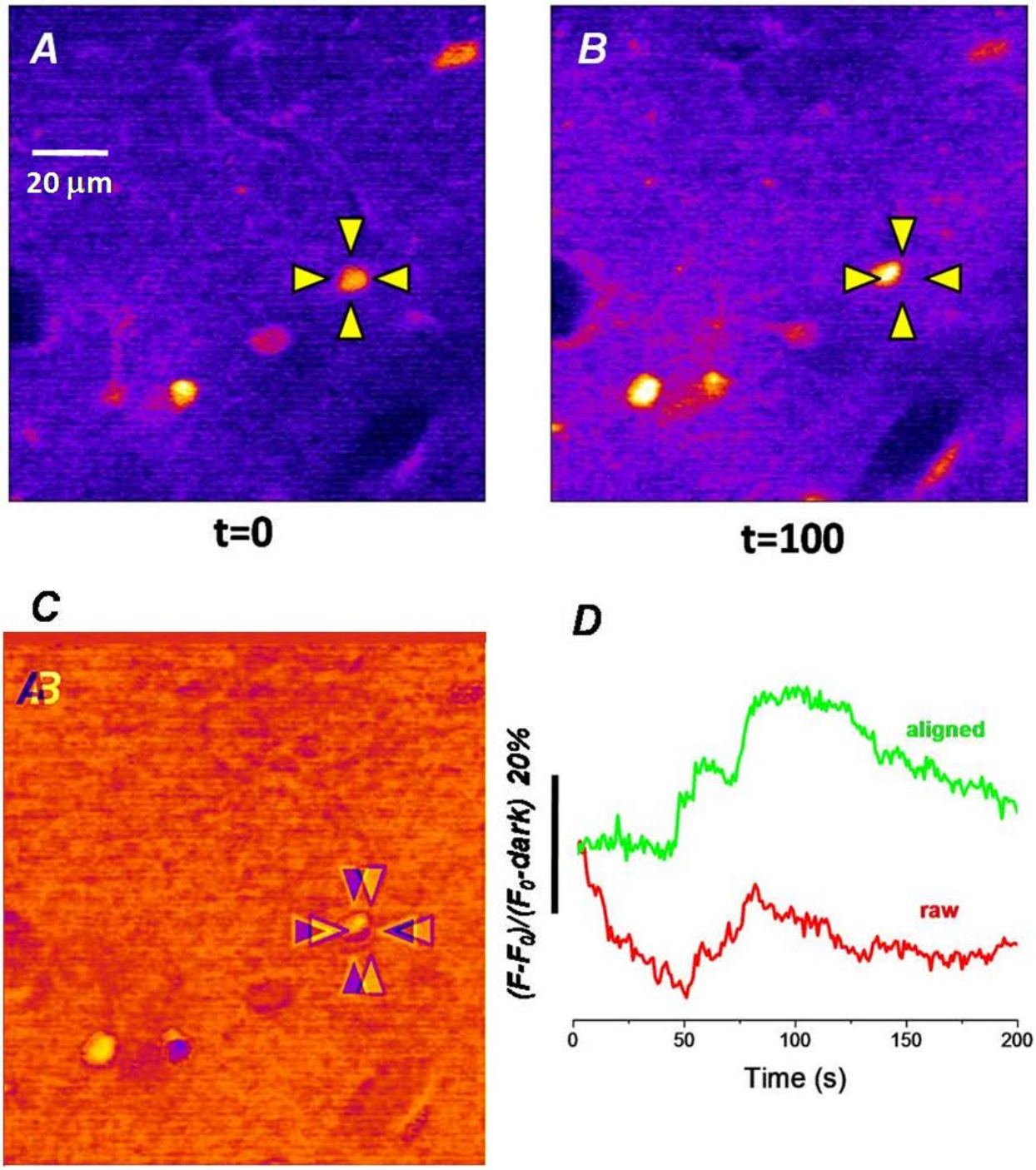

Figure 2.3: Drifting artifacts. A,B) Logarythmic scale color representation of two frames from a time series imaged in EC (frame number indicated below as "t"): blue background signal is the neuropile, "hotter" shapes are cells. Color intensity is relative to fluorescence intensity from OGB 1. The cell highlighted in A) experiences a Calcium transient peaking at 100th frame (B), yet its position is drifted as depicted in C) which is obtained subtracting A from B. "Colder" profiles are relative to frame t=0, hotter ones to frame t=100. Note the slight diagonal drift highlighted by triangles. Drifting artifacts are sometimes "non-homogeneous" as observed in C) where some cells seem to drift less than the indicated one. D) Relative fluctuation of fluorescence intensity (where F and F0 stand for "absolute instantaneous

fluorescence" and "time averaged mean fluorescence" respectively, while dark refere to background PMTnoise) in time as calculated for a static ROI encircling the cell indicated in A). the red track is relative to signal oscillations without any drifting compensation, the green one comes from the same t-series after IRIS alignment instead. After motion artifacts compensation (green), the Calcium-dependent increase in fluorescence in the highlighter cell is greater, less noisy and, more importantly, reliably aligned in time.

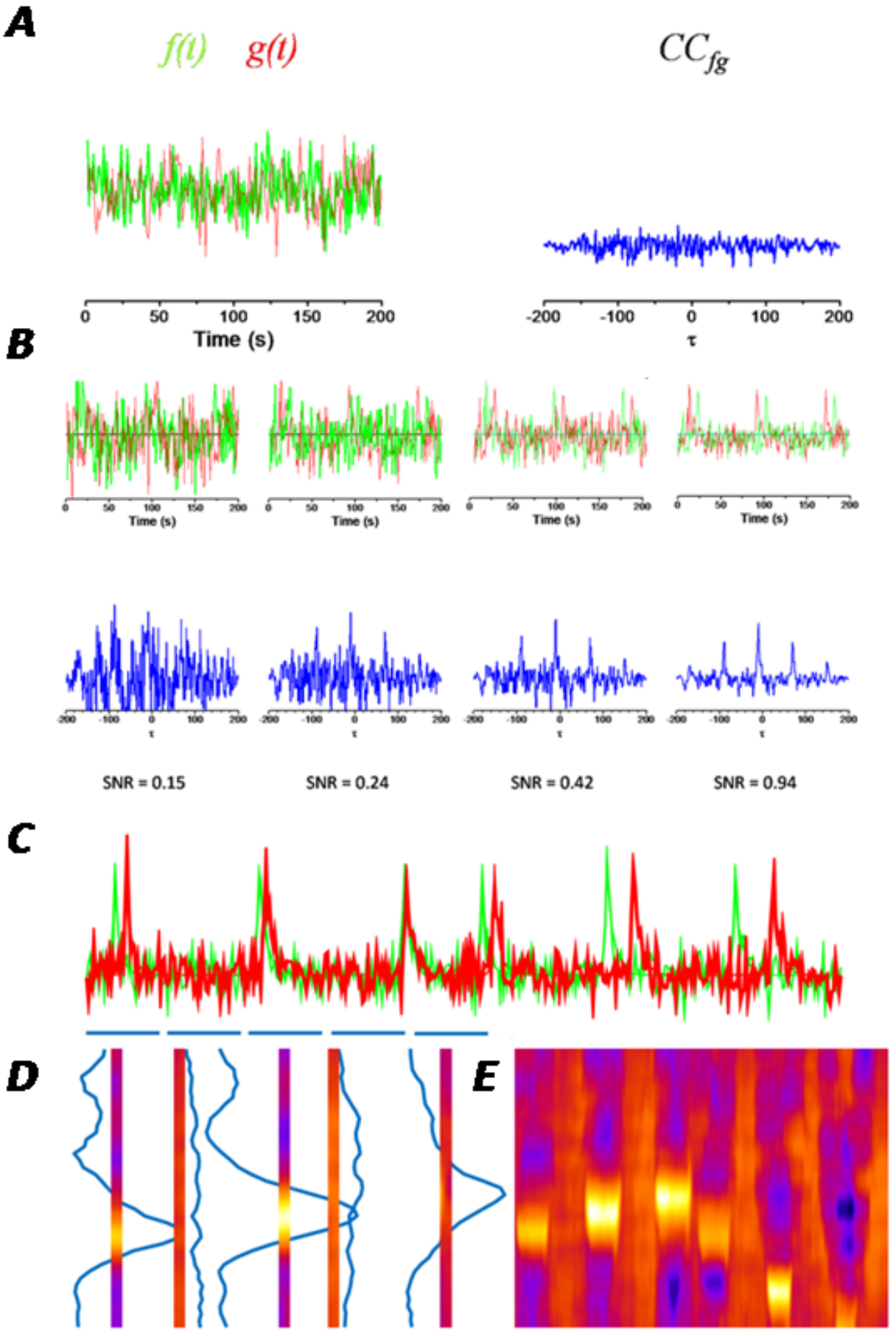
A
f(t)
g(t)
CC_{fg}
0
50
100
150
200
Time (s)
-200
-100
0
100
200
τ
B
Time (s)
τ
SNR = 0.15
SNR = 0.24
SNR = 0.42
SNR = 0.94
C
D
E

Figure 2.4: how to weave a cross-correlation carpet. A) *Left* two arbitrary stochastic function of time represented in red (G_t)and green (F_t) with same statistics (MAX, MIN, μ, sd, duration and aligned). *Right* result of the cross-correlation function $CC_{FG}(f * g)(T) = \int_{Tend}^{Tstart} \overline{f}(\tau)g(T+\tau)d\tau$ for continuous functions, where *T start* and *T end* are values of τ equal to time 0 and time 200 in A) left, or the start and end of the two functions considered. Orizontal axis is the"sliding" τ value or the time lag between F_t and $G_{t-\tau}$ where every value of CC_{FG} is calculated. F* is the conjugate complex of F_t . For discrete functions like those approximating imaging and LFP data, CC_{FG} $(f * g)(n) = \sum_{end}^{start} \overline{f}[m]g[n+m]$. At τs when CC_{FG} gets greater in amplitude, F&G cross correlates better while anti-correlation periods are translated in a deflection of CG_{FG}. B) upper row two periodic functions (F and G) were generated and "contaminated" with random noise of mean amplitude decreasing from left to right. Bottom row the result of CC_{FG} for the functions depicted above. Periodicity is easily spotted in the second plot from left while masked by noise in corresponding F and G plot above. C) Two LFP epochs during interictal events are here simulated adding quasi-periodic impulsive events (of constant amplitude) to F and G without a defined phase relation between the two functions. Blue lines below highlights τ intervals in which the power of the CC_{FG} function is calculated. D) Each vertical line is the intensity-to-color image of the power of CC_{FG} calculated in the windows indicated in C). Hot colors correspond to high power values. Blue lines running between consecutive colored stripes is are the actual plot of the mean power of CC_{FG} calculated inside the same time windows. E) colored stripes are "glued" together in time creating a carpet of CC_{FG}. The same procedure will be applied to some set of data, there F=LFP appropriately decimated and G=ΔF/F.

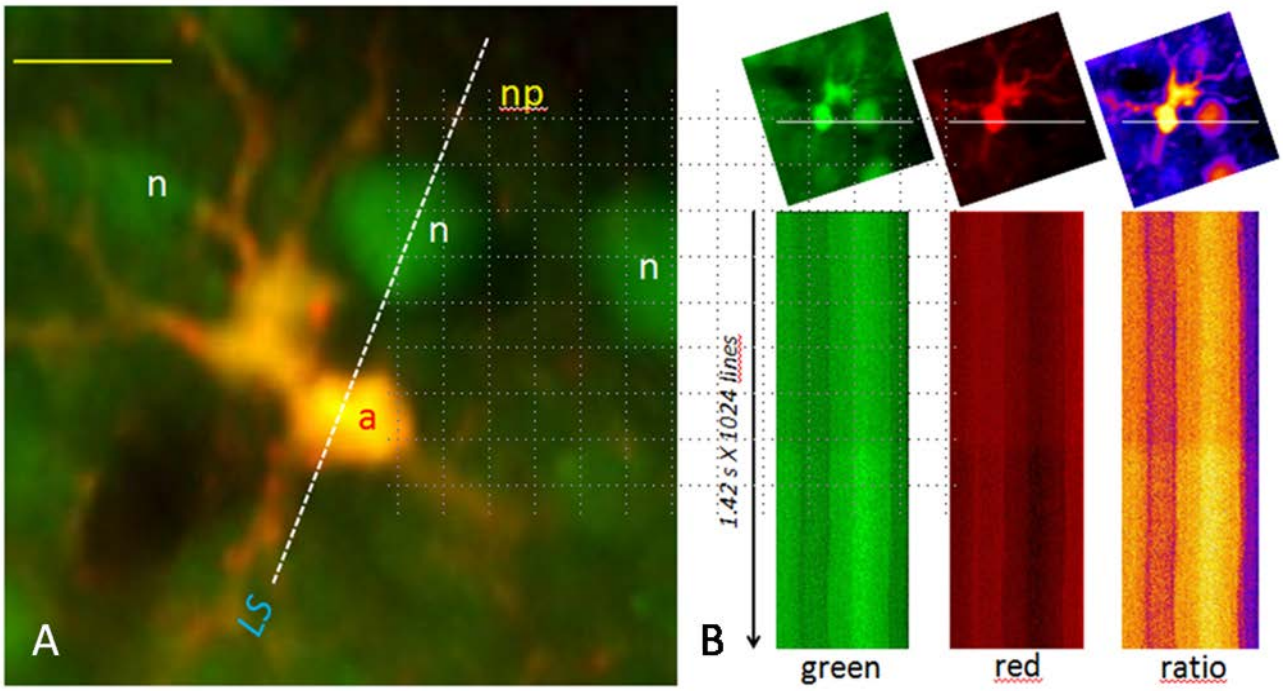

Figure 2.5: How to perform linescan fast acquisitions A) High magnification of an esemplificative field acquired in mouse visual cortex 250 μm deep. scale bar: 20 μm. the dashed line is a trajectory for the line scan mode crossing the soma of a twin astrocyte, a neighboring neuron and two flanking regions of neuropile. Fluorescence intensity is thus acquired only along the line for an arbitrary number of repetitions and in iterative mode in order to compose a "strip" of fluorescence intensity in time. The width of the stripe shall be in pixel that of the dashed line in the field acquired while the length is the chosen number of linear scan iteration. B) Top: the same image in A) separated in green Calcium dependent fluorescence and red Calcium independent-astrocyte specific fluorescence. The third image results dividing green image by the red one once average fluorescence of the two images are normalized. Ratio image is depicted in logarithmic intensity-to-color code. Bottom: changes in color intensity reflect fluorescence intensity variation along the line during the complete iteration, each line in the images being a single line scan. For a 40X objective, 4X magnification, 4.4 ns dwell time, 1024 lines iteration takes 1.5 s to be completed: each line is acquired on a millisecond scale. Variation of fluorescence intensity along the stripe are calculated in the green image for neurons and in the ratio image for astrocytes when needed. Since green fluorescence may change as a consequence of true $\Delta[Ca^{++}]$ or motion artifacts or a combination of both, red channel is used here as a reporter of Calcium independent fluorescence oscillations. Proceding as described for the images above, produces a ratio stripe. Whenever a motion artifacts manifests (drifting, de-focusing or cell swelling) changes in both green and red fluorescence are reported simultanously, conversely green fluorescence alone fluctuate only if a real $\Delta[Ca^{++}]$ take place. Since ROIs surrounding neural somata contains negligible red signal (because of two-photon PSF shape, red pixels bordering a green region and out of focus red fluorescence contaminate, although modestly, the Calcium dependent signal, see the almost-black line in the red stripe in the region across neural soma) the $(\Delta F/F)_t$ for neurons is calculated from green stripe while, when required (depending on the entity of the motion artifact), $(\Delta F/F)_t$ in astrocytes somata, processes or neuropile can be deduced from ratio stripe. In the case of even intense motion artifacts, green "fake fluctuation" are cancelled and in most cases a residual "true fluctuation" emerges with unmasked typical Calcium kinetics when a cellular event is superimposed. Furthermore, when a fluctuation is present in the red channel (motion related) in a region adjacent to a neuron, any concomitant green oscillation in the neuron should be carefully weighted-out.

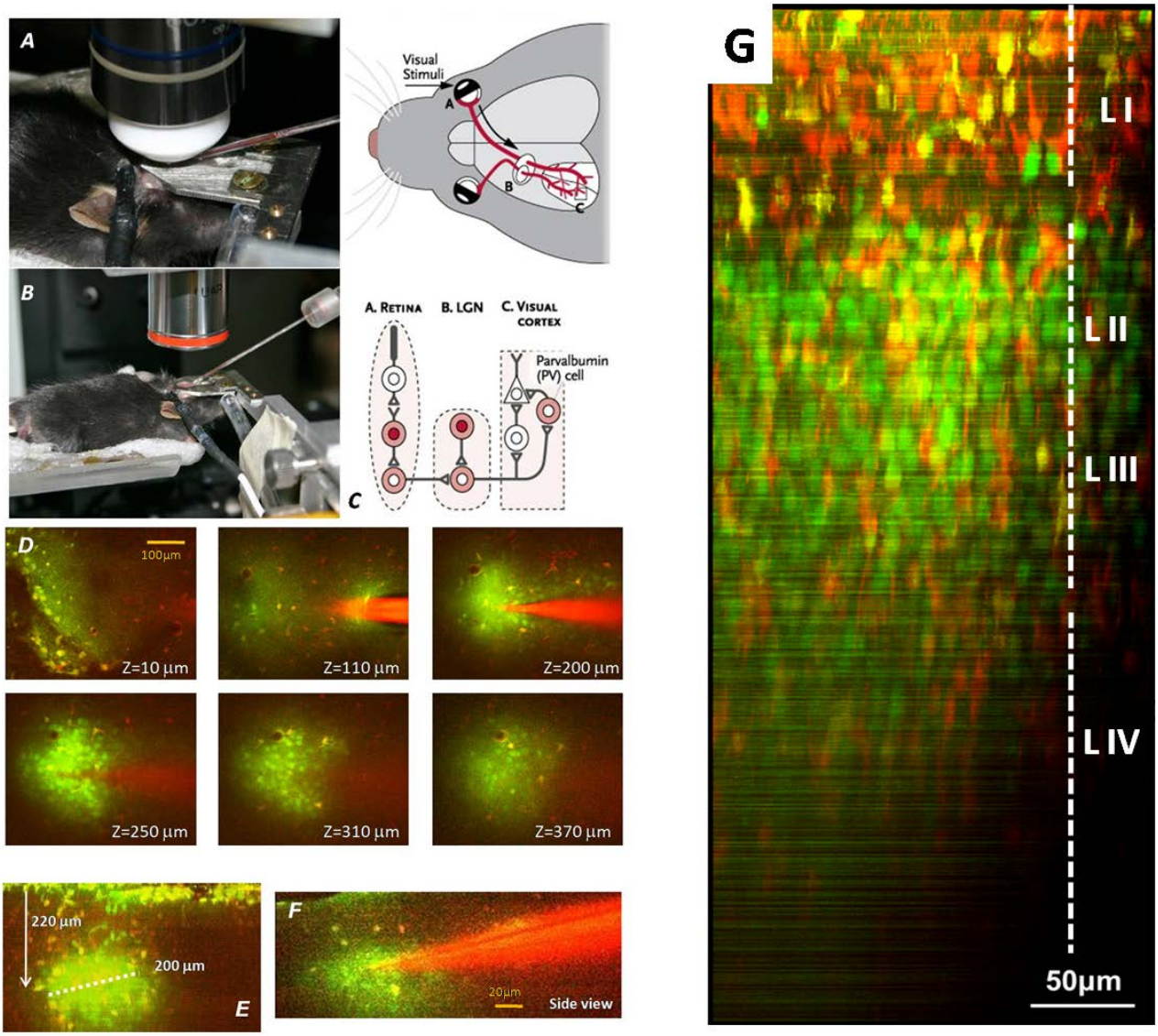

Figure 2.6: Mouse V1 model. A,B) Anesthetized animal is head fixed with a custom made hollow metal frame. Craniotomized region is placed under the objective and kept constantly supefused with aCSF to avoid dura mater sclerotization. Glass pipette with dye solution contains AgCl filament for LFP recording and is inserted inside V1 to a depth of 220 µm with an angle of 23°. The ground reference is visible attached to the back of the mouse head and the respiration aid tube is placed beside the nose of the animal. C) Simplified scheme of the first stages of "visual strams" from the eye to the V1. D) Six frames from a Zseries relative to different depth in V1 1h after OGB 1-AM and SR 101 bolus loading. Depth of optical section is indicated as Z=. the red shaft on the right is the glass pipette the tip of which is placed at 220 µm. Green cells are neurons red-orange ones are astrocytes. A diffuse green staining interveining between cell somata, mainly composed by neural and fine astrocyte processes, is clearly visible at all depths. E) Digital coronal view reconstruction of the injected site to show the extent of stained volume. F) Digital 3D coronal optical section reconstruction showing the position of glass pipette in the context of the velume injected. G) Coronal digital reconstruction of 0-400 µm transverse magnified optical sectioning. Layering of neural cell bodies is clearly visible with interspersed astrocytes somata aggregating toward the surface.

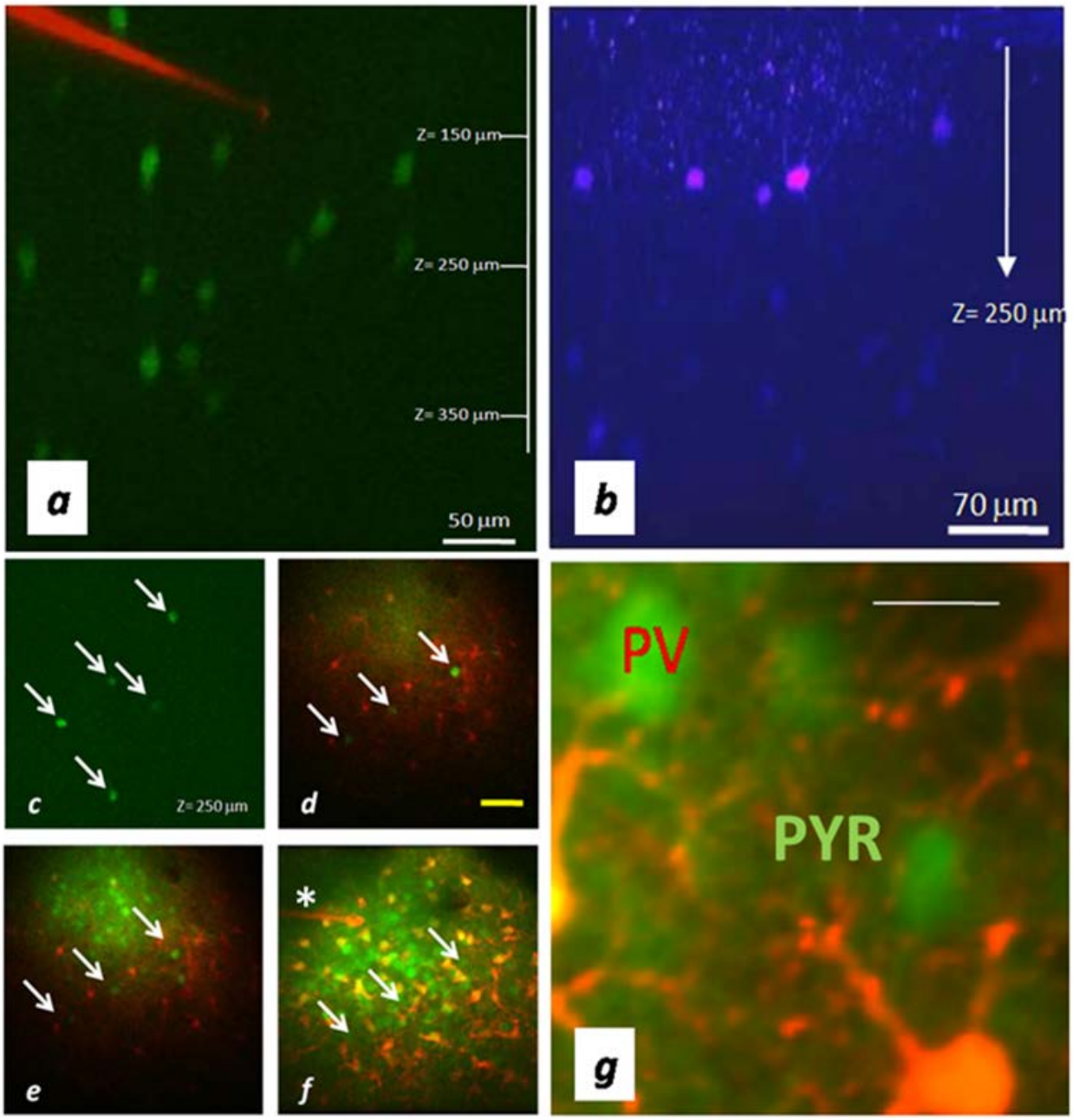

Figure 2.7: mapping GFP-tagged Parvalbumin+ interneuros. A) GAD-67 GFP mice inbred from J. Sanes original line, express GFP exclusively in Parvalbumin containing interneurons (REF ???). the image is coronal digital reconstruction of a Z-series 0-400 µm deep in the V1 cortex of a PV-GFP mouse prior to dye injection. In red is visible the tip of the pipette used for injection and LFP positioned at 150 µm. The image is acquired exciting at 890 nm at the peak for GFP absorption, each green cell is a PV-GFP interneuron. B) another acquisition of PV-GFP digitally reconstructed Z-series displayed in a intensity-to-color logarhytmic scale showing PV-GFP somata, dendritic processes extending in typical bushy shape. Some elongated axonal processes are also visible. C, D E, F) Single frames acquired 250 µm deep in V1 exciting at 820 nm. C) is acquired before dye loading. a flanking region of the excitation spectra peak of GFP allow visualization of PV-GFP cells (arrows). The exact position of these cells is recorded as x;y;z coordinates by the microscope software in order to avoid further ambiguity. D) 1' after dye injection, SR 101 (red) already stains somata and processes of most astrocytes in the field while a faint green shade is barely visible. Three out of five PV-GFP cells

are still well recognizable since no other cell soma have yet loaded OGB. The exact position of these three cells (arrows) is superimposable with image in C. After 30' from dye injection in E) many neurons are labeled in green the intensity of which is comparable with PV cells marked with arrows. After complete loading (1h in F) PV cells from C are no longer distinguishable without recovering coordinates acquired in C. the asterisk (*) indicates a new pipette positioned inside the imaged field. Scale bar in D 80 μm, C, E and F have the same reference. G) Average projection of a time series acquired at high magnification (scale bar 20 μm) showing detailed features of astrocytes processes as well as a couple of neurons. PV is actually one indicated by the arrows in C while PYR is a presumptive pyramidal neuron. No morphological criterion or other discriminants based on fluorescence intensity allow a confident identification of neural cell identity. In GAD 67-GFP expressing mice, a fine mapping of PV+ cells position is always performed before dye loading and software aided re-positioning after 1h allow a correct discrimination.

Chapter 3/ RESULTS:

3.1--- Dishinibition triggers recurrent epileptiform activity in medial enthorhinal cortex.

In the isolated and perfused Guinea pig brain, medial entorhinal cortex is kept alive and functional as demonstrated by local field potential activity and Calcium oscillations triggered by lateral olfactory tract extracellular stimulation. Low frequency afferent activation, result inefficient in eliciting Calcium elevations in astrocytes while neuropile and neurons are easiliy excited. Dishinibition via BMI perfusion starts a pattern of recurrent epileptiform events comprising short periods of interictal activit preceding high frequency ictal seizures of around 10s duration turning into a progressively dissipating afterdischarge phase. Perfused brains, are capable of sustaining several fully blown events at every BMI pulse, each with duration and spectral properties identical to the others. Ictal phases are associated with a strong increase in gamma band power of local field potential spectrum, in the face of a field coordination appearing weaker than both interictal and afterdischarge epochs. Large Calcium elevations are witnessed at each ictal event, pervading the whole imaged field.

Cavia porcellum brain blood supply system, has evolved to be diverted almost completely, through the basilar artery instead of carotids as more frequentely observed among mammals (REF). This rare arrangement turned this animal into a precious experimental model. Easy cannulation of basilar artery allow isolation of the whole brain to be kept alive and functional *in vitro*. *Cavia porcellum* isolated brain preparation, first described in Serafin et al., 1990, (Alonso et al., 1990; Paré et al., 1992; de Curtis, Llinas 1993; Mühlethaler et al., 1993) is an established technique, classically employed to retrieve information concerning electrophysiological behavior of brain regions reducing evident conundrums present when coping with alive animals. One of the most critical, is the difficulty in reaching ventral regions, buried inside cranium. Of prominent interest is the hippocampal para-hippocampal formation, the "gold standard" structure for the study of epileptiform activity (Boido et al., 2012; Biagini et al., 2013). Taking into account the vast complexity of the phenomenon, it is widely accepted that epilepsy is a subject hard to be investigated in simplified systems and any alteration of the naïve physiology, increases the intricacy (Models of Seizures and Epilepsy, Pitkänen et al., Academic Press, 2005; Reddi, Kuruba 2013). Compared to in *vivo data*, electrophysiological activity in *Cavia porcellum* isolated brain preparation, were also demonstrated to be preserved, as well as functional connectivity, blood brain barrier efficiency and homeostasys of extracellular milieu (Mühlenthaler et al., 1993; Librizzi et al., 2001; Mazzetti et al., 2004; Carriero et al., 2009; Biella et al., 2010). Although long studied, epilepsy still remain elusive from several point of view (Chang, Lowenstein 2003). Many autors suspect indeed that mechanisms underlying the establishment of the irritative zone, must be

investigated also in the context of astrocytes-neurons communication (Casadonte, Hydon in "Jasper's Basic Mechanisms of the Epilepsies" 4th edition. Bethesda (MD): National Center for Biotechnology Information (US); 2012; Losi et al., 2012; Gibbons et al., 2012; Devinsky et al., 2013; Crunelli, Carmignoto 2013; Verkhratsky et al., 2013). Although the role of astrocytes in brain physiology have been recentely broadly updated, their role in network disfunctions is still unclear. Furthermore most of the data available comes from *ex-vivo* slice preparations (Koyama 2013), in my opinion a far too simplified and degraded a model to be reguarded as a faithful one. This latter approach is the most exploited in the context of astrocyte research (and neuroscience at large), yet several drawbacks should be kept in mind: 1) only small scale circuitry is maintained, most often intra-layer tangential cortico-cortical connection alone 2) superficial cells in the proximity of cut planes, rapidly decay with unknown effect on deeper cells, while sectioned fibers triggers degenerate in afferent projections. 3) intrinsic rythmogenesis is greately reduced 4) blood-brain barrier is disrupted 5) sensorial stimulation is completely lost 6) blood is removed and extracellular fluid environment replaced with an infinite capacity buffering solution. Taking advantage of the Guinea pig isolated brain preparation we could relax 1-4 adverse conditions and introduce astrocyes into an otherwise electrophysiologically well characterized phenomenon (Condition 5-6 was further ruled out in the in vivo mouse model discussed later). The necessity of an isolated brain comes from the fact that epileptiform activity generation propagation and termination are best described for temportal limbic structures also because of the great incidence of temporal lobe epilepsy (TLE) in humans (Engel 2001). We thus attempted to merge classical LFP recordings with Calcium imaging in mEC of *Cavia porcellum* isolated brain. All Guinea pig experiments were performed together with Laura Uva and/or Federica Trombin from Marco De Curtis lab. Being an innovative approach, our first concern was to test the feasibility of the process and the sensibility of the preparation. Bulk loading procedure (Gaschuck et al., 2006), was adapted to the isolated Guinea pig brain with pretty good results. Given the importance of hippocampal-enthorinal circuit in limbic seizure generation, we focused on mEC, which is also among such areas almost inaccessible *in vivo*. Icy aCSF perfused in the animal at the moment of explantation, grant neuropreservation during the laborious surgical procedure. Henceforth the isolated brain is kept into 35° C aCSF perfusion and immersion until dye injection is completed. After bulk loading, temperature is raised gradually (0.2° C / 15') up to 37° C. LFP and two-photon Calcium imaging is then performed simultaneously in a couple of hours after OGB and SR 101 injection. Slow increase in temperature reduces the risk of aedema further diminished by 10 KDat dextran dissolved into perfusion/immersion aCSF as osmoprotector. Outflow of perfused aCSF is allowed from giugular veins. (further details in REF). In OGB, BAPTA 1 Kd for Calcium is optimal for neurons and astrocytes: Kd 175 nM, reported dynamic range in $[Ca^{2+}]$: 10-1000 nM (Grienberger, Konnerth 2012), Hill coefficient in vivo 1.48, τ rise, τ decay: 0.24 s, 0.38 s , maximum F change 316% (Reiff et al., 2008) making Oregon green BAPTA-1 the Calcium reporter of choice (For two-photon *in vivo* spectral properties and spectral separation strategies see Brondi, Sulis-Sato, et al. 2012). Other fluorescent indicators, although desirable for other properties, have a lower Q.Y. or 2photon Action Cross Section or shorter two-photon excitation wavelength (poorly penetrating) (consult online material from Invitrogen: http://tools.lifetechnologies.com/content/sfs/manuals/mp03010.pdf). Lateral olfactory tract (LOT) electrical stimulation, starts EC neural responses (Uva et al., 2006). In

order to evaluate both LFP recording accuracy and Calcium imaging efficiency, we stimulated LOT (a shallow decurrence extends from bulbs trhough perirhinal cortex) with an extracellular stimulation electrode placed on the olfactory efference pathway recording LFP and imaging concomitant Calcium oscillation in mEC (Figure 3.1). 10 ms/2 mV, 2 Hz reiterated trains of extracellular pulse efficiently discharged LOT and was picked up using LFP recordings 200 μm deep in mEC . Recored potential appeared in LFP epochs with short latency (tens of milliseconds) from pulse onset (triggered from LFP acquisition board with 0 lag). Latency indicates an active propagation against an otherwise passive "far field" effect. Furthermore, LOT stimulation at 35 °C had no effect on LFP recordings in mEC. Each pulse on LOT is recorded in mEC as a huge spike of biphasic polarity. Amplitude and brief duration are hallmarks of hypersynchronous activity. LFP oscillation are often observed after each LOT pulse train, dying away typically in 2-5 s from train end. This indicates local neural activity set into oscillatory mode from the input. No evidences of neural bursting activity was ever observed in LFP as a consequence of LOT pulses, neither during the train nor after. mEC is expected to operate in bursting modality during olfaction, associative processing or in epileptic discharges (Kiernan 2012; Aminoff et al., 2013; Chan et al., 2013). LOT episodic stimulation chosen pattern, is ineffective as a mimicry of physiological inputs. Calcium-dependent fluorescence is nonetheless observed oscillating widely only in synch with electrical stimulation from LOT. Both neuropile and neurons are activated during the train. Interestingly, neural tracks show Calcium oscillations after the train extending longer than those observed in LFP, while neuropile $\Delta F/F$ is silenced altogether at train end. Since LFP signature of oscillating activity is low in amplitude and long in duration, individual neurons might operate in a de-synchronized modality in this phase with little contribution to the neuroplie fluorescence. Also neuropile in the region imaged, is almost completely composed by LOT radiation with little contribution of mEC efferent fibers (Kiernan 2012). Despite the constant amplitude of LOT pulses, recorded LFP show signs of adaptation (reducing in amplitude as the pulses tick by) mirrored in the neuropile $\Delta F/F$ showing a rapid decrease after an initial peak. A second peak is shown in Figure 3.1 possibly due to reduced adaptation in time. Although LFP show no sign of regained responsivity, this might well be a local neuropile biphasic behavior which could be different in different neuropile regions. Neurons on the other hand, display $\Delta F/F$ increasing with train progression slowly returning near 2σ levels after train end. Astrocytes can be easily discerned thanks to SR 101 red fluorescence. Assuming neurons as refractory to red staining and other glial cells invisible due to scarse affinity to –AM based dyes and SR 101 (Nimmerjahn 2012; Schnell et al., 2012), in all data presented in the present work neurons are visualized green and astrocytes yellow-red. Astrocytes show a $\Delta F/F$ profile similar to that of neurons albeit delayed in kinetics (some 0.7 s lag) and strongly reduced in amplitude. This indicate negligible ROI contamination from neuropile's or neuron's into astrocyte ones. As extensively discussed further, hypersynchronous activity triggered by LOT stimulation, is probably not a proficient astrocyte stimulus. Furthermore, no signs of oscillatory Calcium activity is observed in astrocytes after LOT stimulation. These data allowed the validation of the surgical and recording procedures and support reliability of data further presented. Epileptiform activity is

triggered by 2’ arterial perfusion with aCSF containing 2mM Bicuculline meth-iodide (BMI, Sigma) readily recorded in mEC within 5’ from perfusion pulse end (Uva et al., 2005; Gnatvkosky et al., 2010). After perfusion, LFP evolve into sporadic hypersynchronous interictal events (Librizzi, de Curtis 2003; Uva et al., 2009) suddenly replaced by high frequency ictal discharges followed by clonic activity (Uva et al., 2005). BMI is a widely used pro-epileptic compound acting almost exclusively on GABAa channels. Some works report an antagonist action on hyperpolarizing small and maxi comnductance Potassium apamine sensitive channels: SK and BK (Charpak et al., 1998; Huguenard et al., 2009). What was long postulated as a general concept is that any pharmacological treatment producing imbalance in the intrinsic equilibrium between cortical excitatory tone and cortical inhibitory tone has a pro-epileptic effect. In this view any compound with pro-excitatory or inhibitory action (as well as those with “damping” effects like BMI), are regarded as pro-epileptic. Far from being this simple a scenario (see introduction and discussion), we started characterizing the typical alteration in LFP produced under BMI. One of BMI-induced LFP behavior is reported in Figure 3.2. Interictal spikes are described in LFP recordings, as strong synchronized, short-lived (<500 ms) impulsive events (Bautista 2013). Interictal activity (before red arrowhead in Figure 3.2 LFP track) is always scantly represented in this model: few spikes precedes first ictal event rarely found in following epochs until a further BMI pulse is aministered. Electrografic ictal phase (LFP between arrowheads in Figure 3.2) is conventionally defined by 3 parameters: duration > 3s, low synchronization, spectral power increase in >20 Hz bands (Avoli 2003). All recorded ictal phase have similar characteristics as described in Figure 3.2. Extraction of spectral properties, clearly define a low frequency activity preceding ictal discharge (mostly beta and theta bands) which in turn is populated with high frequencies as well as low ones (alpha, beta, gamma and theta, see Figure 3.2). Ictal phase is followed by epochs of increased synchronization and decreased power in gamma band frequencies. Of particular interest is the often observed “slow” interictal event preceding each ictal discharges (red arrowhead in Figure 3.2) (see Conclusions and Librizzi, de Curtis 2003). One of the principal informations provided by LFP, concern the degree of synchrony in the recorded population. As a rule when events are of small amplitude and long duration, population activity are considered poorly coordinated. Ictal activity is a prototypic poorly coordinated event: many frequencies are strongly represented in the power specrum while LFP voltage is low. This is interpred as the result of the “uncoupling” of oscillators with different characteristic frequencies each set free to oscillate reguardless the neighbor. As shown in Figure 3.2 STFT, no fundamental frequency is read in this phase. For reason unknown, strongly coupled cortical neurons become independent. STFT analysis allow an estimation of changes in the power spectrum durin time at different frequencies. We chose to plot the power of STFT since LFP deflection or inflection relative to baseline are not unambiguosely informative of the net sign of the current flowing (depolarizing or hyperpolarizing) but rather of the charge source-sink disposition along the recorded area. Some inference could still be attempted interpreting LFP as a bulk “current clamp”, but I prefere a more ready-to-use approach (for a review on this topic read Buszaki 2011). In the transition toward afterdischarge, LFP show an incremental gain of synchrony paralleled by fall in spectral power at all frequencies: a global oscillator emerges entraining the previousely incoherent population within seconds. Each isolated brain was LFP recorded and imaged concomitantly, while spending time in interictal-ictal or

afterdicharge activity. After each BMI pulse either an ictal event is recorded within 15' or the pulse is considered abortive and another one is administered. LFP without epileptiform activity for a period of 15' after last ictal recorded, is considered silent and a further BMI pulse is delivered. A maximum of 5 BMI pulses were used. Several ictal evens are observed at each BMI perfusion, or, frequently less than 15' elapses between consecutive ictal events at each BMI pulse. Characterization of ictal discharge events frequency at each BMI pulse is presented in Figure 3.3. A constant decrease of ictal presentation chance is observed in recurrent BMI perfusions. Also the number os seizures at each BMI pulse diminishes, which also mean that the brain becomes progressively refractory to epileptiform activity induction although a partial inctease il ictal chance is observed for events beyond the 3rd for the second BMI pulse. After first BMI pulse, probability of 2 consecutive seizures are highest and no more than 4 discharges were observed. Up to 5 consecutive events were observed for the second BMI perfusion and a maximum of 3 for the 3rd one. This could be due to progressive degradation of the preparation, vessel failure or desensitization against BMI. Ictal events, pooled accordingly with event presentation reguardless BMI perfusion or averaged out inside each BMI pulse, have similar duration. Since spectral properties, LFP shape and duration are preserved across ictal events, these were all considered equivalent. In all LFP recording epochs presenting epileptiform activity, three classical phases (*i.e.* interictal, ictal and afterdischarge) can be easily segregated. Discrete spectral analisys is presented in Figure 3.4. Superimposing ictal LFP power spectrum with interictal or afterdischarge ones, conspicuous differences emerge in the gamma band, which is much more represented in ictal phase. Gamma content is larger comparing ictal and interictal phases, while a samller divergence is observed between ictal and afterdischarge. A greater alpha, beta and theta power is also observed in ictal Vs. interictal. Also afterdischarge phase present larger gamma power compared with interictal. Gamma content differences are mirrored in $\Delta F/F$. Evaluating Calcium-dependent fluorescence intensity in frames acquired during single phases, was indeed possible to compare Calcium elevation between ictal and flanking periods. 5 representative frames per each phase were extracted from 10 series (different BMI and ictal presentations) and Calcium-dependent fluorescence intensity averaged across whole image. In each series was calculated the ratio between intensities (ictal/interictal, afterdischarge/interictal and ictal/afterdischarge) and average values across series is plotted in Figure 3.4. Fluorescence intensity is reasonably dependent only upon Calcium oscillations since [OGB] and laser intensity should be considered constant. Series affected with swelling were not included. If swelling was overlooked, this should be detrimental for ictal fluorescence intensity leading to a reduction in differences between ictal and other phases, since tissue bulging is predominantly present during ictal activity (Olsson et al., 2006). $\Delta F/F$ during ictal phase is consistently higher compared with interictal periods and an increase, although not significative, is observed compared with afterdischarge.

Figure 3.1: *Testing Calcium responses in mEC. A) Ventral view of the isolated guinea pig brain. Imaging /extracellular field derivation site, are marked with the red dot (REC) on the caudal margin of mEC. The afferent Later Olfactory Tract (white dashed line, LOT) and the region of external stimulation along LOT (STIM) are also indicated. Black stitch lengths are visible floating in the immersion solotutin extending from sutured carotids and tied brainstem. B) Average projection of two-photon in vivo optical sectioning along Z axis. 300 frames, from the surface down to 250 μm in layer II of mEC, are compressed in this image showing OGB and SR 101 fluorescence excited both at 820 nm. Yellow or red cells are Astrocytes while green signal comes from neural processes and somata. Scale bar: 40 μm. C) Digital 3D coronal reconstruction of the z-stack in B. Note the curvature of the surface highlighted by the white shade below which the glia limitans network extends. White bar marks the upper border of layer II. Scale bar 40 μm. D) Average projection of green fluorescence calculated along 300 frames (150 s) TPLS time series acquired 150 μm deep in mEC and represented with a logarithmic intensity lookup table. 2 neurons, 5 astrocytes and an intermingled region of neuropile are visible. scale bar 30 μm. E) Recording Calcium oscillation triggered by afferent stimulation. top: local field*

potential (LFP) recorded from mEC during two-photon Calcium imaging time-series. Large and fast deflections (boxed in blue dots) of the baseline activity are the signature of propagating bipolar stimulation of the LOT (positive deflections truncated at 1.2 mV for clarity). 10 electrical stimuli applied on the LOT (10 ms/2 mV, at 2 Hz) had 100% chance to be picked up in LFP from mEC. LOT low frequency stimulation like the one shown here, often elicited the onset of fast local field oscillations visible here as smaller and slower deflection in the red track (blue arrowheads). Bottom: LFP-time-matched oscillations of Calcium-dependent fluorescence intensity in a region of neuropile, 2 averaged neurons, 5 averaged astrocytes. Dashed horizontal lines of corresponding colors indicate the 2σ arbitrary threshold for significativity. A Calcium transient is dubbed "significative" (i.e. it is not entirely caused by stochastic noise) when its amplitude crosses the 2σ level of confidence calculated as fluorescence average intensity before the stimulation period in absence of any overt LFP signature. Calcium dependent oscillations were plotted as relative fluorescence intensity variations in time: $(F/F_0)/(F_0\text{-dark})$ where F is the instantaneous fluorescence intensity calculated inside a ROI in each frame, F_0 is the average fluorescence intensity across all frames in the T series calculated inside the same ROI and DARK is the estimated value of "pedestal" imposed by PMT. For each imaging session, DARK value is calculated acquiring few

frames with the same parameters used in T-series but with laser turned off. Different Calcium tracks referes to different ROIs from the same T series. A 20% increase (far above 2σ level) in fluorescence intensity is observed for averaged neurons track in coincidence with LOT stimulation. Fainter oscillations are observed for neuroplile. Astrocytes display a sluggish and weaker oscillation. Neurons and neuropile show a pattern of Calcium increases which do not recapitulate every single LOT pulse and are differet one another. Neurons and Astrocytes display a tripartite oscillation with neuron Calcium rising at the very first LOT pulse and Astrocytes following in apparent antiphase (0.7 s delay between neuron and astrocyte peaks). Neuropile response recapitulate that of neurons only at the beginning of stimulation and at its end while showing a protracted "silence" in between. Sub-liminal fluorewscence oscillations are visible in neurons even

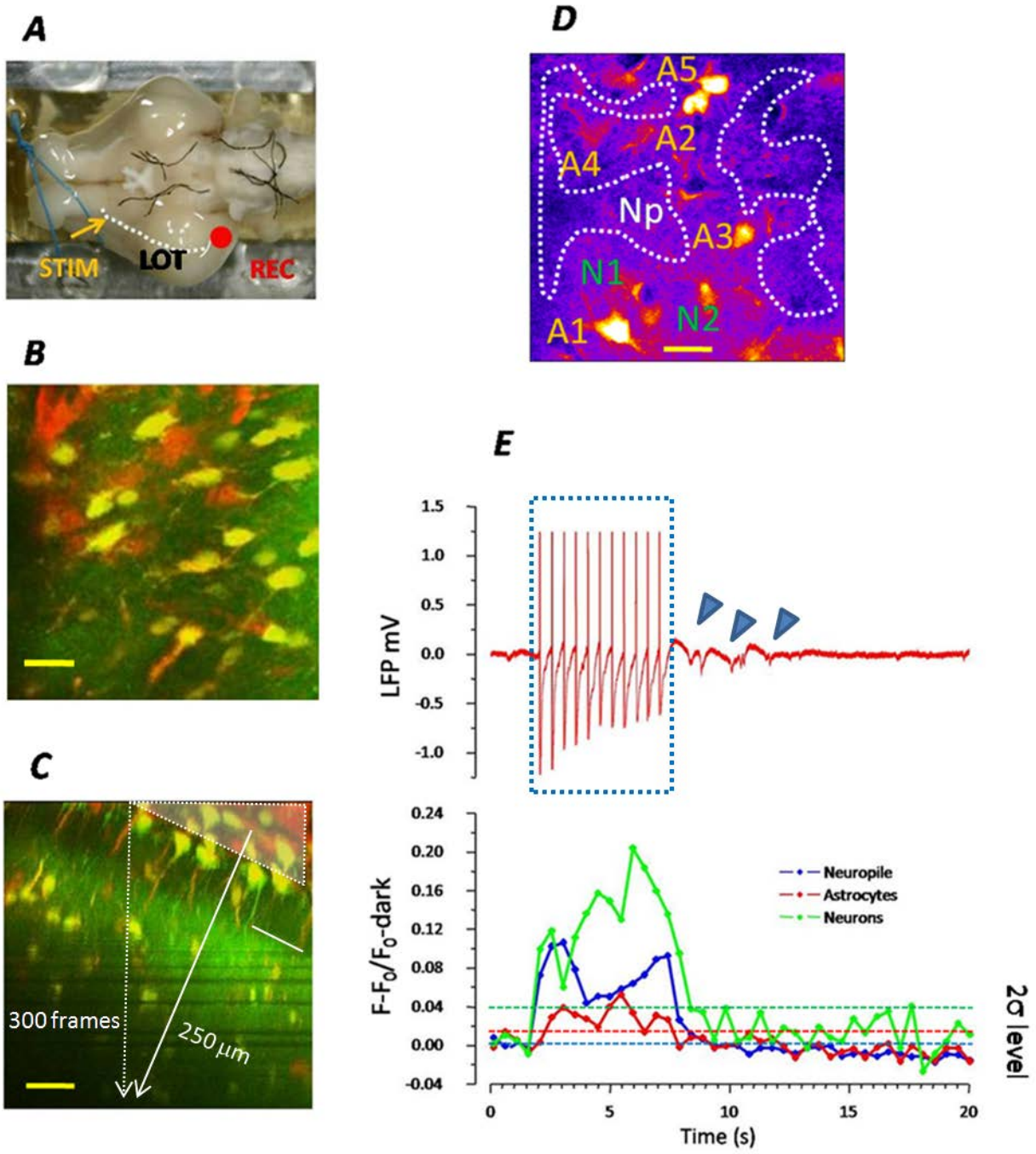

once the LOT stimulation is over, meanwhile neuropile and astrocyte tracks remain flat. No significative Calcium increase is observed prior the stimulation. T-series was acquired at 2 Hz.

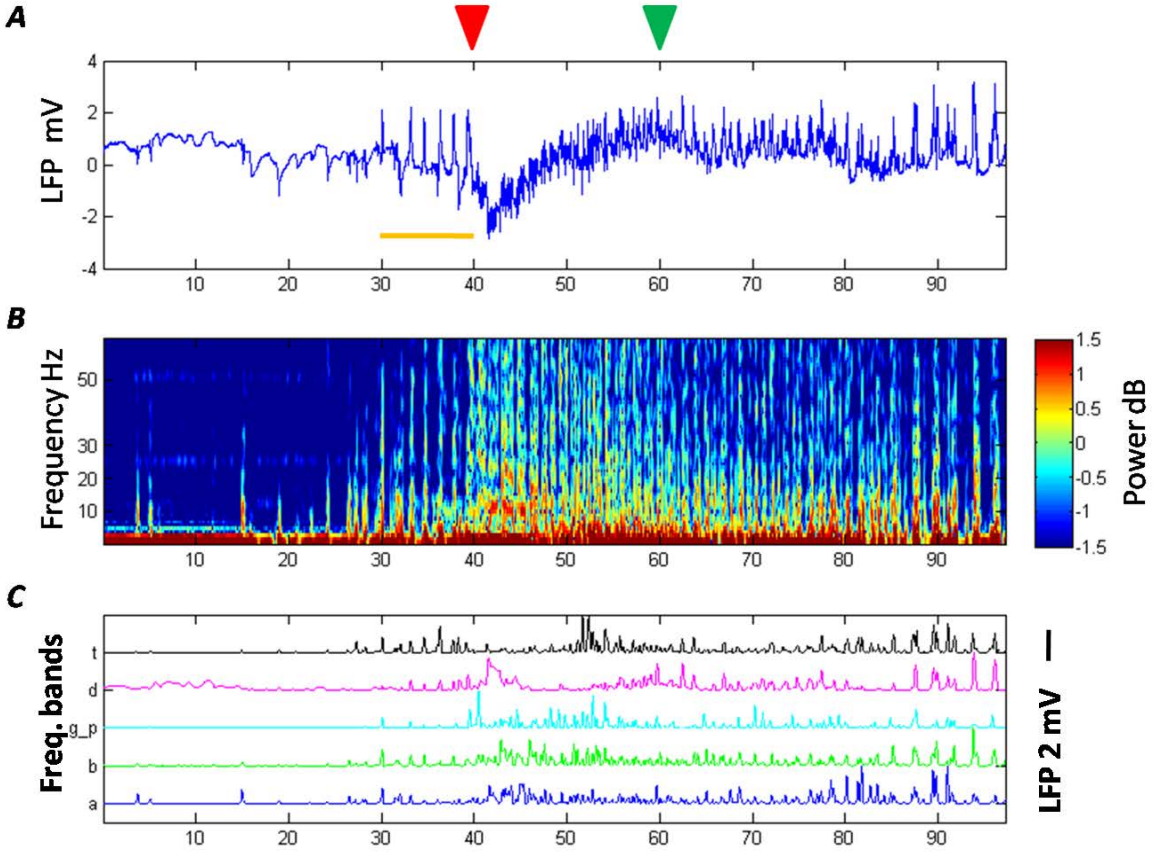

Figure 3.2: *Bicuculline methiodide (BMI) starts epileptiform activity in mEC. A) typical LFP track recorded from mEC after 2 min BMI/aCSF [2mM] perfusion pulse. The baseline activity terminate at around 30 sec from the start of the present recording, when interictal activity ensues (yellow underscore). After few fast interictal events, a larger-slower interictal transient (red arrowhead) marks the onset of ictal activity that is terminated some 20 seconds later with the afterdischarges manifestation (from green arrowhead toward the end of the recording. B) Short-time Fourier transform (STFT) of the LFP shown in A. Power spectrum is depicted in logarhythmic intensity-to-color scale: the minimum value is set as blue. STFT was calculated using a sliding Hanning window 0.5 second wide. Note the impulsive nature of interictal events and the massive elevation of power in the region of ictal phase. C) Bandpass decomposition of A). The classical electrographic bands were considered (α: 8-12 Hz, β: 12-30 Hz, γ: >30 Hz, δ: 0.5-4 Hz, θ: 4-8 Hz.). Ictal events are composed predominantly by activity in the frequency domain of γ, α and β bands. Note also the δ increase at the ictal onset and the θ increase at the ictal termination. Baseline activity shows minor α, δ oscillations. Interictal activity and afterdischarge bursting, being highly impulsive in nature, contaminates all frequency bands as observed also in B. In the Cavia porcellum isolated brain preparation, any event lasting > 3 s with spectral activity above 20 Hz is hereafter considered as ICTAL, "interictal activity" on the other hand, referes to non-baseline, impulsive LFP events of <3 s duration at least 0.5 s apart one another (or non-bursting). Afterdischarge manifestation are non-baseline impulsive LFP events of <3s duration separated <0.5 s clustered in trains (bursting). Brain activity in baseline is otherwise typical of de-afferented brains with dispersed slow waves of shallow amplitude, reminiscent of up/down state oscillations recored in anesthetized animals (see further in the text).*

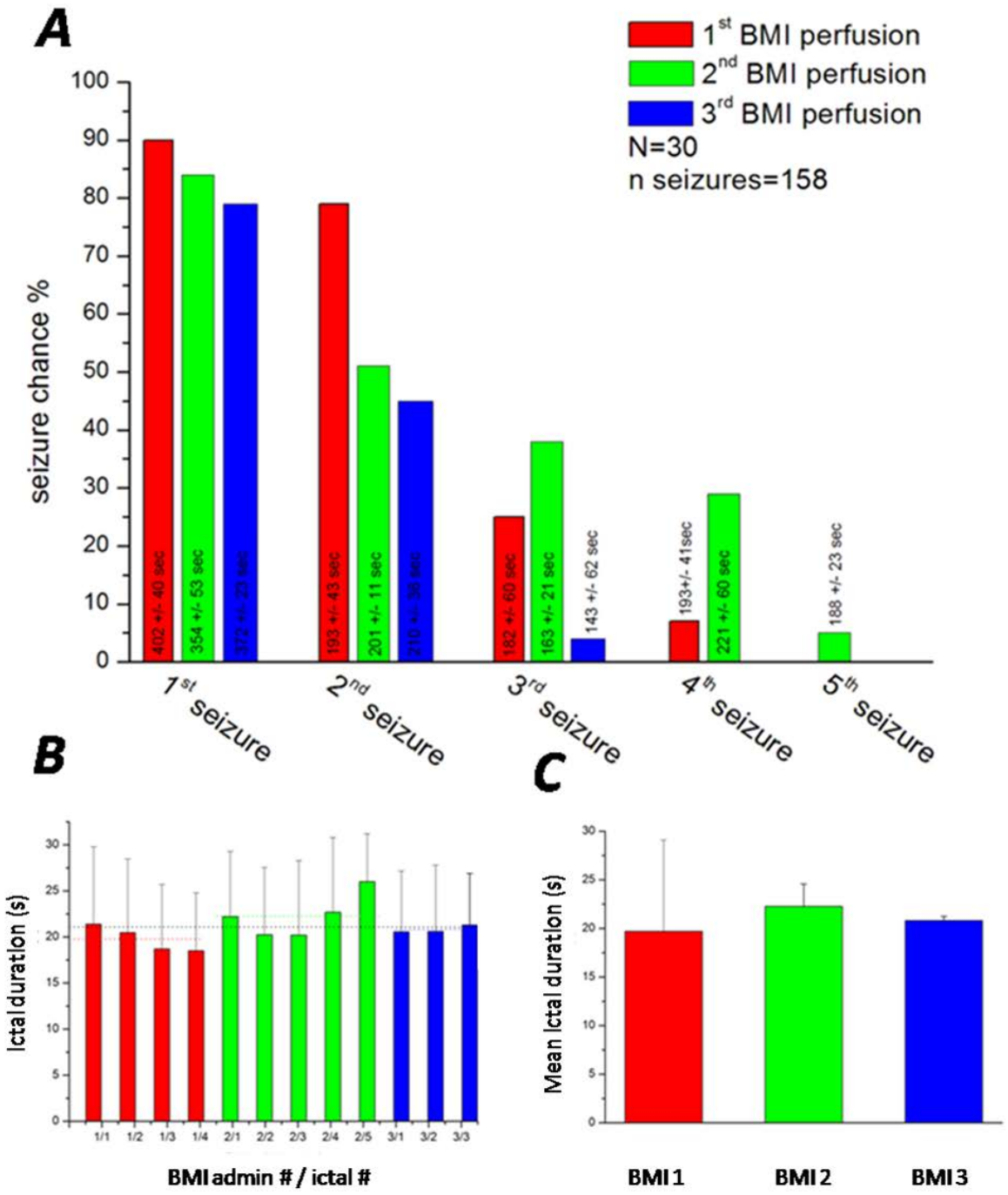

Figure 3.3: Characterization of ictal events occurrence in mEC under BMI. A) Histogram summarizing the progression of ictal activity in time and in recursive BMI administration. Ictal events were identified in LFP according to the criterium described in the text and in figure 3.3. Nth BMI perfusion was considered efficient if at least one ictal events manifested within 15 minutes after 2 minutes perfusion pulse. Events falling beyond 15' were not included in the statistic. Perfusions were classified as 1st, 2nd and 3rd, when efficient in the same brain. BMI pulses further than the third, were not included in the statistics as seldom observed to be efficient. A period of baseline activity of at least 15 minutes must be interleaved before the nth+1 perfusion. Bars height indicate the probability of ictal events after nth

perfusion across all animals (30). For each BMI pulse, several ictal events were often observed, hence, histogram bars are grouped also according to the order of presentation of the events theirselves. “First seizure” probability is here defined as the number of ictal events observed within 15’ from first BMI 2’ pulse divided by the total number of recordings in 30 animals. Different colors refers to successive BMI pulses. The “n^{th} seizure probability” indicates the number of events recorded within 15’ after the n^{th}-1 event for m^{th} BMI pulse, divided by the number of recordings in which m^{th} BMI perfusion was administerd. Any ictal events observed before 2’ perfusion was over in each BMI pulse were rejected from the statistic. Events beyond the 5^{th} at each BMI perfusion was never to be observed. A total of 158 ictal events were recorded from 30 animals. Red bars indicate that 27 ictal events were recorded within 15’ from the first perfusion in a total of 30 experiments. A second ictal event at first BMI exposure, show up in 25/30 cases. The probability of a 3^{rd} and a 4^{th} ictal event after the first BMI exposure, drops down to 25% and 10% respectively. The second perfusion of BMI starts an ictal in 26 aniamls, a second ictal in 15 esperiments, a third one in 12, a fourth in 10 a fifth in 2. The third BMI pulse starts a first ictal with 80% probability, a second one in 43.3% of the cases and a third one in 3.3%. Not in all cases each class of seizure was observed, a general decrease of ictal probability is observed both in recurrent BMI perfusions and in recurrent ictal per each perfusion. Occasionally, no n^{th} ictals were observed (in one case no second and thus no third ictal at second perfusion, in another no ictal at third perfusion, no fourth or fifth seizure at any third perfusion, nor there was any fifth ictal at any first perfusion). Yet, ictal activity might re-appears at further perfusions. Along each bar is reported the time elapsed between a seizure and the preceding one or, in the case of first seizures, the time from BMI pulse and seizure manifestation. Values are mean for 30 experiments with standard deviation. B) Ictal event duration grouped according to BMI administration. Duration was estimated fixing the slow large interictal deflection preceding the high frequency activity as the start of ictal event and the first synchronous afterdischarge event as the ending point (see figure 3.2). Red, green and blue are durations of ictal events at first, second and third BMI administration respectively. There is no significative difference between classes of ictal events neither inside any BMI perfusion group neither across BMI perfusion groups. A trend toward an increase in duration for the second BMI grup of ictals is nevertheless observable. Standar error is reported above bars. C) Average duration for each BMI group, no significative differences are observable. Total mean ictal duration is 21.08 +/- 0.7 s. Furthermore, no significative differences were ever observed among different classes of ictal events on the basis of spectral power profiles, henceforth all ictal manifestations are considered equivalent.

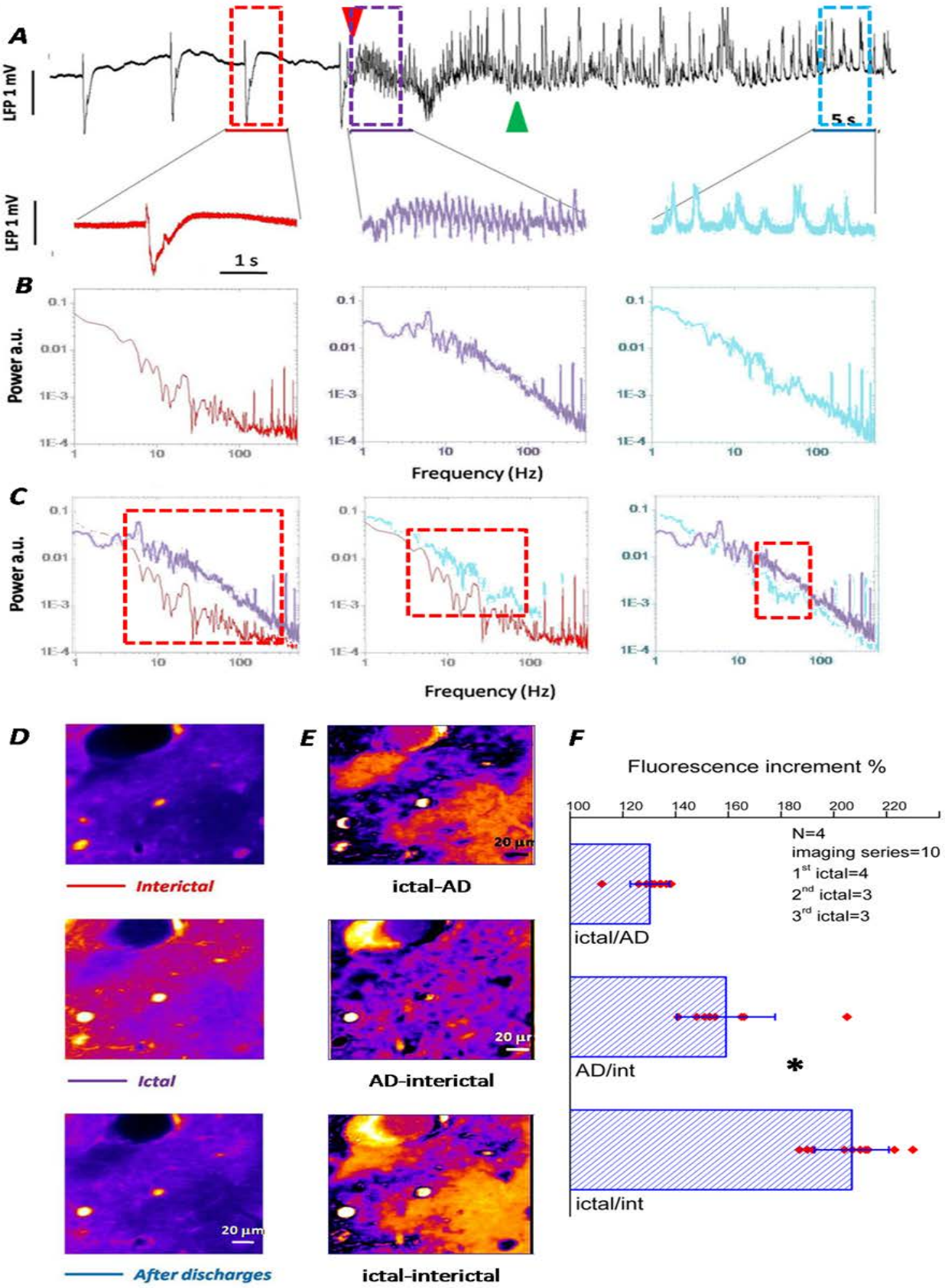
A
LFP 1 mV
5 s
LFP 1 mV
1 s
B
Power a.u.
0.1
0.01
1E-3
1E-4
1
10
100
Frequency (Hz)
C
Power a.u.
Frequency (Hz)
D
Interictal
Ictal
20 µm
After discharges
E
20 µm
ictal-AD
AD-interictal
ictal-interictal
F
Fluorescence increment %
100
120
140
160
180
200
220
N=4
imaging series=10
1st ictal=4
2nd ictal=3
3rd ictal=3
ictal/AD
AD/int
*
ictal/int

Figure 3.4: How can spectral variations in epileptiform activity be read in terms of Calcium oscillations? A) Typical LFP behavior during iterictal, ictal and afterdischarge phases. Ictal events start with the abrupt flattening and thickening of LFP almost invariantly preceded by a "slow interictal event" (red arrowhead). The termination of an ictal event is gradual: coherence emerges in the LFP in the shape of synchronous fast deflections (green arrowhead indicates the first of the series). The first recognizable afterdischarge "spike" marks the termination of the ictal phase. B) Top: magnification of 5s stretches of LFP in A, representing a fast interictal event, the ictal phase and late afterdischardge bursting. Down: power spectra calculated from the LFPs chunks above, normalized for the mean power value of the three samples. C) Superposition of power spectra: ICTAL+INTERICTAL (left), ICTAL+AFTERDISCHARGE (right) and AFTERDISCHARGE+INTERICTAL (center). When compared with interictal spectrum, ictal one show a peak in power inside a huge range (<10->100 Hz) of frequency band as highlighted by the red box. The increase in spectral power is of a lesser extent (below 100 Hz) when afterdischarge and interictal spectra are compared which is further diminished (20-60 Hz) between afterdischarge and ictal spectra (red boxes). Two distinct transitions are observed shifting from ictal to interictal activity: an overall decrement in spectral power and a shrinkage in peak-frequency bandwidth. D) Each image is the average projection of 5 frames from a Calcium-dependent fluorescence T-series acquired concomitant with the LFP in A. Position in time of avery set of 5 frames corresponds to the time windows in A. Intensity of Calcium dependent fluorescence is normalized among images and coded in a logarithmic lookup table. Note the massive and diffuse average [Ca^{2+}] increment during 5s of ictal activity compared with the other images. E) Pixel by pixel differences were calculated between images in C: ICTAL-AFTERDISCHARGE (AD), AD-INTERICTAL and ICTAL-INTERICTAL. Each difference image presents with a peculiar distribution of lit regions and dim ones. F) In 10 imaging T-series encompassing each the whole transition from interictal-ictal-afterdischarge (each phase at least 5 seconds long), 5 frames were pooled representing every LFP phase. Average intensities were calculated across each whole image in all 5 frames set. Three sets of ratios were calculated among the average intensities data set: ICTAL/AD, AD/INTERICTAL and ICTAL/INTERICTAL between values from the same T-series. This allow for a direct comparison of Calcium-dependent fluorescence intensity changes between imaging sessions acquired in different conditions (namely: OGB loading level, laser power and background noise, as other parameters were always kept fixed) and even between different animals. 4 different brains produced a total of 4 1^{st} ictals, 3 2^{nd} ictals and 3 3^{rd} ictals, triggered by 1^{st} BMI in all 4 cases. Bar heights indicate the average value calculated ration, while red dots correspond to single ratio values. The histogram reports a huge (2.060.±0.15 times) increase in Calcium-dependent fluorescence intensity between ictal and interictal phase, a smaller one (1.59±0.18 times) comparing afterdischarge with interictal activity and a tiny one (1.3±0.08 times) between ictal and afterdischarge. This Calcium behavior parallels the 20-60 Hz power contribution observed in spectral comparison in C.

3.2---Two-photon Calcium imaging during ictal phase reveals massive activity in astrocytes.

Ictal onset is mirrored by a biphasic neuropile Calcium increment characterized by an early plateau and a late peak. The latter is aligned in time with ictal termination, when also astrocytes display a large Calcium increase. During ictal phase, astrocytes undergo a steady increase in Calcium under neuropile plateau. Percentage of responsive astrocytes changes dramatically from near 0% during interictal activity into almost 100% in ictal phases.

Figure 3.5 A show a Z-stack aquired in EC from the surface down to 200 μm depth at which signals fade. The intricate structure of astrocyte processes is clearly visible from red stainig. Also a diffuse and strong neuropile green signal is observed. Unfortunately few neurons are imaged being layered below a myelin "capsule" in the mEC cortex (approximatively below 200 μm). In Figure 3.5 Calcium oscillation of averaged 6 astrocytes is plotted compared with neuropile's one and LFP, astrocyte ΔF/F is instead analyzed at single cell level in Figure 3.6. Astrocytes display a flat ΔF/F along all the interictal phase (before the red arrowhead), while neuropile show peaked transients aligned with each LFP event. Neuropile ΔF/F exhibits a slower increase at ictal start developing in a first plateu encoppasing the whole duration of high frequency activity. No appreciable Calcium spikes are observed in this phase in neuropile ΔF/F. Given the LFP high frequency content, ictal event could be under sampled by imaging (2 Hz) thus ΔF/F plateau might results as a sort of low pass filtering. A second rise in neuropile ΔF/F is observed as soon as the ictal phase turns into the clonic activity (green arrowhead). This second increase peaks in few seconds and decay pretty fast (around ten seconds). No sign of fast ΔF/F oscillation are observed neither on top if this later Calcium increase although LFP frequency is much more slower than ictal with clearly discernible impulsive events resembling ictal ones. Interestingly, interictal events always presents with hyperpolarization of LFP while afterdischarges and ictal phases are characterized by depolarization. The difference in LFP polarity might be due to different source/sinc geometry, with ictal and afterdischarge phases generated locally. Although hypersynchronous events can be generated both in hippocampus and in mEC (Avoli et al., 2006; Jiruska et al., 2013) as well as high frequency events, travelling to and from mEC along Schaffer's collaterals (Barbarosie, Avoli, 1997; Luhmann et al., 2000; Wozny et al., 2005), BMI perfused whole brain organize focal ictal activity inside mEC first, spreading toward CA3 (Labyt et al., 2008). Given these premises, LFP hyperpolarization may be interpreted as the telltale sign of hippocampal to mEC efferent activity, while high frequency ictal activity as entorhinal-fugal propagation. Also a large amplitude interictal LFP may arise as a consequence of neural firing entrainment between hippocampus and entorhinal cortex (Jiruska et al., 2013), while tonic phase low amplitude one, would be produced by propagating ictal activity approaching de-synchronized CA3 (Avoli et al., 2006). Progressive transition toward large afterdischarge events, consequentely, may well be the token of a developing synchronization process gaining strength. In this perspective, neuropile ΔF/F should be a faithful mirror of single-cell neural behavior during hypersynchronous interictal activity (as shown later in the context of mouse V1) but a mere average of neural population activity in ictal phase. At the onset of ictal

phase, neurons inside the focus turn into bursting mode uncoupling one-another hence the smooth ΔF/F in focus-fugal neuropile signal averaging out out of phase sural bursts. Conversely, when synchronization is re-gained in afterdischarge phase, neuropile ΔF/F shows interictal-like event while neurons are drifting away from high frequency bursting activity. Transition from hypersynchronous activity/non bursting neurons toward desynchronization/bursting neurons, sees astrocytes completely silent. As in the case of interictal phase astrocytes ΔF/F remains locked until the transition toward afterdischarge activity. Red plot start the rising phase in precise alignmet with the green mark. Astrocyte and secondary neuropile peaks are perfectly aligned. The possibility of ROI contamination from neuropile into asterocytes can be ruled out considering the complete absence of interictal ΔF/F peaks inside astrocytes ROIs. As deducible from these data, astrocyte Calcium is only triggered at the transition from ictal to afterdischarge activity or, at time in which neural firing starts gaining correlation. Calcium elevation in astrocytes fades in around 10s to remain almost silent hereafter (further discussed). The downward transient in red track at ictal onset is interpreted as de-focusing artifact absent in other data further shown. A shift in focal plane is a conceivable description, since a reversible decrease in Calcium or OGB concentration below baseline only in astrocytes is implausible. concentration De-focusing might be due to acute tissue swelling, the magnitude of which is greately variable across expreriments. Most of specimens are indeed subjected to a slowly developing aedema wich impose a Z-focus correction of few microns in several minutes. Nonetheless, instantaneous swelling, is often associated to different scenarios ranging from ischemia to spreading depression or ictal activity as also observed from intrinsic imaging experiments (Witte et al., 2001 Bahar et al., 2006; Mané and Müller, 2012). Acute swelling is a process different from aedema and little de-focusign effects are expected. Should de-focusing happens, neuropile shall be immune (blue track is indeed increasing instead of diminishing) since any neuropile focal plane can be considered homogenous with respect to Calcium behavior as far as little shifts are taken into account and relatively large neuropile ROIs are examined. On the other hand, astrocyte control of vasodynamic properties, might strongly contribute to tissue swelling (Hydon and Carmignoto, 2006), thus larger de-focusing artifacts should be expected in astrocyte expecially in the processes fabric. K^+ buffering, siphoning and pH homeostasys are functions based on water flow thus associated with a propensity in astrocytes swelling (Parpura and Verkhratsky, 2012) exacerbated by intense neural activity. It is thus plausible that transient artifacts like that observed in Figure 3.5, culd indeed be the consequence of astrocyte engagement. In Figure 3.6 Calcium behavior in 3 individual astrocytes is displayed aligned with yet another LFP epoch. In this and other presented examples, no sign of de-focusing is observed and a easier description of astrocyte behavior is offered. ΔF/F of three astrocytes shows a peak in each cell at the end of ictal phase as described in Figure 3.5. Different slopes distinguish sigle cell activities: while the red one is smooth and symmetric, the other two show a first plateau , most visible in the orange one, followed by a peak. Blue and orange tracks are similar to neuropile in figure 3.5. All cells are perfectly aligned in their peak and blue and orange track start rising simultanously with the red one at ictalk start. Since there is no sign of astrocyte Calcium oscillations during afterdischarge phase, when neuropile is “sparkling”, it seems implausible that the first plateau in some cells could be the result of neuropile contamination. This also implies that different astrocytes may display different Calcium behavior in response to ictal activity. The

percentage of astrocytes showing some sort of Calcium increment (above 2σ level, in all cases peaking at transition from ictal to afterdischarge) during ictal activity is > 90% of all *in Cavia* observed astrocytes. 10% of all astrocytes also show transients in interictal phase and all of these also display ictal Calcium increase. Discarding those cells showing interictal Calcium transients (ROI contamination here is considered consistent and astrocyte ROIs classified as ambiguous; further discussions about interictal activity and astrocyte ΔF/F are presented in the context of mouse V1 experiments), 90% of astrocytes behave like in picture #6. A representative average behavior of astrocytes displaying a first plateau is presented in figure 3.7 compared with neuropile and LFP. LFP (black) was decimated to meet imaging frame rate (from 1KHz into 2 Hz) and the amplitude is log-color coded below (same procedure applied for subsequent computations). Each band in the color raster is thus the average value of LFP amplitude inside a time window one imaging frame long. Neuropile ΔF/F first transient is actually steeper than astrocyte one, although starting and terminating concomitantely. Different kinetics suggest different mechanisms operasting in these two districts. If so, astrocytes showing a first plateau, might be activated at ictal start as is the case for neuropile. A same seeding event, seems to start Calcium oscillation in neuropile and astrocytes at the same point in time. If LFP interpretation is correct , this is precisely the moment at which local high frequency activity is generated and starts propagating away. This is also the point in which neurons starts discharging in bursting mode hence the fast rise in neuropile Calcium. In each full ictal epochs acquired, most astrocytes display more or less a first plateau in ΔF/F, starting in-synch with neuropile and growing slowly into a first plateau (>70% of astrocytes display such a behavior). As described in Gòmez-Gonzalo et al. 2010, ΔF/F rises concomitantly in neuropile and astrocytes during full ictal events both in so colled field A and field B (*i.e.* inside ictal focus or in ictal penumbra once invaded, respectively). Notably, when ictal activity is triggered focally in slices (double NMDA pulse), neurons and astrocytes display ΔF/F characterized by a biphasic increase. Neurons show a rapid increase in ΔF/F starting at t1 and evolving in a first plateau (transition into bursting modality), followed by a second peaked increase at t2 (ictal termination) as observed *in Cavia* neuropile. Astrocytes also display an aligned biphasic increase in ΔF/F with a second peak perfectly timed with neurons and a first slower increase. Both neurons and astrocytes only show these biphasic activity in field A. In the 0 Mg+ , double NMDA model when ictal activity propagates into field B, neurons and astrocytes only display a single peak in ΔF/F aligned with second peak in field A. *In Cavia* BMI model, ΔF/F behaves always like a Field A, supporting a scenario in which mEC host a large irritative zone from which ictal activity propagates away. This observation is also in line with the proposed interpretation of LFP polarity inversion. Hippocampus-EC combined slice preparation show indeed fully blown ictal events when challenged with 0 Mg+ or in picrotoxin, even when Schaffer's collateral connection are cut thus disconnected from CA3 supporting the evidence that EC is capable of generating self sustained epileptiform activity (Barbarosie and Avoli, 1997; Avoli and de Curtis, 2011). If we were imaging "fields B" while recording LFP from "Fields A", we would expected discrepancies between ΔF/F and LFP. Due to the inhibitory restrain inpinging on the ictal penumbral area, Field B astrocytes ΔF/F should appear silent while Field A LFP reports

ictal activity (Gòmez-Gonzalo et al., 2006; Trevelyan et al., 2006). Two interictal events are described emanating from CA3(Avoli et al., 2006): fast ones appear to be responsible for the ictal-damping effect over EC neurons. Slow interictal events, on the other hand, seems to be correlated with ictal onset in EC. Once Schaffer's collaterals are sectioned, LFP in EC is devoided of interictal siugnatures and spontaneous ictal events ensue. Mimicking fast interictal events after Schaffer's collateral cut with extracellular 0.1-0.5Hz- stimulation, efficiently prevents spontaneous ictal events in EC. Fast interictal events or low frequency stimulations, reflect into a modest $[K^+]_o$ elevation in EC, while ictal onset is preceded by larger $[K^+]_o$ increments and slow interictal activity. Large $[K^+]_o$ increments seems to be the triggering event igniting ictal activity in seizure-prone structures (Zuckermann and Glaser, 1968; Jansen and Yaari, 1988). Slow interictal events are indeed aboilished in BMI favouring fast ones, thus a mechanism is proposed in which interneuron activation in the form of fast interictal events, act as an hampering factor against local EC clustering of bursting neurons. Once a critical density of bursting neurons coalesce, ictal activity is triggered (Jiruska et al., 2013). $[K^+]_o$ elevation might be responsible for depolarization block in inetrneurons observed just about ictal onset in 0 Mg^{2+}/ NMDA hippocampal slice model, heralded by slow a interictal event. In this transition phase, $[K^+]_o$ reaches ceilng values of around 16 mM (compared with 3 mM in baseline and 4.5 during fast interictal events; Avoli et al., 2013) and the failure of inhibitory drive, should precipitate principal cells into incoherent bursting mode *i.e.* ictal activity (Cammarota et al., 2013). Among several mechanisms, Potassium homeostasis is regulated by astrocyte spatial buffering and siphoning which are observed to be summoned once a $[K^+]_o$ threshold level is attaind. Typical values described in vitro and in vivo are around 10-12 mM (Heinemann and Lux, 1977; Connors et al., 1982; Ransom et al., 1986; Somjen et al., 2002), well below those observed at ictal onset. Once Potassium levels are normalized, interneurons impairment would be relieved and GABA-ergic harnessing of ictal activity re-established. Obviousely, Potassium challenge would be aligned in time with ictal onset only inside Fields A, since neighboring regions would still experience inhibitory veto being locked in fast interictal activity. $[K^+]_o$ increase, is fast and protracts during the whole duration of ictal activity until ictal termination. Fields A first astrocyte $\Delta F/F$ slow elevation at ictal onset, could be the result of bursting neurons activity combined with Potassium increase. Also de-synchronization is timed with Potassium increase and whether coherence degree in neural firing or Potassium challenge is the actual stimulus engaging astrocyte $\Delta F/F$ is still controversial.

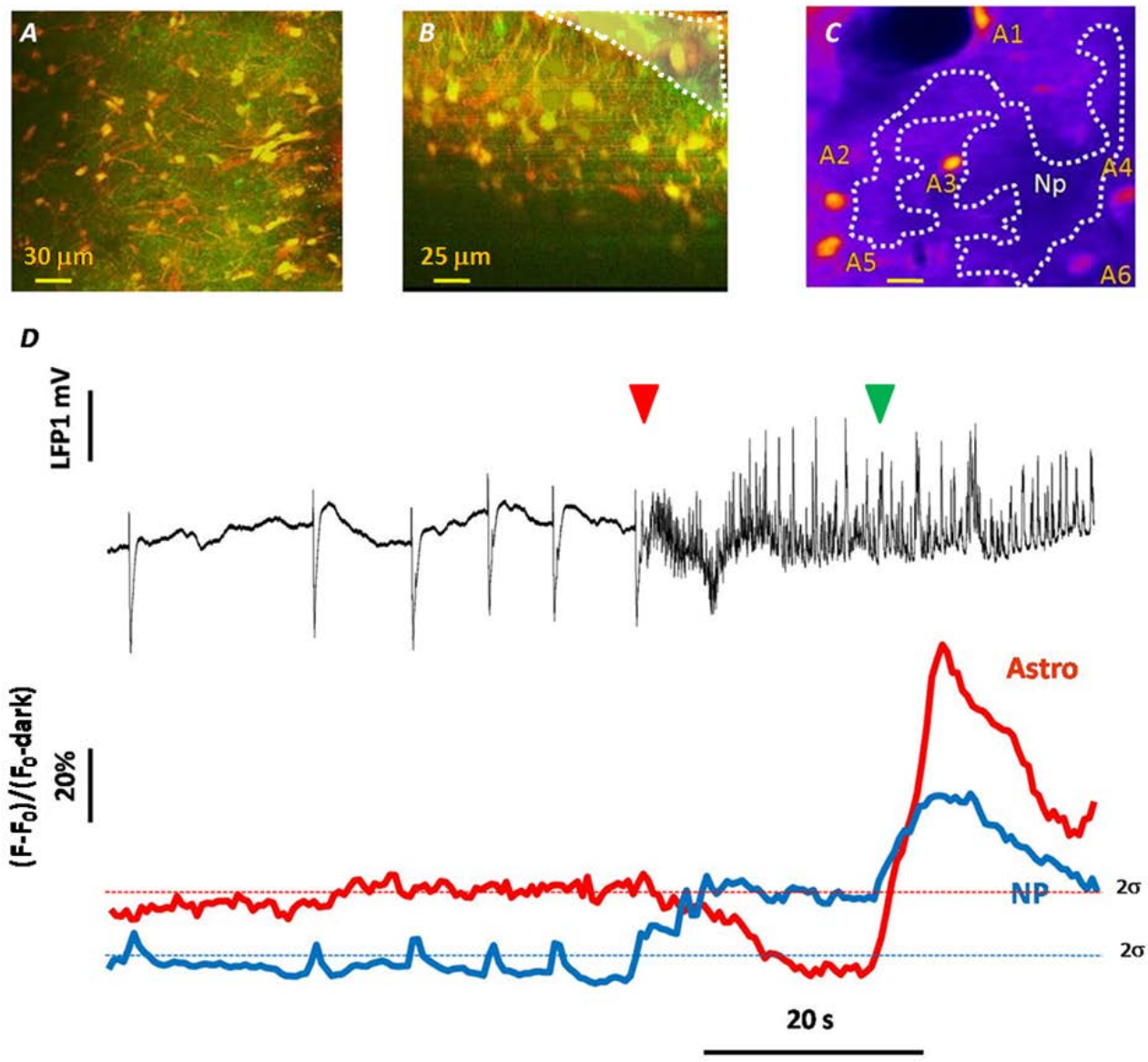

Figure 3.5: Astrocytes and neuropile experience display different Calcium oscillation during epileptiform activity. A) Average projection of a 50 µm thick optical sectioning aquired 150 µm deep into mEC. B) Digital 3D coronal reconstruction of a 200 µm deep Z optical sectioning containing both field A) and C). Dashed shade highlights the mEC surface. C) Logarhythmic color-coded average projection of 30 frame during baseline activity of a T-series containing a 2nd ictal at 1st BMI pulse. T-series was acquired at 150 µm in mEC, "A" and "Np" tags astrocytes and region of neuropile respectively. D) top: LFP recorded near (tip of the pipette placed at the same depth some 100 µm on the left of the field in C) the field imaged in C during a "first BMI/second ictal" event. The whole sequence: iterictal-ictal-afterdischarges is recorded. Red and green arrowheads mark the ictal start and ictal termination respectively. Bottom: oscillation of Calcium dependent fluorescence intensity in time simultaneously recorded with the LFP above. Blue and red tracks are relative to nuropile and averaged 6 astrocytes from field C. Dashed lines indicate the 2σ threshold level. During interictal phase (before red arrowhead), neuropile Calcium transients faithfully mirror interictal spikes while astrocyte Calcium-dependent fluorescence remains flat. No Calcium activity is observed between interictal events at

all. At ictal onset (red arrowhead) neuropile shows a first increase in Calcium dependent fluorescence rapidly peaking to a plateau. This steady Calcium increase, lasts some 20'' until ictal termination is reached (green arrowhead). At this moment a second increase in neuropile Calcium is observed of approximately the same extent as the previous one both in duration and intensity yet, a wax and waning shape replace the plateau. Astrocytes red trace display a single massive increase aligned with the second peak in neuropile, some 20 seconds from ictal start, at ictal termination (green arrowhead). A neuropile-to-astrocyte ROIs contamination is ruled out by the absence of any trace of neuropile interictal Calcium transients or ictal plateau in the red trace. On the other hand, the clear similarity between astrocyte and neuropile peak at ictal termination suggest quite the opposite effect: neuropile second peak could be at least in part, of astrocyte contribution.

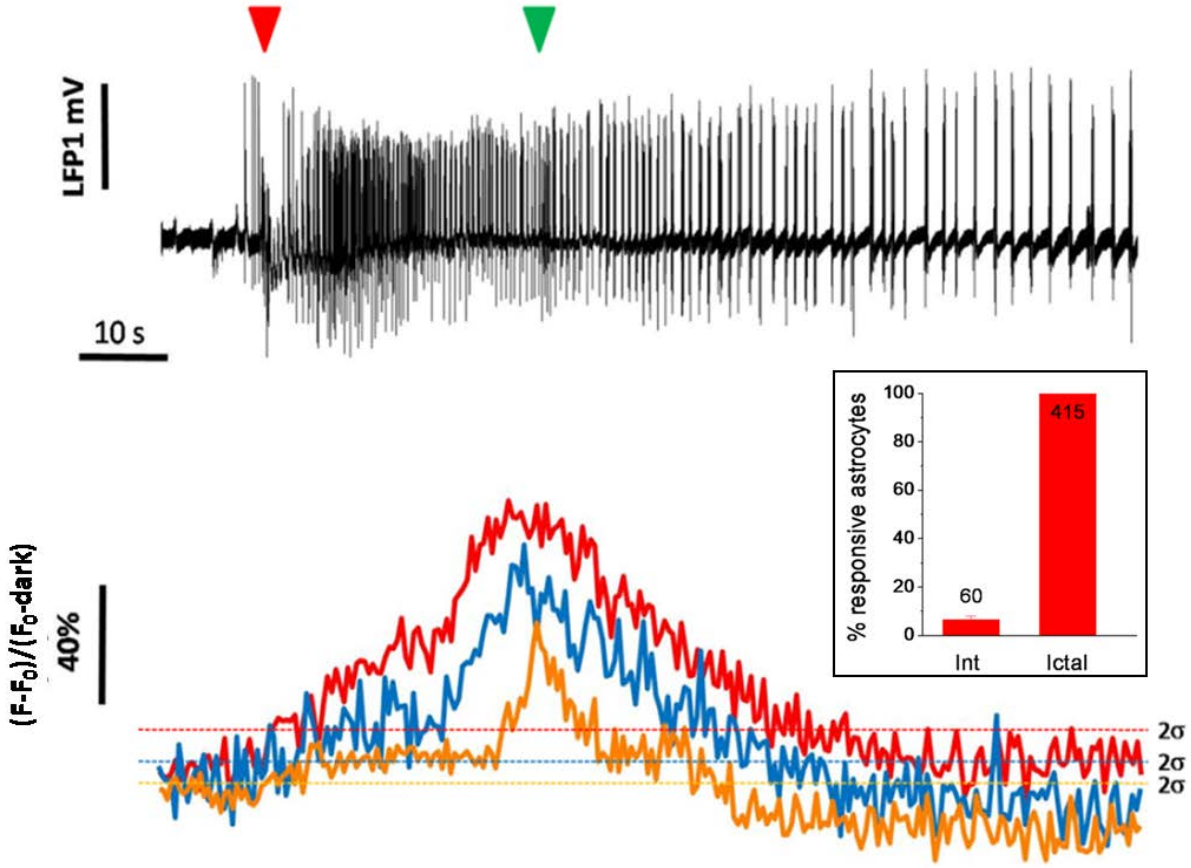

Figure 3.6: Imaging ictal activity with single cell resolution. Top: LFP from a 1st BMI 3rd ictal event. Arrowheads sign the start/end of ictal activity. Bottom: Fluctuation in Calcium-dependent fluorescence intensity from a two-photon time series acquired simultaneously with LFP above. Calcium oscillations of three astrocytes are shown, dashed lines mark the 2σ level. A massive and synchronous increase in astrocyte Calcium is present peaking sharply at termination time (green arrowhead) 22 second away from ictal start. Different Astrocytes display rising phases differing in slope, nevertheless, all Calcium transients starts at ictal onset and peak at ictal termination. Some cells (orange trace for example) show a slight increase at ictal start developing in a first plateau reminiscent of the neuropile behavior. Some other (the red trace) display a slow increase straight to the peak at ictal termination with no signs of a preceding plateau. Different astrocyte ROIs could be affected by different amount of neuropile bleedthrough: the more the contamination the larger the first plateau. Alternatively, astrocytes could show either two actual Calcium transients like those observed in neuropile, or a sigle slower one over which bleedthrough may add on. No sign of significative Calcium oscillations are to be observed during the afterdischarge phase. Insert: red bars height represents the probability (expressed in %) of detection of an astrocyte Calcium transient during ictal events Vs interictal phase. Calcium events and LFP deflection were considered concomitants if: 1) Calcium events were above 2σ level during the event and 2) Calcium oscillations peak fell in time within the LFP event with ± 0.3 s tolerance. Statistic is relative only to those astrocyets for which both ictal and interictal ΔF/F data are available (495 cells, 22 BMI perfusions for a total of 73 ictal events and 152 interictal spikes in 11 animals). More than 90% of them displayed calcium increase during ictal activity (452 cells). Less then 10% of astrocytes also responded to interictal events (41 cells, all of them were also responsive to ictal activity). A small fraction of all astrocytes included in the statistic (4%), remained silent to both

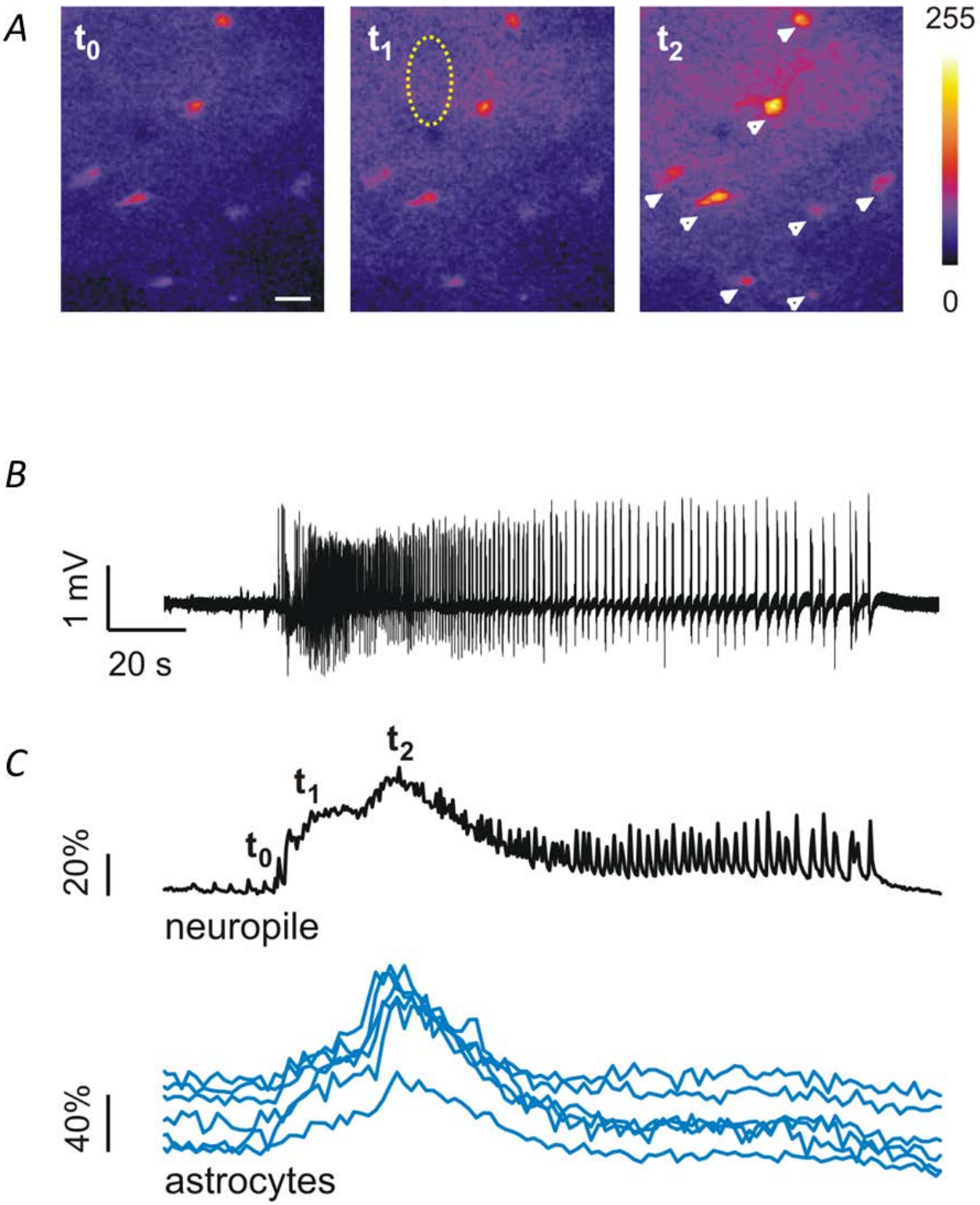

interictal and ictal activity, while not a cell was observed to display Calcium transients during interictal activity but not in ictal phase (not shown).

Figure 3.7: Discrete Calcium oscillations in astrocytes are associated with LFP de-synchronizatio. A) single frames extracted from a two-photon Calcium imaging t-series acquired 250 μm deep in mEC. t0, t1, t2 refere to ictal onset, ictal phase, ictal termination respectively, indicating times reported in the LFP epoch below. White arrowheads indicate astrocytes, the yellow oval a region of neuropile. Images are intensity-to-color coded. Scale bar: 20 μm B) LFP from a 2nd ictal 1st BMI recorded from mEC. A short interictal, ictal and afterdischarge phases are visible before the restoration of baseline values. t0, t1 and t2 indicates times at which imaging frames in A were extracted C) Calcium dependent fluorescence intensity fluctuations from field in A. $\Delta F/F$ tracks from 6 astrocytes and a region of neuropile are shown. Neuropile Calcium starts rising as soon as ictal activity ensues (t0). A second peak at ictal termination (t2) follows a 20s first plateau. Coincident with the second peak in neuropile is located the main peak in astrocytes Calcium. During afterdischarge activity, neuropile fluorescence exhibits fast transients aligned to each LFP spike increasing in amplitude as electrical deflections grow larger and sparser. In this region Astrocytes exhibits no significant Calcium activity apart from some subthreshold oscillations. Astrocyte $\Delta F/F$ start rising together with neuropile, yet rising phase is slower while neuropile readily reaches a plateau. Concomitant with neuropile second peak at t2, is the major astrocyte $\Delta F/F$ increase. Astrocytes $\Delta F/F$ tracks are strongly synchronized although intensities are variable across cells.

3.3--- Synchronization of astrocyte is maximum during ictal activity.

The degree of coordination between local electrical activity and Calcium oscillations is evaluated plotting the variations in time of cross correlation power among the two signals, during epileptiform activity. Different neuropile regions display variable degree of synchronization with local field potential, also cross-correlation power peaks appear scattered among different areas although average values result elevated along the whole ictal event. Cross correlation between single astrocytes Calcium signal and local field potential, on the other hand, result lower in average while an intense synchronization event is observed in all cells, precisely at ictal onset. Astrocyte coordination also appear stronger than neuropile one.

Astrocyte vesicular release depndes upon intracellular Calcium elevation (Bezzi et al., 1998; 2004; Parpura and Haydon, 2000; Pasti et al., 2001; Fellin et al., 2004) proven to elicit glutammatergic responses in neurons (Haydon et al., 2001; Zhang et al., 2004; Marchaland et al., 2008). Furthermore, astrocyte signaling have been proved to generate paroxysmal depolarization shift in neurons (Kang et al., 2005; Tian et al., 2005, Fellin and Haydon, 2005; Rogawsky, 2005; Seifert et al., 2006) which is the hallmark of interictal neural activity and. Given the critical role of astrocytes in modulating neural activity and also considering the vast territory under control of each astrocyte, it is plausible that any synchronous $\Delta F/F$ event in a cohort of astrocytes would exert an effect over a far larger population of neurons. If the gliotransmitter release is synchronous, neurons would then be instructed with a synchronous input. Neurons on the other hand, talks to astrocytes through neurotransmitter receptors, most of which are G-coupled proteins starting Calcium signaling events culminating in intracellular Calcium elevation. when synchronous neural events occur, astrocytes should exhibit a transient synchronous $\Delta F/F$ as a readout. As a result from this interplay, LFP should be synchronized by any large enough astrocyte coherent $\Delta F/F$ event and any synchronous LFP event shall trigger large astrocyte $\Delta F/F$ (Fellin et al., 2006). This sequence of events would be plausible only if a simple positive feedforeward loop is operating between astrocytes and neurons. A simple observation should be deduced from such a simple scenario: the emergence of synfire chains once, somehow, the seed of hypersynchronization is installed. Both synchronization among neural activity (*e.g.* fast interictal events) or cohordinated astrocyte Calcium increase (Calcium waves, siphoning, special buffering, extravasation etc. etc.) would be sufficient to recruit ever larger territories into a spreading fire of synchronization. Obviosely this is not the case and CNS must posses some “escaping mechanisms” from the hypersynchronous trap. A temporal displacement between neural and astrocyte input/output functions could be part of this mechanism. A “transfer function” could computed describing the coupling between duration and synchronization degree in neural firing on one hand and time constant of Calcium rising in

astrocytes and threshold responsivity to neurotransmitters, on the other. Furthermore, physiological gliosecretion is a complex phenomenon and several opposing effects over neural target are demonstrated operating in parallel or in intricate series (for a comprehensive review see Perez-Alvarez and Araque, 2013). A large scale correlative analysis between LFP pattern alterations and $\Delta F/F$ in different astrocytes, could prove useful in this respect. Temporal dynamics of the power of cross correlation function calculated between any two $\Delta F/F$ traks, provide valuable information about coherence between ROIs. LFP on the other hand may be used as a reporter of neural network synchronization (Buzsaki et al., 2012). From the "electrical active cells" standpoint, LFP amplitude is considered to be co-variating together with coherence degree in neural firing. Analysis of the variation in power of cross correlation function calculated between LFP and $\Delta F/F$ in time, is here used to estimate single cell contribution to the bulk electrical activity. This approach is particularly valuable incorporating electrically silent astrocytes in the calculation. In Figure 3.8 is presented the result of one of these analysis. In A is a typical first ictal, second BMI activity decimated to match imaging period and amplitude-to-color coded. Large intensity events in LFP correspond to hot bands. Below is reported neuropile and averaged 7 astrocytes $\Delta F/F$ behavior acquired during LFP. Below is the cross-correlogram computed between individual neuropile sub-regions or each astrocyte ROI and LFP intensity. Power of cross correlation is calculated in each imaging frame with which a single value of LFP intensity is associated. Three periods in cross correlogram are highlighted in B, corresponding to ictal-ictal phase (boxed red), early AD phase (boxed green) and late AD phase-baseline (boxed blue). Black horizontal bar in B indicates the duration of LFP ictal event. Observing neuropile lanes, power of cross correlation is already above average baseline value preceding ictal star although, as deducible from LFP power lane, no clear interictal events are present in pre-ictal phase. A clear early increase in cross-correlogram power is detectable precisely at ictal onset (red arrowhead). Surprisingly, not all neuropile ROIs behave the same. Increase in synchronization is not aligned in time for all neuropile ROIs and some of them also display poor correlation. Also duration and intensity of the synchronous period jitter considerably among different lanes. Observing last two neuropile lanes and the first two, 3 points in times exist where average neuropile synchronization with LFP experiences strongest increases. Yet differen ROIs behaves independentely. All neuropile lanes display a short lived episode of synchrony between ictal start and termination. A general and aligned rapid fall in neuropile-to-LFP synchronization is observed at ictal termination. Also astrocyte lanes show a fall in synchronization around this time. In astrocyte lanes the degree of synchronization is very weak in pre-ictal phase and shortly after ictal start. All astrocytes experience their strongest increase in cross-correlation synchronously within few seconds from ictal start. Althoug $\Delta F/F$ starts increasing at ictal onset, correlation wanes readily as LFP progress into high frequency activity. Correlation in astrocytes terminates rapidly into a region of very low power extending throughout the early AD phase when $\Delta F/F$ for both neuropile and astrocytes are proceding into the second peak. Meanwhile neuropile lanes show average higher correlation but de-synchronized one another. No apparent correlation exists between np cross correlation lanes and those of astrocytes, except amidst ictal activity.

Neuropile and astrocytes lanes show average high correlation across afterdischarge phase. Cross correlation is less coherent in neuropile lanes than in astrocite ones, the latter behaving almost in block, with a slow increase toward the right border of green box. Here average $\Delta F/F$ in neuropile is spiking while astrocyte one is silent. Inside the blue box, cross correlation in astrocytes and neuropile display quite the same pattern as in the red one until an abrupt fall. This is ther time at which LFP show the last afterdischarge event and turns into baseline flat activity. Henceforth neuropile correlation remains low but stronger than astrocytes, a behavior mirrored in $\Delta F/F$, where neuropile is absolutely flat (as LFP) and astrocytes are sub-thershold oscillating. In Figure 3.9 is depicted the temporal evolution of cross correlation power of three regions of neuropile and three astrocytes. Panel A show the time evolution of the power of cross correlation in the red box of figure 3.8. 3 neuropile lanes (top) and 3 astrocyte lanes are reported. Neuropile present a pedestal extending all along ictal intial phase (see B), well time matched in all 3 lanes. Over this few “spikes” of increased power are visible. These are not synchronized between none of the different neuropile profiles. Astrocyte profile of synchronization show a much more uniform behavior which starts shortly after neuropile initial rising correlation. Curiosely, peaks in neuropile crosscorrelogram appear to be in antiphase when compared with those in astrocytes, except for the central peak. From the last peak in correlation, astrocyte tracks slowly decrease toward minimum values with variable amplitudes in different astrocytes. in neuropile instead an abrupt decrement in correlation is observed synchronous in all 3 regions. As depicted in panel B, increment in correlation power rises and fall within 10 seconds from ictal start while $\Delta F/F$ is still rising in both neuropile and astrocytes to the first plateau. If LFP amplitude is interpreted correctly as a measure of neural population coherence in firing activity, then the peak amplitude-synchronization is observed in correspondence with the slow interictal at ictal start. Here is the point in time when $\Delta F/F$ is triggered and start increasing. Cross correlogram reveal here just the beginning of increased coherence further growing shortly after, when LFP amplitude is strongly reduced. If slow interictal events preciding ictal ones are the sign of inhibition failure inside Field A and depolarizazion block in interneurons, the increase in correlation startin in neuropile, could be attributed to the recruitment of principal neurons in bursting mode. Neuropile signal cannot be deconvolved here in sub-regions belonging each to a single-cell output, thus each neuropile ROI is an average representation of neural behavior. It is also impossible to tell apart regions in neuropile comprising signals invading mEC from CA3 or the other way around. Large amplitude slow interictal LFP events poorly correlate with $\Delta F/F$, indicating either a wide range desynchronization event or an under-representation of afferent signals in the region imaged. The second possibility is ruled out in further discussions while the previous one, is supported by the fall in LFP amplitude starting with ictal onset. Afterall a large LFP event may arise, even when a large territory is integrated in which the number of active units is increased. Slow interictal events are thus interpreted here as a massive enrollment of mEC with comprising de-phasing firing neurons. The decrease in LFP amplitude following is then the result of both interneuron depolarization block and prosecution of the desynchronization phase inside a field A. Bursting mode, as read from $\Delta F/F$ measured in neuropile during afferent activity (Field A propagating toward Field B), shall be populated at each frame, by several $\Delta F/F$ transients belonging to different neurons with no phase relation. The increase in $\Delta F/F$ then descend from the increase in firing frequency since no further

increment in LFP amplitude is observed and no additional recruitment is to be expected. Increase in firing frequency in random-phased neurons would infact increase the chance of stochastic resonance in a fixed time frame *i.e.* imaging frame period. This is true for neuropile regions the composition of which is tangled, but is not necessarily true for astrocytes somata. Here the input might well be mixed but what $\Delta F/F$ reveals is the summation of inputs at the level of the cell soma. $\Delta F/F$ here is somehow a reporter of astrocyte capability of temporal summation of inputs. Signals incoming with progressively higher frequency shall be summated more efficiently leading to a steady increase in Calcium. The rate at which Calcium rises in astrocytes is indeed slower than neuropile probably due to the process of astrocyte integration wich obviousely can't keep the pace with electrical propagation in neurons. Neuropile cross correlation will reveal a sudden increase as the neural population recruited strts firing at higher rates ($\Delta F/F$ increase) with steady LFP amplitude, a trend mirrored with delay in astrocytes being owerwhelmed in neural bombardment. The loss of correlation before the end of first $\Delta F/F$ plateau might be caused by a parallel dilution in firing rates which could be revealed by single unit or intracellular recordings from pyramids in this phase (Losi et al., 2010).

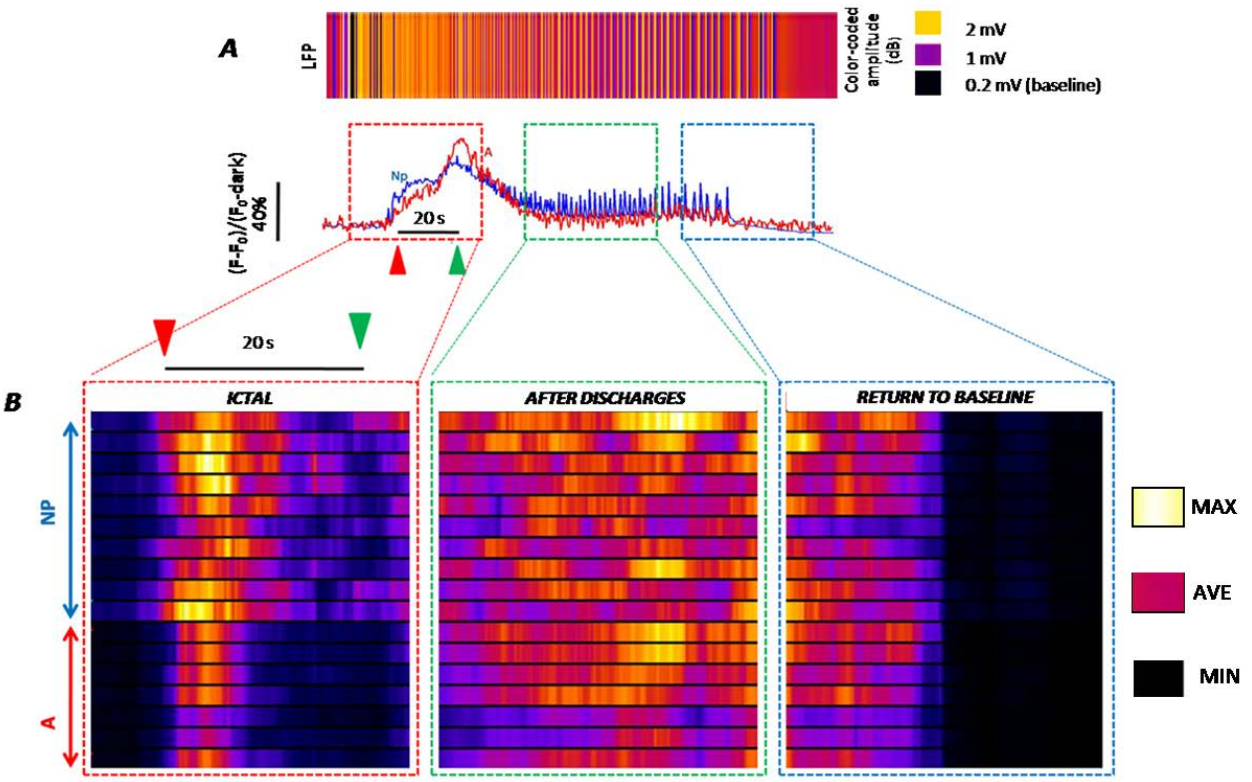

Figue 3.8: Astrocyte synchronization in ictal activity. A) Same data described in figure 3.6. Boxed regions indicates ictal, afterdischarge and return to baseline phases. Red arrowhead and green one marks the ictal start and ictal termination respectively. B) Cross correlation raster plot between LFP and ΔF/F calculated in the boxed region in A. In each lane of the raster is color-coded the value of the power of the cross-correlation function calculated between Calcium-dependent fluorescence intensity oscillations (ΔF/F) and LFP. Each lane corresponds to the cross-correlation calculated for single ROIs. The lower the power of cross-correlation the "colder" the color (on the right are reported maximum, average and minimum values as references). ΔF/F allows normalization between cells loaded with different concentration of OGB enabling a direct comparison of relative ΔF/F amplitudes. LFP trace is properly decimated to fit the sampling period of ΔF/F and average LFP intensity normalized to average ΔF/F estimated across all ROIs. 10 regions of neuropile (NP lanes) and seven astrocytes (A lanes) are included in the raster. Ictal box: High cross correlation power is observed first in neuropile. All NP lanes display hot colors starting precisely at ictal onset (red arrowhead). Cross correlation power fades away rapidly in neuropile regions reaching average values before ictal termination (green arrowhead). Synchronization between different neuropile regions is not stringent as peak cross correlation values are not aligned jittering abaut some 10 s. Toward ictal termination alignment is much lower fading into an erratic pattern. Astrocytes, on the other hand, appear extremely synchronized. Peak values are reached shortly after ictal onset in a confined time window not mirrored in neuropile lanes. Synchronization loss is also synchronized compared to that of neuropile. Two astrocytes apper almost silent. Overall ictal Neuropile average cross correlation remains higher than that of astrocytes. Afterdischarge box: neuropile lanes display "hot" values along the whole afterdischarge phase, yet pretty de-synchronized. First and 8th lanes show a continuous increase of power toward the end of the of the boxed region rapidly fading while other lanes display sporadic power bursts. Coherence between

lanes wax and wane. Astrocyte lanes are much more synchronized one another showing a pattern similar to that of neuropile 1st and 8th lanes. Astrocyte cross correlation average power remains nonetheless lower than that of neutopile. Return to baseline box: Neuropile and astrocyte lanes show a decreasing cross correlation power down to minimum values at the afterdischarge termination. All lanes appear fairly synchronized one another with no intense bursts. When LFP reaches baseline levels all lanes fades to black. Eventually neuropile lanes present synchronized patches of low power absent in astrocytes.

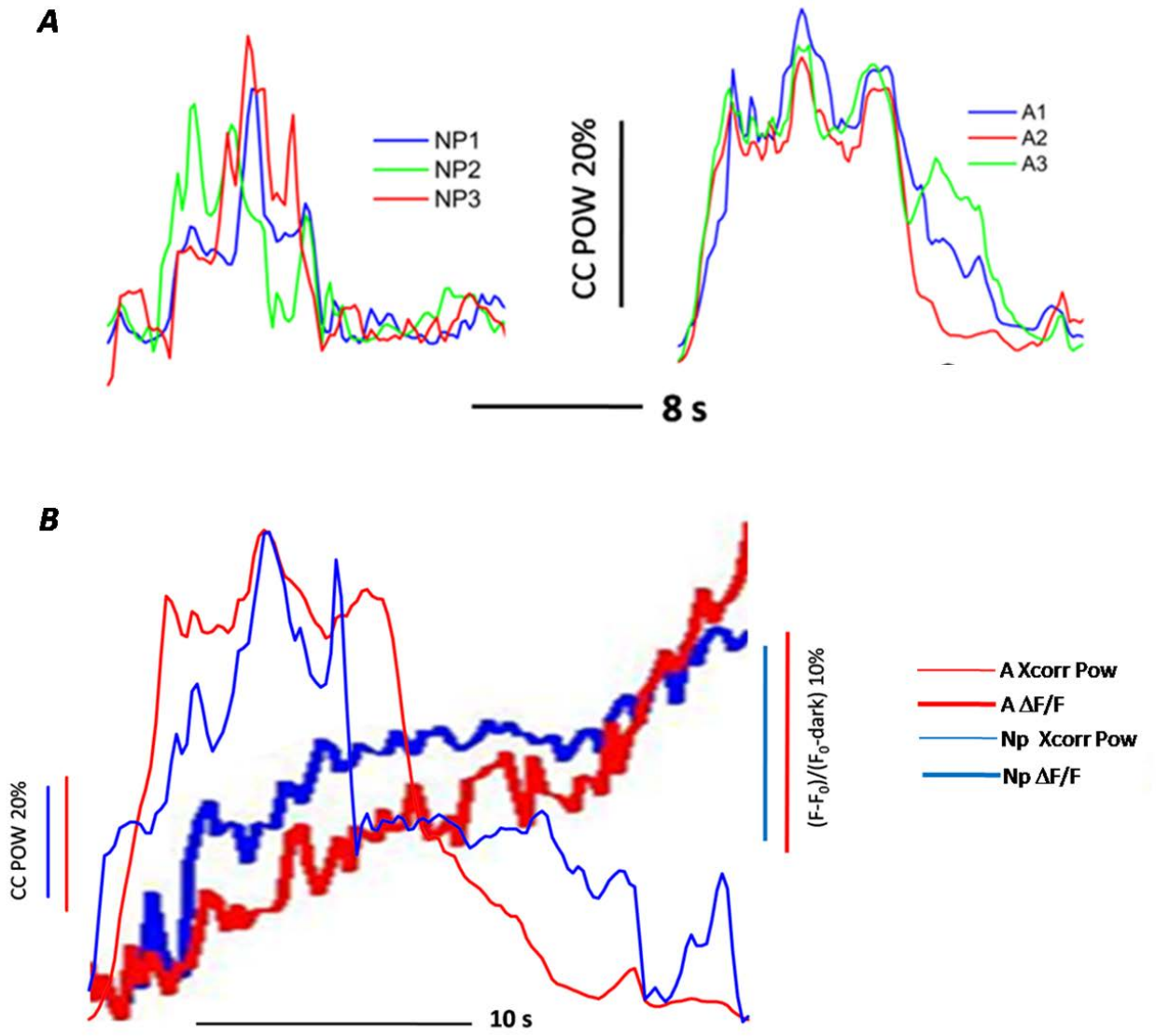

Figure 3.9: *Cross-correlation between Calcium-dependent fluorescence and local field potential is maximum at ictal onset. A) cross correlation analysis relative to ictal box in figure 3.8. Plotted are the cross-correlation power oscillations in time of 6 representative lanes. Top graph is relative to first 3 "Np" lanes, bottom graph presents first 3 "A" lanes. Neuropile crosscorrelograms are asynchronous and display variable number of "peaks" over an extended "pedestal". Rising phase start at ictal onset with some jitter. The end of the pedestal is well aligned before ictal termination. A fast central peak over the pedestal is aligned in all neuropile taces. Astrocyte cross-correlograms are highly synchronous Power reaches rapidly a pedestal level over which three peaks emerge. Astrocytes display a slower decrement of power toward ictal termination where synchronization is lost. All astrocyte transients. B) Thick lines are ΔF/F while the thin ones are cross-correlogram average power from A. Superimposing ΔF/F with cross correlogram power oscillations, reveals an antiphase relation. Synchronization in both neuropil and Astrocytes reach the peak before Calcium transients. Further increase in Calcium dependent fluorescence toward ictal termination, is not mirrored in cross-correlogram power which is decreasing in this phase. Central peak in cross-correlogram is aligned among neuropile and Astrocytes. Blue thin line rising phase precedes that of astreocytes at ictal onset while red thin trace reach the first peak before neuropile.*

3.4--- Activation of astrocyte Calcium elevation triggers ictal events.

Microinjection of PAR-1 receptor agonist starts Calcium elevations in a small patch of astrocytes. As a consequence, an ictal event is precipitated in a context in which seizures are unlikely to manifest spontaneously. Triggered ictal events are shorter in duration than spontaneous ones, yet spectral properties are indistinguishable. Moreover, as the PAR-1 agonist injection starts, interictal activity is readily obliterated in favour of an high frequency electrical phase, terminating abruptly with a "slow" interictal event few seconds after microinjection end, leading into the actual ictal phase. Astrocyte triggered Calcium rise, results biphasic, with a slow rising phase followed by a steep increase. Neuropile Calcium present a strong increment delayed with respect to the early astrocyte increase, wich is also perfectly aligned with late astrocyte peak. Calcium increase in astrocytes first appear in the cell closest to the injecting pipette tip and is broadcasted across cells faster than the estimated diffusion of PAR-1 agonist itself. A paracrine mechanism could be responsible for the fast recruitment of further astrocytes, the speed of which is in agreement with ATP-dependent astrocyte-to-astrocyte communication. Triggered Calcium peak in both astrocytes and neuropile die away withing the duration of ictal activity, henceforth, neuropile displays a typical afterdischarge pattern of Calcium oscillation, while astrocytes remain silent altogether.

The role of astrocytes in neural network synchronization, is sporadically highlighted in literature mostly due to the cumbersome task of manipulating glial cells without a direct effect on neurons. Data presented so far suggest that astrocytes are recruited during the transition from a coherent neural network activity to an incoherent high frequency one. Whether astrocyes are responsible for phase transition or merely captured in neural attractors, is a matter of debate (). To avoid circular causality, one should be able to manipulate at will and separately, either neural or astrocyte network, switching them on or off at will. Dissection of such an intricate mesh is not yet possible with the available techniques. Nonetheless, it is possible to trigger astrocyte Calcium elevations at least in a restricted territory, operating on G-coupled astrocytes receptors. Proteasa-activated receptor-1 (PAR-1) is expressed in astrocytes endfeet (Striggow et al., 2001; Wang et al., 2002 Lee et al., 2007; Shigetomi et al., 2008), upon cleavage (physiologically started by serine protease such as thrombin) part of the receptor act as agonist, triggering Gq activation. Synthetic mimetic peptides like TFLLR efficiently activates PAR-1 receptors leading to intracellular Calcium increase in astrocytes (de Garavilla et al., 2001). We thus decided to employ TFLLR to elicit astrocyte-restricted Calcium increase before spontaneous ictal events, during interictal activity. If astrocytes are endowed with some Calcium-dependent mechanism capable of phase transition effects over neurons, then exogenous activation of Calcium increase, shall produce a kick toward phase shift. As described above and in deeper details below, astrocytes exhibit strong Calcium increments during ictal activity remaining silent in interictal periods. Triggering Calcium increase on top of ictal ones, would be then largely ineffective, therefore we chose to activate PAR-1 during interictal activity. Microinjections of TFLLR 200 μM in aCSF are delivered in mEC after 3rd ictal 3rd BMI perfusions at least 15' after the last observed ictal events. As described in Figure 3.2, at this

point, further ictal events are only summoned by additional BMI perfusion, otherwise LFP is thereafter stable with sporadic interictal events. Concomitantly, LFP and recurrent sessions of Calcium imaging are acquired in the region of TFLLR pulse. In slice model (Gòmez-Gonzalo et al., 2010), TFLLR (puffed 10 μM), proved to be sufficient to trigger conspicuous Calcium elevations followed by SICs in nearby patched neurons bathed with TTX. No Calcium elevations at all are observed in neurons in the presence of D-AP5/TTX and TFLLR indicating that PAR-1 activation leads to glutamate release from astrocytes impinging on neural NMDA receptors. In Picrotoxin/0 Mg^{2+} a single TFLLR pulse is enough to start an ictal event, while in the double NMDA model, PAR-1 agonist is proved to be efficient only as an NMDA vicarious.. The proposed model in wich astrocytes participates in an excitatory loop with neurons, contemplates that, provided a sufficient excitatory drive into neural network, astrocytes would be bypassed altogether in the ictal generation mechanism. A threshold of excitability exhists then, beyond which neurons precipitate into ictal phase no matter whether pushed by astrocytes or exclusively by neuron-to-neuron interaction. Picrotoxin/0Mg^{2+}, would set the network recurrently over this threshold (being a non-competitive anthagonist for GABAa receptors, Picrotoxin would clamp inhibition constantely at reduced efficiency, leading to frequent and spontaneous failures of interneuron barrage), while double 4-AP model would set it just about the threshold (4-AP providing excitatory drive interfering with re-polarization). Little push is thus needed in PTX/0 Mg^{2+}, while a stronger kick is required in the 4-AP model. Single NMDA or TFLLR pulse is indeed efficient in 4-AP 0 Mg2+, while a double NMDA or NMDA/TFLLR is necessary in 4-AP. BMI, in this respect, would be a much milder treatment, since no further excitatory drive is provided (like NMDA or 0 Mg^{2+}) and GABAa channels are impeded in a competitive fashion. Competition at GABAa receptors would actually result in an increase in interneuron average firing (since interneuron-principal cells feedback loop would require stronger GABA release to be efficient) and an increased tendency toward synfire chains of pyramidal firing. This semms to be the case since hypersynchronous events, present in the BMI perfused *Cavia* brain, are virtually absent in the other two models. Nevertheless, the 4-AP model require double NMDA pulses in order to exhibit critical activity which are not spontaneous, while BMI model display recurrent spontaneous events. Considering the occurrence of spontaneous events (*i.e.* not exogenously triggered by further manipulations) as an estimation of the system proximity to ictal threshold, BMI-perfused *Cavia* brain should be considered half a way between 4-AP and PTX/0 Mg^{2+}. In this context Astrocyte contribution might result critical in the absence of an intense excitatory drive. To be taken into account is also the isolated Guinea pig brain preserved circuitry which is obviousely lost in slice preparations, the contribution of which to the threshold setting is far from being elucidated. No descriptions of TFLLR effects in a BMI-induced epileptiform activity was previousely presented. In Figure 3.10 is described the effect of single TFLLR pulse while mEC is entrained in hypersynchronous interictal events. In this phase CA3 fast interictal events should be harnessing the mEC tendency to critical activity and large territories of entrained neurons are firing synchronously. A single TFLLR pulse is enough to trigger a full blown ictal evet in this context. Spectral properties of evoked seizure, are indistinguishable from spontaneous ones, while duration is considerably and significatively shorter (average: 12.5 ± 5 s in 7 trials in 3 animals, Vs 21.08 ± 0.7 s $P < 0.001$ s for 3rd ictal 3rd BMI spontaneous events). Evident increase in power in the gamma, beta and alpha region of the spectrum also indicate an involvement of several firing

units mirrored in the thichening of LFP. A large slow interictal event precedes all TFLLR-induced ictal events. A period of LFP baseline perturbation underlines 5 seconds of microinjection. This is characterized by a rapid increase in high frequency content preceding ictal start and a possible "shielding-effect" of injection on the recording electrode seems thus implausible also because spectral alterations are not observed in control injections. Increment oin high frequencyes proceeds after injection stops, with a approximately steady rate until ictal event ensues. Interictal activity n this phase disappeard but a chance coincidence is not ruled out. Nevertheless, increment in high frequency spectral power and disappearance of hypersynchronous events can be interpreted as the hallmark of a phase transition in neural network assembly. Speculatively enough, gamma band population of spectrum, might also be interpreted as the result of fast spiking interneuron recruitment (Csicsvari et al., 2003; Traub et al., 2003; Cunningham et al., 2004; Traub et al., 2005), interpreted by some authors as the sign for a phase shift in neural coupling (Timofeev et al., 2012; Khazipov et al., 2013). TFLLR single pulse have an estimated 72% probability of success in this model, to be excluded is otherwise a plausible effect of pressure-injection over Volume-regulated anion channels (VRACs, Okada et al., 2009) since control pulses (aCSF + SR101 alone) are tested with no avail. After termination of TFLLR evoked ictal events, no further seizures are detected in LFP unless BMI is re-perfused. TFLLR 200 μM in aCSF is added with SR 101 (20 μM) to monitor ejection efficiency and to evaluate possible the extent of injected solution. Injection of SR101 in aCSF alone never started any ictal events. SR 101 spread volume is to be considered a good reporter for TFLLR diffusion (SR 101 M.W.: 606.71 solubility: 1 mg/ml in methanol; TFLLR M.W.: 647.82, solubility: 1 mg/ml in 20% acetone-water). In Figure 3.11 is presented an example of Calcium imaging during TFLLR injectiuon. Injecting pipette is visible in the imaged field, two flanking regions of neuropile and several astrocytes are indicated. Both neuropile regions exhibits similar behavior: fast transients mirroring each interictal event, a flat period during TFLLR injection, a large increment preceding ictal onset protruding into ictal activity and fast afterdischarge peaks. As observed in LFP, TFLLR shuts hypersynchronous activity and no $\Delta F/F$ increase is observed in neuropile while LFP exhibit high frequency power thickening. A flat period of about 10 s elapses before neuropile $\Delta F/F$ maximum increase abruptly rising to peak before LFP slow interictal event preceding ictal. Neuropile peak is divided into an early phase of a couple of seconds, in which high frequency $\Delta F/F$ is observed, evolving into a brief plateau readily decreasing before ictal termination. Once $\Delta F/F$ is restored into near-baseline levels, ictal activity is already terminated and afterdischarge phase ensues, with neuropile Calcium spiking. Astrocytes on the other hand, show a quite different $\Delta F/F$ profile: silence during interictal events, a slow rising phase during TFLLR injection, a large increase preceding ictal onset, a short plateau and a slow decaying phase into silence again terminating at ictal end. Most notably, astrocytes show a $\Delta F/F$ rising phase during the increase in LFP high frequency activity preceding ictal. Here neuropile is completely silet. Different astrocytes show different amplitude of early $\Delta F/F$ increase. Astrocyte peak is aligned with the end of the first half of neuropile $\Delta F/F$ peak. No evidence of spiking activity in astrocytes $\Delta F/F$ is present. Alla astrocytes appear to be synchronized (but see further) and the return to baseline phase

exceeds neuropile's one. No afterdischarge or interictal activity is detectable in astrocyte ΔF/F, excluding ROI contamination. Since different astrocytes display different kinetics in early ΔF/F transient, I estimated TFLLR diffusion using SR 101 as a reporter to see whether astrocytes closer to the injecting pipette werte first to display ΔF/F increase and how fast Calcium activity propagated through astrocyte syncitium. Considering an average ΔF/F in astrocytes, TFLLR triggers a rising phase in 4 ± 2 s from injection end and a ΔF/F peak in 6.23 ± 25 s. Reguardless position with respect to the tip of injecting pipette,, astrocytes show a synchronized late peak, while first rise jitter as described further. Astrocytes and neuropile late peaks are aligned as reveald from lag 0 maximum in cross correlation between ΔF/F. Both enuropile and astrocyte ΔF/F peak manifest before overt ictal activity, also preceding slow interictal LFT event. Increase in LFP spectral power in the high frequency regimen is instead perfectly timed with early astrocyte ΔF/F rising phase. Furthermore, a steady increase in 30-50 Hz power is observed as a consequence of TFLLR injection and astrocytes ΔF/F faithfully keeps the pace. Before slow intertictal event, neuropile ΔF/F starts showing high frequency fast oscillations and astrocyte ones starts rising to second peak. Once astrocyte and neuropile ΔF/F reach the late plateu the ictal preceding slow interictal event, manifests. At this point LFP is in ictal mode while ΔF/F is slowly restored to baseline values. From this perspective, TFLLR seems to be responsible for a slow recruitment of ever larger astrocytes territories until a coordinated threshold increase is reached. This the moment in which ΔF/F peaks first in neuropile. Probably neural excitability is pushed here across ictal generation threshold but in a region beyond imaged field. This result from the delay in LFP recording of ictal start assumed to be coincident with slow interictal event. Thus neuropile integrated measure would report the shift in neural phase while astrocytes at this point will respond to further Calcium increasing inputwhile still rising due to TFLLR. Neuropile input shall act as a rebound on local astrocytes pushing further Calcium increment. Ictal activity is then readily reported in LFP. Imaged field could well be a Field B in this case, acquired in the close proximity to the irritative zone. It is tentatively speculated that few astrocytes are focally triggered with local PAR-1 agonist injection and both a TFLLR diffusing-reinforcing effect and a paracrine Calcium propagation is thus set into action. A region neglected from imaging is experiencing phase transition when neuropile ΔF/F reports early spiked activity, precipitating an inhibitory failure which is propagated isotropically and reported by LFP. At this point ictal is unrestrained and reverberates in imaging field while astrocytes are already recovering from first Calcium "wave" shifting ΔF/F to the late peak. Early rising phase in astrocytes can be analyzed in more details separating individual ΔF/F tracks as shown in Figure 3.13. Slow ΔF/F transient show a shallow peak before the late large one is reached. The position in time of this early peak jitters among different cells. Using SR 101 as TFLLR diffusion reporter and early peak as a reading of Calcium propagation among neurons, it is possible to evaluate the speed of propagation of each phenomena. Red fluorescence diffuse with an average speed of 9.3 ± 0.6 μm/s while early ΔF/F peak is propagates in astrocytes with an average speed of 18.7 ± 1.6 s. First astocyte to display ΔF/F early peak is the imaging fields is the closest one to the injecting pipettes, A1 in Figure 3.13. If Calcium elevation was exclusively due to TFLLR reaching ever larger territoties, red fluorescence wold propagate faster than green one. As observed here instead, astrocytes early peak diffuse through somata as a function of the distance from the first activated one. Also the

domain in which SR 101 fluorescence is best detected after TFLLR pulse, is stretched as described in Figure 3.12, 13, upword in the imaged field. In Figure 3.13 is reported the progression of early peak in astrocytes choosing 4 cells displaying consecutive peak in time, astrocytes from SR 101 invaded region are all delayed compared with A4 of Figure 3.13. Calcium dependent fluorescence in region 2 is indeed still flat when A1 already show early peak, while red fluorescence is decaying from region 1. This also indicate that probably efficient TFLLR concentration is only attained closest to the injecting pipette, (no evaluation of SR 101 3D diffusion profile is, nevertheless, presented here). Few astrocytes would be first triggered as TFLLR is delivered and propagation of Calcium across syncitium would be started by a paracrine effect since no sign of neural activation is detected at least from neuropile. Astorcyte early peak propagation is in line with described Calcium diffusion in the syncitium sustained by ATP secretion (16-20 μm/s, Haas et al., 2006).

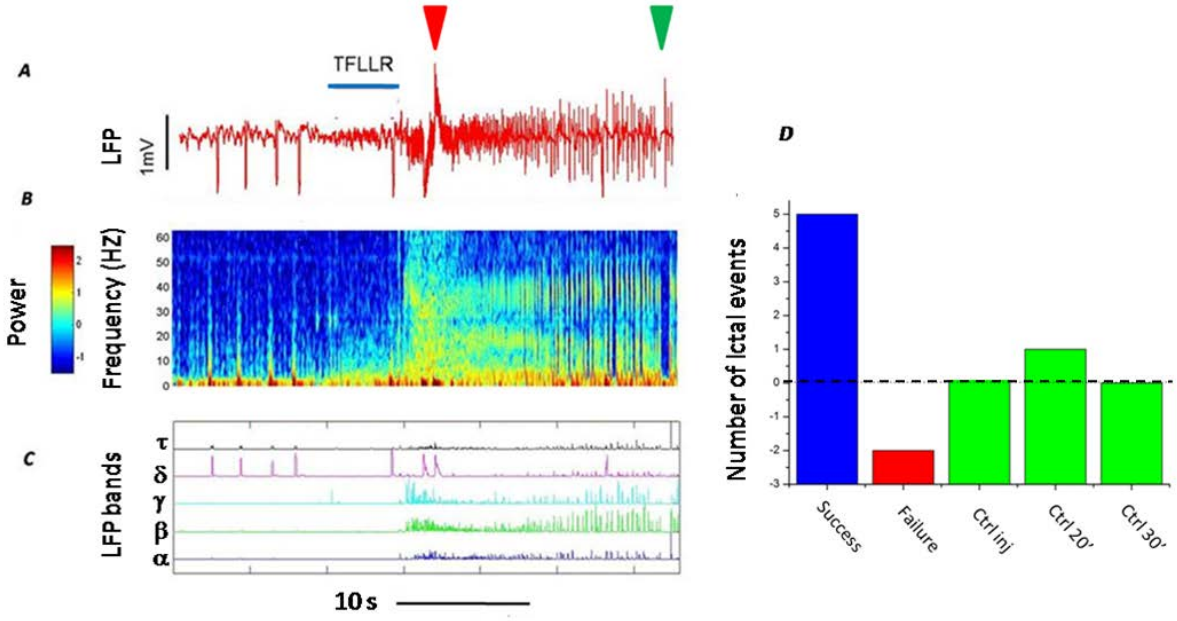

Figure 3.10: Ignition of ictal events. A) LFP during ongoing interictal activity recorded 15' after a third perfusion/third ictal event. At this point no further spontaneous ictal events are expected (see figure 3.3). Blue line indicates pressure-injection of TFLLR (200 μM in aCSF at 0.5 p.s.i. for 5 s). A low LFP amplitude phase ensues after TFLLR injection turning into a bursting one shortly after. LFP shape is indistinguishable from spontaneous ictal/afterdischarge events although shorter in duration compared with average 3rd ictal/3rd perfusion (12.5 ± 5 s Vs. 143 ± 42 s). B) STFT analysis of the LFP in A. Spectral features of TFLLR-triggered ictal event are similar to spontaneous ones. Note the marked increase in 10-30 Hz power band shortly after injection start and constantly increasing suddenely peaking at ictal start (red arrowhead). A greater increase in 10-50 Hz band is concomitant with the slow interictal event just before ictal onset when TFLLR injection is already terminated. In the following 10 seconds a typical ictal STFT developes into an afterdischarge pattern. C) Frequency band decomposition of LFP shows a strong increase in gamma activity after TFLLR injection and during the slow wave before red arrowhead. D) Quantification of TFLLR effect. Positive effect was considered when a 5 s injection of TFLLR was followed by a ictal within 15s (average delay is 4 ± 2 s). Statistics presented here are relative to trials conducted in low ictal chance, namely >15' after a second BMI/fifth ictal or 15' after a third BMI/third ictal or 15' after a first BMI/fourth ictal. Regrettably too few experiments were conducted (N=3), nevertheless a 62% of success could be estimated for TFLLR using these criteria. Furthermore, only one case of spontaneous ictal event (no TFLLR injection) after 20' from previous one is recorded in one animal (ctrl 20') and none after 30' (ctrl 30'). In 2 cases after the injection no ictal events were observed (not even spontaneous ones) instead restored after a further BMI perfusion (failure). TFLLR containing solution was also added with 20μM SR-101 in order to visualize ejection and discard possible ejection failure. Control were performed injecting aCSF + SR 101 without PAR-1 agonist. 3 injections were made in the same conditions described for TFLLR in this case (ctrl inj). No effect of SR 101 was ever observed.

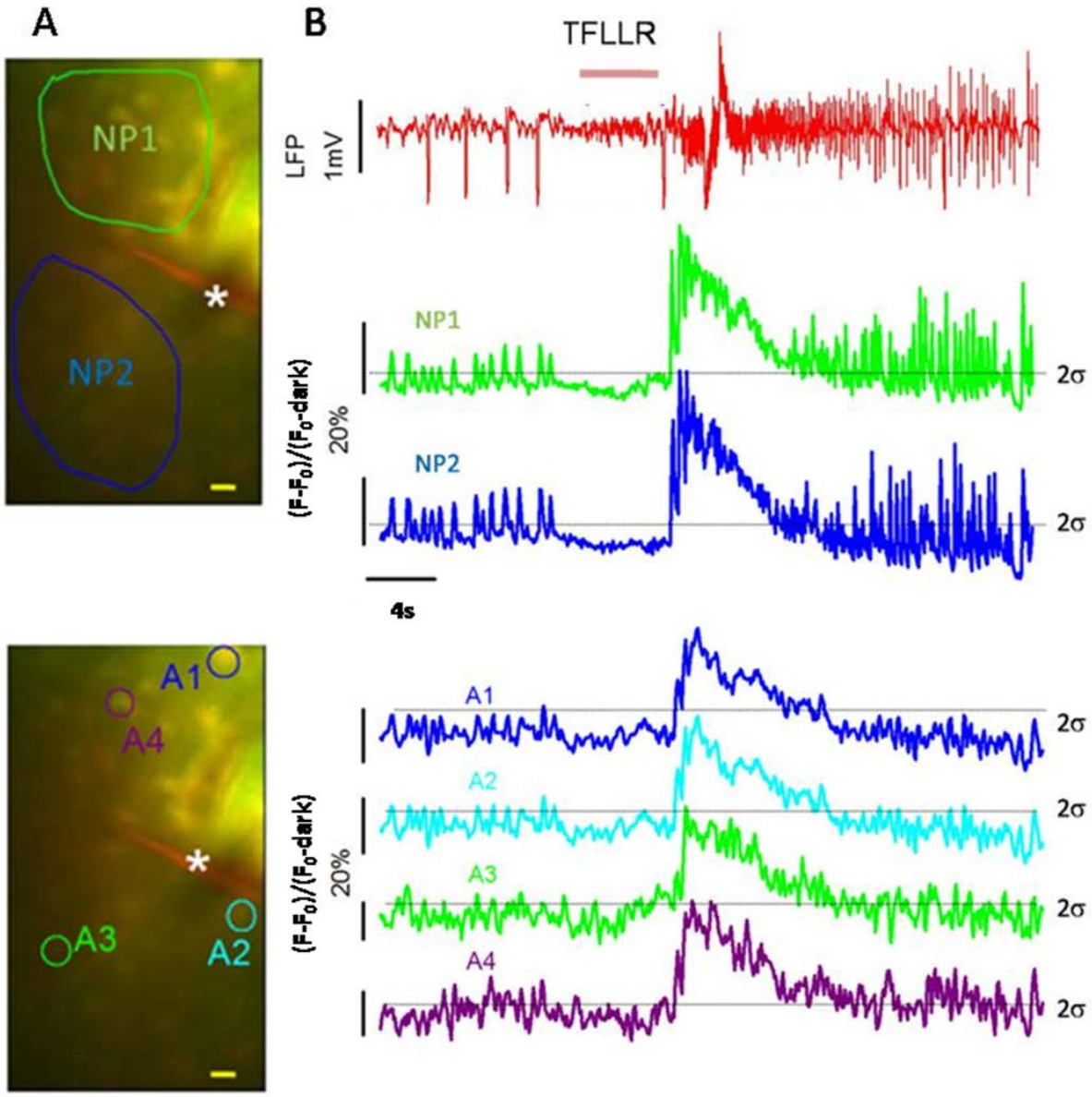

***Figure* 3.11:** Astrocyte Calcium elevation precedes ictal onset in TFLLR injection. A) Imaged field at 150 μm in EC. Top two region of neuropile are highlighted. Bottom: same field with 4 astrocytes indicated. The injection pipette is visible being loaded with SR 101 together with TFLLR. (*). Calibration bar 20 μm. B) In red the LFP described in figure 3.10. Horizontal red line indicates the 5 s injection of TFLLR during ongoing interictal activity. Below: $\Delta F/F$ for the two regions of neuropile and astrocytes in A, acquired concomitantly with LFP. Horizontal lines indicates the arbitrary 2σ level of confidence. Before TFLLR injection, neuropile shows Calcium events at each interictal spike. Shortly after TFLLR injection, a large neuropile Calcium increase precedes ictal onset. Neuropile Calcium peaks just before the slow wave leading into ictal phase. Neuropile Calcium transients experience a short lived plateau during early ictal activity then decrease quickly reguardless the sustained high frequency oscillations in LFP. No "second peak" is to be observed at the termination time as described for BMI spontaneous epileptiform events (see figure 3.5 and 3.6). Fast Calcium oscillations are clearly visible during afterdischarge phase. Calcium transients in the two neuropile region analyzed

here are highly synchronous during interictal phase, at the onset of ictal activity and although to a lesser extent, in afterdischarge activity. ΔF/F for astrocytes show a single sysnchronous massive increase in all astrocytes with no delay with respect to the neuropile. On the other hand, rising phase kinetics in astrocytes seems to be more sluggish compared to neuropile. Astrocytes alone also display a shallow and slow increase in Calcium during TFLLR injection preceding neuropile. This increment its unlikely the consequence of cell swelling or tissue deformation under pressure challenge since control injection with SR 101 (same condition as in TFLLR) never produced any Calcium deflections. a second weak peak later on (still before ictal termination) is visible at least in A1, A2 and A3 of which neuropile seems to be completely bereft of. Fast oscillation in interictal events or during developing of afterdischarges are not detectable in astrocytes. During TFLLR injection LFP is silenced abruptly. Although an artifact here could be suspected possibly due to volume flow “masking” the electrode from the field, no sign of Calcium oscillations are to be observed in this region. Indeed, if LFP here was not silenced, traces of activity should be reported from neuropile ΔF/F at least.

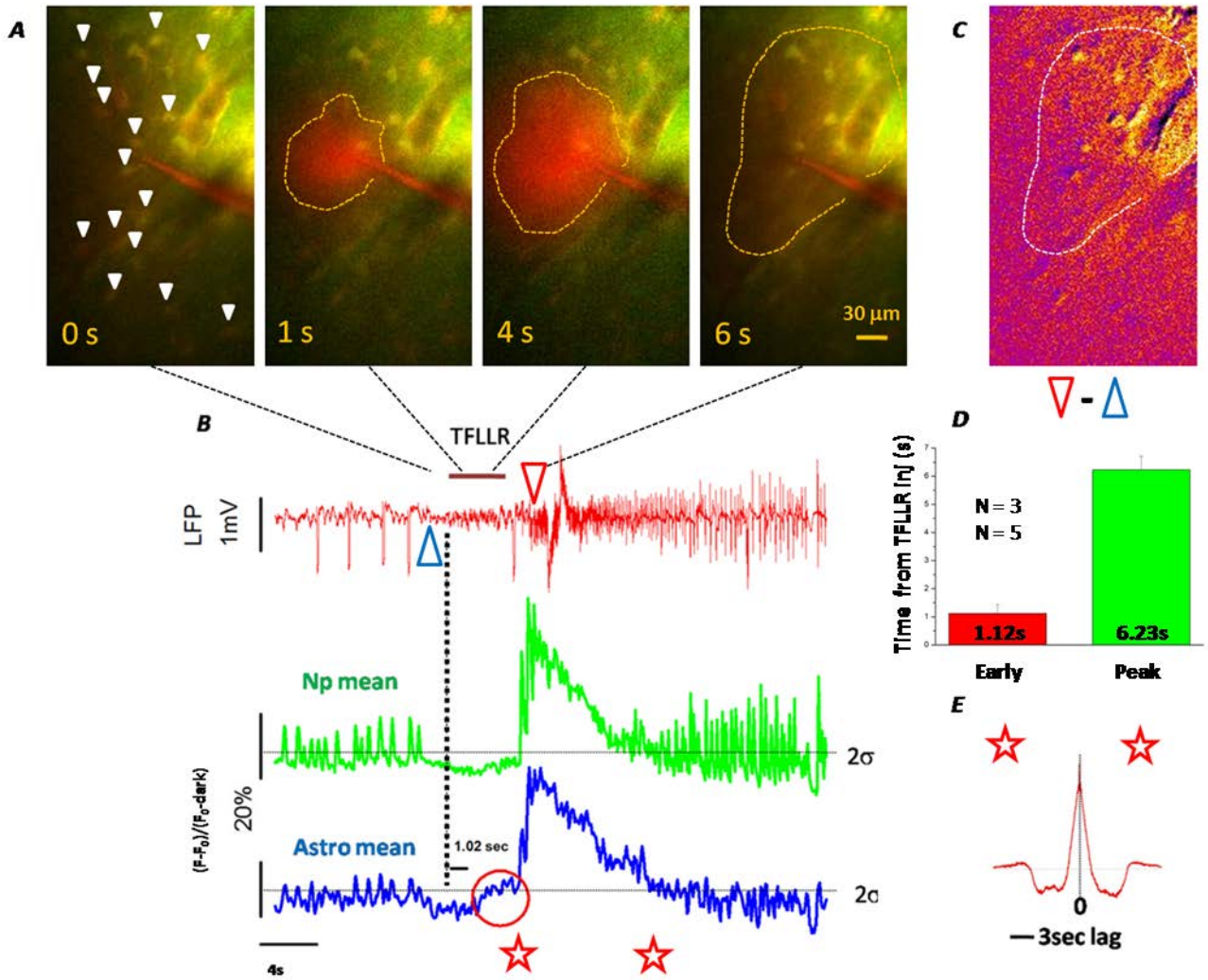

Figure 3.12: TFLLR microinjection recruits large astrocyte territories. A) Four frames extracted from the same imaging series in Figure 3.11, taken just before TFLLR injection start (0 s), 1 second after injection start (1 s), 4 seconds after injection start (4 s) and at 1 second after injection end (6 s). Red shade is the diffusion front of SR 101, highlighted by the yellow dashed line. Diffusion of TFLLR is inferred from the red halo of SR 101. No leakage of SR 101 and thus presumably of TFLLR, is observed before pressure pulse (0 s frame). Diffusion appears to be inhomogeneous privileging the upper portion of the field. After pressure is stopped the red halo keeps diffusing (6 s image show a larger and fainter red area). The red shaft is the pipette tip loaded with aCSF containing TFLLR and SR 101. White arrowheads indicate the position of 15 astrocytes B) top: LFP showing TFLLR triggered ictal event. Red bar indicates the position in time of TFLLR injection. Blue and red triangle mark the position in time of two frames used to calculate image C. The vertical dashed line serves as a temporal reference for ΔF/F plots beneath and is aligned with TFLLR injection start. Bottom: ΔF/F oscillations calculated for neuropile as the mean of ROIs in image # 12 and astrocytes as mean values in 15 ROIs in A. Red circle highlights the occurrence of a weak Calcium transient only present in astrocytes during TFLLR administration starting around 1 s after pression is applied to the pipette. In this experiment 13/15 astrocytes displayed the early Calcium transient, and none of them remained silent during the ictal event. During developing of afterdischarge activity, neuropile display conspicuos pulsatile Calcium increases completely absent from

astrocytes mean. Red stars below the plot indicates the portion of ΔF/F used for E. C) Logarhythm color coded image from Calcium dependent fluorescence obtained subtracting the frame acquired at the time indicated by the blue triangle from the one acquired in correspondence of the red one. The image represents the difference in OGB fluorescence comparing the timepoint of the ictal peak in ΔF/F at 6 s after TFLLR injection, with a timepoint preceding TFLLR administration. Hotter regions correspond to higher Calcium dependent fluorescence in the later frame compared with the erlier one. The dashed white line is the same as in A frame 6 s, which is also in the same temporal position of the red triangle thus no further TFLLR diffusion has occurred. TFLLR is a peptide thus it is reasonable to assume a wider diffusion front for SR 101. Although the hottest region is contained into the white perimeter, several Astrocytes far away from the border are also lit. D) Statistic relative to all 5 TFLLR success (n) in 3 animals (N). A total of 52 astrocytes were counted, 38/52 astrocytes displayed the early increase in Calcium. Red column is relative to these astrocytes and indicates the mean delay from TFLLR injection begin to the start of early Calcium raise. The green bar is relative to the mean delay fron TFLLR to ictal Calcium peak in all responsive astrocytes (48/52). A low standar error bar indicates that distribution of calcium oscillations timing across experiments is homogeneous and narrow, and, astrocytes are pretty well synchronized by TFLLR injection. F) Cross correlation calculated between ΔF/F in neuropile and mean astrocyte between time positions indicated by the red stars. The perfectly aligned lag-0 peak indicates synchrony between Calcium oscillation in neuropile and astrocytes at the point of ΔF/F large peak.

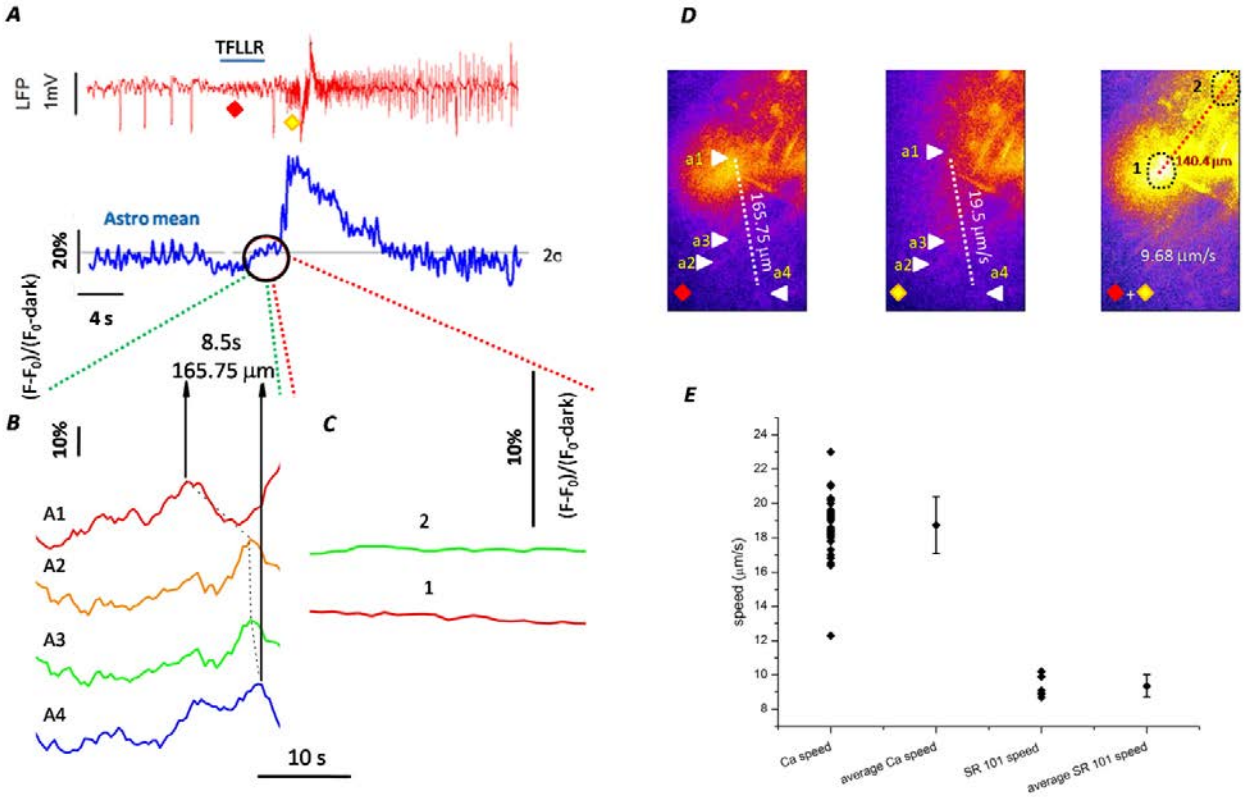

Figure 3.13: Astrocyte Calcium propagation speed. A) LFP and Calcium-dependent fluorescence oscillation described in Figure 3.12. Black circle highlights the slow Calcium rise in Astrocytes preceding ictal start. Red and Yellow diamonds indicate the time at which images in D are pooled. B) Four ΔF/F tracks from different astrocytes running during the pre-ictal Calcium rise. A1-4 are progressively further from the injection pipette tip. All show a double peaked transient shortly after TFLLR injection end. The position in time of the topmost peak in each astrocyte track is used to calculate the Calcium propagation speed. Red track is the one showing first the pre-ictal peak, not surprisingly comes from the astrocyte in front of the injection pipette. All ΔF/F track were corrected for acquisition time distortions imposed by scanning mode that could be relevant considering small differences in time between distant cells. Distance between cell A1 and A2 is indicated as well as the time intervening between top peaks in both cells. C) Calcium-independent SR 101 fluorescence intensity behavior during the period in the black circle in A. Green and Red refere to region 1 and 2 in D respectively. ΔF/F in B and in C are aligned in time. ΔF/F is flat for both region 1 and region 2 with a slanting profile for red trace indicating that at the time considered, SR 101 is diffusing away from region 1 and has not yet reached region 2. Red fluorescence peak is reached at the time of TFLLR injection start then, although injection is kept going for several seconds, SR 101 slowly diffuse possibly due to a partial clogging of the pipette tip. D) Frames extracted from the Calcium-independent SR 101 fluorescence at time points indicated on LFP in A by the colored diamonds. Left: peak in SR 101 fluorescence at the start of TFLLR injection Center: red fluorescence just before ictal start 1 s away from the end of TFLLR injection. Right: image obtained summing the other two, in order to highlight the diffusion front progression. Images are logarithmic intensity-to-color coded. White triangles mark the position of four astrocytes, the ΔF/F of which is displayed in B. Distance (calculated from software provided µm-per-pixel measure) between A4 and A1 is indicated in white in the image on the left, while Calcium peak propagation speed is reported on the image in the center. Calcium speed propagation was estimated dividing distance between A1 and A4 by the time lag between A1 and A4 pre-ictal ΔF/F peak. Diffusion speed of TFLLR containing solution was estimated dividing distance from region 1 and region 2 (image on the right) by the time lag between red fluorescence peaks observed in region 1 and region 2. E)

Average speed of Calcium propagation was calculated among 40 astrocytes and SR 101 from 5 pulses (only efficient ones) performed in a total of 3 animals. The histogram presents speed distributions and corresponding average values (average Calcium propagation speed: 18.7 ± 1.6,μm/s average SR 101 diffusion speed: 9.3 ± 0.6 μm/s).

3.5---Astrocytes are (almost) silent during hypersynchronous events in epileptic mEC.

High speed line-scan acquisitions, reveals absence of any significant Calcium transients in astrocytes during interictal activity. Contamination between neuropile regions and astrocyte ones also result negligible.

Data presented so far, were acquired at frame rates around 1-4 Hz. Fast interictal events are around 200 ms long, thus the possibility of a inadequate sampling is consistent. A typical image acquired containing one interictal event results indeed divided in two regions with clearly different average levels of Calcium dependent fluorescence intensity. The two regions are composed by scanning lines acquired before the time point of interictal event occurrence and lines imaged from the onset of impulsive event to its end and further. Such events are so fast that an instantaneous step in ΔF/F is observed across the two regions. Typical acquisitions are 256X256 in pixel resolution with 4.4 μs pixel dwell time, for an average duration of scanned frames around 0.2 s. each frame is then composed of pixels acquired in different times for an average duration comparable to the interictal event itself: obvious undersamplig and aliasing phenomena may occur. Cellular bodies occupy small spots in a 40X objective 1X zoom images, thus a small duration in time when scanned. Each average value of ΔF/F aquired inside a whole cell has an average duration of apound 0.1 ms at low mag (some 30 pixels in area) and is separated from the next by a frame period. An average 0.1 s of “darkness” fill the time between frames. In these intervals galvos are reset to starting position, laser power is shielded and fluorescence data are not acquired. LFP acquisition is performed at 1 KHz sampling rate which is beyond scanning capabilities at full frame acquisition. It is possible, nevertheless, to arbitrarly define the path along which laser is scanned, on a customizable scanning path. One option is to draw an horizontal straight line along which a series on arbitrary number of scans can be reiterated. An arbitrary number of lines are scanned in unidirectional way (back and forth scan is not allowed) each distant from the next a “line-flyback time” (around half the time spent in scanning). This produce a striped image where spatial coordinates are encoded in the width of the stripe and temporal coordinates correspond to the length of the striped image (1 ms for a 256 pixel long line and 4 μs dwell time). Time between each iteration (a period of average 0.3 s duration) allow to moderate possible damaging effects of continuous laser scanning insisting on the same cell for lon periods. With this sampling rate a far better characterization of fast events was possible. In figure 3.14 is presented a line-scan acquisition of a single interictal event. Between ictal events a variable period of hypersynchronous activity is interspersed with baseline epochs and seldom observed spike-wave complexes. Interictal events frequency is highly variable and tipically few are observed. A line-scan acquisition across a region of neuropile and one astrocyte during one hypersynchronous event is shown. Neuropile

ΔF/F transient start is perfectly aligned with the onset of LFP event. Duration of neuropile ΔF/F exceeds that of LFP transient, in average: 0.7 ± 0.05 s (20 interictal line-scan analyzed). Astrocyte Calcium behavior during interictal events as deduced from line-scan acquisitions is comparable with that observed with conventional scanning mode: no signs of Calcium oscillation. This procedure excludes that fast Calcium oscillations were neglected altogether when acquiring OGB fluorescence from astrocytes in wide-field scanning mode. Several types of Calcium behavior are described for astrocytes, ranging from fast "sparkles" to large "waves", both *in vitro* and *in vivo*, all of them with kinetics beyond the millisecond range (Ubl and Reiser, 1997; Pasti et al., 2001; Kuga et al., 2011; Li et al., 2012; Verkhratsky and Parpura, 2013; Shigetomi et al, 2013; Tong et al., 2013). Calcium oscillation in astrocytes somata may also result as a build-up mechanism starting from processes and propagating into bulky cytoplasm only when spatial summation is sustained enough in time (Volterra and Meldolesi, 2005; Jourdain et al., 2007; Di Castro et al., 2011) . Although few thick processes were resolved in the Guinea pig model, a piece of analysis is presented in the next session. Suspecting a protective role against ictal events, hypersynchronous interictal spikes are further examined in more suited model: the BMI-superfused mouse V1 *in vivo* presented later on, since interictal events are pretty scanty in the BMI perfused *Cavia* brain.

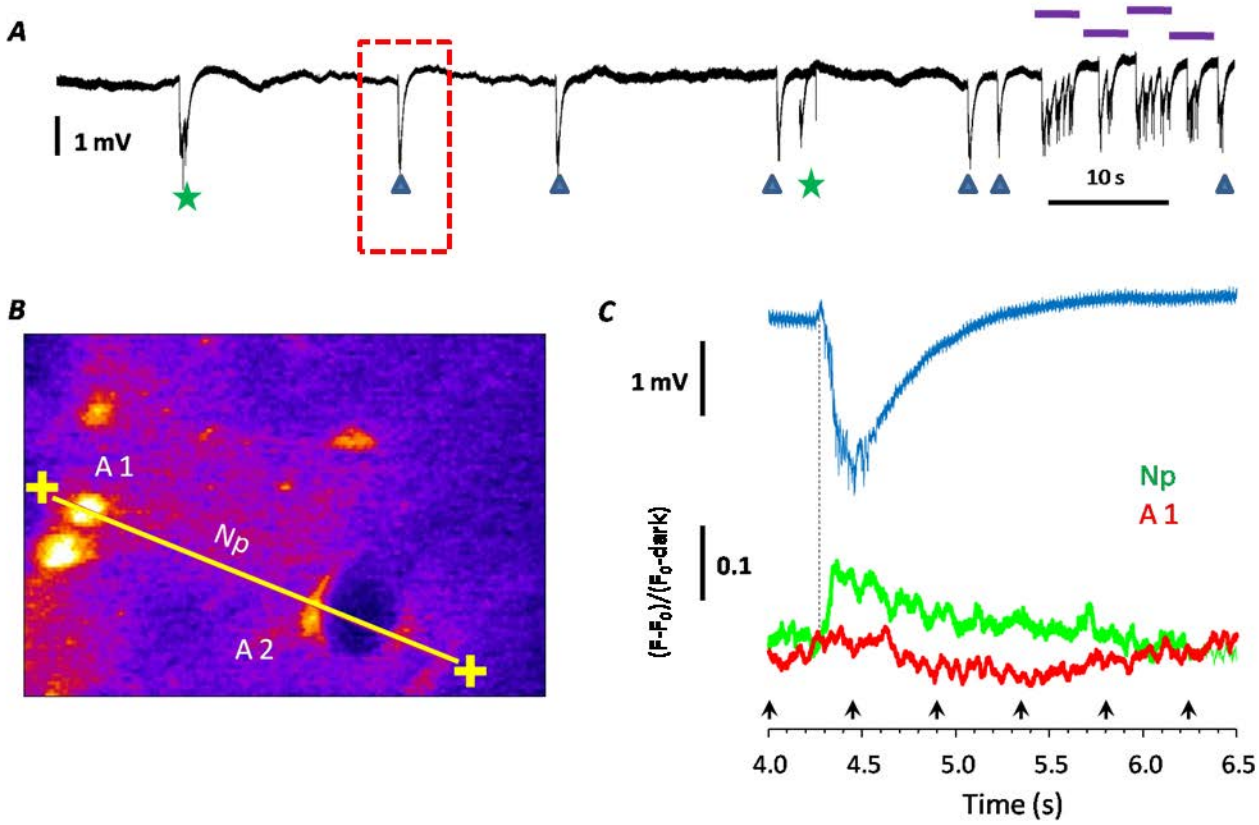

Figure 3.14 : Astrocytes are almost silent during fast interictal activity A) LFP from mEC recording during interictal activity after second BMI pulse. Fast spikes (arrowheads) are interspersed with some rather slower ones (star) and some spike-wave complexes (bars). These deflections are peculiar of epochs between two ictal events reguardless the BMI pulse cardinality. Interictal activity may greately vary in duration and in frequency of events while individual deflections are rather stereotyped. A single fast interictal event is captured during line-scan fast acquisition (dashed box). B) Single frame from a Calcium-dependent fluorescence T-series acquisition. Intensity is logarithmic color-coded. A1, A2 are two astrocytes, while NP is a region of neuropile. ROIs, in this case, are sections of the yellow line along which a linescan acquisition was performed between yellow crosses. Each ROI is chosen in order to fit with the location of cells in the whole field. C) Top: LFP of 2.5 s of LS total duration. A typical single fast interictal event is scanned. Bottom: $\Delta F/F$ extracted from LS for neuropile and astrocyte A1. Only neuropile show significative Calcium increase aligned with interictal event (vertical dotted line as a time reference). The astrocyte remain silent throughout the event, before and after it.

3.6--- A-synchronous ictal events trigger intense endfeet activity.

Short lived Calcium oscillations have been described in several circumstances at the level of individual astrocyte processes, of which bulky cytoplasm appears to be completely bereft of. We observed that fast interictal activity have no Calcium counterpart at all in first order processes or vessel-enwrapping endfeet. Conversely, high frequency-long lasting ictal activity is associated with intense Calcium elevations in both processes and endfeet. This points toward a differential homeostatic regulation of blood supply being poorly challenged during hypersynchronous events and massively recruited in high frequency ictal activity.

Another discussed issue concerning networks and ictal activity, deals with metabolic consequences of seizures and how astrocytes might be involved in vasodynamic homeostasis (Magistretti, 2006; Allaman et al., 2011; Bélanger et al., 2011; Itoh and Suzuki, 2012; Stobart and Anderson, 2013). To evaluate energy costs and homeostatic strategies the fMRI approach is largely employed also suitable for human applications. BOLD signal is instructive of tissue oxygen consumption and was used to describe a biphasic response in TLE patients (Kobayashi et al., 2006). fMRI experiments suffer from several drawbacks amongst which poor spatial and temporal resolution are the worst. Imaging experiment conducted in slice preparations report conflicting avidences concerning neuro-vascular coupling in model of epilepsy (Vanzetta et al., 2010; Bettus et al., 2011; Zhao et al., 2011; Winker et al., 2012). *In vivo* imaging of intrinsic signal experiments points toward large increase of perfusion and sudden ipoperfusion at ictal onset and arrest respectively (Schwartz and Bonhoeffer, 2001; Bahar et al., 2006). also these experiments are characterized by low spatial and temporal resolution. M. Gomez-Gonzalo *et al*.(2011) report evidences of astrocytes direct implication in vasoactive modulation during epileptiform activity. We tested this hypothesis *in vivo*, by means of conventional and LS Calcium imaging during BMI induced epileptiform activity in Guinea pig isolated brain EC. In Figure 3.15 is reported the behavior observed in $\Delta F/F$ of neuropile, astrocyes and perivascular endfeet during ictal and interictal activity.Typical biphasic $\Delta F/F$ deflections of neuropile and the delayed monophasic one in astrocytes already described for ictal phases are shown. $\Delta F/F$ track from two endfeet is also reported. Note the peaked $\Delta F/F$ transient aligned with astrocyte's one and the shallow plateau preceding that. The possibility of neuropile signal contamination is excluded confroting AD phase in endfeet and neuropile: no sign of neuropile transients are observed in endfeet. Also the kinetic of the endfeet peak is much faster than that of neuropile. Even astrocyte cell bodies display Calcium behavior different from that observed in endfeet: two different processes seems to be acting in difeerent astrocytes cell districts. Calcium elevation in endfeet either spontaneous or triggered ones, are documented to start vasoactive responses which produces different outcome on blood perfusion depending upon the present vasoconstriction level (Mulligan and McVicar, 2004; Haydon and Carmignoto, 2006; Metea and

Newmann, 2006; Iadecola and Nedergaaard, 2007; Gordon et al., 2009;). Also Calcium elevation in astrocyte somata produces, with low fidelity, calcium elevation in endfeet that are in cytoplasmatic continuity with triggered cell (Straub et al. 2006). Although correlation between Calcium elevation in processes and endfeet was never investigated, once an astrocyte cell soma experience a large Calcium elevation it seems plausible all processes emanating from it will receive the Calcium wave (Di Castro et al., 2011). Conversely, spontaneous Calcium elevations at the level of the soma are rarely observed in low regimen of electrical activity while processes are intensely yet locally stimulated. Increasing neural activity shall in turn translate into an increased astrocyte process Calcium activity. Finally, when some processes undertake intense Calcium fluctuations a somatocentric Calcium wave could propagate. This might be enough to trigger CICR phenomena starting a retrograde somatofugal Calcium wave invading alla processe even those relatively silet until that moment. Indications that endfeet are experiencing Calcium transients of low magnitude before observed somatic ones, hints in this direction. During ictal aactivity thus, perifereal processes activation might precede astrocyte somata and once a threshold is gained, somatofugal CICRI could be released. If this point of view was proven right, the early and slow increase in astrocyte soma $\Delta F/F$ preceding ictal termination and starting just ahead of neuropile's one, could be the telltale sign of somatocentric integrated Calcium pulses conveyed by periferic processes. In this perspective, these early and slow transients are indeed steady rising slopes until a point is reached where time derivative of somata $\Delta F/F$ gets suddenly extremely higher. This could be the time at which afferent Calcium inputs are summated overthreshold and start a all-or-nothing intense back propagation. From endfeet point of view, some local interplay with neuropile could start the slow and shallow early transient. This could remain local or propagate (I'd rather suspect the former being more plausible given the morfofunctional specialization of endfeet) while Calcium from all activated processes accumulates in the soma. During early transient, endfeet might promote vasodilation (relatively low levels of NO and PGEs are produced in low Calcium regimen having vasodilataive effects if low enough or vasocontricting if high Mulligan and McVicar, 2004). Once somatofugal Calcium wave reaches endfeet, massive increase in Calcium is raised wich could be responsible for vasoconstriction. During interictal events, on the other hand, rarely fluctuation are observed in endfeet $\Delta F/F$ and often falling below noise fluctuations. No vasodilation nor vasoconstriction is described for interictal activity. Meanwhile as described above, neuropile show $\Delta F/F$ spikes perfectly matching those in LFP and astrocyte somata $\Delta F/F$ are flat. Responses in endfeet $\Delta F/F$ are quantified in Figure 3.15. From thesa set of data, two possible scenarios emerge: either somatofugal Calcium propagation invades processes and endfeet or metabolic homeostasis of ictal activity require astrocyte endfeet activation. No sign of interictal commitment of astrocyte endfeet is oibserved suggesting for a metabolic low-cost modality.

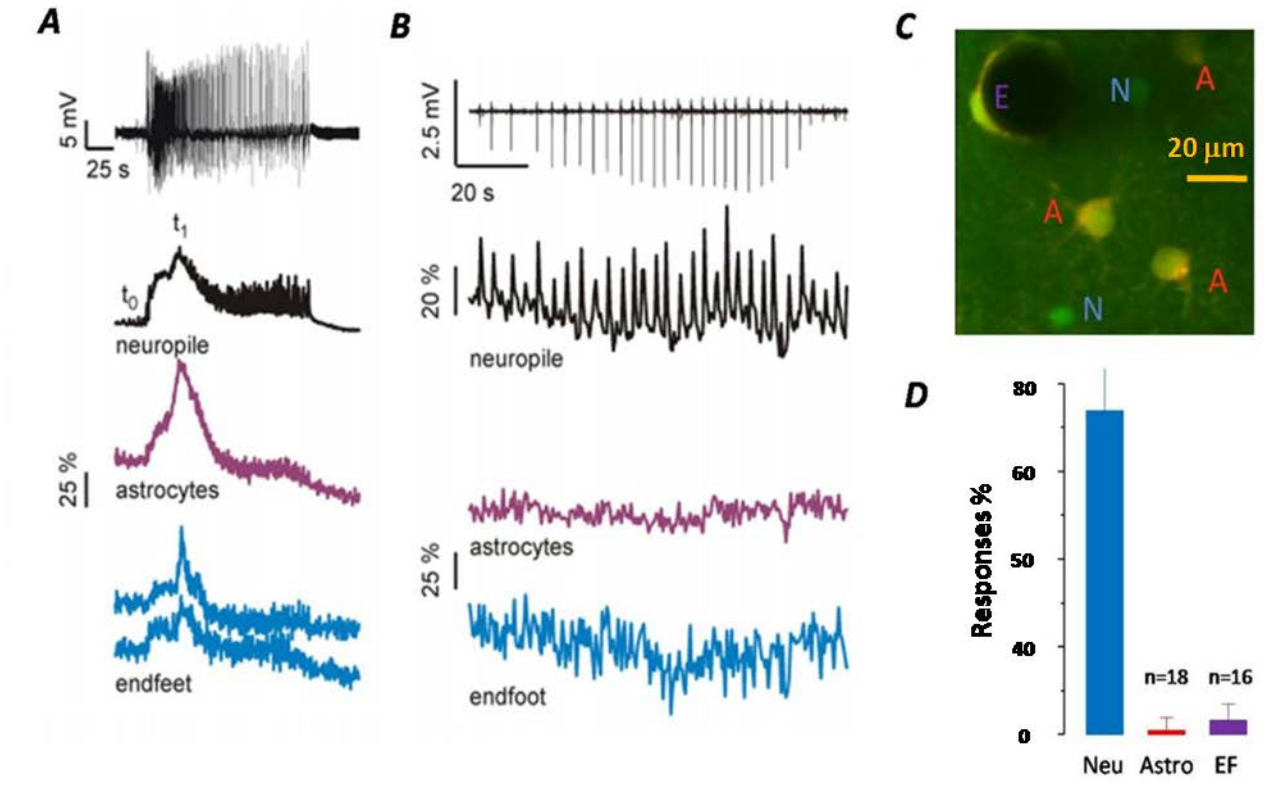

Figure 3.15: *Endfeet Calcium behavior in epileptiform activity. A) black top track is the LFP recorded in mEC during a full epileptiform event. Black track below is the Calcium dependent ΔF/F for neuropile where t_0 and t_1 mark the onset of ictal activity and its termination respectively. Purple plot is ΔF/F relative to an astrocyte soma representative of mean astrocyte behavior: a single prominent peak in Calcium is reached a t_1 (around 20 s after ictal start). Blue tracks at the bottom are ΔF/F of two endfeet in the same field. Note the marked early Calcium transients aligned with neuropile's t_0 and the second one at t_1 aligned with astrocyte soma. Athough some degree of neuropile signal contamination in endfeet is plausible, peak at t_1 in endfeet display kinetics different from those in neuropile, furthermore, no contamination whatsoever is observed during afterdischarge activity which is nonetheless conspicuous in neuropile. Conversely, Calcium increase between t_0 and t_1 in neuropile seems to be faithfully mirrored in endfeet. B) Interictal activity in LFP and corresponding ΔF/F in neuropile (black). Each fast event in the field is mirrored by a transient in ΔF/F , conversely no sign of Calcium dependent fluorescence fluctuation is observed in ΔF/F relative to either astrocytes or endfeet. C) Average projection of a typical time series in mEC showing astrocytes and neuron somata, neuropile and blood vessels-enwrapping endfeet. D) Histogram summarizing the occurrence of ΔF/F transients during interictal activity (70 events in 3 animals): neuropile (5 regions in 5 different time series) display an average 73% fidelity while astrocyte somata and endfeet are almost non responsive (1% and 3% respectively).*

3.7--- Low activation of astrocyes during up/down states.

Spontaneous cortical sleep activity is dominated by the "up-down oscillator": neurons are entrained in a rhythmic under-threshold fluctuation of membrane potential. Only seldom neurons are observed to fire short trains of action potentials under anesthesia, unless sensorial stimulation is brought about. In this regimen of low neural "pressure" astrocytes show signs of Calcium activity with very low probability, which also appear to be poorly correlated with local field potential. Processes from different astrocytes, collectively show "flickering" Calcium oscillations mostly aligned in time with neural ones. Processes emanating from a same soma display, remarkably, uncorrelated Calcium oscillations one another. Neuropile Calcium transients, more than neurons, perfectly mirror local field activity with nearly 100% accuracy during up-states. Calcium oscillations in principal cells result far more accurate in "detecting" up-states than Parvalbumin containing interneurons, which, on top of a lower frequency of Calcium ascillations, also display an homogeneous probability of Calcium "spikes" both during up and down states.

During non-R.E.M. sleep, cortical mantle entertain slow frequency activity, disengaged from sensorial processing or executive tasks. At the level of neural population this is manifested as a quasi-periodic oscillation of EEG, ECoG or LFP. Short periods of low intensity depolarizations, UP states, are recorded interspersed with epochs of "silence", DOWN states. frequency may change in time and in relation to the depth of the sleep stage (Steriade, 2004; Steriade, 2006; Destexhe et al., 2007; Compte et al., 2008; Chauvette et al., 2010). Although isolated neocortex is capable of intrinsic rhytmogenesis (Borg-Graham, 2001; Santos et al., 2010; Sanchez-Vives et al., 2010; Mohajerani et al., 2013;), in the living animal up-down states are almost exclusively dictated by Thalamus (Timofeev, 2011; Timofeev and Chauvette, 2011; Errington et al., 2012, Ushimaru et al., 2012). During sleep, Ach, Histamine, 5-HT, and other subcortical modulators are diminished, as a result, thalamic neurons hyperpolarize and turn into intrinsic bursting units (also termed Central Pattern Generators, a sort of Pace-Makers) (Lee and Dan, 2012). Volleys of excitation are distributed to the cortex in a pulsatile way and local neurons experience a rhythmic subthreshold depolarizations spaced by input-silent periods. Only seldom some neuron in the population are driven suprathreshold in an apparently stochastic way (Bonjean et al., 2012; Marzano et al., 2013). Nevertheless, when discharged, only few AP are fired since bursting mode is impeded as a result of diminished input resistance due to the lack of activation of Potassium channels operated by Ach, Histamine and other neuromodulators. In Figure 3.16 E is described the typical spectral signature of up-down state oscillatory activity, charachterized by the modest population of low frequencies (<10) bands during up-states and a flat FFT power in downstates. Neuropile $\Delta F/F$ show a sparsely packed spiky events, each of low amplitude and duration, perfectly aligned with the start of an up

transient . ΔF/F profile in neurons is radically different: only few Calcium oscilation are observed each of which falls inside an LFP up-state with some jitter. A Single cell show variability in firing rate across time and different cells apper to be uncorrelated in ΔF/F. At each up state few cells are active and the next one most probably have a different set of cell with observed ΔF/F transient. When a neural ΔF/F is detected, a neuropile one is always present and aligned. During Down states both neuropile and single cells are silent. Since most of up states are reflected at the single cell level with a subthreshold depolarization, cellular Calcium increase could be too small to be reported by OGB. Subthreshold oscillation are reported for OGB Calcium imaging using high framerate, high laser powers and deconvolution algorhytms (Helmchen, 2011). On the other hand, single spikes are detectable in conventional Calcium imaging although with the need for avery good S/N. Astrocyte behavior during UP-Down states activity is illustrated in Figure 3.17. Astrocytes somata show some ΔF/F transient aligned with LFP Up states. Compared with neurons, these transients are of longer duration, and of shallower intensity. Also temporal alignment with LFP is highly jittering. It is sometime difficult to tell an astrocyte ΔF/F aligned with up state in LFP since many of them are of longer duration and/or starts before/outside LFP-upstate. an arbitrary time window was selected into which any ΔF/F was considered inside/outside perfect alignment with LFP upstate. This frame have the same duration of average up-state (1.2 ± 0.3s). Events starting before – 1.3 s from upstate onset and those starting after + 1.3 s from up state onset are counted OUT from the upstate. Events with the INSIDE onset but lasting longer than the up state are also considered INSIDE. Neurons and neuropile easily fall inside this window and astrocytes display ΔF/F more frequentely longer than upstate. as a general rule, neuropile (and neural) ΔF/F starts before astrocytes transients. Situation in astrocyte processes is quite different: few ΔF/F are detectable in a much more noisy trace (processes are pretty well resolved, yet small in representative pixel areas) as fast, quite intense, peaked deflections. Most of these events are aligned with neuropile. Some process ΔF/F show little oscillations under upstates which results often ambiguous because of noise. When a clear process ΔF/F is present, not necessarily a correspondent one is observed in somata. No apparet correlation emerges even between processes and the soma of origin, in these conditions. A situation the other way around is instead often observed with somata in view: when a clear astrocyte soma ΔF/F appears, a “blink” in its processes is observed. Probability of process ΔF/F was not included in the calculations since chance of imaging well resolved, stable processes with high S/N was too low. one of such series is depicted in figures 3.18. Here the relation between several processes ΔF/F is compared with ΔF/F from the soma from which they emanate. Some processes either remain silent or S/N is too low to allow detection of significative ΔF/F. P3 P4 and P5 in panel C show intermittent ΔF/F spikes. Time alignment among processe is variable and some perfectly time-matched events are observed. One endfoot is also included in the analysis. A single detectable increase in ΔF/F is observed near the end of the series. Most of blinking events in processes are aligned with neuropile trace. Astrocyte soma show few transients which rarely collimate in time with neuropile. Sometimes a coherent relatively wide blink is observed in processes and a closely preceding or following soma event is

detected. Yet no clear relation between timing or number of process ΔF/F and somatic behavior can so far only be suspected. Delayed response of astocytes compared to neuron and neuropile one, are not nerely the effect of low time resolution as deducible from figure 3.19. Fast (1 ms resolution) linescan acquisitions reveal the early onset of neuronal ΔF/F with almost precise start at the onset of LFP oscillation. Astrocytes are lagging behind. Reported here is a fast somatic astrociye ΔF/F transient, even longer once behave similarly. During sleep or deep anesthesia, Ach subcortical inputs are suppressed, thus Layer II-III neural membranes are locked in low input resistance and harly oscillates in synch, also bursting probability is greately reduced. Local astrocytes receive low neurotransmitters and remain predominantely silent. When Colinergic receptor agonists are injected in anesthetized animals, astrocytes are massively aroused and neurons increase their input resistance. The same effect is obliterated when astrocyte Ach-induced Calcium elevation is forbidden (IP3R2-KO mice). Furthermore, cholinergic-dependent plasticity, is crucial in mnestic tracks fixation (Leach et al., 2013; Minces et al., 2013) which results impaired in IP3R2-KO mice and rescued by d-serine local administration. This observation also lead to the acknowledgment of astrocytes as the gate keepers of cortical wakefulness (Takata et al., 2012). As presented in figure 3.20, cross correlogram between ΔF/F and LFP up-down activity, is characterized by periods of oscillations with associated average high or low cross correlation power. Timed with each up state individual ROIs in neuropile, would show up with matching cross correlation power increase. Some neuropile lanes are less cross correlated along time while most present an average high cross correlation that is intermittently lost. Neurons lanes behave pretty much the same way although average cross correlation appear smaller. Some neurons only seldom correlate. Astrocyte lanes are the faintest in average, nevertheless, few episodes of high cross correlation are present. Observing all lanes, cross correlation tend to be oscillating in phase for neuropile and neurons while astrocytes seems to cohordinate only randomly. Periods of extended Down states, like those highlighted in box 3,4 seems to be associated with minima in cross correlation power, which ensue synchronously along all lanes. When compared with that of epileptiform activity, cross correlogram from up-down activity, appears more scattered, without salient events. Figure 3.21 show the quantification of the probability with which a ΔF/F transient is observed falling inside an up-state or in a downstate. Neuropile ΔF/F of increasing size display increasing fidelity with LFP and almost no events are observed inside a Down state. Also pyramids have a great skewness toward upstates although average probability, compared with neuropile is smaller. Parvalbumin interneurons instead, display an even distribution between up and down statete coincidence. Although total frequency of PV+ ΔF/F firing is comparable with pyramids, chanche of up-state matching is lower in favour of a higher probability of firing away from upstates. Concerning astrocytes, total frequency of ΔF/F peaks in baseline activity result reduced when compared with neurons, also distribution of ΔF/F do not prefere between up or down states (average coincidence chances: Neuropile up: 73 ± 5%---down: 4 ± 1%; Pyramids up: 22 ± 5%---down: 2 ± 1%; Parvalbumin up: 11 ± 4%---down: 12 ± 3%; Astrocytes up: 5 ± 3%---down: 4 ± 3%). No apparent correlation emerges between coincidence chances of any classes and frequency in up-down state activity (0.1-0.3 Hz).

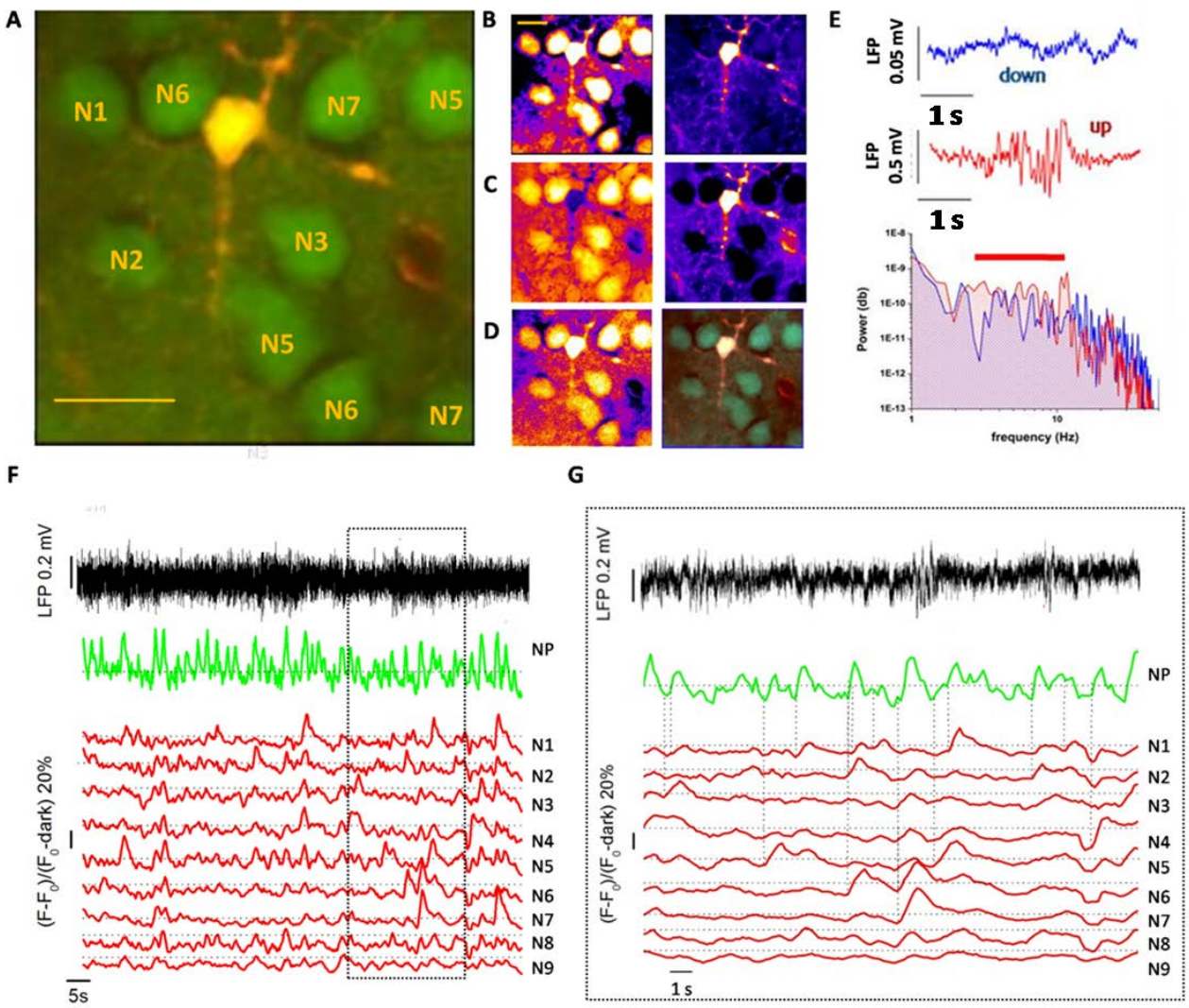

Figure 3.16: V1 neuronal baseline activity at single cell resolution. A) average projection of a time series acquired 250 μm deep in V1 during baseline activity. A single astrocyte (yellow) and 7 neurons (N) are visible. scale bar: 25 μm. B, C, D) Fluorescence intensity-to-color logarithmic scale representations of time series obtained from field in A. B) Left: Calcium dependent fluorescence reveal intense signal from neurons as well as from astrocyte and process. Scale bar 20 μm Right: Calcium independent fluorescence. First order and second order proximal processes are well resolved. C) Left: Average projection of ratio time series obtained from green channel/red channels once normalized each other frame by frame. Right: Same image as in Left with inverted lookup table, discrete domains of intense activity in astrocyte process are emphasized. D) Left:Standard deviation projection of green channel highlights region of neuropile, astrocyte soma and neuronal somata mostly active during the time series. Compare color "hotness" of neurons 5 and 7 and of astrocyte soma with image B Left. Right: merge of C Right (log color coded) with D Left (green). Bright hot colors reflects domains in the astrocytes most active in the time series while more intense green neural somata correspond to more active neurons. E) top: LFP of a isolated downstate, electrical activity is almost silenced. Middle: A single up-state is depicted in red. Typical short-lived small oscillations in the LFP are associated with sub-threshold oscillations in most L II/III neurons, a minority of which discharges APs. Up and down states alternates

constantely during deep sleep/anesthesia in the cortex. Bottom: Power spectra of baseline (blue) and upstates (red) compared (Log Power/Log Frequency). Spectra result from FFT of averaged 10 up states and 10 downstates extracted from LFP as 5 seconds epochos. All upstates were aligned at the onset of each event while downstates were aligned 1 secon after the termination of the previous downstate). The red bar highlights a region where red (averaged up-states) spectral power exceeds the blue one in slow frequency regimen (within 10 Hz) typical of slow wave activity. F) Simultaneous recording of baseline LFP activity (black) and $\Delta F/F$ relative to nine neurons and a region of neuropile. Neuropile Calcium oscillations (green) faithfully mirror each deflection in the LFP while only occasional up states are reported as Calcium fluctuations in single neuros. Neuron 5 and 7 are the most active. As a population, neurons appear to be scantly synchronized with LFP which indeed appears characterized by weak oscillations (average up-stats frequency: 0.3 ± 0.1 Hz, average intensity: 0.6 ± 0.2 mV, average duration: 0.1 ± 0.07 s. Counts relative to 100 upstates in 3 animals). Region of the LFP populated by downstates are indeed devoided by any oscillations in neuronal $\Delta F/F$. G) Boxed region in F magnified in time to emphasize few $\Delta F/F$ peaks in neurons (red) and neuropile (green) as well as LFP upstates. Vertical dotted lines align in time neuropile oscillation onsets with neural tracks. Whenever at least one neuron is active, there is a neuropile transient. No apparent correlection exist between amplitude of LFP up states and probability of neuronal $\Delta F/F$ elevation (also discussed further).

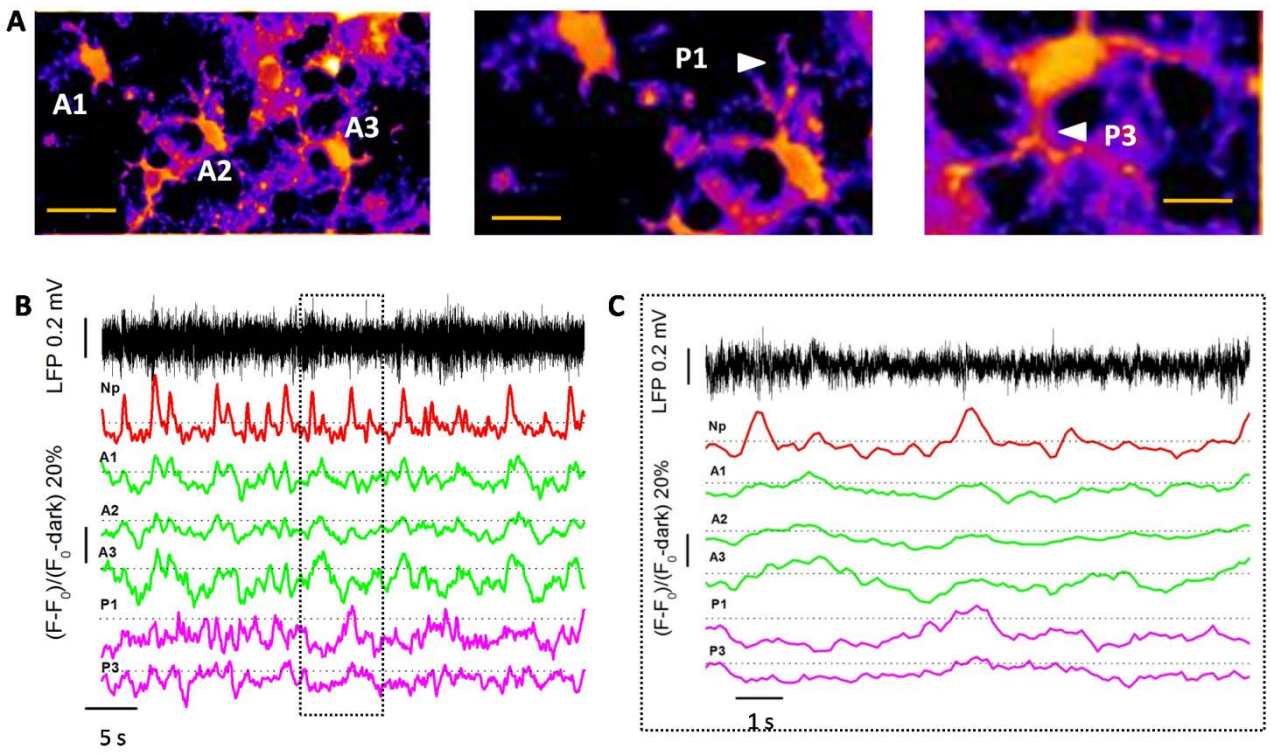

Figure 3.17 :V1 astrocyte baseline activity with sub-cellular resolution. A) Average projection of a ratio time series (green fluorescence/red fluorescence) represented with inverted logarithmic intensity-to-color lookup table to emphasize astrocytes somata, first and second order processes. Astrocyte A3 is the same as in figure 3.17. Scale bar 25 μm. Center: magnification of region in A Left, with A1 and A2, branched first order P1 process of A2 clearly visible. Scale bar 20 μm Right:magnification of region in A left with A3 (rotated -90°). Highly branched P3 process is visible. Scale bar 12 μm. B) LFP up/down states activity in black and simultaneous ΔF/F in neuropile (red) three astrocytes (green) and two first order processes (magenta). Astrocyte transients are much more sluggish compared to those observed in neurons (further discussed). The chance of astrocyte responses seems homogeneous and the overlap between neuropile oscillations and astrocyte ones is considerably lower than that observed in figure 3.16. Processes ΔF/F are more noisy than somata's yet few distinct events are still visible. C) Magnification in time of boxed region in B.Transients in P1 and P3 peaks together with neuropile although raising with a slower kinetic. Cell bodies appear desynchronized from LFP and neuropile.

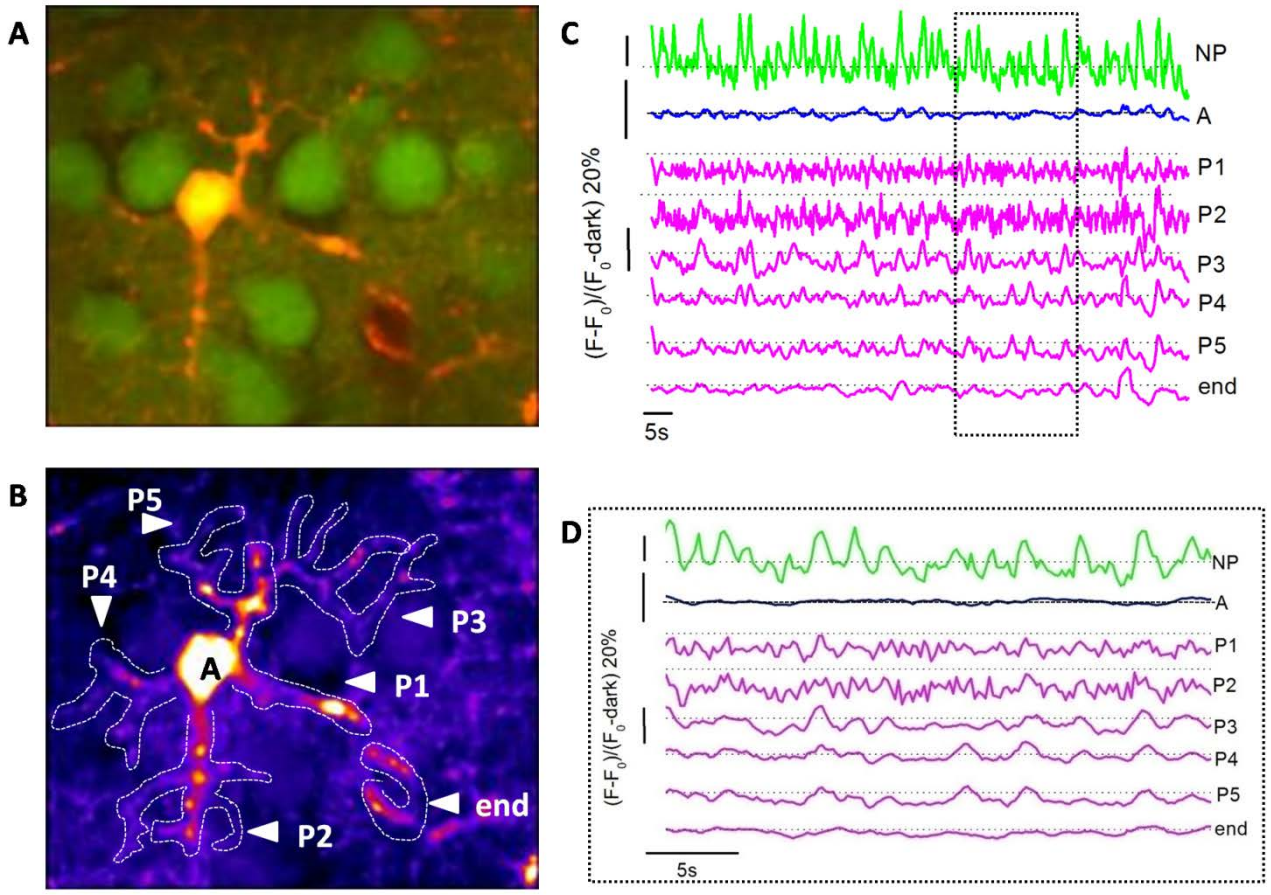

Figure 3.18: Closer inspection of single astrocyte baseline activity. A) single astrocyte also present in figure 3.17, here from a different T-series. B) The ratio time series is average-projected in inverted logarithmic intensity-to-color lookup table, five processes (P_n) and a terminal endfoot (end) are indicated. C) LFP is now omitted being Neuropile $\Delta F/F$ (green) a faithful surrogate. Endfoot display only an isolated significative $\Delta(F/F)t$ increment in the proximity of the end of the time series, remaining otherwise silent. Astrocyte cell body appear almost silent also compared with A1, A2 and A3 in figure 3.17. Since processes transients are present only in few ROIs and in an intermittent fashion, neuropile contamination into processes $\Delta F/F$ could be excluded: two consecutive neuropile oscillations have little chance to be mirrored by processes $\Delta F/F$. This is more evident in D) which is a magnification in time of the boxed region in C. Differences between this time series and that in Figure 3.17 could descend from the different frequency of upstates events between these two eppochs.

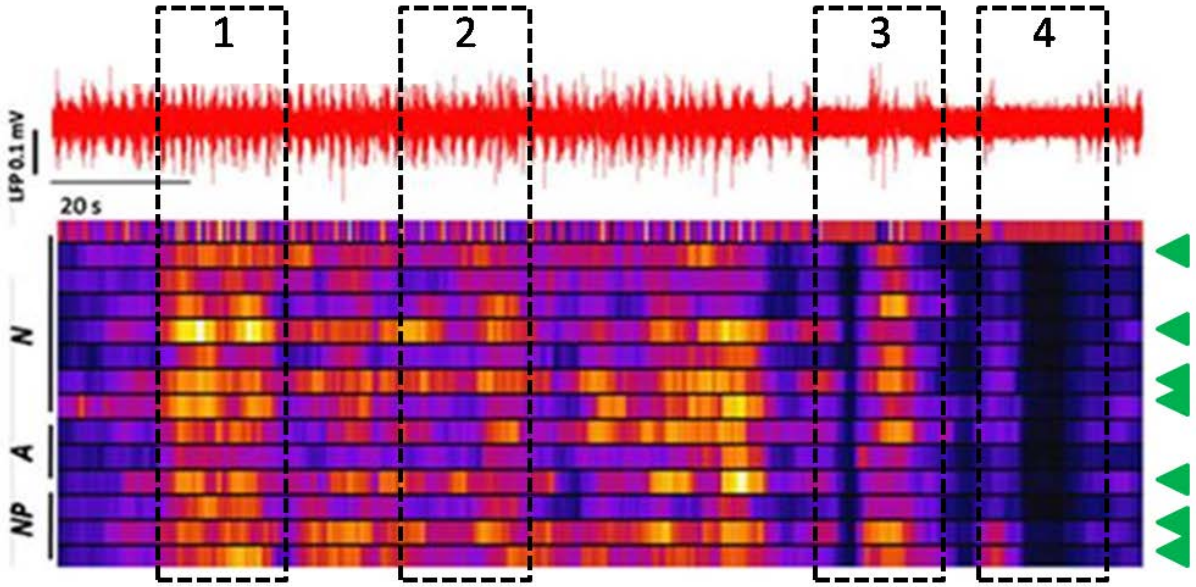

Figure 3.19: High speed acquisition of astrocyte Calcium transients during an Up-state. A) Left panel depicts the LS reference in the imaged field. Below is the LS Calcium dependent signal intensity color coded in logarhytmic scale plotted in time (vertical, total duration 1.34 s). the right panel show LFP with an up-state in black and corresponding ΔF/F track for the astrocyte (green) and neuron (red) visible in top left panel. Neural ΔF/F increases at the very onset of the up-state deflection in LFP, while astrocyte one is delayed. Times indicated referes to this single image and are not average durations. Durations were calculated as the distance in time between first deviation from baseline and peak ΔF/F. B) leftmost two bars in the histogram ("up---n" and "up---a") represents average time lag between first baseline ΔF/F deviation and upstate onset (up---n average value: 0.25 ± 0.06 s, up---a average value: 0.42 ± 0.07 s). Rightmost two bars ("n rise" and "a rise") indicates duration of time-to-peak values in ΔF/F calculated from 30 linescans comprising each a single upstate. Only linescans having first baseline ΔF/F deviation after upstate onset are included (n rise average value: 0.22 ± 0.03 s, a rise average value: 0.08 ± 0.1 s).

***Figure 3.20*:** Cross correlation of ΔF/F and LFP during baseline activity. Red track is a long LFP recorded during deep anesthesia up/down state activity. Frequency of events is not constant, periods of dense activity alternates with epochs of LFP silence. Cross correlogram power between neuropile, neurons and astrocytes ΔF/F and LFP is represented in log color scale . First lane in the raster-plot is log color coded intensity of LFP appropriately decimated in sampling number to match that of ΔF/F. N, A and NP lanes refere to neurons, astrocytes and neuropile respectively. Each raw is relative to ΔF/F of a single ROI around cell somata or comprising neuropile areas. Power of cross correlation cange in time along each lane and different classe of raws present very different patters. Single neurons show very different patterns of cross correlation power with LFP although the average coherence across the whole epoch remain pretty high. Neuropile regions display the best matching pattern with LFP, nevertheless, different lanes are intermittently poorly correlated. Astrocytes are weakly synchronous with LFP exept for few intense events. Even between different lanes in A the coordination appear to be poor. Green arrowheads indicate lanes with most precise matching between LFP and ΔF/F. Despite the great variability in the pattern of cross correlation among different classes, few regions in the LFP are associated with peaks of coordination across all lanes as highlighted by boxed regions. Box 1 present a transversal high power of cross correlation in the face of pretty “standard” up/down activity which is also not the highest in frequency. A transient up-state higher frequency epoch is highlighted in box 2, raster plot below show pretty low values in all lanes. Box 3 indicates a period of weak activity punctuated with 2 high frequency up-state events of which only the first one is mirrored by increase in the power of cross correlation in all lanes except for A. Box 4 comprises the longest period of silence in LFP in the recording associated with high synchronous low power cross correlation along all alnes. As a general consideration, long or short periods of silence are more frequentely associated with overall synchronization.

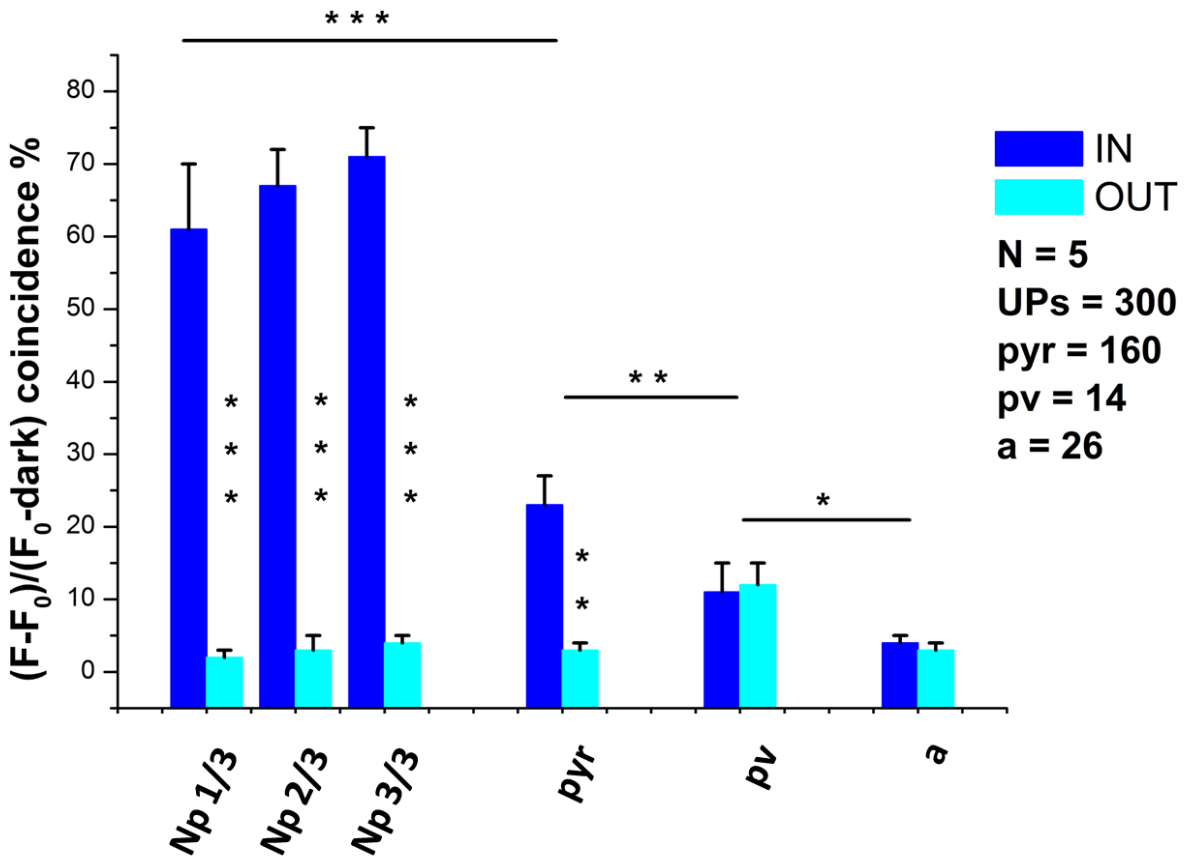

Figure 3.21: *Quantification of coincidence probability between ΔF/F and LFP events in baseline activity. Blue bars height is proportional to the probability, expressed in %, with which a class of ROI presents a ΔF/F transient coincident with a LFP up-state. % referes to averaged values for 160 pyramidal (PYR), 14 Parvalbumin (PV) neurons, 15 regions of neuropile and 26 astrocytes in 5 experiments. Neuropile regions are of increasing size being the "np 3/3" area the largest in each field. Coincidence between ΔF/F and LFP was accepted when ΔF/F events starts within an arbitrary confidence window of + 0.6 seconds (average up state duration) from the nearest up state event start, spotted on the LFP track. A total of 300 upstates was counted with different frequencies (0.2 ± 0.1 Hz in average). Cyan bars represent the probability per each ROI class that a ΔF/F transient appears outside upstate confidence time window. Neuropile display an almost 100% average probability of coincidence that grows as the area of the ROI is increased (an increment of 2/3 in the area size correspond to a significative increase in coincidence %). Large neuropile areas ΔF/F can indeed be used as faithful reporter for LFP activity. Pyramidal neurons are the second best ROI class matching LFP although with poor accuracy, far below 50% chanche coincidence. Chance of coincidence is highly significative compared with "out of up" for pyramidal neurons. PV+ interneurons on the other hand show both a non significative difference in P% matching upstates compared with "out of up". The overall probability of ΔF/F transients in PV remain low during upstates as well as out of them. PV coincidence probability is significative lower then pyramidal neurons. Astrocytes show the lowest average chance of coincidence with upstates, significatively lower then PV. In Astrocytes the probability of ΔF/F transients outside an upstate is not significatively different from the coincidence probability. (*: P < 0.01, **: P < 0.001, ***: P < 0.0001 for paired t-tests).*

3.8--- Photic stimulation increase astrocyte activity.

The sleeping cortex engages sustained electrical activity when solicited with the appropriate sensorial stimulus. Photic stimulation triggers a distinctive field response associated with a spectral increase of gamma band frequencies. In this context, both neuropile and neurons show conspicuous Calcium elevation aligned with every stimulus presentation. Parvalbumin positive interneurs and astrocytes show an increased frequency of Calcium oscillations compared with spontaneous activity albeit with no selectivity toward visual evoked potentials. Astrocyte processes show Calcium peaks aligned with principal neurons which appear coordinated among processes belonging to the same cell.

Anesthetized animals preserve the capability of visual processing (Niell and Stryker, 2010). Visual stimulation is enough to elicit a transition in network state, from spontaneous sleep oscillations to higher frequency activity and associated coherence shift. Here a simple wide field equiluminant flash stimulus was used delivered to the eye contralater to the V1 imaged. Stimulation is exclusively monocular and imaging/LFP were conducted in V1 (Bregma -2.18; -5.20 mm). Up states are easily distinguishable from V.E.P. on the basis of much longer duration (2.3 ± 0.5 s for a 50 ms stimulus), greater amplitude and spectral signatures as reported in Figure 3.22 for typical V.E.Ps.. Also a constant delay from flash onset in observed (average 100 ms, the position in time of the visual stimulation is acquired together with LFP). Stimuli as short as 50 ms are enough to trigger a robust V.E.P. Increasing illumination intensities (measured as relative value of monitor contrast with respect to a pre-set minimum) triggers V.E.P. of increasing amplitude. Also a slight increase in peak frequency in FFT analysis is observed for higer luminance (see figure 3.22, B). Fast linescan acquisitions reveal the delayed V.E.P. response to a visual stimulus in both neuropile an pyramidal neuron $\Delta F/F$. Calcium transient rising phases is not perfectly aligned between the two tracks, with neuropile leading. During episodic FLASH stimulation, also up-down state oscillation persisted. LFP signature of the two different events clearly allow an accurate separation also confirmed by superposition of FLASH triggering signal in time. Amplitude of Calcium transients are consistently bigger during V.E.P. compared with up-states and also durations are longer. Individual principal cells show Calcium increases with most of the FLASHES. These transients apper wider in average than those observed in baseline. Different neurons display different pattern of $\Delta F/F$ which are variable in time. As an average behavior, all principal neurons and neuropile regions, display a coincidence probability between $\Delta F/F$ deflections and LFP V.E.Ps. higher than observed for upstates. The frequency of responding cells is also increased. A decrease in coincidence probability is instead observed for PV interneurons with respect to up-down states, although the difference is not significative. Also the precision of the coincidence probability for PV cells appear poor as

observed for up-down states, with no clear preference for “inside V.E.P.” Vs. “outside V.E.P.”. Astrocytes on the other hand, show a non significative increase in coincidence also associated with a poor precision (see Figure 3.25). Astrocyte processes behave much more like principal cells (see Figure 3.24), with frequent shallow oscillation coincident with visual stimuli superimposed on a oscillating baseline. Different processes emanating from an individual astrocyte, behave differentely one another, in the face of an almost flat soma. Too few processes are unfortunately sampled to perform a meaningful comparison between spontaneous activity and visual triggered one. One interestin feature is that when astrocyte soma display a calcium increase coincident with a FLASH, all its processes also In Figure 3.28 is reported the $\Delta(f/F)_t$ behavior of a single astrocyte and 6 processes emanating from it, during episodic FLASH stimulations. A brief period of up-down baseline (see the neuropile for reference and box C) activity is characterized by few soma $\Delta(f/F)_t$ deflections and processes “blink”. In sosme cases processes show multiple peaked activity in single flashes. Astrocyte still preserve up state activity inbetween flashes. As described before, in spontaneous modality, the same soma-to-processes correlation is observed.

Figure 3.22: *Signature of visual processing. A) representative magnification of single events in LFP, V.E.P.: visually evoked potentials (average duration 2.6 ± 0.8 s, average intensity: 0.7 ± 0.4 mV calculated on 100 V.E.P. from 3 animals), baseline: a downstate, UP: an upstate. FLASH marks the position in time of 50 ms blue photic stimulation in the case of V.E.P. B) calibration of LFP responses in different regimen of full screen FLASH contrast stimulation. In the graph, power spectra of LFP epochs are comparated: different colors refere to different light contras stimulation episodes. A baseline screen luminosity is kept constant (0 set an arbitrary value for the lowest intensity of the screen illumination used in baselines epochs) between stimulation episodes and baseline power graph correspond to no-stimulation (up-down states). Progressive increment in contrast are tested for 50 ms full screen flash (values on the left report the incremented contrast of FLASH compared to 0 baseline level). Each slope is in log Power/Log Frequency and*

is the FFT calculated on 10 averaged consecutive LFP traces recorded in the same stimulation regimen (aligned on the FLASH start and of 4 s duration). Note the drift in the power spectra peaks (arrows) toward higher frequency as the FLASH contrast increases. Being the tacks normalized for a common average value of power amplitude, the increase in power of the peaks appear as a consequence of increasing FLASH contrast. Frequency bands populated during photic FLASH stimulations falls in the gamma band (30-70 Hz). C) Line Scan during FLASH stimulation. 1 is the reference imaged field containing a pyramidal neuron and a region of neuropile across the LS line (Scale bar 12 μm). 2 is the LS ΔF/F of 1.7s duration (1024 lines). Right: upper panel represent the STFT performed on the LFP below containing a single V.E.P. apisode. Note the increment in gamma band power in correspondence of the V.E.P. response in LFP (aligned in time). Position of FLASH in time is indicated in blue. Note that the LFP V.E.P. is delayed with respect to the

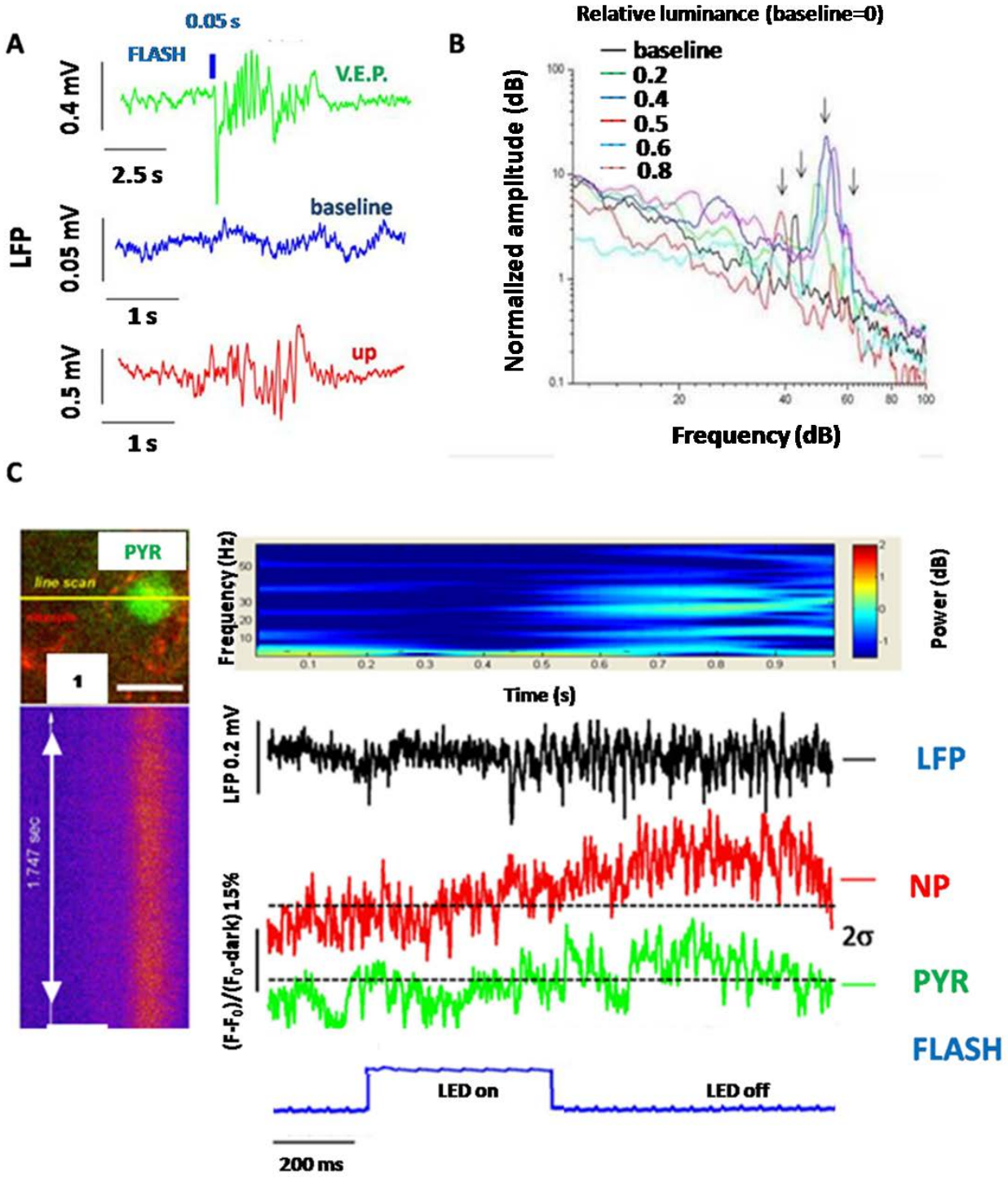

FLASH (500 ms). ΔF/F in red for neuropile and in green for pyramidal neuron in C 1.horizontal black dotted lines represent the arbitrary 2σ level of confidence, calculated on flat baseline ΔF/F periods. As quantified further, each FLASH stimulation triggers a neuropile ΔF/F deflection which can then be used as a reporter of LFP activity. Responses to FLASH can be discerned from upstates in LFP power spectrum, duration of events and amplitude, while in ΔF/F the tracking of FLASH time position is essential.

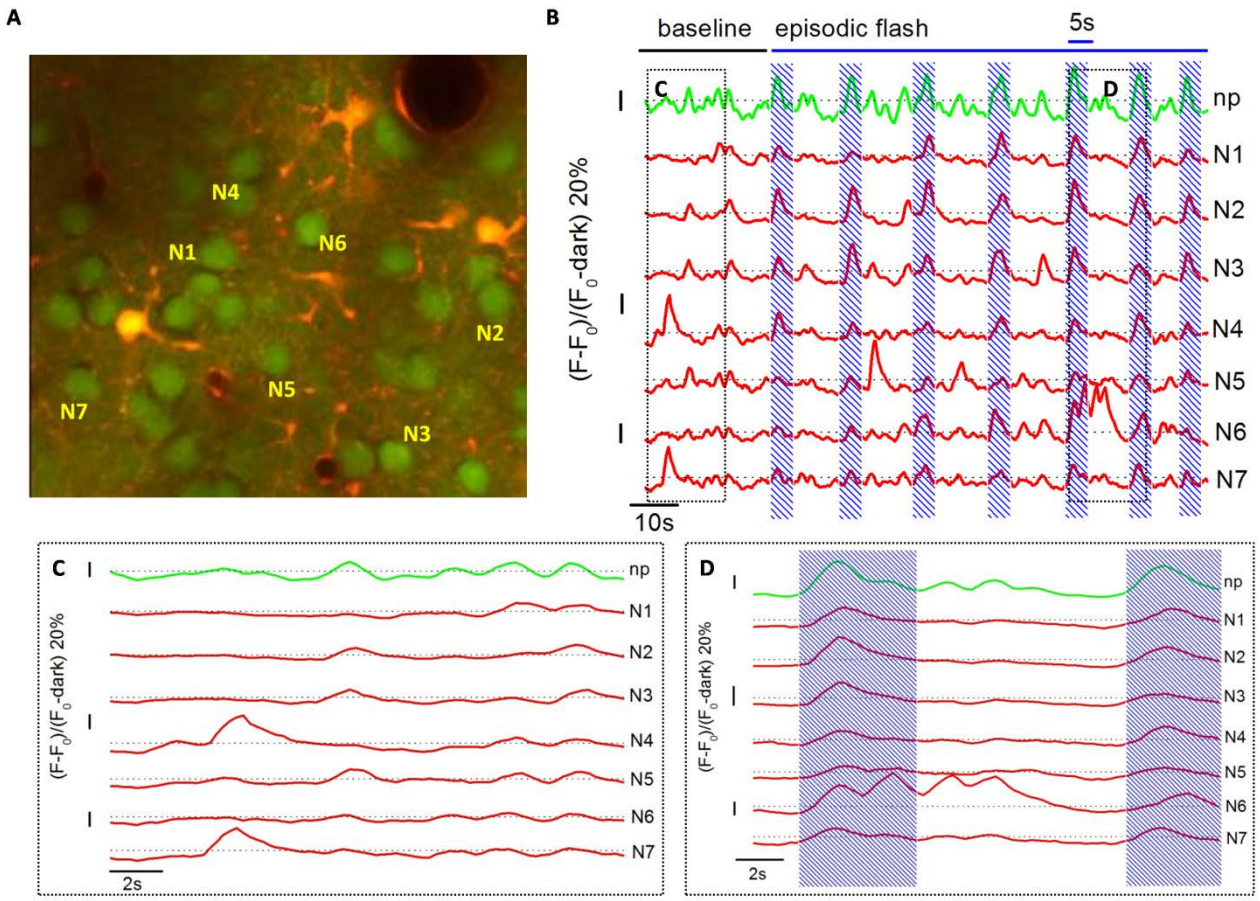

Figure 3.23: V1 neural visual processing with single cell resolution. A) Imaged field acquired 250 μm deep in V1. Several neurons and astrocytes are clearly visible, the ΔF/F is reported. B) Green tack represents neuropile ΔF/F during a time series acquisition comprising a short period of baseline (black horizontal bar) and episodic FLASH (contrast 0.8) stimulations (blue horizontal bar). The position in time of each 5s FLASH stimulation is highlighted by the blue vertical shade. Each green ΔF/F peak falls precisely inside a FLASH episode, while uncorrelated ones are dispersed between FLASHES and in baseline initial epoch, in correspondence with up states. Red traks are relative to neurons indicated in A). few ΔF/F deflections are observed during baseline activity, while more frequent and more intense ones fall inside FLASH stimulation 5 s periods. Most of the neurons response to most of the FLASHES, N7 remains almost silent exept for a couple of transients during flashes and a wide deflection in baseline. N6 produces what appear to be a burst of activity in response to a single FLASH. C, D) magnification in time of boxed region in B: during baseline and FLASH stimulation respectively. A poor alignement in baseline regimen between neuropile and neurons is evident in C, while great coherence during FLASH 5 s stimulation episodes is well documented in D. correlation between ΔF/F from neuorons and neuropile is almost lost again between FLASHES.

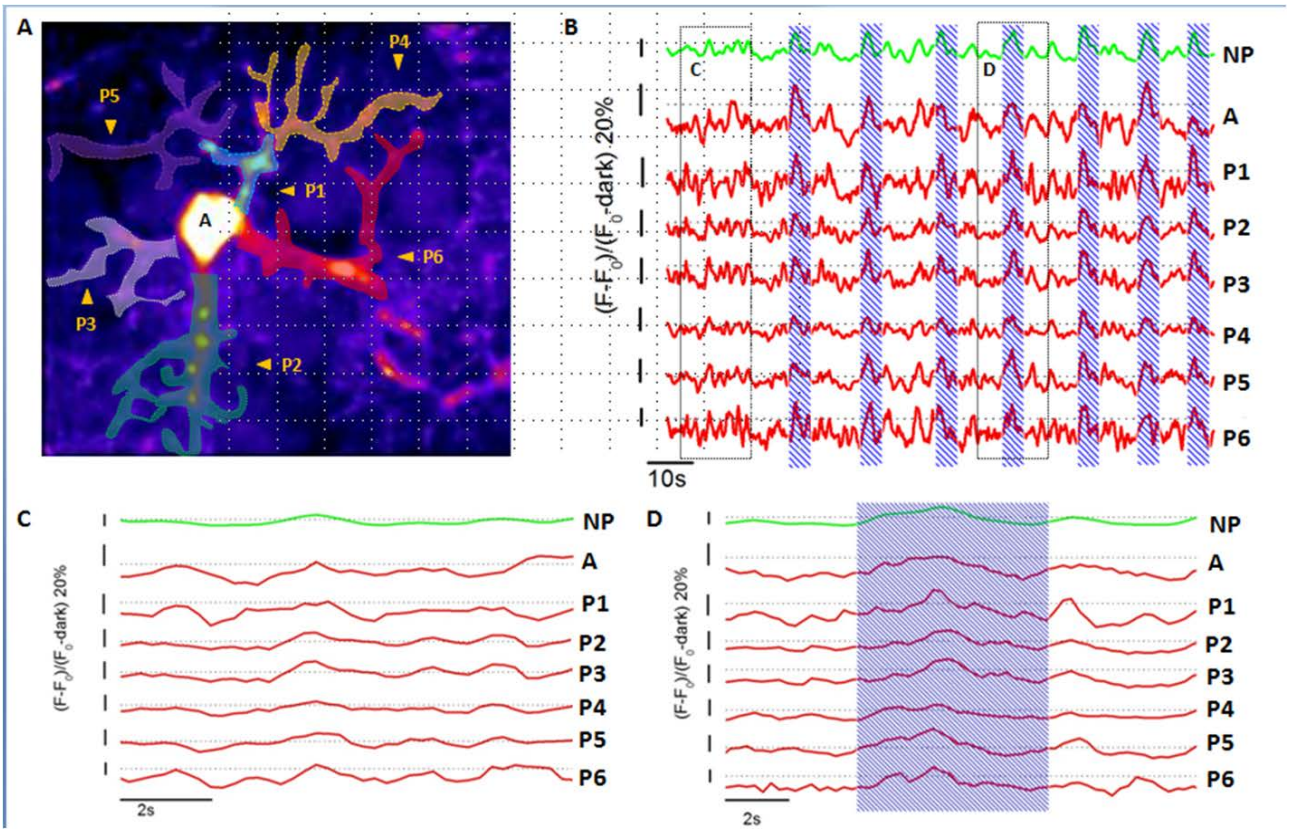

Figure 3.24: V1 astrocyte visual processing with sub-cellular resolution. A) Average projection of a ratio time series from the same experiment in Figure 3.23. Field is cropped on a single astrocyte to highlight processes (P). B) top is the green track of neuropile ΔF/F, below are ΔF/F of astrocyte soma and 6 processes. Processes display frequent ΔF/F oscillations either inside FLASH stimulation or between them. "Blinking" activity persists in pre-FLASH baseline period. Not all the processes ΔF/F deflections are mirrored in astrocyte soma that is, on the other hand more responsive inside FLASH periods than outside them. Not all flashes contain ΔF/F in all processes and in soma. Peak coincidence between neuropile ΔF/F and astrocyte soma appear precise while processe display some jittering both with respect to astrocyte soma and to neuropile. Boxed regions are magnified in C,D) here the fast kinetics of processe ΔF/F fluctuation is evident together with temporal displacement of their peaks compared with astrocyte soma and neuropile. All processes seem to be very active during FLASH stimulation and given the discrepancy between neuropile kinetics and peak timing compared with those of processes, these transients appear to be authentic instead of some neuropile contamination.

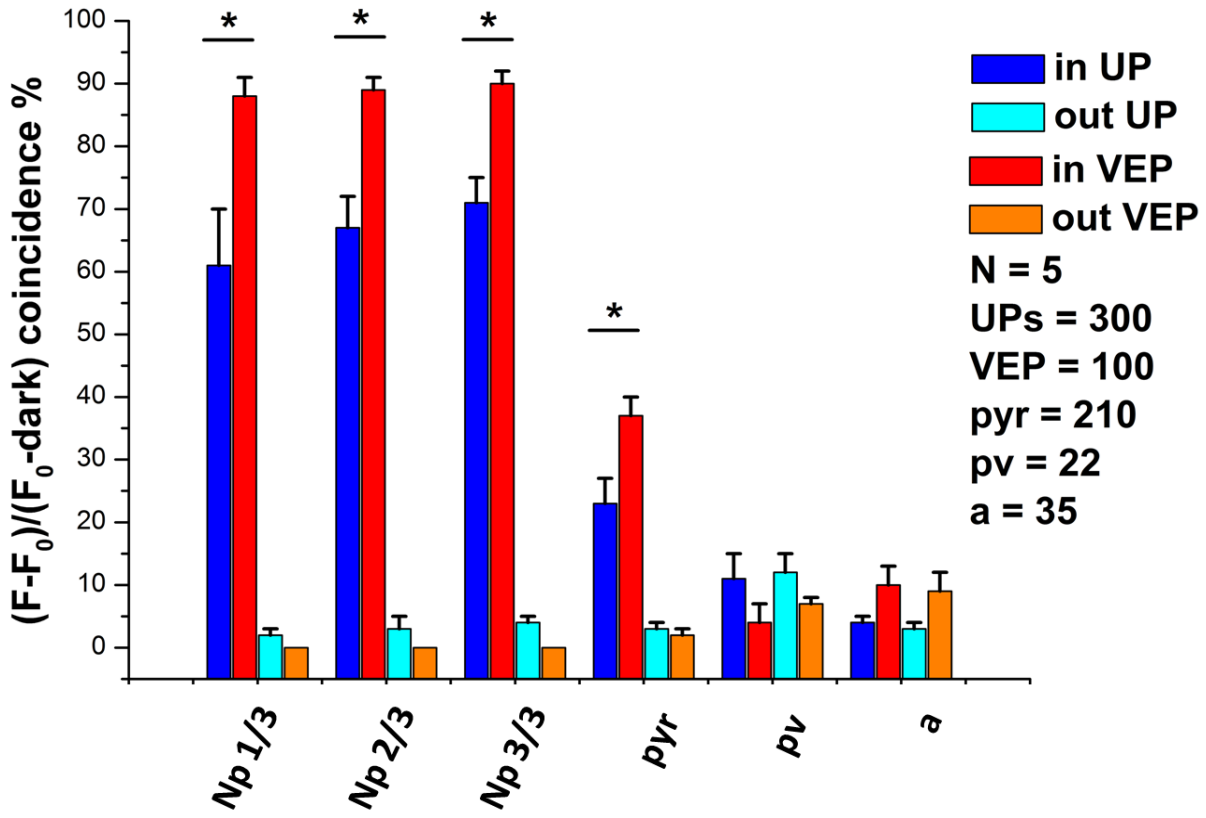

Figure 3.25: Quantification of the coincidence probability (expressed as % of the total ΔF/F fluctuation number) between ΔF/F events and V.E.P. events (Bright colors) compared with up state events (Pale colors). Coincidence of ΔF/F transients with LFP V.E.P.(discerned from upstates inequivocably from the simultaneous acquisition of FLASH timing, shape and duration of LFP event allowing for distinction of upstates triggered by FLASH itself) is counted if ΔF/F starts within LFP event + 0.3 s (average latency from FLASH start). All events preceding FLASH start are discarded. Out of V.E.P probability referes to ΔF/F events falling outside V.E.P. LFP events. Similar consideration also described in Figure 3.21, are valide for upstates. Neuropile coincidence is always higher than is for upstates (the difference is significative for all classes of neuropile areas) while probability of ΔF/F transients outside V.E.P. drops to 0. Pyramidal cells have significative higer probability to exhibit ΔF/F coincident with V.E.Ps. compared with upstates. Pyramidal cells out of V.E.P. probability is comaparable with their out of upstates ones. Quite the opposite is observed for PV interneurons: on one hand the coincidence probability with V.E.P. is lower than upstates and, on the other hand, out of V.E.P. probability is greater than out of upstates, comparable with the probability of upstate coincidence. Astrocytes increase their coincidence ΔF/F probability during V.E.P. compared with upstates while probability of out of V.E.P. remains low.

3.9--- Reduction of inhibition in V1 induces sustained interictal activity.

In contrast with what observed in isolated Guinea pig brain enthorinal cortex, mouse V1 respond to Bicuculline-induced dishinibition producing only hypersynchronous events. Shortly after superfusion of the cortex with GABAa anthagonist, up-down states oscillations are lost and sustained interictal activity rapidly builds up into stereotyped rhythmic intense field hyperpolarizations. Long lasting periods of "silence" are observed in between consecutive field events.

When we started with the mouse model, we forecasted, that BMI superfusion could have produced ictal events, similar to those observed in Guinea pig. We based our expectations of data obtained from experiments conducted mainly in slices but we soon realized that this was not an accurate prediction. Not a single ictal event was ever observed using BMI at different concentrations either superfused or microinjected in the cortex (different depths of injection or differebt cortical locations were also tested). As reported above, interictal activity is suspected by several authors, to be protective against ictogenesis. In Cavia, hypersynchronous events are scanty and possibly this protective effect could be weak. In V1 strong interictal events are much more frequent and endure for hours without collapsing. This was actually a great chanche to explore interictal activity for two main reason: such an higly synchronized activity could be of great interest from the astrocyte point of view and moderating interictal events might result is the generation of a focal irritative zone. As represented in Figure 3.26, cortical superfusion with BMI 2mM produces hypersynchronous events typical of interictal epileptiform activity. These present a "linear" phase, during which the peak amplitude is reached, a "double exponential phase" of gradual re-polarization of LFP toward baseline levels and an "afterphase" often comprising some small upward transiets. Note that all interictal events may present small variation both in amplitude and duration (discussed further) yet every single one is characterized by a large hyperpolarization of the A.C-recorded LFP. As soon as the first interictal event is observed, physiological up-down states are cancelled altogether from LFP as long as interictal spiking is present. Typical low power low frequency sleep oscillations, reproduced in panel A STFT, turns into impulsive events with strong periodicity. Since each spike in LFP is restricted to 0.2 s (average duration: 0.23 ± 0.05 s) and a large deflection (1.1 ± 0.5 mV) is compressed in such a small duration, uncertainty over contributing frequencies is a consequence. STFT of representative 20 s of interictal LFP activity (Panel B), show periodic impulses invading all frequency bands. Esemplified in Figure 3.27, spectral characterization of interictal events suffering from this limitation (1KHz LFP sampling rate is insufficient to retrieve better data) is poorly informative. A period of silent LFP is interposed between two consecutive hypersynchronous events. These flat intervals contains short lived regions of high frequency activity as revealed by STFT, flanking the interictal spike. The origin of these events is unlikely buried in the interictal surges of power in the spectrum since STFT sliding rectangular window amplitude is chosen to be half the duration of typical interictal events and these transients are variable in both duration and spectral signature, with no relation to the impulsive event parameter. A period of STFT silence is always observed following these events

often extended for few seconds. Frequently another brief burst of activity precedes the instantaneous increase in power of the next interictal event.. Interpretation of hypersynchronous LFP events is quite easy. LFP is a measure of the variation of electrical field in time, the field in turn, is a vector whose intensity is proportional to the difference in electrical potential (a scalar) separated by a certain distance. LFP readings changes when: field vector changes intensity (electrical potential difference is changed), direction of the vector is changed with respect to the measuring electrode (location of the points between which the field is defined are changed with respect to the fixed frame of reference) or, more often, a non conservative combination of both. LFP is also a measure averaged over a volume of around 50-100 μm in diameter (approximate evaluation for pipette tip of 2 μm) and any variation in the reading is the result of combination of field changes generated by the activity of several cells. The contribution of each cell to the LFP also depends on its distance from the electrode with closer ones contributing the most. Since the electrode is positioned in L II/III, a deflection in LFP is generally interpreted with a local depolarization. A depolarization as big as that observed in interictal events is only possible with the contribution of a large number of cells. These must be cohordinated in their activity to overlap their effect on the field to this extent. Furthermore, instantaneous synchronization is also required to constrict the population event in 0.02 s (average duration of time to peak of interictal events, described further). From these simplified premises follows that the interictal peak should be equivalent to a massive coherent large depolarization of all (or nearly) the cell contributing significatively to the LFP recording, while the high frequency region following, could be the tail of population bursting activity rapidly degenerating their coherence. The exponential phase of repolarization could be an artifact due to LFP undersampling and might cast a shadow over the onset of bursting activity, smoothing out high frequency, yet a more interesting description is discussed later on. Population discharge might start as a singularity but different cells having different AP firing profile, shall cause rapid decoherence to the trace. Moreover pyramidal cells, the most aboundant neural class in the cortex, quickly adapt when triggered to high frequencies, contributing to the flattening of the trace. Fewer cells like Parvalbumin containing neurons, are capable of tonic firing for protracted periods at very high frequencies (up 200 Hz). These and the tail of bursting from pyramids might sustain high power spectral periods observed in LFP following an interictal event. Those brief “puffs” of high frequency before the onset of an interictal spike, could be the result of normal thalamic incoming excitatory volley. Castro-Alamanca (2000) report instead ongoing interictal activicy once thalamus is silenced with TTX. Further details on the onset of interictal event are not to be retrieved from these data since impulsivity of hypersynchronous events retropropagates uncertainty artifact.This is in fact deducible from the symmetric shape of the peak in STFT (see Figure 3.27) deriving from an highly asymmetric LFP event. Thus, interictal events observed in LFP, are considerable efferent events of L II/III origin. Although extremely similar one another, some variability in interictal amplitude and shape emerges. Literature reports CSD analysis demonstrating that two sets of alternating interictal events may emerge as a result of cortical BMI dishinibition (Castro-Alamanca 2000), the sources of wich reside into L II or LV/VI.

Figure 3.28 shows a charachterization of BMI dose-effect. It is important to note that amplitude and frequency of hypersynchronous events, increases with [BMI] until 2 mM, concentration at which frequency and amplitude are maximum (IC50 evaluated with *Dicentra cucullaria* extract = 3 μm, also small conductance apamine-sensitive Potassium channels are blocked by BMI). After supefusion, 2' are generally enough to observe the first event at any concentration. In < 0.06 mM frequency and amplitude of events remain erratic and eventually hypersynchronous activity fades into baseline, for higher doses a steady state of spiking LFP frequency is readily gaind enduring for hours. This steady state is reached with a phase of increasing frequency and amplitude, that is shorter at higher doses until 2 mM. once the steady state is gained, sporadic "misplaced" interictal events are observed with a minimum inter-event interval of 0.8 s (read further). In order to better charachterize interictal events Figure 3.33 show the distribution of 4 chosen parameter from LFP across spikes. Time to peak define how fast is the linear phase of initial bursting activity. The peak amplitude is proportional to the extent of cells in the integrated volume of LFP, recruited to participate to the phase of maximum synchrony. Together time to peak and peak amplitude, define how coherent is the event. Duration measure the entire extent of the interictal manifestation, including the region of de-synchronization as this would prove useful to detedct transitions out of the interictal steady state. Even in the case in which time to peak and peak amplitude remain constant, some sub populations of participating neurons might already start escaping the phase. This should be translated into an elongation of the total duration because of increased "afterphase" then at the expense of time to peak and peak amplitude. The escape from hypersynchrony could be a plausible mechanism leading into desynchronized ictal events. Peak duration is another parameter sensible to decoherence. If a subset of cells de-synchronizes, some accessory fluctuations should be observed in the exponential phase. This could happen even if linear phase is maintained. Picking one random interictal event from any LFP epochs, one could refere to the steady state statistics in order to cathegorize the event as a "typical one " or "atypical one" (read further). Peak amplitude show a clear bimodal distribution. Two clusters of interictal event are present from the start (as observed in Castro-Alamanca 2000). Also a nice correlation between fluctuation of the parameter inside each cluster is suspectable (paired t test rejected a single distribution with $p < 0.001$). Total duration distribution is strongly unimodal, while time to peak and peak duration values decreases exponentially from the interictal start into stable levels within some 40 events. At the steady state peak amplitude bimodal distribution is combined with strongly preserved other parameters. This support the idea that all steady state interictal events are "cloned" events with two different origins: distal ones are less intense because field is generated at more distant regions from the LFP electrode. Assuming that no field is recorded if generated beyond the volume of integration, the region of overlap should sit inside ~200 μm from the electrode tip (integration volume should be measured more accurately, but read Buzsaki et al. 2012). Same alternating amplitude in interictal events can also be a consequence of a variability in the number of cells participating at each field spike without the need for a "double source". Finally, since interictal events are the the result of large populations of neurons discharging brief trains of APs, astrocytes bombarded with such an intense activity are expected to produce some $\Delta F/F$ signal in response, which surprisingly is not the case as shown further.

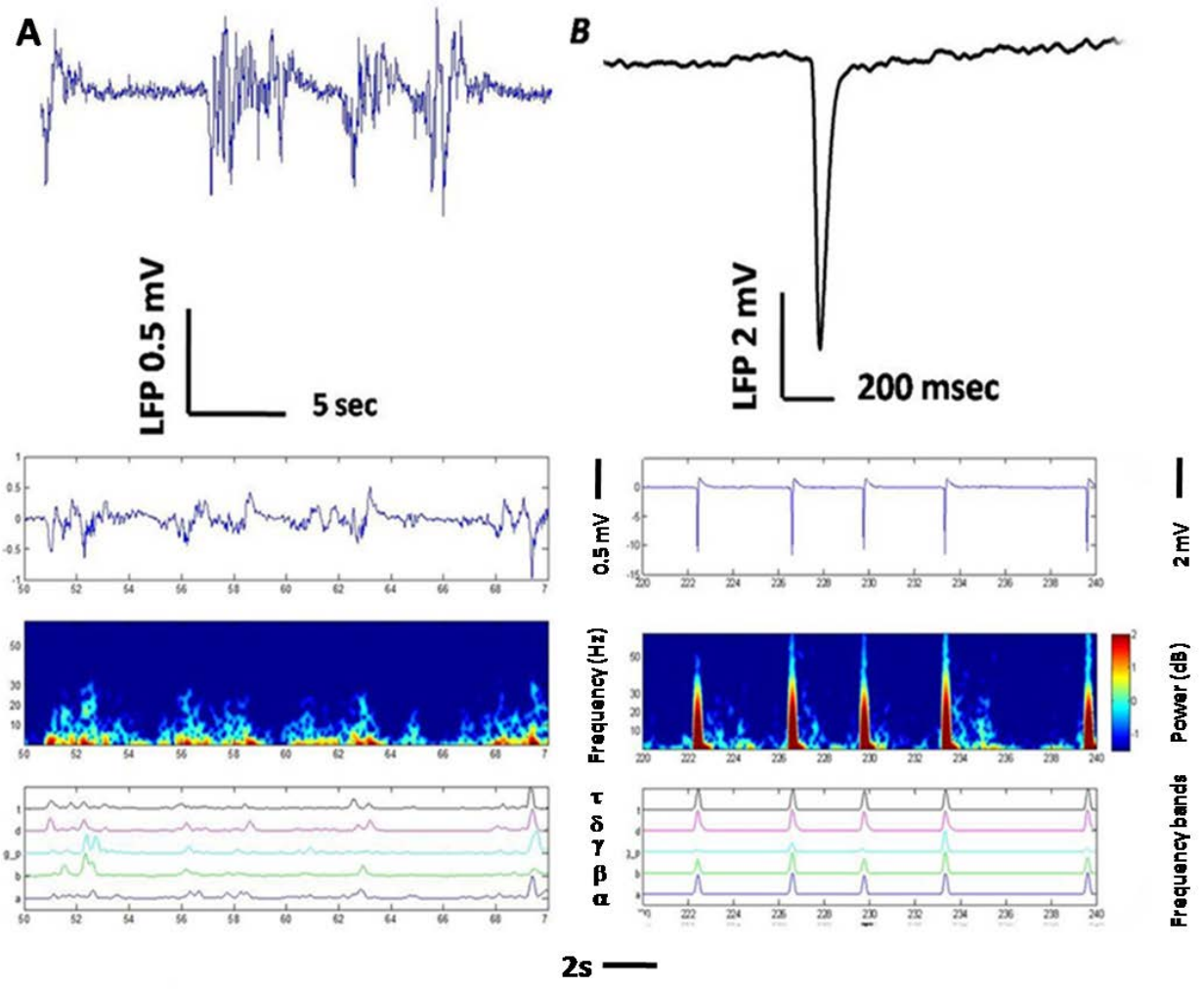

Figure 3.26: *BMI triggers hypersynchronous LFP events. A) top: LFP presenting few up/down states. Bottom: STFT of 20s LFP epoch showing low frequency low power events .D) top: Typical BMI-induced interictal hypersynchronous events. note that up state activity is disappeared from the trace during interictal phase. Bottom: STFT of 20 s LFP during interictal activity. Periodic stereotyped events are clearly visible as extremely impulsive and intense deflections. Between consecutive events power spectrum drops gradually to 0 power remaining silent until the next event sometimes heralded by brief power increase in low frequencies bands. below STFT plot are reported the frequency band decomposition of LFP. Interictal events populate the whole spectrum although with different contribution in different bands. Most populated ones appear to be* α, γ *and* τ. *The large amplitude (typical average value: 1.1 ± 0.05 mV) and short duration (0.22 ± 0.05 s) of interictal LFP events are interpreted as the product of higly synchronous short bursts activity of a large population of neurons.*

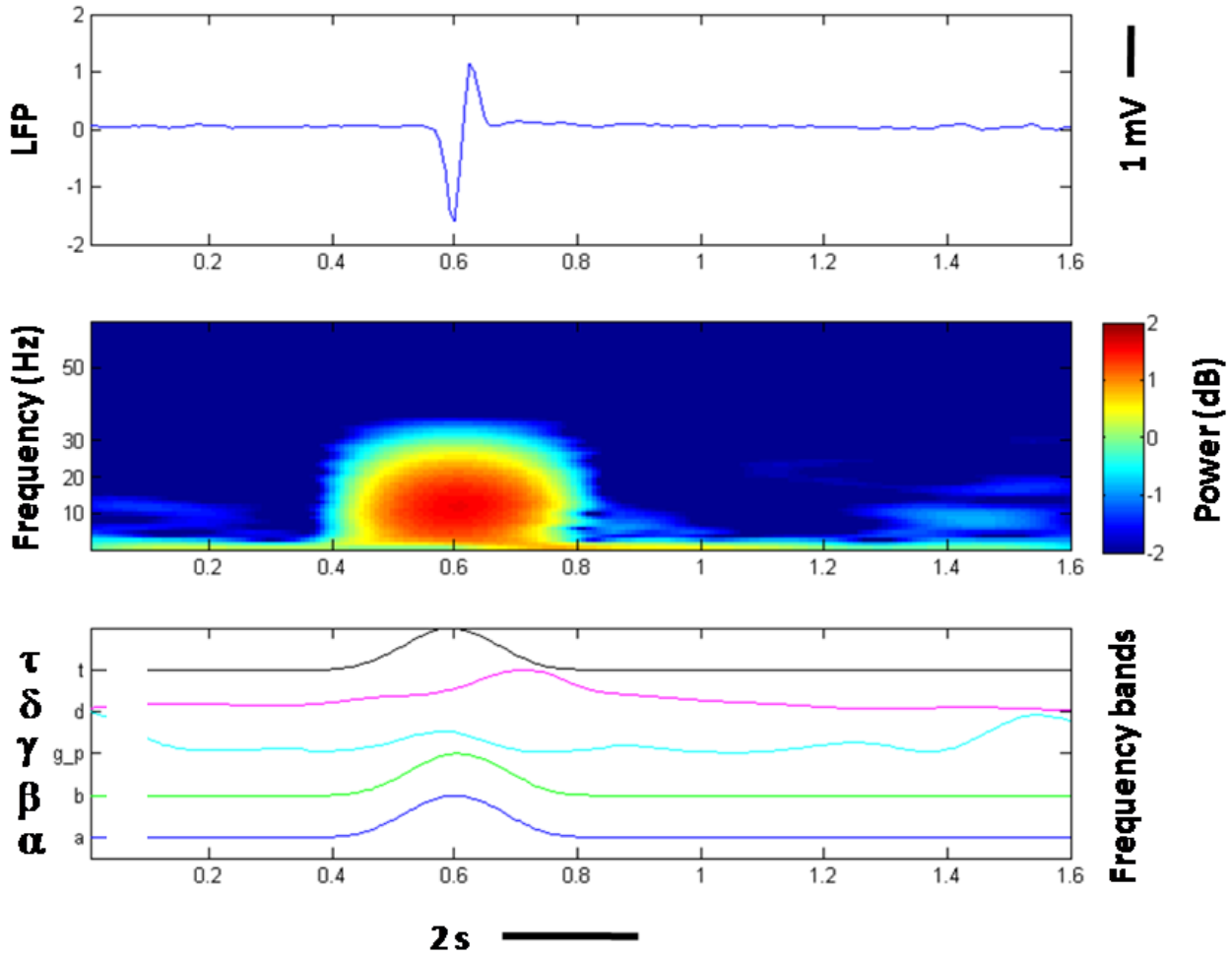

Figure 3.27: Impulsive hypersynchronous interictal events.Top: single LFP interictal event. Center: STFT analysis of a LFP event above, give little help is decomposing contributing characteristic frequencies. Region between adjacent interictal events are still well resolved in low frequency activity which is indeed greately reduced compared with upstates otherwise poorly recognizable in LFP. Exceptions are visible in close proximity of the rising phase of an interictal event or just after its termination. Band decomposition of LFP (bottom) support this consideration with the presence of, although weak, delta activity after termination of single events and gamma activity on the right side of the plot, region preceding the next interictal event.

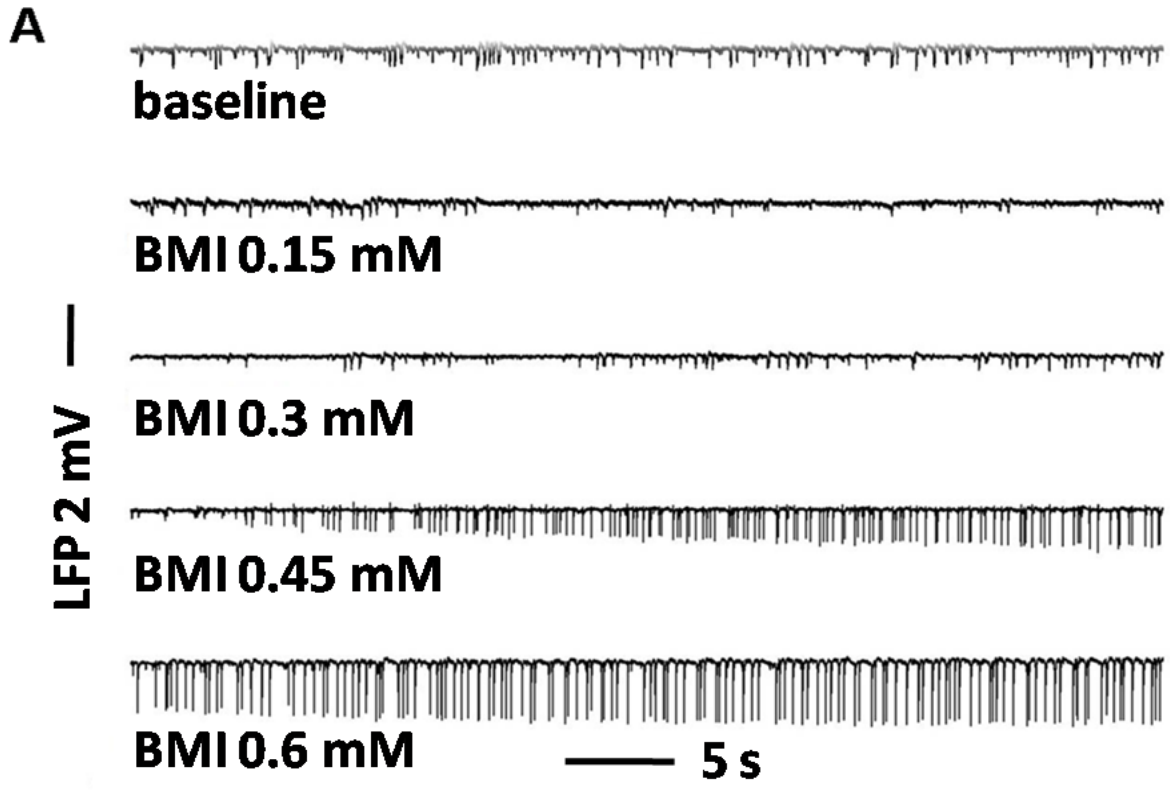
A
baseline
BMI 0.15 mM
BMI 0.3 mM
BMI 0.45 mM
BMI 0.6 mM
LFP 2 mV
5 s

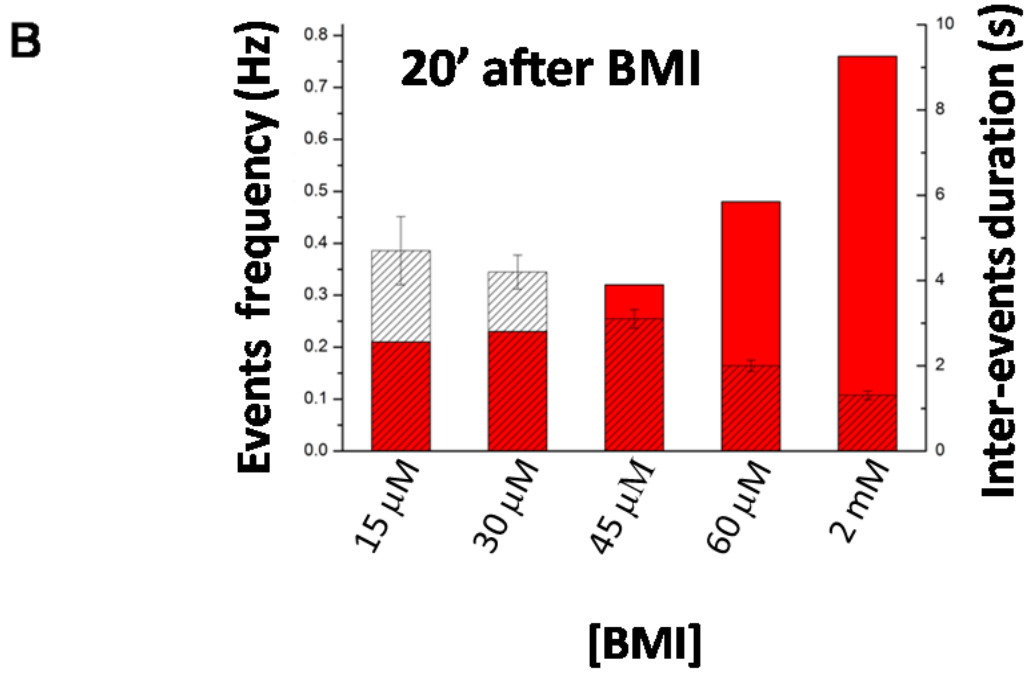
B
20' after BMI
Events frequency (Hz)
Inter-events duration (s)
0.0
0.1
0.2
0.3
0.4
0.5
0.6
0.7
0.8
0
2
4
6
8
10
15 μM
30 μM
45 μM
60 μM
2 mM
[BMI]

Figure 3.28: BMI dose-effect quntification. A) top track is a baseline epoch presenting typical up-down states activity. Within 2’ from superfusion of BMI 0.015 mM, up-down state frequency decays. With 0.03 mM BMI up-down states are abolished and few apparentely random low voltage interictal events appear. Within 2’ from superfusion with BMI 0.045 mM frequent interictal events manifest in the LFP, gradually increasing in amplitude and frequency. BMI 0.06 mM or above starts a high voltage hypersinchronous activity with amplitude and frequency increasing very fast until a steady ste is reached. A typical frequency of interictal events (1.4 ± 0.2 s) is reached in few minutes (depending on the dose) for [BMI]> 1 mM, running most of the times until the end of the experiment without evident alterations. For doses below 0.03 mM interictal events quickly appear but are weaker in amplitude and tend to disappear within a couple of hours leaving LFP to up-down states again. B) Red histogram is relative to the frequencies of interictal events observed at different [BMI] indicated on horizontal axis. As expected, the trend in inter-events interval histogram (shaded bars), is inverted when compared with the red one. Interestingly enough, dispersion around the mean value drops quickly when inter-events interval approaches 0.8s and no furder decrement is ever observed, or, no interictal event have ever been observed following another one closer than 0.8 s. this is true for all doses at all frequencies. 100 events were included in the statistic from a single animal.

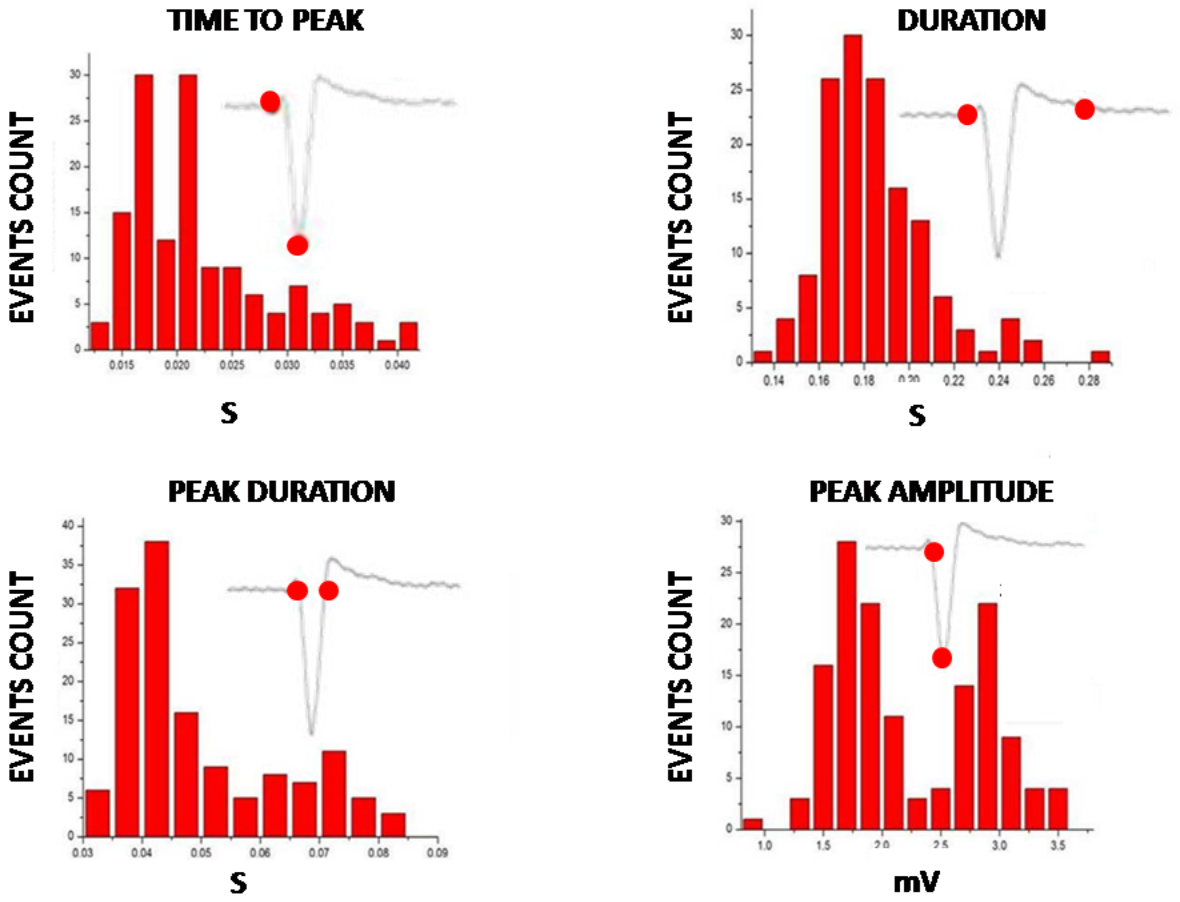

Figure 3.29: *Characteristic features of interictal events. Red histograms represent the frequency count distribution of each parameter which is esemplified, on a typical interictal event, with two red dots. Analysis referes to steady-stete interictal activity. An average baseline Voltage value is evaluated for each recording epoch and used to segregate single interictal events. Top Left: "time to peak" is defined as the duration in seconds from the first significative deviation from baseline to the negative peak of the event. Average value: 0.018 ± 0.005 s. Top Right: "total duration" of interictal events calculated between first deflection from baseline and regain of baseline typical baseline voltage values after the positive rebound phase. Average value: 0.19 ± 0.06 s. Bottom left: "peak duration" is defined as the duration of the spike alone from average baseline value, down to the peak and back again. Average value: 0.045 ± 0.003 s. Bottom right: "peak amplitude" defined as the average LFP peak intensity. Two populations of interictal events stems out when considering peak amplitude: average values: 1.75 ± 0.2 mV, 2.55 ± 0.3 mV. Red histograms comes from 200 events from 2 animals during sustained steady state interictal activity triggered with 2 mM superfused BMI at least 1h in advance of the first interictal event included in the statistic. The steady state itself is definewd as the epochs in LFP where interictal frequency changes the least (average frequency 1.25 ± 0.8 s in these 2 animals, stabilized within one 20 minutes from BMI superfusion and lasting in both cases until the sacrifice).*

3.10--- Astrocytes are (almost) silent during hypersynchronous events in V1.

As observed in the Guinea pig isolated brain model, interictal activity is associated with intense Calcium oscillations in neuropile showing great accuracy with local field events. Also neurons (both excitatory and fast spiking inhibitory cells) display a near 100% coincidence of Calcium transients and field spikes. Astrocytes, on the other hand, remain almost silent, with the exception of sporadic Calcium oscillations in processes. At each interictal event, Parvalbumin positive interneurons always display calcium transients with a rising phase delayed with respect to principal cells. Calcium peaks in excitatory neurons more slowly than in inhibitory ones and remains higher for a longer period even in absence of any field signature of neural firing, suggesting of an intricate interplay between inhibition and excitation during interictal activity. Cross-correlograms during sustained interictal activity, reveal a certain degree of modulation of neural synchronization waxing and waining across the whole population, with no distinctive alterations in local field potentials.

Analysis of $\Delta F/F$ performed during steady state interictala activity, presented in Figure 3.30, confirm data obtained in the Guinea pig isolated brain. Neurons and neuropile mirror precisely each interictal event with a Calcium transients peaks at the LFP peak, with little jitter around it. Differences are not to be observed from $\Delta F/F$ between small and large interictal events. Even amplitude of Calcium transients oscillates to some small extent, but lower or higher amplitude $\Delta F/F$ events are equally frequent at high amplitude LFP spikes as well as at low ones. No $\Delta F/F$ at all is ever observed between interictal spikes. In conventional scanning mode, sampling period could be too long to capture events in the “afterphase” that results apparentely “Calcium silent”. The same is also true for the exponential repolarization phase, but high speed conventional scannings and LS analysis are also presented further. Neural behavior was seldom observable in Guinea pig brain, in the mouse instead, large population of cells are asily imaged, with opportunity to characterize $\Delta F/F$ in different cellular classes. In Figure 3.30, is presented the behavior of $\Delta F/F$ in 4 neuron, 2 astrocyte and few processes acquired at high speed in conventional TPLSM time series (5 Hz frame period). Neuropile and neurons faithfully reflect each interictal LFP event with a spike in $\Delta F/F$ Astrocytes $\Delta F/F$ remain below 2σ level throughout almost the whole interictal activity steady state period. Occasional Calcium transients are observed in correspondence with neuropile and neuronal ones under LFP deflections (discussed later). An interesting issue descends from aforementioned considerations about two populations of interictal events having different layer origins. Given that both high an low amplitude LFP events are all associated with a $\Delta F/F$ oscillation in LII/III the two “generators” should be synchronous only in correspondence of the highest amplitude interictal events, one of the two also must remain silent during low amplitude events. From this follws also that the generator with higher frequency must be in LII/III since $\Delta F/F$ from neurons in other layers is not detected when LII/III is imaged. If this was not the case, neuropile signal could report deeper layer activity aligned with low amplitude LFP events while LII/III should remain silent or lag behind at best. The delay, in any case, could be enough to be under our

temporal resolution power. What could be expected in this case is ΔF/F in LII/III neurons jitter in time with respect to neuropile being in average delayed when low amplitude events occur in LFP. An alternative hypothesis would be that all ΔF/F are "in time" but fewer neurons from a single generator contributes to lower amplitude events. Chance to observe silent neurons would be low anyway given the high number of cells and the relatively small difference in LFP peak amplitudes. As presented below, high temporal resolution acquisitions, did not allow further clarifications. In overt contrast with astrocyte soma behavior, processes display high coincidence between ΔF/F and LFP events, resembling neural activity. Line scan acquisitions presented in Figure 3.31 better charachterize ΔF/F during interictal events. Few observed astrocyte somatic Calcium elevations (panel A) appear triggered at the same timepoint as neuropile and neurons but exhibits a more sluggish rising phase when compared with Parvalbumin interneurons and neuropile. No correlation between astrocyte response chance and amplitude of the interictal LFP event has emerged. A linescan esemplificative of astrocyte lacking ΔF/F peaks is presented in panel B. this is also instructive of the lack of contamination from neuropile inside astrocyte ROIs. In panel C are reported statistics relative to the chance of coincidence between ΔF/F in each cell class and LFP occurrence of interictal events. No ΔF/F with onset preceding interictal start (eventhoug the full exent of the transient extended inside LFP deflection) wa accepted as coincident. Coincident events were instead accepted if the starting phase of ΔF/F fell within 200 ms from the end of the LFP spike. Any ΔF/F elsewhere fell in the cathegory "out of interictal" (200 interictal events, 80 different pyramidal cells, 20 PV ,30 astrocytes in 3 animals). As compared with V.E.P. and up-down states statistics, panel C report a slight increase in the coincidence probability for astrocytes, a dramatic increase in precision for PV, a great increase in Pyr and no or little increase in NP. (average values are respectively: 18.2 ± 2%, 95.5 ± 2%, 92 ± 3%, 95.7 ± 1%). Overall, out of interictal coincidence fell toward 0. From high temporal resolution acquisitions also emerged a difference in ΔF/F timing comparing pyramidal neurons and Parvalbumin ones. Depicted in Figure 3.32 is a linescan acquired across somata of neighboring putative principal cell and a Parvalbumin containing GFP interneuron comprising a single interictal event observed in LFP. Both cells are responsive and ΔF/F are coincident with LFP spike, yet, ΔF/F rising phase in pyramidal cell display a slower kinetic. As a consequence PV reaches ΔF/F peak faster than pyramidal cell and fall back to baseline while the principal cell Calcium level remains higher. Aligning ΔF/F from 20 LS acquisitions an average significative difference in time to peak of 34 ± 6 ms is observed. This observation may turn helpful when considering a plausible role of interneurons in the genesis or restrain of interictal events. Cross correlogram in Figure 3.33 is performed between ΔF/F from pyramidal neurons, regions of neuropile and astrocytes during a steady syate interictal activity epoch. Compared with Figure 3.20 relative to the baseline Cross correlogram, a great increase in average synchrony between LFP events and ΔF/F is observed. What surprises is the absence of a clearly periodic tiling of the lanes as expected if all interictal events were precisely mirrored in ΔF/F . the time jitter between Calcium elevations and LFP events results of variable dutration and oscillating in time. Some regions of the cross correlogram presents very intense powers for prolonged

periods, punctuated with epochs of low correlation. This is true for neurons and neuropile lanes with dynamics differing from lane to lane although quite similar. Astrocyte lanes alone remain poorly correlated along all the recorded period. No apparent relation sussists between LFP events of higher/lower amplitude and the power on crosscorrelation among different lines.

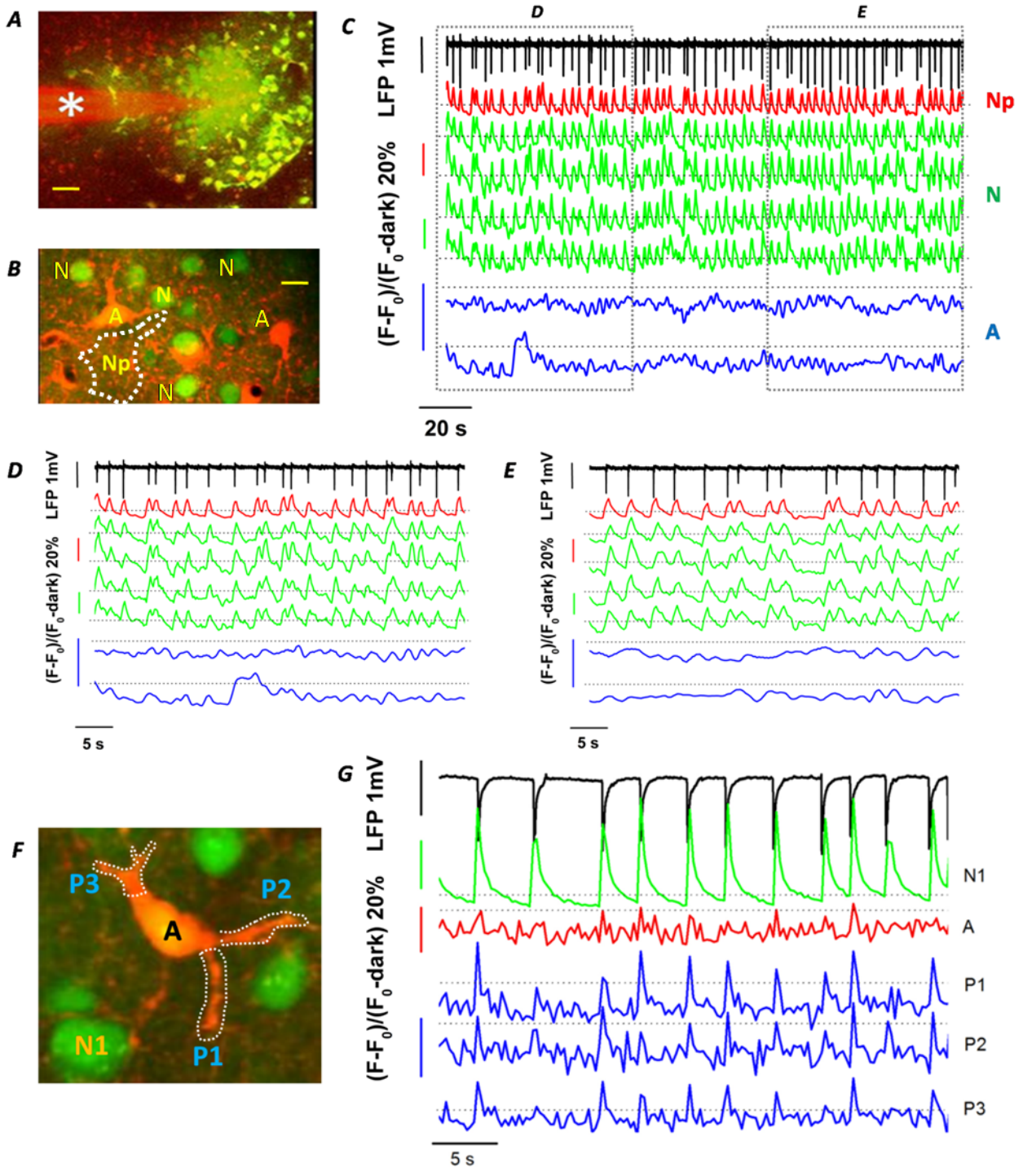

Figure 3.30: *Imaging hypersynchronous activity. A) Average projection of a low magnification Z-series from V1 surface down to 250 μm. A large green bolus is visible at the center of the image where the red tip of the pipette (*) is placed (scale bar 80 μm). B) Average projection of a time series acquired at 200 μm inside the central bolus in A. 4 neurns, 2 astrocytes and a region of neuropile are indicated, the ΔF/F of which is described in C. extracellular electrode is placed near the imaged field (within 100 μm). C) Black line is the LFP during steady state interictal activity triggered*

by superfusion with 2 mM BMI in aCSF administered 1h before the presented epoch. Neuropile ΔF/F is plotted in red, while neurons and astrocytes are indicated in green and blue respectively. Nuropile and neural ΔF/F recapitulate faithfully interictal events. all cells considered display a Calcium transient for each LFP spike mirroring neuropile track. Noteworthy, each Calcium transient is conspicuously higher than any observed during baseline or visual stimulation although LFP transients are short lived (discussed further). Region of flat ΔF/F are otherwise found between adjacent interictal events with no exceptions. ΔF/F profiles relative to Astrocytes show few hints of Calcium fluctuation in this epoch, with the exception of a single slow transient in a cell. Given the frequency and height of Calcium-dependent fluorescence spiking activity measured in neuropile and neurons, flatness of astrocyte ones, also advocates for a negligible astrocyte ROI contamination. D,E) Magnification or two representative regions in ΔF/F profile. Astrocyte transient is highlighted in D. The fluctuation is slower than neural or neuropile ones yet is aligned at least in the onset phase, with an interictal LFP event which also means that it starts together with neural and neuropile spike (more time resolved analysis is presented further). Astrocyte peak terminates inside a region of LFP silence where neural and neuropile ΔF/F are already at baseline. Peaks like this one are seldom observed in astrocytes during interictal activity (further quantified). Most of the ΔF/F in astrocytes behaves as exemplified in E. No evident Calcium oscillations are to be observed eventhough a flickering oscillation around baseline average value seems to be more prominent than in baseline o stimulation conditions. This increased noise in astrocyte ΔF/F appear to be uncorrelated with LFP and impulsive events being uniformely distributed across the tracks. F) Average projection of an high magnification T-series in the same field in A. Beside a neuron and an astrocyte, three first order astrocyte processes are well resolved. G) ΔF/F relative to the ROIs indicated in F. Neuron and astrocyte behave as described above. All three processes present frequent Calcium spikes. Each spike is aligned with an interictal event in LFP. Not all the LFP hypersynchronous events are mirrored in processes tracks yet ΔF/F appear to be highly coherent with LFP. Not all the ΔF/F transients are alike: most of them are extremely fast and precisely aligned with LFP maximum deflection and neural ΔF/F Calcium peak. Decay phase in astrocyte processes ΔF/F peaks, is otherwise completely different from neural ones. Neurons display a complex double exponential behavior (further described), while processes show short lived impulsive peak with a simple monoexponential decay phase (which is also faster than neural one). Amplitude of ΔF/F transients in processes is also considerably lower than observed in neurons or neuropile. As observed for astrocyte somata, also processes show a ΔF/F noisy behavior. Unfortunately, astrocyte processes are seldom resolved well enough to allow a statistical analysis of their Calcium behavior.

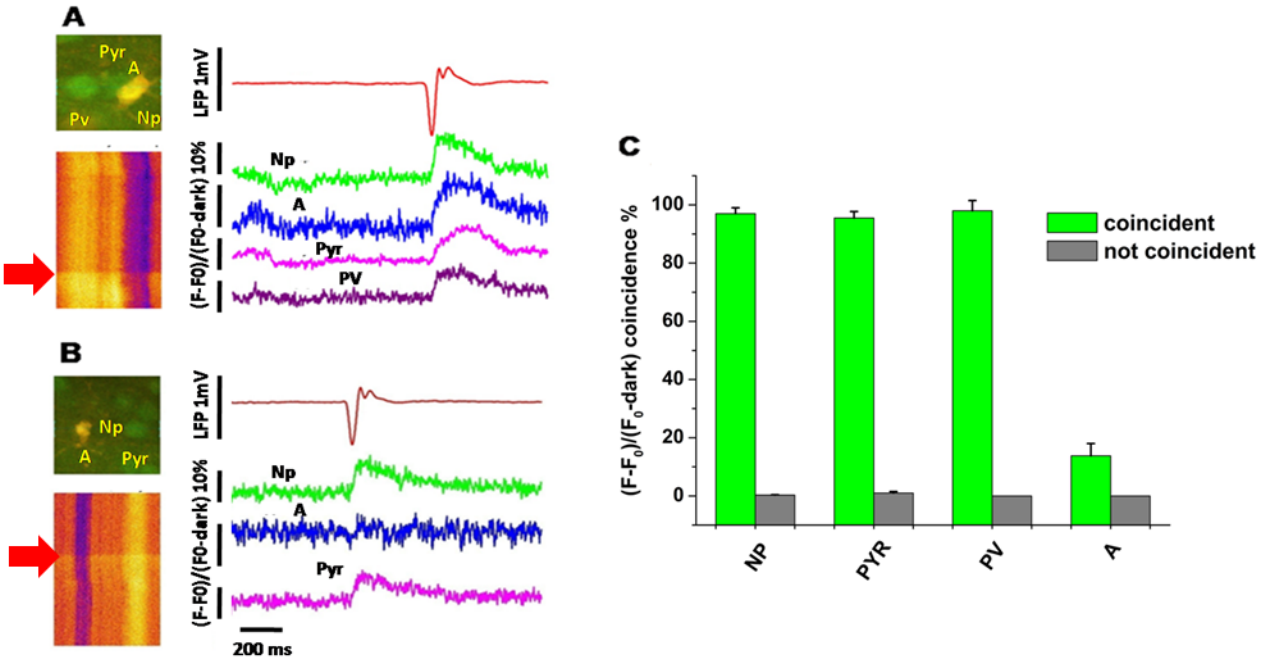

Figure 3.31: High temporal resolution analysis of interictal activity. A) Top: magnified reference field over which linescan acquisitions were performed. A GFP-positive Parvalbumin-containing interneuron is visible on the left, flanking a GFP- putative pyramidal one. Beside this is visible an astrocyte. Line scan is performed across the three cell somata extending few microns on both sides in thin regions of neuropile. Bottom: The Calcium-dependent fluorescence intensity variation in time extracted from a linescan acquisition, is visualized in color-coded scale. Length of the colored stripe is proportional to linescan duration (1.34 s in this case). Each vertical shaded columns is relative to the above cell soma. The red arrow indicate the point in time where an interictal event falls as deduced from LFP recorded simultaneously. Right: $\Delta F/F$ behavior of neuropile, putative pyramidal neuron, parvalbumin neuron and astrocyte from the linescan on the left. Red line is the concomitant LFP showing a typical hypersynchronous event. All cells below show a Calcium transient below the interictal event. $\Delta F/F$ peak onset is precisely aligned across cells and with LFP peak. A fast rise in Calcium transient is observed for neuropile (the fastest) and PV cell (second faster). These ROIs also present a fast regain of baseline $\Delta F/F$ levels. Astrocyte show a faster Calcium rise than GFP- neuron which also extends the oscillation a little longer. The sign of a previous interictal event is visible in $\Delta F/F$ at the beginning of the linescan analysis. B) A similar acquisition is performed in a field lacking a PV neuron. As described in $\Delta F/F$ on the right, astrocyte here is silent to the interictal event. Although neuropile $\Delta F/F$ transient appear prettymuch the same here as presented in A, GFP- neuron show a fainter response. Further observation could fend off uncertainty on the nature of pyramidal neurons $\Delta F/F$ responses in the case of a responsive nearby astrocyte. Also a correlation between astrocyte $\Delta F/F$ responses and proximity to PV neurons is still lacking. C) Quantification of coincidence probability of $\Delta F/F$ transient with interictal LFP event. Coincidence was accepted whenever a $\Delta F/F$ onset fell within interictal event with a tolerance of + 200 ms after termination of LFP episode. No $\Delta F/F$ transient was ever observed preceding interictal start. All Calcium transients falling outside interictal events were collected as out of interictal and plotted in grey. NP. PV, PYR display a near 100% coherence with LFP while a probability near 0% of is observed for “out of interictal” category. Astrocytes are distinctively more responsive to interictal compared with out of interictal events.

When compared with upstate or VEP coincidence probability, no significative difference emerges for astrocytes (a total of 200 interictal events were counted of which 30 were in LS modality).

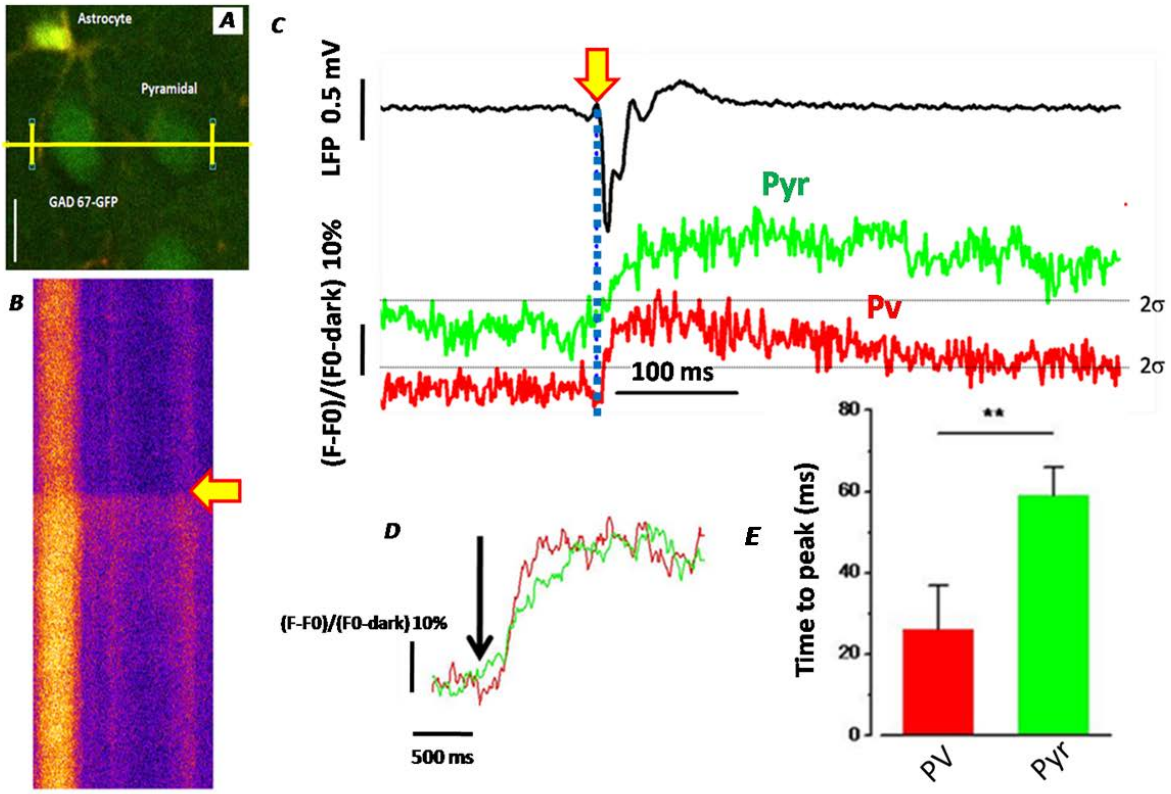

Figure 3.32: V1 pyramids Vs. fast spaking interneurons during hypersynchronous events. A) Reference frame depicting a GFP+ parvalbumin-containing interneuron, a putative pyramidal neuron and ojne astrocyte. Yellow line indicates the trajectory of linescan acquisition intersecting GFP+ and GFP- neurons (scale bar 12 μm). B) ΔF/F relative to a line scan in the field in A. Note the instantaneous rise in fluorescence where the interictal event peaks (yellow arrow). C) Black thrack is the LFP relative to a single LS containing one interictal event starting at yellow arrow. Below is the ΔF/F of PYR (green) and PV (red) in A. a consistent difference in Calcium behavior is observed between PV and PYR. Using the dotted vertical line as a temporal reference (aligned with interictal start), it is clearly visible the onset of PYR ΔF/F compared with that of PV. Interneurons present a delayed start of ΔF/F. Also time to ΔF/F peak is different with PYR reaching the maximum later than PV. Also PV compared with PYR, quickly descends within 100 ms leaving pyramids on a ΔF/F plateau. D) Two ΔF/F interictal peaks are aligned at their start and only the rising phase is magnified. An average 10 ± 2 ms are required to align in time PV with PYR ΔF/F in 20 line scans from 2 mice in steady-state interictal activity. E) quantification of PV Vs PYR time to peak. PV reaches peak some 40 ms before PYR (20 line scans average difference: 34 ± 6 ms)

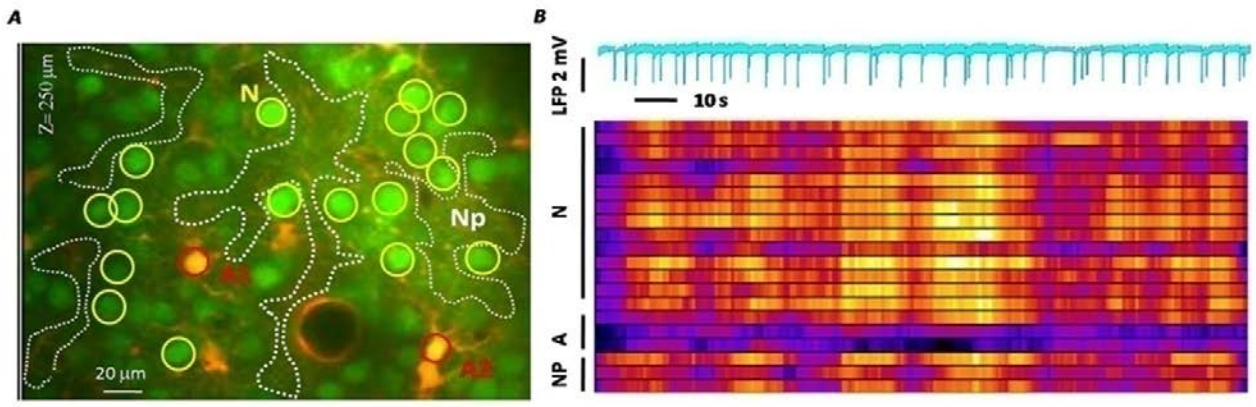

Figure 3.33: *ΔF/F-LFP cross correlogram during V1 interictal steady state. A) average projection of a T-series 250 µm deep acquired during interictal steady-state activity triggered 1h in advance superfusing V1 with 2 mM BMI in aCSF. Several neurons are visible as well as two Astrocytes. Scale bar 40 µm. B) Cyan track is the LFP recorded concomitant with T-series. Note the rigid periodicity and homogeneity in amplitude and duration of interictal events. The first lane in cross correlogram below, is the color-coded intensity of LFP decimated according to imaging frame period. Next lanes are relative to neurons followed by 2 astrocytes and 3 regions of neuropile. Cross correlation power appear to be overall high for neurons. As a general rule, both neuropile and neurons, show a peak in cross-correlation power for each LFP event. Each peak is coherent across all neural and neuropil lanes although variable in intensity. The cross-correlation function is nevertheless not a mirror image of the periodic LFP. Different neural lanes alternate intermittent phase-lock ΔF/F activity with periods of low coherence. Given the approximate 100% fidelity of coincidence between ΔF/F and LFP for neurons, this erratic behavior can easily be a consequence of ascillating amplitude of ΔF/F transients across ΔF/F events. The same is true for neuropile lanes. Although more uniform, crosscorrelogram in neuropile also wax and wanes. Of peculiar interest, is the presence of a region of highest cross-correlation power in the central region of the raster plot. In this window both neuropile and neural lanes, show a surge of hot colors unrelated with either frequency or amplitude in LFP spikes which remain similar to the rest of the epoch. Astrocyes alone maintain a constant low cross correlation profile reguardless neural, neuropil and LFP activity. Few spots of higher power, although small compared to neurons and neuropil, are disseminated without apparent relation to the pattern of other lanes or LFP. This goes together the low chance of coincidence in astrocyte ΔF/F during interictal activity.*

3.11---"Low-synch" interictal events trigger massive responses in astrocytes.

After a couple of hours after bicuculline superfusion, a class of "de-synchronized" events appear sporadically beside hypersynchronous ones. These "atypical" transients are associated with a gamma band power increase in field potential and with "typical" Calcium behavior in excitatory as well as in inhibitory fast spiking interneurons. Astrocytes display instead, large Calcium fluctuations with great coincidence probability, never to be observed during "typical" interictal events. also duration of astrocyte transients aligned with "atypical" interictal spikes results considerably longer in duration when compared with few observed for "typical" hypersynchronous events.

Hypersynchronous steady state do not last forever, after 2h of sustained stereotyped activity some alterations eventually manifest in the parameters selectd to define a "normal interictal events". Sporadic clusters of "irregular interictal events" disseminates amidst normal ones with variable frequency, although very low. Eventually, all of a sudden, the last interictal event leaves LFP in a normal up-down state activity. In Figure 3.34 are reported LFP and $\Delta F/F$ during these late steady states. Neuron average $\Delta F/F$, as usual, reflects each interictal event either regular or irregular. Red circle in the LFP indicates the presence of a small cluster of irregular interictal events (clusters frequency, duration and density of irregular events are not classified being greately variable in all these aspects, other quantifications with respect of these events are described below) the shape of one of these is magnified in red box. Beside each cluster, only regular interictal events are present. When LFP goes through a cluster, $\Delta F/F$ in astrocytes have a greately increased probability to show significative transients. Also STFT of these events is radically different. A surge of high frequencies is now present at the peak time of the event and protract ahead of this. Since the impulsive artifact of these events is also reduce compared with normal interictal spikes, the emergence of the high frequency activity could the result of reduced synchronization in irregular events unmasking bursting activity. Also time to peak, peak duration and peak amplitude are characteristic in irregular events, but total event duration is the parameter changing the most and was used to define an irregular event (histogram in Figure 3.39, 0.4 ± 0.05 s Vs 0.13 ± 0.05 s of regular events). Power specra comparison, reveal an increase in gamma band during irregular events. In Figure 3.35 is characterized the occurrence of these events in time, as interictal regular activity keeps going on. Using total event duration as a discriminator (red dots are inter evet times comprising at least one irregular event), frequency count of inter-event interval between any consecutive two events from -70' from the first observed irregular event up to + 120' is plotted. Before time 0 in this series, average inter event interval (all regular ones) remains around 1.8 sec without significative oscillations, once the first irregular event is observed (a single one is present in the red circle), average inter-interictal event among all the other regular events is already drifted significatively (here was 3.2 s). as time goes by, average regular-regular interevent time is further

drifted toward 4 s. Irregular-regular or irregular-irregular interevent intervals had the same distributions (red dots) centered at 7 s. considering the frequency of such irregular events (number per type of event is reported in the graphs), the drifting in interevent interval is not due to the "wheight" of increased "red" times, rather, the presence of irregular events marks the "out of steady state phase". Appropriately dispersion around average "black times" is indeed increased greately since time point 0. Irregular events comes in two sorts: the one described before and a symmetrical one with same event duration distribution but with the high frequency region preceding the interictal peak. In each cases the probability of a coincident astrocyte ΔF/F peak is highly increased compared with regular events. ΔF/F is counted inside an irregular event within an arbitrary window of ± 200 ms. When astrocytes ΔF/F coincides with LFP, onset of the Calcium event start some 100 ms earlier than the LFP peak being this preceded or followed by the high frequency region as depicted in Figure 3.36. A first low intensity Calcium oscillation is observed aligned at -100 ms followed by another one in irregular events or by 3-4 events in the other case. In the first kind of interictal irregular event, the highest peak in astrocyte (second peak) is delayed by some 30 ms from the peak in neurons or neuropile. In the second case-irregular event, the third peak in astrocye follows neuronal one of similar amount of time. Pyramidal cells, as well as PV and neuropile, display a ΔF/F similar in all parts to what observed for regular events. coincidence probability for astrocytes increases up to 60% while other statistics remain the same as in regular events. Statistics relative to these irregular events are reported in Figure 3.36. So far no cross correlogram was performed between ΔF/F and LFP in irregular interictal activity, a significative decrease in correlation power is to be expected during clusters of irregular events. It is also presumable that a general decay in cross correlation power would be observed instead also given the sporadic appearance of irregular events. Anyway, irregular interictal events, are themselves less synchronous LFP oscillations than regular one and appear when regular events starts losing their synchrony. Transition into up-down state LFP activity ensues within 120-150' from first irregular clusters.

***Figure 3.34**: Emergence of de-synchronization. A) average projection of a time series acquired at 250 μm in V1 2h;40' after [BMI] 2mM superfusion. Several neurons (red circles) and astrocytes (yellow circles) are visible. scale bar 40 μm. B) LFP in black presents interictal activity, below ΔF/F relative to averaged astrocyte (red) and averaged neurons (green). Neural ΔF/F mirror faithfully each interictal event while average astrocytes ΔF/F show a significative transient only under region 3 (red dotted circle on LFP) being flat elsewhere. C) single LFP events extracted from LFP regions with corresponding numbers. Only in region 2 slower, "irregular" events are found. Irregular events seems to appear in random clusters interspersed with regular ones.D) Magnification of a single "irregular" event from region 2 in LFP. Red circle define the total duration and blue dots the peak amplitude, as described for "regular" ones. Ripples of activity are present preceding (as in this case) or following (as in C) the impulsive phase. These are not similar neither to up-down states nor to VEP activity, as described further here. E) Discrimination of such events is possible comparing total duration with "regular" ones. In the case of "irregular" interictal events duration is considerably longer than typical ones (371 ± 102 ms Vs 202 ± 12 Ms for "regular" ones, calculated from 3 animals for a total of 932 regular events and 42 irregular ones). The other parameters used to define a "typical" interictal events, show no divergence in these "irregular" events. F) FFT spectra of regular events compared with irregular ones. 42 power spectra were calculated from each class of events the average power spectrum was then calculated in each class then normalized for maximum values. 42 single events per class was used, extracting time frames 1.3 s long from LFP. Each time frame*

contained a single comlete interictal event that was segregated into regular or irregular comparing the duration parameter. An event was dubbed irregular whenever duration parameter exceeded typical one at least by 2σ the regular distribution. Average irregular power spectra differ from regular one for an increase in 30-40 Hz (boxed region). G,H) STFT for sigle "typical" and "irregular" events compared. In irregular events a consistent power increment in high frequency band (γ band region: 30-40 Hz) is observed near the peak of impulsive phase. In irregular events, after the impulsive phase, a burst of 10-30 Hz activity also "contaminate" what otherwise would be a regular spectrum in this region. Impulsive phase and inter-event phase are indistinguishable between regular and irregular events. Given the

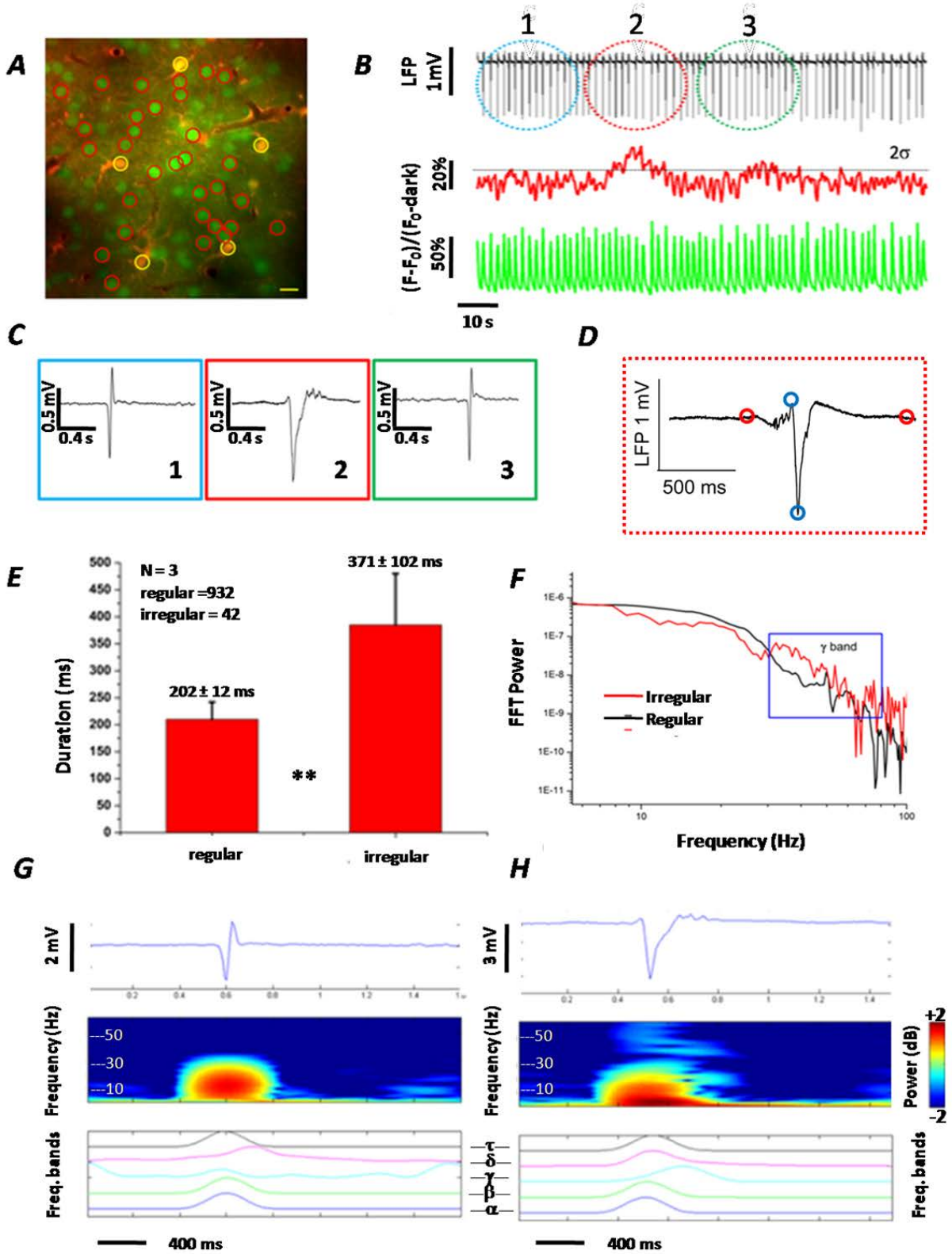

longer duration, the shape of LFP and its spectral properties, an emerging de-synchronization could be suspected of what is elsewhere a steady-state of recurrent stereotyped events.

Figure 3.35: Irregular interictal events disrupts periodicity. A) four frequency counts scatterplots relative to measured interevents interval starting with events 70' before the appearance of the first group of irregular interictal

events during steady state activity. This is confirmed by the highly skew distribution peaked around 1.3 s (vertical red line, with dispersion represented as horizontal black line). A s time goes by, the number of events starts to decrease while inter-event interval increases (-50', -20'). At time 0 a first clouster of irregular events is detected (red circle). Here regular events have an average interevent interval around 3s. B) 10' later a new more conspicuous cluster of irregular events appears (red spots) having an average inter-event interval of 7.25 s while regular ones maintains more or less inter event interval parameter around 3s. two populations of interictal events emerges at last, defined by different total duration and inter events interval both longer than the regular ones. Average values set readidly on separated distributions of inter events interval and remain significatively different (black dots Vs. red ones at 60' and 120', $P < 0.001$ for paired t-test). C) once appeared, irregular events have little chance to manifest. Histogram show the percentage of irregular events at progressively loger times from BMI 2 mM superfusion. Binning at 20', first events manifest after 1h, peaking around 100-120'. Percentage of irregular events remains constant even after 180'. Irregular counts was performed from sweeps of 900 s each covering a span of 180' from BMI administration in 4 animals.

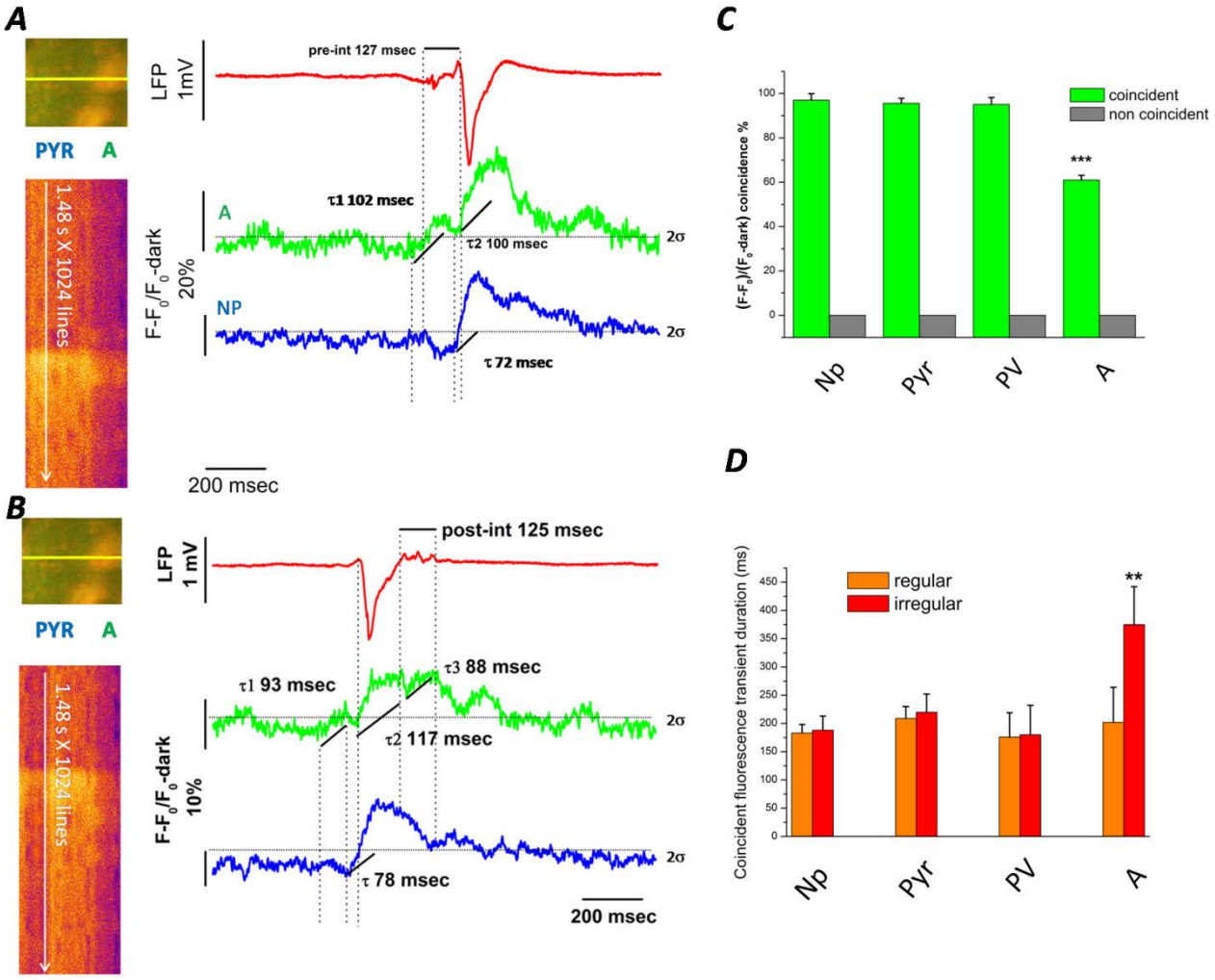

Figure 3.36: *Astrocytes prefere irregular interictal activity.A,B) Reference frame and line scan ΔF/F oscillations in the presence of two different irregular interictal events. A single GFP- neuron and one astrocytes are depicted. Two sets of events emerges in time, both having longer total duration parameter, one is characterized by a dilated fluctuation in LFP preceding the onset of an otherwise regula interictal event (20 events have ripple centered at -127 ± 10 ms). In these events ΔF/F relative to neurons is aligned with the onset of impulsive event (blue track), while astrocytes present a surprising small peak aligned with pre-impulsive LFP oscillation (peaking in -102 ± 12 ms from spike in LFP). Moreover, astrocytes peaks a second time just about interictal termination in these events, some 0.03 sec delayed with respect to neurons. The other group of irregular interictal events (B), present an oscillation in the LFP just afater the*

impulsive phase of interictal event (20 events have ripple centered at +125 ± 7 ms) of duration comparable with the case in A. In these events, neurons behave just like the other group i.e. just like regular interictal events, while astrocytes display 3 peaks: the first preceding (–93 ± 11 ms) the onset of impulsive spike, a second one aligned with LFP maximum deflection (and neural response) and a third one delayed from neurons ΔF/F onset (+88 ± 15 ms from neural ΔF/F onset), often a fouth one is observed as in figure. C) Coincidence probability between an irregular LFP event and ΔF/F is depoicted in the histoghram green bars. Out of irregular events probability is represented by gray bars. Pyramidal and parvalbumin neurons as well as neuropil behave as if in "regular" interictal activity with a near 100% coincidence and 0% out of events ΔF/F transients. Astrocytes show an astonishing increase in coincidence probability reaching 60% . Furthermore, no out of interictal events ΔF/F oscillation are detected during irregular activity. Also the coincidence probability for astrocytes is unchanged for regular events separating irregular ones. D) ΔF/F duration is also significatively affected in astrocytes. Given the presence of accessory peaks only during irregular interictal events in astrocytes, the duration of ΔF/F is considerably longer (376 ± 57 ms). No differences emerge, on the other hand, for neurons or neuropile comparing ΔF/F from regular and irregular events. astrocyte ΔF/F regular transients have a duration comparable with that of neurons and neuropile (198 ± 65 ms). Frequency of events the type described in A do not differ from events depicted in B. Also ΔF/F duration in astrocytes does not change among different irregular events.

3.12---Photic stimulation unmask the existence of an absolute refractory period between interictal spikes.

As a consequence of Bicuculline-induced dishinibition, the visual cortex becomes unable to properly process visual stimuli: an interictal event is recorded in response to photic stimulation instead of a physiological visual evoked potential. Since the actual shape of evoked and spontaneous field potential events are indistinguishable, the visual cortex is then no longer capable of discriminating between darkness and visul cues. Randomizing the timing of photic stimulation with respect to interictal spiking frequency, unmasked a period following each hypersynchronous event during which the cortex is completely blind since no field signature at all is recorded. Bicuculline dishinibition turns the cortex into an anharmonic oscillator with a precise accrual phase and a refractory period. Discharging the system with an external "kick" (photic stimulation), produce an "all or none" response, re-starting the cycle.

Visual processing has the characteristic V.E.P. LFP profile reflecting a complex series of events in V1, involving precise timing of cell firing, distinctive frequency bands, cell classes specialization and hierarchical layering of information flux (Hubener 2003; Hubener and Bonhoeffer, 2006; Bonin et al., 2011; Andermann et al., 2011; Glickfeld et al., 2013; Hubener REF???). This is true for complex visual stimulation as well as simple one. The ability to interpret the visual world rely on this very property. Also recalls, imagination or dreams trigger cortical neural activity similar to visual stimuli processing (Horikawa et al., 2013; Fox et al., 2013; Marx, 2013). To test whether V1 under BMI effect is still able to organize electrical patterns of visual activity, we simply administered flashes to the eye contralateral to the imaged cortex while acquiring LFP and $\Delta F/F$. Single photic stimulation stats an interictal event in LFP. No V.E.Ps. was ever observed under BMI. In Figiure 3.37 is depicted LFP and LS $\Delta F/F$ of an epiosodic flash stimulation. Hereis reported the behavior of a region of neuropile, and a PV neuron. Spectral properties of the interictal event triggered are identical to any other regular interictal event and LFP show a typical hypersynchronous spike (parameters defined for steady state interictal events are recapitulated for flash triggered events). PV and neuropile show synchronous single peaked events starting at interictal onset and peaking at LFP maximum deflection as observed in spontaneous interictal events. The very same is observed for pyramidal neurons also presenting the already discussed faster onset with respect to PV. Astrocytes, as expected events, show no difference in $\Delta F/F$ profile or coincidence chance, compared with spontaneous interictal events. A constant delay of 20 ms (23 ± 8 ms in 40 flash triggered interictal events in 4 animals) is observed from the onset of interictal event triggered by the flash and the visual stimulation start. Delay is observed in LFP (15 ± 7 ms with respect to the interictal event first deviation from the baseline, before peak hyperpolarization or 27 ± 4 ms considering time to peak)

and in ΔF/F. comparing Figure 3.23 with Figure 3.37, becomes clear that V1 responsivity is altered in steady-state interictal activity, with physiological V.E.Ps. presenting a longer dealy from the stimulus onset. (103 ± 10 ms Vs. 23 ± 8 ms, $p < 0.001$) This is true for flashes of variable duration and intensity (0.2 s flash is enough to trigger an interictal event), the position of which is randomized in time from 0.2 to 120 s apart also excluding possible aliasing between interictal periodicity and led presentations. In this reguard, inter-event interval between consecutive interictal events is not altered by the presence of the flash, as the spontaneous interictal event will follow the triggered one with the usual 2 s delay (2.5 ± 0.8 s). In order to evaluate the efficacy with which the flash was able to start an interictal event, single sporadic flashes and trains of hundreds of flashes with fixed periods was tested during LFP. As depicted in Figure 3.38, a 500 ms episodic (0.2 Hz) flash starts itericta events with an accuracy of 81%. For episodic stimulation, the probability of failure was 100% each time an interictal event preceded flash position in time by ≤ 0.8 s. When success probability is evaluated for flashes falling ≥ 0.8 s from the preceding interictal event (spontaneous or flash triggered), the score grows up to 100%. During steady-state interictal activity V1 is turned in a binary switch: the network is either silent or entrained in hypersynchronous events. V1 state oscillates periodically between these two states with a nearly constant periodicity, like an harmonic oscillator of 2.5 s periodicity. A kick in the system (visual stimulation) during the accrual phase, precipitates the discharge phase. After each discharge, the system re-start the accrual phase with unperturbed duration. The flash starts invariably an iterictal spike if another spontaneous interictal event is beyond 0.8s from the time at which the flash is started, or, no responses are observed if the flash is delivered within 0.8 s from an interictal spike. Furthermore, neither a spontaneous event is ever observed falling within 0.8s from the preceding one. For each interictal event spontaneous or flash-triggered, the distance from the preceding event is subtracted from the distance to the following one (Min Delta t). this value is plotted for all 600 events in Figure 3.38. A clustered populations of interictal-interictal times emerges being the pontaneous ones all aligned around 2.5 s. Other scattered events are flash triggered. Distribution is peked at 2.5 s, no interictal events is less then 0.8s from the preceding one and green bars in Figure 3.38 represent distribution of flash induced events. An absolute refractory time exist that abolishes any discharge from V1, once a hypersynchronous event has happened. These observation are reminiscent of the classical behavior of an anharmonic oscillator (described in the introduction) with an accrual phase around 2.5 s (inter-events interval for spontaneous events) and a refractory period of 0.8 s. Actually, no matter how intense was the flash, no events was ever observed within the absolute refractory period and each interictal events belong to a “clonal population” of identical events. Triggered events are indeed indistinguishable from spontaneous ones in a “tapping the faucet” behavior. In the anharmonic oscillator, an input delivered during the accrual phase to be effective must carry enough energy the amount of which decreases as the duty cicle approaches accomplishemnt. In this perspective, flash stimulation results associated with enough “energy” to discharge the oscillator at each point beyond the refractory period. From an adaptive point of view, sustained interictal activity of the type described, results in a dramatic

impairment of signal processing capability. Neural activity is indeed forbidden during refractory period no matter how strong the inputs are and for a pretty long period actually, which shall be far too long for efficient visual processing in a natural environmental context with fast changing features (*e.g.* 1 Hz for 0.01 cpd sliding sine waves, see Ledue et al., 2012). The structure of visual processing is also profoundly compromised, instead of a V.E.P. pattern an hypersynchronous event emerges in LFP, which is the result of a synfire chain activation. In a typical 200 ms interictal event the hyerarchical structure of signal processing in V1 is compressed in monolithic block of all or none synfire. Thus, either V1 si blind to visual stimulation or an hypersynchronous event is misfired instead of a complex V.E.P. If a signal is not delivered instead, a spike identical to that produced in response to the visual stimulation, is generated ectopically and periodically. V1 is then bombarded with “dazzling lights” everytime a flash is presented, is blind for the following 0.8s then either another flash falls or an “illusory” one is generated intrinsically. Humans report phosphenes during parietal interictal activity, to such an extent that may result incompatible with normal visual-depending tasks *e.g.* present reduced ability to operate machinery and slowed reflexes to visual cues (Krestell et al., 2011). Far more frightsome must be the effect of hypersynchronous events discharging the limbic system. TLE affected people are often able to sense the incoming seizure, the so-called “aura”. Oftentimes this represent a great resource since auras can start hours before the ictal event strikes, giving the person the chance to find a secure shelter in order to avoid accidents caused by sudden loss of consciuousness associated with seizures. In many cases auras starts just ahead of the seizure and give no help at all. Sometimes can be terribly pervasive, starting days in advance. Auras are described in many different ways by different epileptic patients depending on the region generating the epileptiform activity. Most frequent are: overt fear unrelated with environmental contest, inability to execute normal daylife tasks (as if one is unable to retrieve the information required), strange sense of extraniation, lost familiarity with usual ambient or people, de-ja vù, exaltation (read F. Dostoevskij, “the idiot” for instance), strange taste or alterated corporal-vegetative functions. Feelings reported during auras are of clinical value since areas interested will be most probably those flooded with the ictal event. Yet another aspect of interictal activity is quite interesting. Since an intense discharge of a large population of neurons is what we observe, what impact could be expected at the level of neural plasticity? Interictal events at the synaptic level are indeed short low frequency pulses reminiscent of LTD protocols. On the other side, long lasting Calcium increases could be experienced by each neuron possibly contributing in triggering potentiation phenomena. Most importantely, what happens to the hippocampal autoassociator system when an hypersynchronous event starts? Do recentely lerned tasks/memories consolidate better when interictal activity is present? Does memory fixation result impaired or mnestic track are being shuffled? What are the cellular mechanisms contributing to the generation of hypersynchronous events and are these protective against ictal onset? Concerning both Calcium elevation is individual cells and a possible generating mechanism sustaining interictal activity against ictal one, read further.

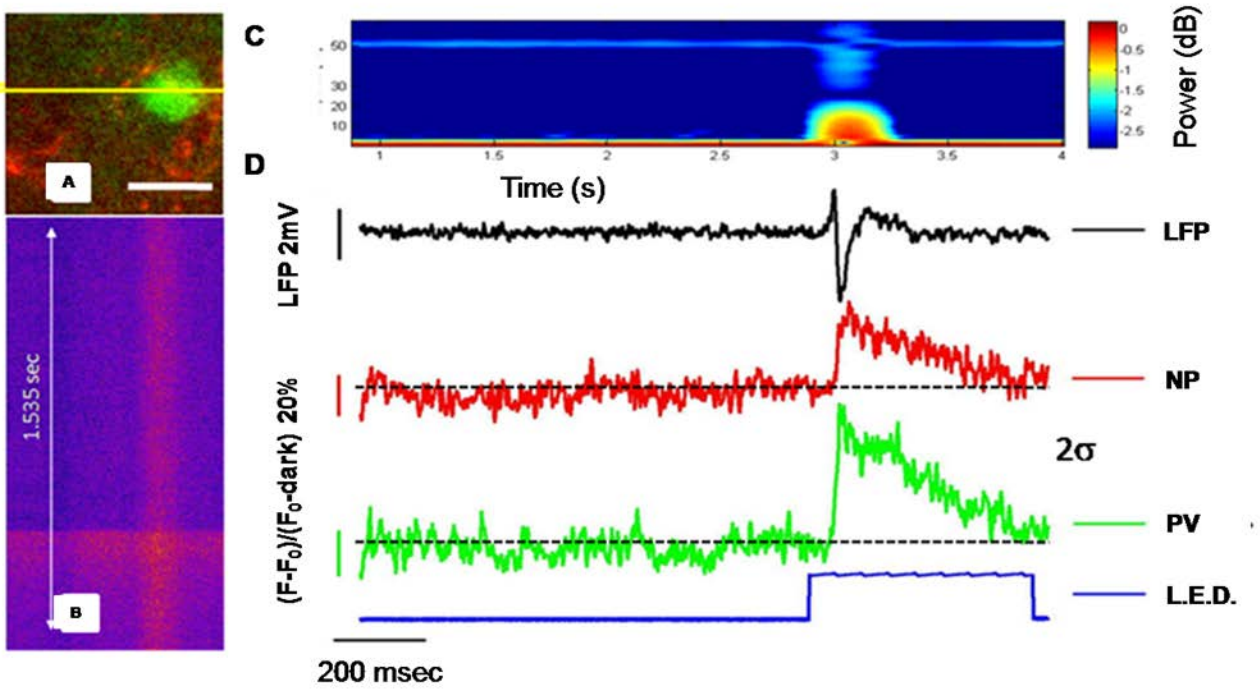

Figure 3.37: Visual processing is impared during interictal hypersynchronous activity. A) Reference frame depicting a single GFP+ parvalbumin neuron and a region of neuropile from 250 μm deep V1 over which a line scan was perfomed. Scale bar 20 μm. B) ΔF/F fluctuation across the yellow line in A, during steady-state interictal activity and photic stimulation. Position in time of stimulation is coincident with the horizontal band abservable near the bottom of the ΔF/F. C) STFT of the LFP acquired during the line scan in B. The typical spectral signatures of a regular interictal event are clearly distinguishable. The blue line at the bottom of the figure, represent the photic stimulation position and duration. During steady-state interictal activity (40' from superfusion) episodic photic stimulation was administered with random frequency. Each flash (0.8 contrast) was 500 ms long contralater to the injected V1. Black is the LFP reporting a regular intterictal event starting at the flash onset. During interictal activity, no VEP was ever observed from animals with normal VEPs before BMI superfusion. VEP rescue is observed in LFP from animals left in washing aCSF solution after superfusion with BMI, only once interictal activity is disappeared and up-down states are restored. Red and Green lines are the ΔF/F in time from neuropile and PV neuron in A. no differences are observed between interictal ΔF/F and flash triggered ones. Since VEPs are the LFP epiphenomena of visual processing, BMI induced interictal events, completely disrupt V1 phisiological function in a reversible fashon.

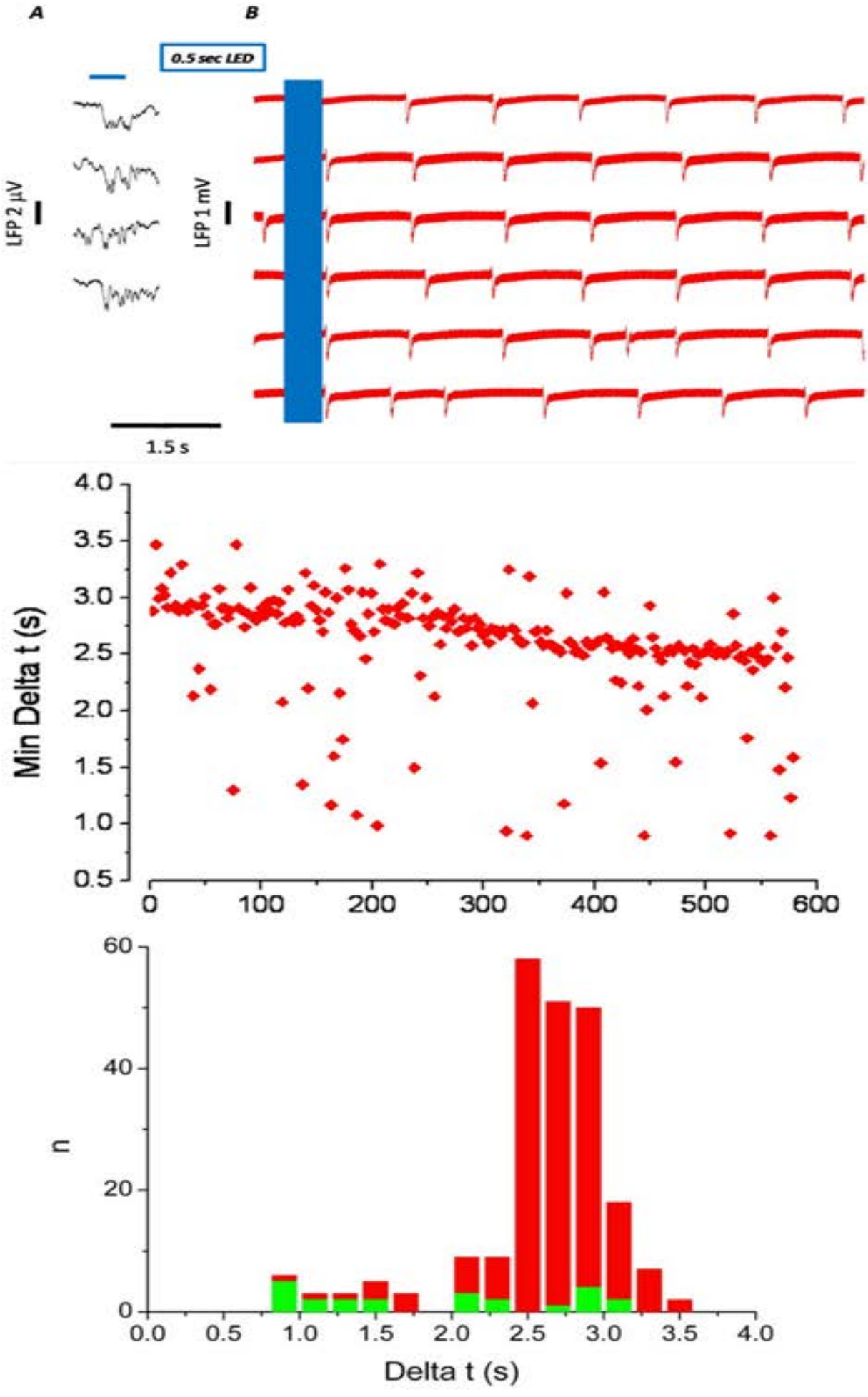
A
B
0.5 sec LED
LFP 2 µV
LFP 1 mV
1.5 s
Min Delta t (s)
4.0
3.5
3.0
2.5
2.0
1.5
1.0
0.5
0
100
200
300
400
500
600
n
60
40
20
0
0.0
0.5
1.0
1.5
2.0
2.5
3.0
3.5
4.0
Delta t (s)

Figure 3.38: On the existence of an absolute refractory period after each interictal event. A) few typical V.E.Ps. triggered by 500 ms (horizontal blue bar) blue l.e.d. flashed in baseline deep anesthesia. B) 6 sweeps of LFP during steady state interictal activity with episodic l.e.d. visual stimulation (500 ms). All tracks were aligned at l.e.d. onset cropped to show an equal amount of LFP recording in each. Blue bar extended across LFPs represents the photic stimulation. 5 tracks out of 6 show an interictal event aligned at the l.e.d. stimulation start. Since spontaneous Interictal events are also present during episodic flash stimulation, a scatterplot in C) top, describe the dispersion of mean delta t across all 600 events. "Min Delta t" defined as time elapsing from the j^{th} interictal and the preceding one - time elapsing from the same j^{th} interictal to the following one. blue dots men delta t with an interictal events with a flash aligned (low frequency of flash stimulation avoid a mean delta t with two interictal events triggered by the photic stimulation), indistinguishable from spontaneous ones represented as red dots. Two distinct populations of red Vs blue dots emerges (KS test returns a rejected hypothesys for all dots belonging to the same distribution). Red dots are dispersed on a line intersecting mean delta t around 3 s, which is the average period of the current interictal spontaneous activity. C) Bottom, frequency count of interictal events numerosity (n) at each bin of "Delta t" value. "Delta t" is the time elapsed from a j^{th} interictal to the j^{th-1}. red bars indicates spontaneous events peaking at inter event interval of 2.5s, green bars are l.e.d. triggered interictal events. since l.e.d. is not in any phase with interictal activity, one should expect all possible Delta t or Min Delta t only in the case that all the time between interictal events were expendable in LFP hypersynchronous events.Data support quite another possibility. Since no events ever fall below 0.8 s from the preceding one or no events follow a triggered one before 0.8 sec, there must be some "refractory" period just ahead any single interictal event that prevents the occurrence of spontaneous events as well as visual triggered ones.

3.13--- Astrocytes show strong activation at the onset of hypersynchronous activity.

The short period intervening between Bicuculline superfusion and appearance of the first interictal event in the local field recording, is characterized by a substantial increase in gamma band power, while up-down states turns into more synchronous events. Neurons and neuropile exhibit increasing Calcium activity as the synchronization in electrical activity builds up. Before the first interictal event, astrocytes display a strong Calcium activity with slow oscillations in correspondence with field events. Calcium oscillations in astrocytes terminate abruptly with the presentation of the first interictal spikes.

Interictal activity induced by BMI superfusion, do not start *ex nihilo* with typical interictal events reverberating *ad libitum*, a transient phase of rapidly evolving LFP parameter is instead observed. This transition phase starts 2' after BMI application and some earlier cellular events might be instructive toward the generation of the first hypersynchronous population event. Hereafter the game is already almost over: feedforeward excitation begets excitation and in the absence of inhibitory brakes ever larger populations are recruited. A sign for this is observed in the temporal progression of time-to-peak LFP parameter that from high values, that is low coherence, falls rapidly in fast ones, or high coherence. In the BMI superfusion model, GABAa anthagonist is allowed to freely diffuse across the cortex thus obvious dilution effects are to be expected and a dorsoventral gradient would be established. Also a temporal gradient is to be expected in BMI effect. Most of the GABA-ergic inputs impinges at the soma level (predominantely fast spiking afferences) the shallowest of which is actually stratified in Layer II-III. Although imaging is performed at 250-300 μm from dural surface and an owerwhelming concentration of BMI is delivered, spatiotemporal pattern of dishinibition development, could be an uncomfortable variable easily overlooked. We then moved our attention to the early phase intercurring from BMI superfusion to the first interictal event recognizable in the LFP delivering dishinibition treatment with a focal microinjection (2 mM, 5''). This allows a confinement of BMI effect to the imaged field. As depicted in Figure 3.39, LFP shows a peculiar increase in high frequencies just before the presentation of the firse interictal event. Up-down states are already washed away and BMI has been injected 10'' earlier. STFT here is charachterized by a general elevation of power in lower and higher frequency, with brief burst of high frequency activity in the region of 10-30 Hz. A sudden fall of power at all frequencies is observed few seconds after the marked first interictal event recognizable (red bar in panel B, C). What follows is the typical sequence of impulsive events. $\Delta F/F$ present drastic differences among neuropile, neurons astrocytes (Figure 3.40). Neuropile show a phase in $\Delta F/F$ characterized by enlarged Calcium activity presenting intermittent shallow spiked plateau. These are interspersed with periods of "silence". The frequency of Calcium transients slowly increases toward the end of the "interictal onset" epoch. Meanwhile LFP track, show

increasing frequency of transients progressively becoming more impulsive and large starting from a baseline-like activity. ΔF/F neuropile events grows in amplitude while reducing plateu pedestal. These considerations points toward a gradually increasing synchrony in neaural activity until overt interictal events shows up. At this point neuropile ΔF/F is indistinguishable from that described for steady-state interictal activity. Synchronization between neuropile and ΔF/F and LFP is, nevertheless, conserved throughout the onset phase. Neural ΔF/F recapitulate neuropile one, yet single cells are far less synchronized with LFP before the appearance of the first interictal events (red bar). Also cell-to-cell synchronization from poor grows higher with LFP impulsivity. First interictal events represented here comes in a bunch of closely packed spikes, separated by silent periods shorter than 0.8s *i.e.* the absolute refractory period seems to be violated. Later interictal events falls instead rigorousely timed with inter-event-intervals > 0.8s (periodicity typical of steady state interictal activity already described). Duration of neural individual ΔF/F events present a marked variability, always starting with the LFP transient, until typical interictal events are observed. From this point even ΔF/F oscillations becomes stereotyped. Neuropile ΔF/F spikes are instead homogeneous in duration near first interictal events. Most surprisingly, during the low coherence phase preceding first interictal events, astrocytes show intense ΔF/F activity. In figure 3.40 is depicted the Calcium behavior of a strongly activated astrocyte and three weakly blinking cells. Sluggish and wide transients falls apparently scattered along LFP first half becoming progressively shorter. A1 present a massive and slow Calcium increase (box C) protracting for the whole rest of the acquisition. Over this slow wave, several spiky transients are observed. These are tightly timed with LFP events. In all astrocytes, early ΔF/F events are variable in duration and alignment with LFP while later ones becomes homogeneous and always presenting a rising phase starting ahead LFP and neuropile or neural one (thus ROI contamination shall be neglected). No sign of drifting or swelling are nevertheless observed for any astrocytes as reported by the red channel remaining flat along the whole acquisition (not shown).

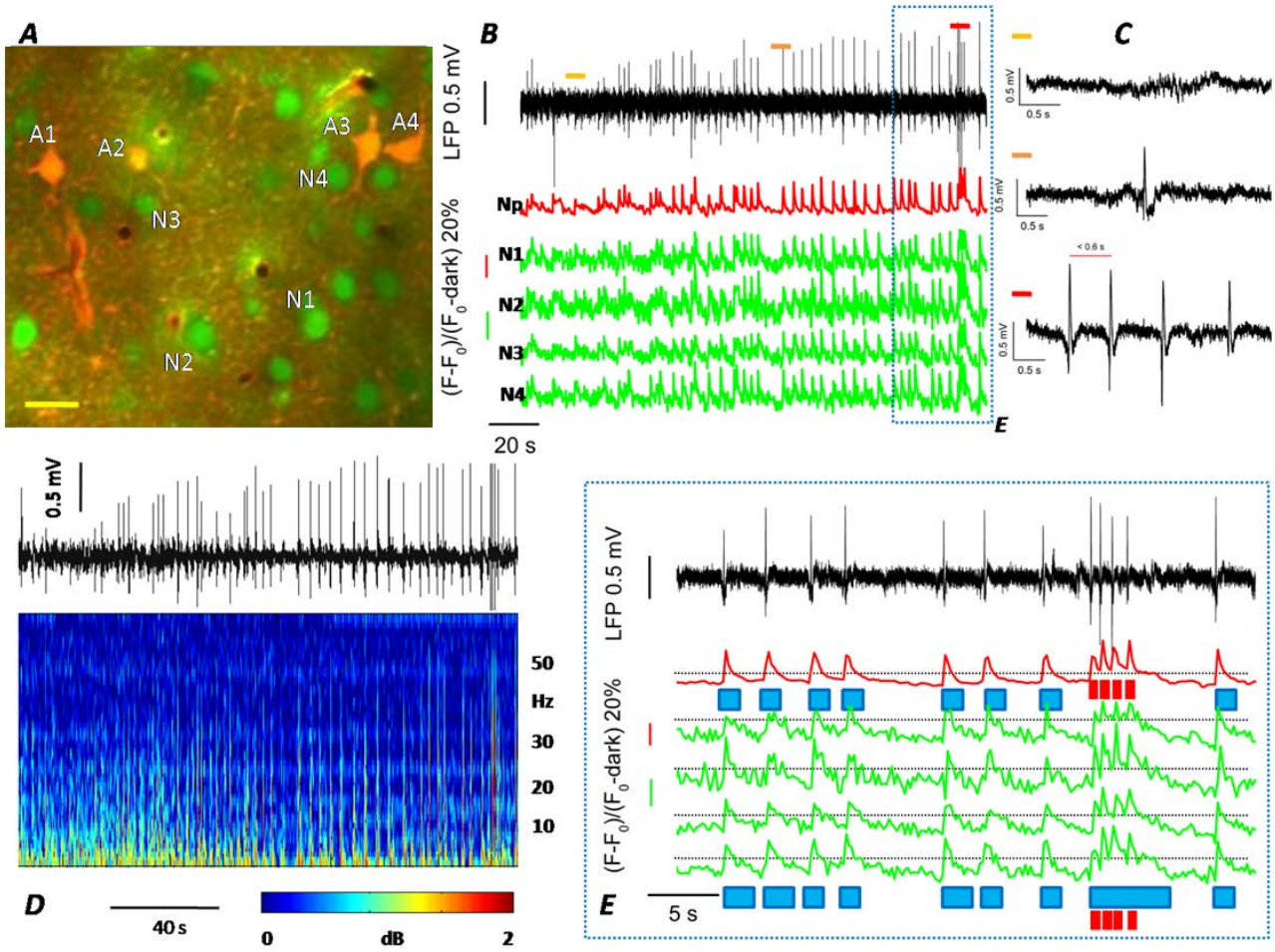

Figure 3.39: *Onset of generalized interictal activity. A) Average projection of a Time series series acquired at 250 μm across the period (3 ± 1.30 'in averaged 10 animals) between BMI superfusion and appearance of the first hypersynchronous events. B) LFP and time matched ΔF/F below starts about 2' after BMI 2mM supefusion, time at which interictal activity is expected to start. In the first half of LFP track intermittent bursting activity is visible quickly turning into hypersynchronus ones. The first detectable interictal event developes with time from sdome sort of semi-baseline activity (yellow bar), through truncated interictal events (orange bar) eventually into fully blown interictal spikes (red bar). After the epoch presented here, a typical interictal activity was observed. Below the LFP is the ΔF/F relative to four neurons and a neuropile region. Neuropile show long lasting ΔF/F oscillation punctuated with spikes at the beginning of onset activity, developing into single spikes advancing toward the center of LFP and eventually turning into typical ointerictal ones in the last third of the epoch. ΔF/F events in the first part appear to be uncorrelated with LFP while, since truncated spikes appear, ΔF/F obtain coherence with LFP. Neurons are almost silent during the first part breaking the symmetry so far observed with neuropile. ΔF/F spikes appear with LFP truncated events and expand further as LFP gain synchrony. Neural Calcium transients are aligned with LFP. C) Magnification of three segments of LFP representing the three phases of onset deveolpement. Top line is representative of a "reduced baseline" typical of the early phase of onset activity. Little signs of up/down states are observed. Center, show a single truncated interictal*

event with inverted spike polarity compared to typical ones and a marked ripple activity preceding and following the spike. Also the amplitude is reduced compared with regular interictal events. Bottom, correspond to the burst of LFP activity toward the end of the epoch in B. here three truncated interictal events are gaining negative polarity and a reduction in ripple activity is also visible. D) STFT of LFP in B. an increase in 30-40 Hz activity is visible toward the early phase of the onset. Here no synchronous events are visible and STFT is greatly different from that of spontaneous up/down or VEP activity. Energy is released continuously at high frequencies. Power starts decreasing when truncated events appear, during the central part of the LFP. As events gain amplitude and impulsivity, power signature in high frequency bands drops further. Toward the end of the epoch, power is organized in pulses remaining low elsewhere as if all the energy is released in intermittent fashon only where synchronous events falls in LFP. At the end of the epoch STFT has already turned into a typical interictal one. E) Magnification of ΔF/F analysis in boxed region in B. High synchronization between neuronal and neuropile ΔF/F is obtained. Also duration of ΔF/F transients are homogeneous between neuropile and neurons (indicated by blue and red blocks below neuroplie and neural tracks). This region of onset activity could be considered similar to interictal steady state, but a burst of spikes is present in the LFP to which all neurons and neuropile respond with high frequency ΔF/F oscillation. Since this sporadic event marks the sudden increase in amplitude and inversion in polarity of truncated interictal spike, the next event could be identified as the first typical interictal spike.

.

Figure 3.40 Astrocytes are aroused by generalized onset activity. A) Same field as in Figure 3.39. B) ΔF/F relative to four astrocytes and neuropile. The latter one is described in the previous figure. Three astocytes remain almost silent during the onset activity except few shallow and long transients dispersed along the trace. All astrocytes show a marked and quick increase in ΔF/F in correspondence with the burst toward the end of the recording. A1 show dramatic ΔF/F oscillations along the whole onset activity. Large isolated slow oscillations are present during neural silence while neuropile display bursting ΔF/F. each astrocyte oscillation in this phase is aligned with neuropile yet present a slower kinetic and is devoided from those ΔF/F spikes overriding neuropile plateaus. Toward the middle of onset activity, A1 ΔF/F changes into a biphasic oscillation: a slower and larger one starting here and protracting until the first typical interictal event, and a fast one characterized by alternating peaks. In C) is depicted the start of the slow rising phase. Most fast transient peaks with a LFP and neuropile event yet is triggered much earlier. Some A1 transients comprise more neuropile ΔF/F and LFP oscillation (like the first one). The duration of A1 ΔF/F is highly erratic (blue underscores) compared to thet of neuropile. Other astrocytes show fewer oscillations of a lesser extent in amplitude yet correlated to A1. D) Magnificagtion of the last part of this onset epoch. A1 reduces ΔF/F oscillations both in frequency, amplitude and accuracy with respect to neuropile and LFP. ΔF/F peaks are somewhat larger than the previous box. Other astrocytes also are more silent. A last surge in ΔF/F is aligned with the burst of four truncated

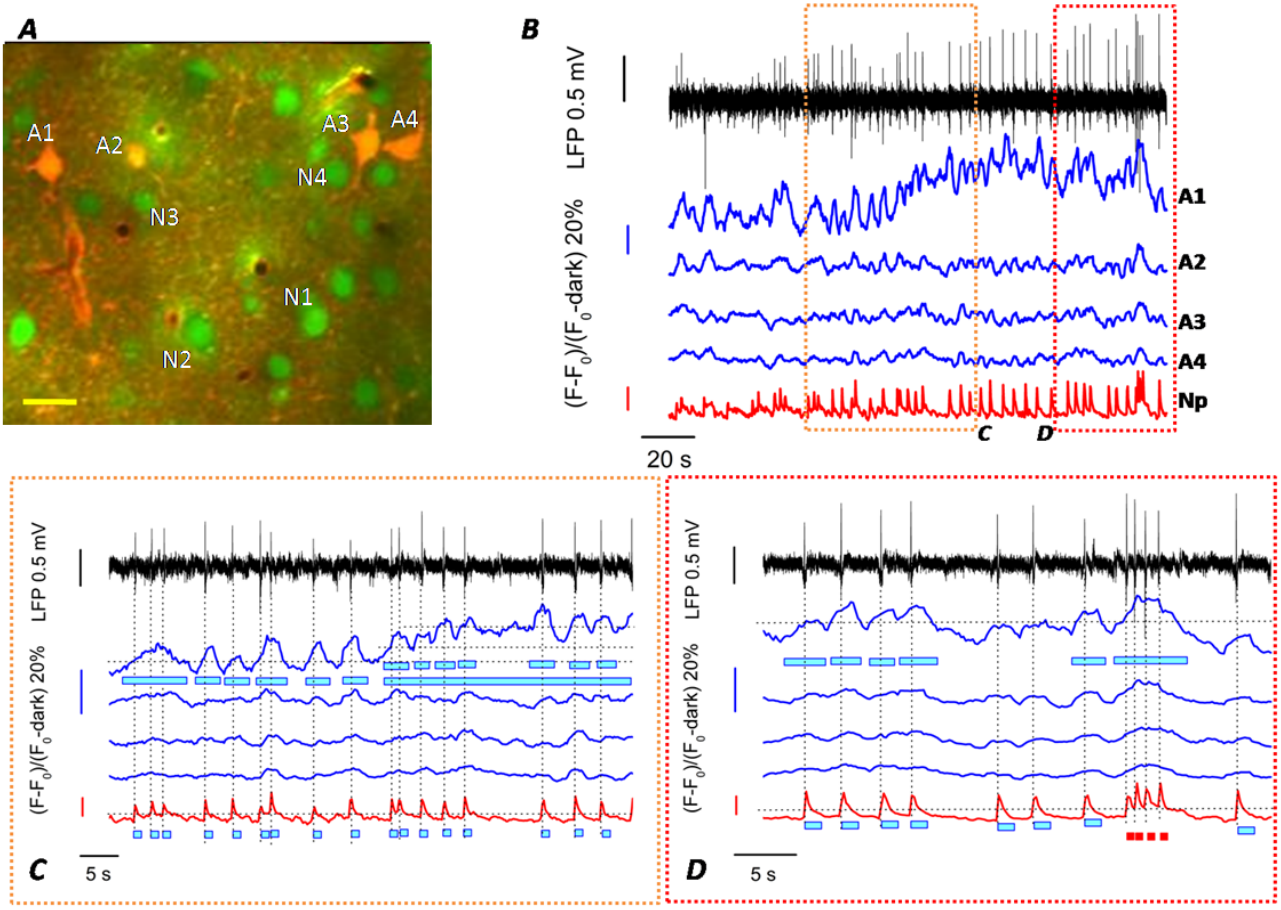

interictal events at the end of the LFP. Note that here a single A1 ΔF/F slope replaces a 4-spiked neuropile oscillation. The first typical interictal events following this burst, appear to be a ΔF/F oscillation under threshold for all astrocytes.

3.14--- Calcium in neurons remains higher than baseline levels during interictal activity.

Interictal events are associated with impulsive Calcium increase of great magnitude readily recovering into a baseline level which endures several seconds before the next hypersynchronous spike. Comparing Calcium signal magnitude in baseline activity (before Bicuculline administration) with periods during interictal phase, a consistent increase in relative Calcium concentration is revealed in neurons and neuropile between consecutive hypersynchronous events. Notably, Calcium levels in astrocytes appear homogenous across baseline and interictal phases. This tonic Calcium elevation outlasts typical Calcium re-normalization kinetics and is always present in spite of a complete silenced electrical activity. Little is known about the impacts of such a protracted Calcium elevation on cellular physiology.

Shape of neuronal Calcium spikes during interictal activity, results quite different from the previousely presented ones for spontaneous and visually evoked activities: ΔF/F are asymmetric with a fast rising phase and a biphasic decay. Neuropile presents a single exponential decay curve recovering baseline levels from each Calcium peak. Increasing the imaging sampling rate allows the unmasking of a prolonged period after Calcium peak, in which intracellular Calcium remains high despite the absence of overt neuronal firing. This is not to be attributed to OGB intrinsic decay dynamic which is monoexponential (http://tools.lifetechnologies.com/content/sfs/manuals/mp03010.pdf). The slow decay phase conforms indeed with whole cell data performed in BMI perfused Guinea pig isolated brain (de Curtis et al., 1999) in which 4 stages of principal cells Vm oscillations are described under hypersynchronous events. A first CNQX-sensitive depolarization triggers the fast QX-314 blocked bursting activity after which a so-called Paroxysmal Depolarizing Shift (PDS, Matsumoto and Ajmone-Marsan, 1964; Prince, 1968; Schwartzkroin and Wyler, 1980; Gean and Chou, 1991; de Curtis and Avanzini, 2001; Timofeev et al., 2002; Schiller, 2004; Ure and Altrup, 2006; Gorji and Speckman, 2009) is observed. PDS results from a sustained, Adenilate cyclase dependent, increase of intracellular Calcium lasting about 100 ms (de Curtis et al., 1999) clamping neural Vm into a non-firing modality with slightly depolarized potentials. PDS are on synaptic origin, meaning that a massive AMPA input is converted into Calcium elevation above some yet poorly charaqcterized threshold: hypersynchronous synaptic events have thus a great chance to elicit these Calcium plateu. Bursting activity preceding PDS, is of short duration and in ΔF/F could corresponds with the underresolved peak. PDS phase terminates in a residual NMDA current, the sign of which in the ΔF/F could be found in the slow decay component of Calcium behavior. These considerations are also instrumental for interpretation of results discussed further concerning the genesis of micro ictal events. PDS Calcium plateu although prolonged, is intermittent, possibly inpinging on Calcium dependent plasticity mechanisms. Also the pulsatile nature of interictal activity, could be seen as reiterating low frequency strong stimulation. Considering that interictal phase usually pervades a considerable part of epileptic patients life, elucidations on the role of interictal activity down to cellular level would be desirable. Neurodegeneration, excitotoxicity, plastic rewiring are among most common phenotypes associated with status epilepticus yet which is the contribution of interictal phase is still obscure. If interictal activity acts as a brake against seizure, it could also be responsible for at least some undesired cellular events or even paradoxically, paving the way for increased recurrency of seizures in the long term. Triggering interictal activity with BMI superfusion, allow the possibility to compare to some extent, neural physiology during spontaneous activity and epileptiform one, taking advantage of Calcium readings as a reporter of cellular “health”. Once bulk loading procedure culminates in a stable staining (1h post injection is usually enough), no alteration in OGB intracellular concentration is to be expected. Extracellular OGB would thus be already washed away and trapped indicator won’t escape unless cellular membranes becomes compromised. Furthermore, appreciable hydrolysis of OGB is achieved in about 24h (40 °C, pH 7 aCSF) and no enzymatic digestion was ever reported at least in neurons. assuming a steady state for OGB, Calcium dependent fluorescence would only change in time as a consequence of actual Calcium variations, once excitation laser power and acquisition parameters are granted fixed. We performed a relative comparison between basal and interictal Calcium

intracellular concentration in 3 animals. Calcium dependent fluorescence was collected from several cells, sorting data in time in order to segregate fluorescence intensity readings only in down states or between consecutive interictal events. LFP helped defining time appropriate time windows with which pooling data. During interictal activity, frames extracted from imaging series were always captured for times > 1 s from LFP event and well beyond the end of $\Delta F/F$ complete decay. As shown previousely, both in downstates and between interictal events, $\Delta F/F$ tracks are flat. We assumed fluorescence intensity in these phases as representative of basal Calcium concentrations. In each animal, fluorescence was excited at constant laser power and acquisition settings, same parameters were kept constnt across animals. To normalize for obvious differences in OGB concentrations between animals, only average values for each cellular class in each condition were compared (surprisingly, standard deviation resulted very small). In Figure 3.41 is reported the large difference between baseline and interictal phases in Calcium-dependent fluorescence levels for a representative field and for averaged 3 animals. A dramatic 3 fold increase in fluorescence is observed for neurons and neuropile, while astrocytes display no significative variation. Since peak fluorescence amplitude and decay phases are altogether discarded from the analysis, if no constitutive Calcium increment was present during interictal activity, one should expect either a conserved value of fluorescence or even lower one for interictal phase. This derive from the consideration that during spontaneous activity, coordination between neurons is poor and when LFP readings reveal a downstate, it is reasonable to admit that not every single neuron would be clamped in non-oscillating phase, the escape of scattered cells from entrainment in this condition is hard to be detected. Should this be the case, $\Delta F/F$ tracks in individual cells would reveal oscillations and the cell would be discarded. In interictal phases instead, given the extraordinary synchrony in Calcium activity, the possibility that single cells would behave erratically in the face of flat LFP tracks should be considered lower than baseline. Even in this case, $\Delta F/F$ would reveal oscillation, and once again the cell would have been discarded. No data are yet available for animals regaining baseline activity after several hours of interictal phase, since it is rare to observe complete regain of up-down state activity which is seldom obtained after 6-8h from BMI perfusion time at which the integrity of the model could be doubtful. We can't tell whether this observed Calcium is therefore reversible, but even if not, 6h of constant 3 fold Calcium levels should be considered enough to suspect the activation of some sort of Calcium dependent cell reprogramming. This long lasting Calcium elevation, have yet another counterpart on a shorter time scale, namely the interictal Calcium peak. $\Delta F/F$ peaks triggered by interictal events present a double exponential decay phase characterized in Figure 3.42. Here a single event is highlighted with time constants produced by a double exponential fitting. Average time constants of 70 events in 3 animals are also reported. This phase leads into the recovery of interictal baseline Calcium levels. Duration of $\Delta F/F$ complete recovery to baseline after interictal peak is comparable with whole cell recording performed in BMI treated entorhinal cortex in Guinea pig (de Curtis et al., 1999). Superimposing *Cavia* Vm and mouse $\Delta F/F$, bursting phase appear aligned with the peak of Calcium-dependent fluorescence (imaging undersampling and

OGB kinetics taken into account), while the double exponential phase is mirrored in the PDS plateau. The prolonged period of flat ΔF/F have corresponding signature in Vm which remains smooth when -71 mV was the resting potential. PDS is exclusively Calcium dependent and abolished when EDTA is intracellularly injected. Since PDS is not obliterated when QX314 is administerd, blocking NaV-dependent firing, the strong Calcium elevation associated is to be considered ignited by incoming synaptic input (Glutammate ionotropic receptor anthagonists CNQX+AP5 dissipates PDS). Also steady current injection starts PDS in the presence of QX314. Thus synchronous incoming synaptic inputs triggers both short bursting events and strong Calcium elevation lasting about 300 ms. A mechanism by virtue of which, Calcium-activated slow inhibitory after-hyperpolarization Potassium currents (*sIAHP*) are gate-contolled by counteracting action of PKA Vs PP-1 and PP-2A, is well characterized both in ippocampal and cortica pyramidal neurons (Timofeev et al., 2002; Villalobos et al., 2011; Andrade et al., 2012; Witkowski et al., 2012; Pderzani et al., 2013). These currents are sustained by channels homologous to apamine sensitive Potassium rectifier with a markedly protracted inactivation time constant which results, surprisingly enough, of 0.8-1s. Gating of these *sIAHP* channels (locus still unknown), is operated by sustained Calcium elevations, is apamine insensitive and modulated by a variety of factors inpinging on cAMP downstream signaling (firing rate, cholinergic tone, serotonin and Estradiol levels, for instance). The net effect of gated *sIAHP* is the clamping of Vm away from threshold in a hyperpolarized state. As long as *sIAHP* conductance is operating, pyramidal neurons are not capable of firing. Given the long time constant of *sIAHP* channels, principal cells turns into phasic firing modality, concentrating short bursts in periodical time windows of 0.8-1s. The double exponential decay phase after each interictal event, is interpreted here as follows: phase 1 corresponds to renormalization of Calcium levels triggered by AP firing, while phase 2 would be the trace of waning PDS. Different Calcium buffering mechanisms might be operating in the two phases. The strong Calcium rise shall than be reponsibel for *sIAHP* activation. During normal baseline activity, cortical pyramidal neuron never experience such an extreme Calcium increase and sIAHP are “normally” closed. In these conditions, neurons are able of tonic-adaptic firing. Intracellular Calcium during interictal activity might be enough to trigger a constitutive activation of *sIAHP* or each interictal peak could be otherwise responsible for gating. sIAHP EC50 is around 300 nM (Andrade et al., 2012) while a tenfold lower level is estimated as pyramidal baseline Calcium level (Berridge, 1998; Maravall et al., 2000). Since a 3fold increase is observed in Calcium levels inbetween interictal events, it is rather unplausible that the prolonged Calcium elevation could be a tonic triggering factor fot *sIAHP* gating. Peak amplitude of interictal ΔF/F, accounts for an above 10fold increase well within sIAHP gating threshold. Among neuronal Calcium buffering systems, hippocalcin would be a good candidate for Calcium renormalization from PDS (Kd around 100-150 nM, Burgoyne, 2007) while Calmodulin would be set in action for greater increases, such as interictal acute bursting (Calmodulin Kd being in the micromolar range, Klee et al., 1980). Such a biphasic Calcium buffering would thus be mirrored in the presented double exponential ΔF/F decay curve. The constituve Calcium elevation during interictal activity from around 60 nM estimation in resting neurons to (Maravall et al., 2000) to the threefold increase documented here shall then be a sign of hippocalcin activation which is observed to be involved in hippocampal LTD (Colingridge et al., 2006; Anastassios et al., 2008).

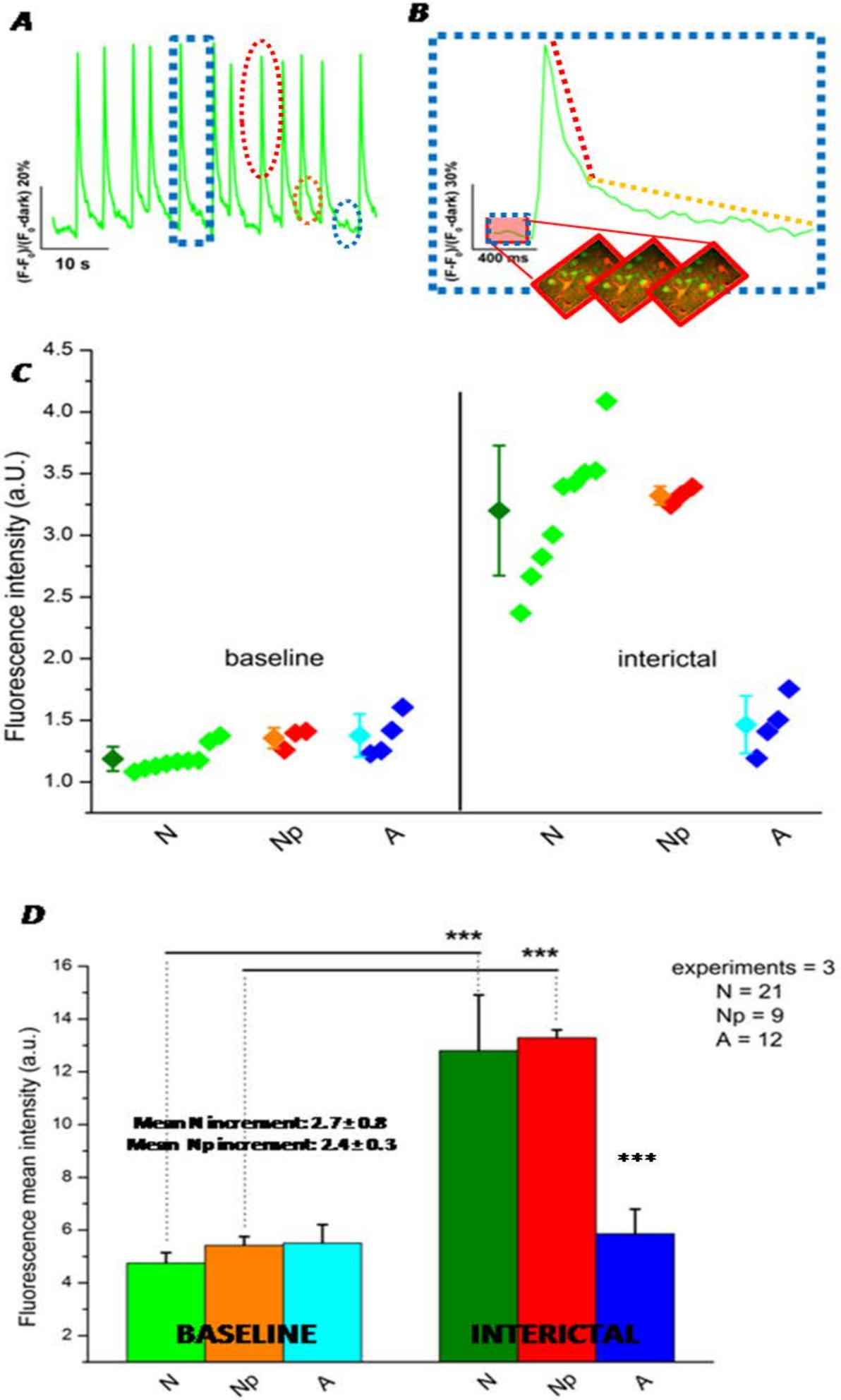
A
B
(F-F0)/(F0-dark) 20%
10 s
(F-F0)/(F0-dark) 30%
400 ms
C
Fluorescence intensity (a.U.)
baseline
interictal
N
Np
A
D
Fluorescence mean intensity (a.u.)
***
***
***
Mean N increment: 2.7±0.8
Mean Np increment: 2.4±0.3
BASELINE
INTERICTAL
experiments = 3
N = 21
Np = 9
A = 12

Figure 3.41: Calcium in neurons remains higher than baseline after each inter-interictal event. A) ΔF/F from a representative neuron during typical interictal activity. Three recursive phases are present at each interictal LFP event: a fast ΔF/F rising phase (red circle), a slower decay (orange circle) and a low ΔF/F "silent" period before the next event (blue circle). A single spike in ΔF/F is highlighted and magnified in B). Here the three phases are clearly distinguishable. The decay phase presents always a long slope extinguishing in a flat line of variable duration. This last epoch is associated with LFP spectal silence. Duration of first and second phases are stereotyped, only a small variation in amplitude is observed between cells and interictal events in individual cells. Both evoked and spontaneous interictal events only develop this ΔF/F shape when at least 0.8s elapsed from the previous spike. Spontaneous or triggered interictal events are only observed after the complete decay of the second (orange) slope after the ΔF/F maximum (blue circle).. OGB Kd and kinetic grant for a complete recovery of bulk fluorescence after each burst of AP within milliseconds. Given the fact that at each interictal event, only a burst of few AP is generated at the peak of LFP spike followed by "silence", $[Ca]_i$ should be elevated by APs then left free to renormalize. This would produce a $[Ca]_I$ baseline level after each ΔF/F peak within few milliseconds instead of the two exponential decay phases described here and further. (de Curtis et al., 1999), (Kd 170 nM http://www.lifetechnologies.com/it/en/home/references/molecular-probes-the-handbook/indicators-for-ca2-mg2-zn2-and-other-metal-ions/fluorescent-ca2-indicators-excited-with-visible-light.html, detection of individual action potentials are described for 100 Hz imaging sampling at the level of the soma, as described in Helmchen, 2011), Since the decay of fluorescence terminates with the second exponential decay phase, within 0.3s, third phase should be considered as a period of stable "baseline" Calcium concentration Calcium dependent fluorescence intensity in the third phase shuld therefore change, compared with "before BMI" up-down states baselines, only if: laser power/PMT gain is changed in the meanwhile, $[OGB]_i$ is not stable, topological cues are altered or if a steady $[Ca]_I$ elevation occurs. Calcium dependent fluorescence intensity is extracted from 3 frames during late phase 3 (choisen in time in order to be as close as possible to the rising phase of a ΔF/F interictal spike and as far as possible from the termination of a preceding second exponential decay phase), from a bunch of selected interictal events (100) presenting extended flat ΔF/F before the following interictal event. A series of phase 3 interictal Calcium-dependent fluorescence intensities data set is extracted from several neurons and averaged out. B) Calcium-dependent fluorescence intensity is also extracted from the same neurons before interictal activity, during down-states (100, away from LFP upstates in order to avoid sub-theshold ΔF/F oscillations and occasional APs). Series of three frames from different neurons are collected keeping laser power and PMT gain constant. $[OGB]_i$ is reported to remain constant after 2h from the loading (Garaschuk and Konnerth, 2010). Baseline Calcium dependet fluorescence intensity are collected here after 2h from loading. Geometrical issues could also be relaxed since no evidence of aedema are observed in selected experiments and no apparent change in shape/proportions of either neurons or astrocytes are ever observed after interictal activity onset. Average fluorescence obtained in each ROI is used to normalize [OGB] differences between different cells. Scatter plot presents average Calcium dependent fluorescent intensities for 10 neurons, 3 regions of neuropil and 4 astrocites, calculated during baseline and during phase 3 interictal activity. A total of 300 frames contributed for each condition in each cell. Interictal events and downstates were randomly selected but never consecutive. Dark points indicates the average ΔF/F among cells of the same class. Standard deviation is also reported. During baseline no significative difference is to be observed among cells or neuropil regions all showing an uniform "down-state" Calcium-dependent fluorescence intensity. During interictal activity a large difference is observed only comparing average astrocyte value with neuron/neuropile ones. Comparing baseline values with interictal ones, a great difference emrges for neuron and neuropile showing an almost 3-fold increase in interictal activity while in astrocytes, average fluorescence remains comparable with baseline level. D) ΔF/F is averaged across ROI classes (neurons, astrocytes and neuropile) in the same conditions (baseline or interictal activity) in different animals (3) in order to obtain the histogram reported. Although few cells were so far included, a large difference is observed for neurons and neuropil between conditions and between neuron/neuropil and astrocytes during interictal activity.

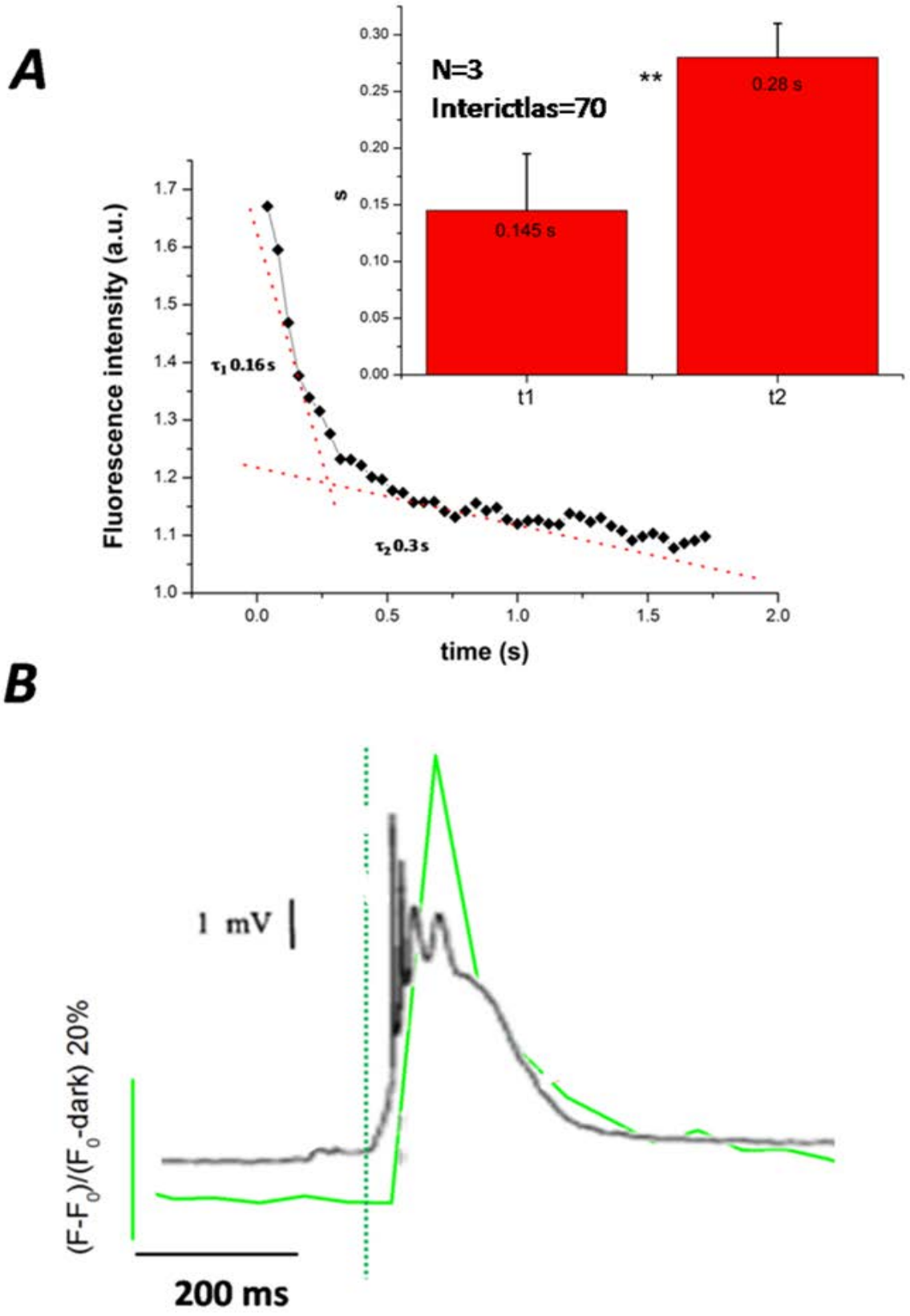

Figure 3.42: Interictal absolute refractory period might be supported by a Calcium dependent mechanism. A) ΔF/F during phase 1 and phase 2 interictal event from a representative neuron acquired at high speed (26 Hz). Double exponential fit produced two separated time constants τ1: 0.16 s and τ2: 0.3 s. The existence of a double exponential

decay curve is suggestive of a mechanism responsible for Calcium buffering, operating in two independent steps. Average calculated over 3 animals in 70 interictal events produced τ values reported in the histogram on the right (phase 1: 0.145 ± 0.05 s, phase 2: 0.28 ± 0.03 s). B) Top: a typical mouse $\Delta F/F$ (green line) from a pyramidal neuron during an interictal event is superimposed with a intracellular recording (black line) from mEC pyramidal neuron in Cavia porcellum (deCurtis et al., 1999). LFP provided in the same figure allowed correct positioning of the $\Delta F/F$ onset time (vertical dotted line). Intracellular recording show spiking activity overriding a depolarization plateau observed at each interictal event in Cavia. Brief small oscillations precedes interictal onset while sustained depolarization persist after burst. Phase 2 in $\Delta F/F$ might correspond to the so-called paroxysmal depolarizing shift (PDS) described in Cavia (de Curtis et al., 1999) at each interictal event. This is the plateau depolarization following AP bursting presented in the intracellular recording. PDS is calcium dependent and present an average duration of 400-500 ms.

3.15--- Collapse of absolute refractory period leads to micro-ictal activity.

Paroxysmal depolarization shift is often described together with interictal events, a phenomenon in which neuronal membrane voltage is "clamped" to underthreshold depolarized levels and long lasting Calcium elevation is observed. This scenario is triggered at each interictal episode and last up to a second. Meanwhile, a Calcium activated outward Potassium current is recorded which is responsible for the re-polarization of principal cells. As long as this current is sustained, no further action potential firing is allowed for the cell. Interestingly, time constant of this hyperpolarizing current is perfectly compatible with the absolute refractory period previousely described. Superfusing the visual cortex during interictal activity with a compound capable to shut down Calcium dependent outward Potassium current, hypersynchronous events are observed to get progressively packed closer one another until absolute refractory period is violated. At this very point interictal events start to vanish from the field recording and bursts of high frequency activity is recorded instead. Henceforth, high frequency events pops out scattered in time, each of variable duration around 4 s. Spectral properties of such events closely resemble those of ictal activity.

How strong is the dishinibition during interictal activity is unclear. Different concentrations of BMI starts hypersynchronous events with different amplitudes and frequency yet conserving shape ranging from 0.03-2 mM. Since there is no further increment in amplitude or frequency for doses above 2 mM it seems that this is a saturating dose, enough to exert complete effect on the volume inside which LFP is recorded. Lower doses should be active on smaller volumes, hence the reduced amplitude of the events. But still at low doses, when a bunch of cells organize an hypersynchronous activity among them, "monolithic" stereotyped events manifests. This is confirmed by data from microinjections, where the volume of dishinibition must be the smallest observed. Even in these conditions, interictal activity emerges, although reduced in amplitude and longevity. There must be a "no return zone" below which BMI results too few to overcome GABA effect. What happens there is still unknown. A firing ring of inhibition could harness the propagation of interictal events that do not spread all over the cortex (e.g. for V1 superfusions no motor effects are observed, that manifest instead when craniotomy was performed much more rostrally, these includes rapid ritmic twitching or vibration of back and limbs musculature, together with "face washing" or "yawning" authomatisms). Also inside hypersynchronous region, GABAa activity is unlikely to be completely removed. Large hypersynchronous events also interests PV neurons and, most likely other interneurons (no deviation from "one interictal-one $\Delta F/F$ peak " rule in any neural cells analyzed was ever observed). Brief waves of GABA could be enough to kick BMI away from receptors at least at the peak of interictal spikes, probably triggering its termination. Most importantely, GABAb receptors remain fully operative in BMI and MUST play some role. In the Guinea pig brain a 20% of dishinibition is estimated to be obtained with arterial perfusion In the abnsence of a Current clamp recording in supefused mouse BMI interictal activity we cannot tell if inhibitory block is actually complete. Although partial, some GABA-independent intrinsic silencing mechanism must be triggered by interictal events in each cell since, at least in PV, $\Delta F/F$ ends just as LFP completes the deflection and silence is obserd henceforth until next event strikes. It is unlikely that some 2 s of silence are maintained by a 200 ms GABA burst even taking

into account GABAb effect. From Voltage clamp evidences reported in Figure 3.42, principal cells invariably enters PDS after each interictal bursting activity. This is a long lasting (up to seconds) period of high intracellular Calcim that correlates with the termination of firing. Three Calcium activated Potassium hyperpolarizing currents are the major candidates in sustaining intrinsic inhibition. Two of such currents are apamin sensitive fast conductance readily inactivating. A slower one, the *sIAHP*, is mediated by a large conductance channel that has not yet been isolated although widely present in neocortical neurons, this is also finely modulated but subcortical mediators like Ach and is involved in synchronization phenomena (Pennefather et al., 1999; Fohering et al., 2003; Kato et al., 2003; Buno et al., 2006; Power and Sah, 2008; Kohling et al., 2012). When gated, this inhibitory current shut firing and shunt excitatory currents for 06-1 s. We then tested the effect of a *sIAHP* blocker on interictal activity and $\Delta F/F$. The only potent and selective one available is UCL 2077 (Tocris) wich, when superfused, exerts two strong effects: 1) if the cortex is in ongoing interictal activity, ALL impulsive events are washed away within few menutes and 2) if delivered before BMI, NO interictal event is to be observed after GABAa antagonist is puperfused. In Figure 3.43 is reported the LFP and STFT effect of UCL 2077 during ongoing interictal activity some 10' after superfusion in comparison with up-down state and interictal activity. Powerful surges of high frequency bursts of activity emerges instead of iterictal events and an overall increased high frequency power is observed. These high frequency events are rhythmical but are not spaced by total silece as in interictal activity. In panel B, is reported one of such events magnified. They all starts with a wide deflaction and goes on for 1-3 s as high frequency oscillations punctuated with sudden spikes. The maximum amplitude is dramatically reduced and duration extremely extended when compared to interictal events. Furthermore, spectral properties, duration and amplitude are clearly not those of up-down states. Average duration is erratic within first few menutes then is stabilized around 3 s while amplitude remains around 1/3 that of up states and 1/5-1/8 compared with interictal events measured in the same animal. These events start as synchronized activity (somehow reminiscent of in Cavia slow interictal event preceding each ictal phase), but the much smaller deflection compared with interictal one, suggest the contribution of a much smaller population of synchronous cells. Also the exit phase from interictal bursting is quite peculiar when UCL 2077 is superfused. In Figure 3.44 an acquisition of an early UCL 2077 trace is reported: steady state interictal activity, with typical hypersynchronous events and the mirroring neuronal $\Delta F/F$ activity, is compared with a recording 20' after UCL 2077 superfusion. Under UCL highly packed interictal events distributed in discrete bursts of coherent spikes. Note the starting high frequency of such events in each train, which adapts readily. Neural cells in green show a $\Delta F/F$ mirroring each of these events with a strong Calcium increase, identical to those observed in interictyal events. Average distance between events in a train is initially around 1 s but as UCL effect goes on, ever closer events are observed. Eventually, later events fall closer than 0.8s apart. in a couple of minutes from this point LFP is further changed into that of figure 3.45 and 3.46. $\Delta F/F$ in neuropile is always perfectly aligned with

LFP in UCL 2077 events, while neural ones starts as typical interictal Calcium transient to be turned slowly in “out-of-pace” events, with $\Delta F/F$ peak jittering with respect to LFP peaks.

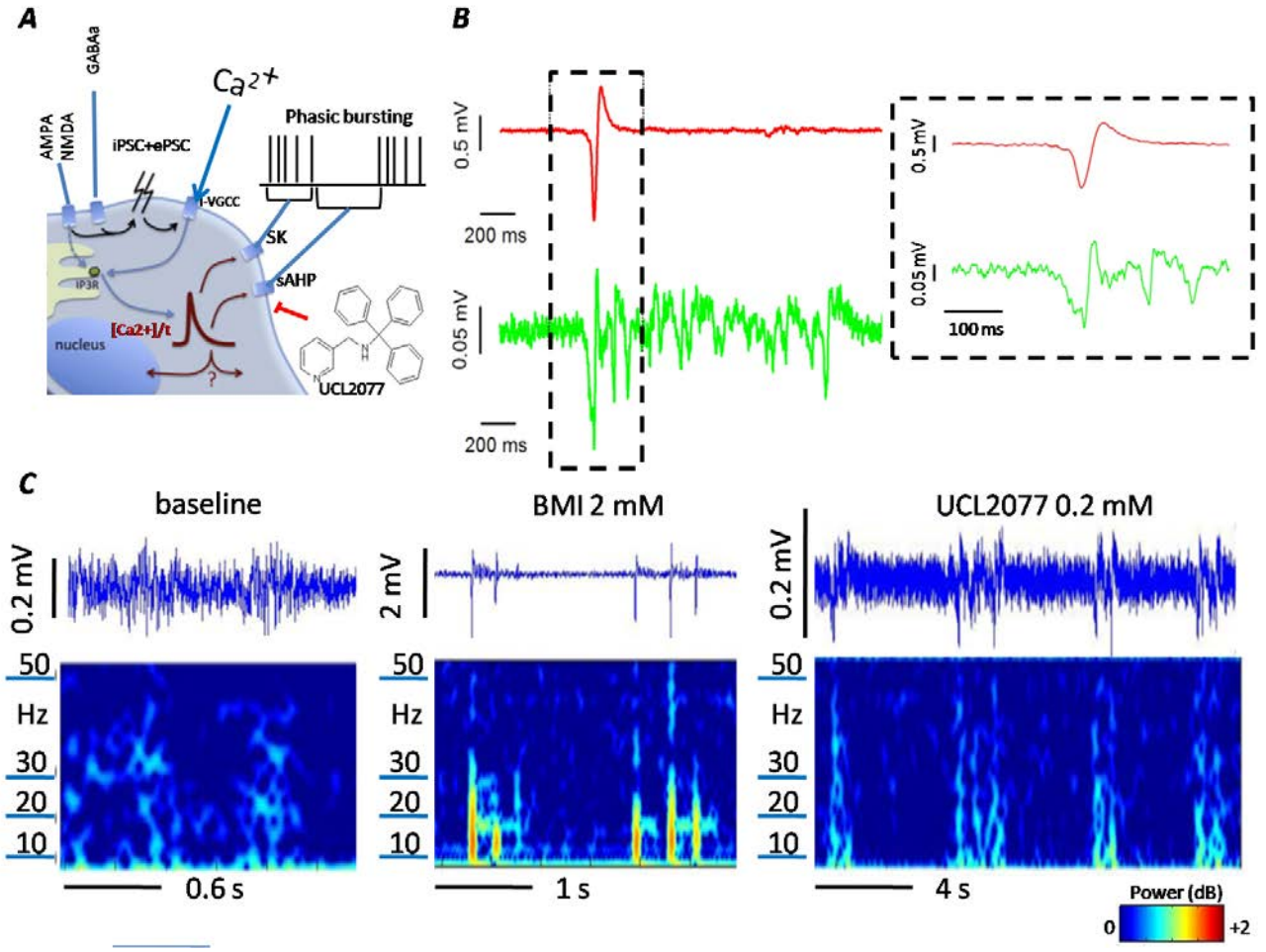

Figure 3.43: *UCL2077 abolishes interictal activity. A) UCL 2077 is potent selective inhibitor of Calcium-triggered Potassium outward slow currents ($_{s}I_{AHP}$). Proposed mechanism of gating and action of $_{s}I_{AHP}$ on the firing behavior of model growth hormone releasing neurons (GHRN) from neurohypophisis (adapted from Kohling et al., 2012). Channel mediating $_{s}I_{AHP}$ current turn a tonic-adapting cell into a "peace.maker" one, imposing at each burst a strong iperpolarization of fixed duration initiated by bursting activity itself. These currents , we suppose, operate in Pyramidal cells during high Calcium challenge triggered by sustaining interictal activity. B) In red typical interictal LFP beforeUCL2077 superfusion, in green LFP induced by UCL 2077 when administered during ongoing interictal activity. Interictal events vanish from the LFP replaced by high frequency-low duration episodes (the hallmark of de-synchronization). these events are reminiscent of ictal events described for BMI perfused Cavia brain. Both average amplitude and duration of these events differ significatively from all LFP patterns described so far in this work (3.6 ± 0.4 s; 0.24 ± 0.05 mV). Magnification of aligned interictal and "micro-ictal" events is depicted in the insert. While interictal events terminates shortly after the peak, an high frequency phase ensues in micro-ictal events once negative phase is terminated. C) Spectral signatures of baseline, interictal and micro ictal activity compared as revealed by STFT analysis. Micro-ictal events present an increase in power density inside 30-40 Hz frequency band with respect to up/down states and interictal activity. Distribution of such events apper completely bereft of any periodicity.*

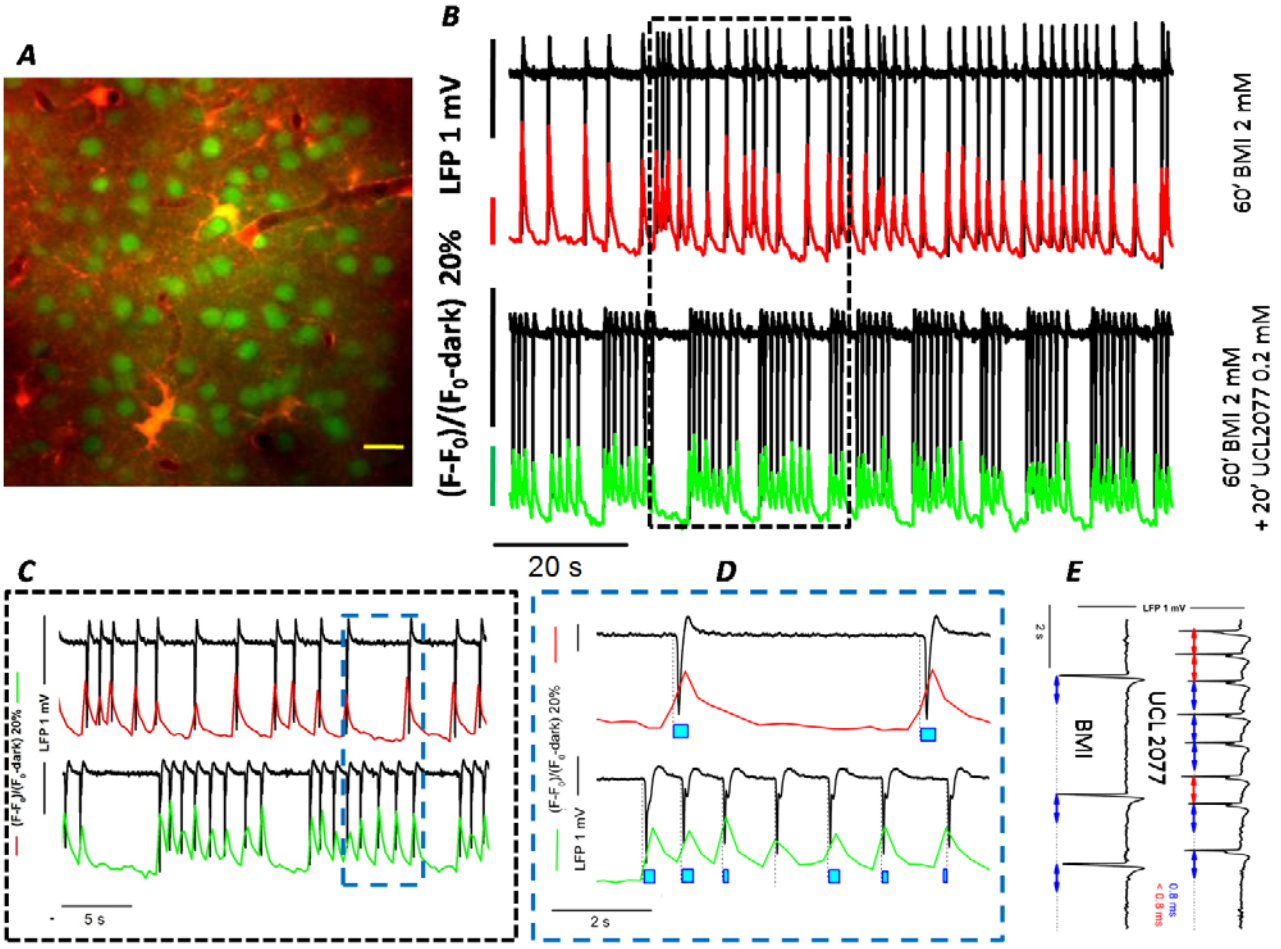

Figure 3.44: Crushing absolute refractory period. A) Average projection of a T-series performed 250 μm deep in V1 after superfusion of UCL2077 during interictal steady-state. Several neurons and astrocytes are visible. Here a fast conventional scanning acquisition was performed (scalebar 40 μm). B) Top: LFP activity during interictal phase preceding UCL 2077 administration (60' from BMI superfusion) and Bottom: ttransition from hypersynchronous events toward microictal ones (20' from UCL2077 superfusion). Both LFP have similar amplitude but completely different activity patterns. Within 15-20' from UCL 2077 superfusion, short, high-frequency bursts, manifest replacing typical interictal spikes. Single event inside a burst closely resemble isolated interictal events (in shape, amplitude and duration). Periodicity is lost within each burst: LFP spike frequency adapts. ΔF/F reported in red and green are both relative to individual representative neurons visible in A. Same neuron is imaged before and after UCL2077. Neural ΔF/F preserves the sharp correlation with LFP producing trains of spikes each terminating on the shoulder of the next. C) Magnification of boxed area in B. Each LFP spike is mirrored by a neural "interictal-like" ΔF/F oscillation. Here "phase 3" (see Figure 3.41) of interictal ΔF/F events is completely lost between consecutive spikes, to be observed again between consecutive bursts. A period of silence is also present between consecutive bursts. Each burst contain an almost fixed number of spikes (8 ± 2 in 40 bursts) varying very little in amplitude. Above, a pre-UCL2077 ΔF/F series from the same neuron is reported for comparison (red and correspondent LFP in black). D) Further magnificagtion of boxed region in C. Duration of single ΔF/F spikes inside each burst may change erratically as compared to "cloned" events in interictal activity (blue underscores represents the duration of highlighted event). E) Although highly dense in

spikes, initial bursts respect the 0.8 s rule for absolute refractory period. In 30’ from UCL2077 superfusion, a sudden change in spike frequency herald LFP shift toward micro-ictal activity. Single spikes get closer than 0.8 s. Spiking activity terminates shortly after, leaving the cortex into a pulsatile micro-ictal activity. In the rightmost track, some spikes violates the 0.8 s rule (interictal activity is reported for comparison), blue and red lines underscore normal latency and shorter than 0.8s one respectively.

3.16---Astrocytes are massively recruited during micro-ictal events.

Calcium imaging during "micro ictal" events reveals intense activity in neuropile and neurons perfectly aligned with local field oscillations. More precisely, principal cells and neuropile present Calcium spikes peaking inside field events while Parvalbumin interneurons fire preferentially in short time windows adjacent to micro ictals. Alignment in Calcium traces from different cells is variable in time, a sign of low synchronization in the network as confirmed by the low amplitude/long duration of field oscillations. Astrocyte somata show also an intense Calcium activity which is greately increased in frequency when comapared with both physiological and interictal activity. Coincidence between Calcium events and field oscillations is maximum during micro ictal phases. Astrocyte processes appear very active with Calcium peaks well aligned. Coincidence probability of Calcium transients with field events in neuropile remains flat in all conditions tested so far, while neurons follow a law best approximated by the variation of synchronization as extrapolated by field recording. Astrocyte coincidence probability instead, is best predicted by the gamma-over-alpha ratio in spectral power.

In Figure 3.45 is depicted the LFP in UCL 2077 superfusion during steady state interictal activity. An overall low amplitude LFP is punctuated with small events the duration of which is stabilized around 3 s (3.5 ± 0.6 s in 3 animals). $\Delta F/F$ in neuropile is deeply distorted compared with interictal or baseline activity. Frequent oscillations of small amplitude are disseminated each centered inside an LFP event. Duration and shape of each $\Delta F/F$ peak is highly variable and periods of $\Delta F/F$ silence are concomitant with LFP fluctuations. Neural $\Delta F/F$ faithfully mirrors neuropile although cell-to-cell coordination appear poor. Neural peaks are indeed all timed with LFP events, yet Calcium peaks are not synchronous among cells each presenting large variability across LFP event. Different principal cells display $\Delta F/F$ peaking in different times inside LFP events with no preference neither for the onset nor for the end. A peculiar distribution of $\Delta F/F$ transients with respect to LFP oscillation is otherwise observed for PV-positive cells as described in Figure 3.47, 48 and later discussed. Astrocytes appear highly active, with brief and longer transients. Two highlighted periods in LFP are anlarged in Figure 3.46, a prolonged silent period is aligned with one observed in neurons and neuropile, flanked by sluggish oscillations concomitant with LFP events. $\Delta F/F$ transients are timed with "micro ictal onsets" and well synchronized among different cells. Processes are also highly active with peaked transients all aligned one another and with somata peaks. Coordination between processes appear higer than neurons. To better observe UCL 2077 induced events, we performed a series of LS acquisitions collecting pyramidal, parvalbumin neurons and astrocytes $\Delta F/F$ as presented in Figure 3.47. Astrocytes always fire toward the second half of the event and always a double peaked deflection is present (green shades). Parvalbumin neurons, instead, concentrate their firing outside each event, in two narrow $\Delta F/F$ transients flanking the LFP oscillation. Pyramidal, neurons display a single spike near that of astrocytes. No significative $\Delta F/F$ events are observed for neuropile, astrocytes, processes or principal cells falling

outside LFP events. UCL 2077 LFP keeps going with intermittent events separated by smaller fluctuation, for around 1 h then a dissipation in frequency is observed and eventually up-down states emerges. In the steady phase of UCL events, beside already described low amplitude $\Delta F/F$ events in astrocytes, some big deflections are observed, starting inside a single UCL event and protracting for few seconds (one such event is boxed in Figure 3.46). Neurons, neuropile and LFP $\Delta F/F$ behavior also present larger oscillations in correspondence of these events. To evaluate the coincidence probability of $\Delta F/F$ with "micro-ictal" events, we chose a window of ± 0.5 s around each LFP oscillation and counted "out" each event falling outside. In Figure 3.48 is reported the coincidence probability for the various cell classes observed. Pyramidal neurons show a decreased "inside probability" compared to interictal events with no increase of "outside" ones. Neuropile still shows a near 100% coincidence with near 0 out probability. As already described, PV interneurons show greater out probability exceeding the inside one (5 ± 5 % inside Vs 73 ± 2% outside). Astrocytes present a coincidence probability extremely high, comparable with that of neuropile as well as a ner 0 ouside probability. As a consequence of observation concerning LFP and spectral signature, $\Delta(F/F)_t$ oscillations and coincidence probabilities, I dub these UCL events as "focal micro-ictal" . These events seems confined into a small domain as deducible from the low amplitude and short diration of LFP signature. Also $\Delta F/F$ profile is radically different from that observed in Cavia, probably due to the focal nature of the event itself. A closer resemblance is instead to be observed comparing UCL 2077 behavior with TFLLR experiments. In both cases the high frequency LFP territory could be small in size. Among other variables examinable, LFP provides insights into the degree of synchronization of recorded events and about their spectral properties. Spectral signatures are higly indicative of several aspects of neural computation, like wakefulkness state, memory retrieval, exploration behavior, pattern recogniction, sesory processing and epileptiform activity, for instance (Lagier et al., 2004; Verret et al., 2012; Thut et al., 2012; Ainsworth et al., 2012; Henry and Obleser, 2012; Buzsaki and Watson, 2012; Guitart-Masip et al., 2013; de Graagf et al., 2013; Vijayan et al., 2013; Yamagishi and Anderson, 2013). Gamma power is one of such diagnostic featurE. In Figure 3.49 we present a cathegorization of synchronization degree of LFP events expressed as amplitude over duration. LFP amplitude correlates directly with synchronization degree, while duration present an inverse correlation (Buzsaki et al., 2012). Their ratio will then grow as synchronization increases. in order to normalize amplitudes across experiments, we used the average baseline amplitude value estimated in downstates (periods of silence *in Cavia*). Gamma power was evaluated from STFT analysis and presented as the ratio of calculated power in 30-40 Hz Vs. 10-20 Hz bands. Coincidence precision is expressed as the difference between average coincidence probability observed inside-outside LFP events. Neuropile show a flat slope of coincidence precision across all LFP events examined. Principal cells and PV-positive ones display a peak for interictal events (regular and irregular ones), with parvalbumin interneurons strongly preferring out of events during microictal oscillations. Neurons coincidence seems to follow synchronization degree while astrocytes does not. Gamma contents is actually a better "predictor " for coincidence precision in astrocytes. Gamma activity

have been shown to be related to interneuron activation and cortical sub-region segregation, the hallmark of local computation, which appear to be disfunctional in several pathologies (Kiduff et al., 2011; Fishell and Rudy, 2011; Lewis et al., 2012; Volman et al., 2011; Verret et al., 2012; Caputi et al., 2013; DeFelipe et al., 2013).

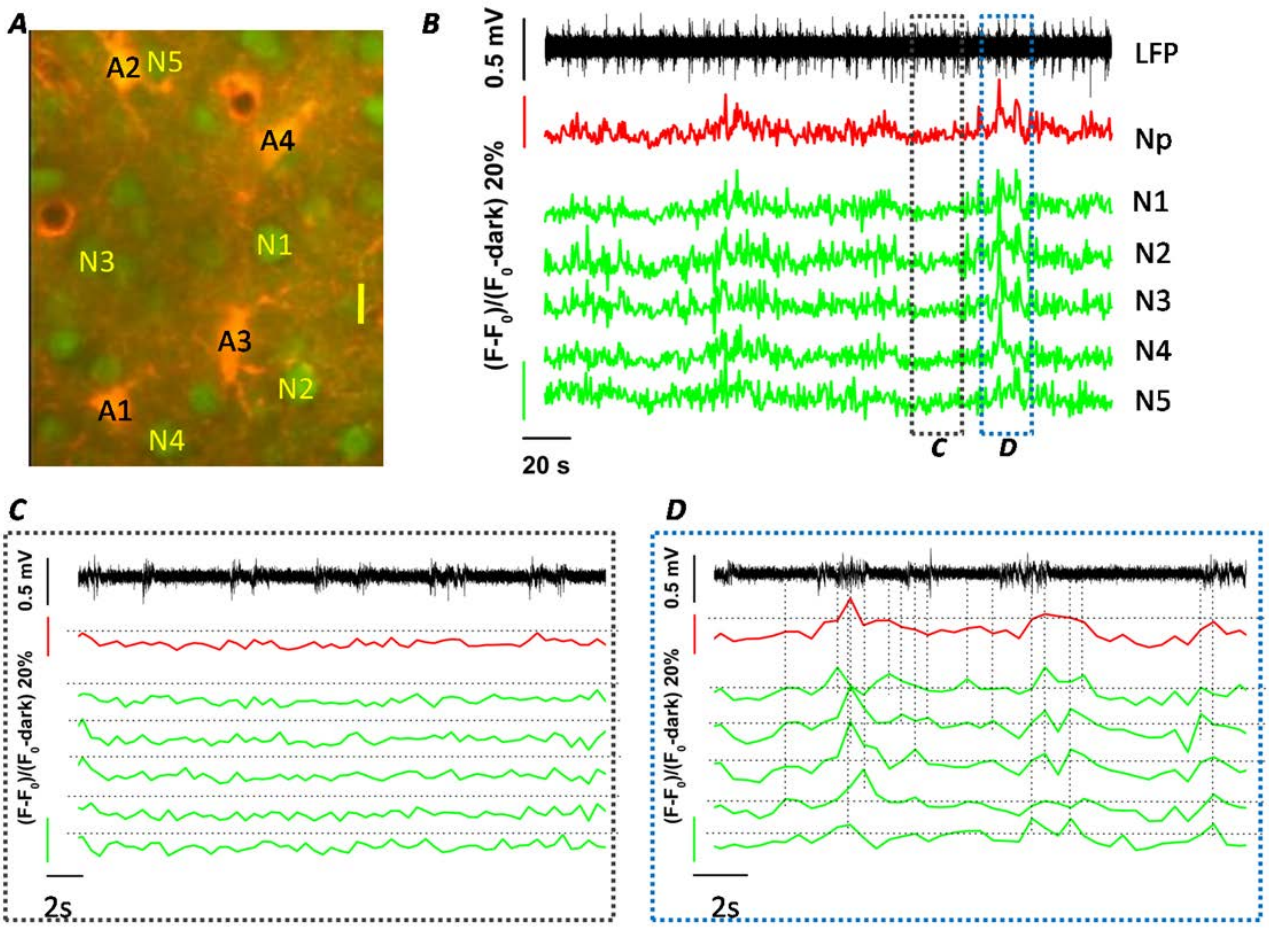

Figure 3.45: de-synchronized neural activity during micro ictal events. A) Average projection of a time series acquired at 200 μm in V1 after UCL 2077 supefusion, 50' after BMI induced interictal activity (scale bar 20 μm). B) LFP in black show frequent micro-ictal events 40' after LFP described in figure 3.44. No interictal events are visible. Red track is the ΔF/F from neuropile. Far from being similar to physiological or interictal activity, neuropile ΔF/F show complex behavior characterized by frequent fast peaks, slower oscillations and few periods of flatness. Individual neurons mirrors neuropile track, with a prevalence of fast peaks. Occasional intense ΔF/F falls apparently random across LFP. C) Magnification of a period of ΔF/F silence boxed in black in B. Despite LFP recurrent activity in this region appear indistinguishable from other section of acquisition, ΔF/F is almost completely flat in neuropile and neurons as well. D) Blue boxed region in B is magnified here. A stretch of intense ΔF/F activity is associated with a LFP section which is similar to tha in C. Events are not always triggered at the onset of each micro-ictal. A large jitter is observed also with respect to peak value in ΔF/F and LFP. This is most evident for neural tracks. Each neuron present a rising ΔF/F aligned with different points inside each micro-ictal events. Duration of ΔF/F transients is also variable and peak values jitter in time below LFP events (vertical dotted lines serve as temporal reference for peaks ΔF/F with respect to LFP). Coordination of neural population is compromised in micro-ictal events as reveald also from the average low intensity of LFP. Nevertheless, all ΔF/F falls inside a micro-ictal event. No individual neurons appear silent when other neuron dispay ΔF/F oscillations .

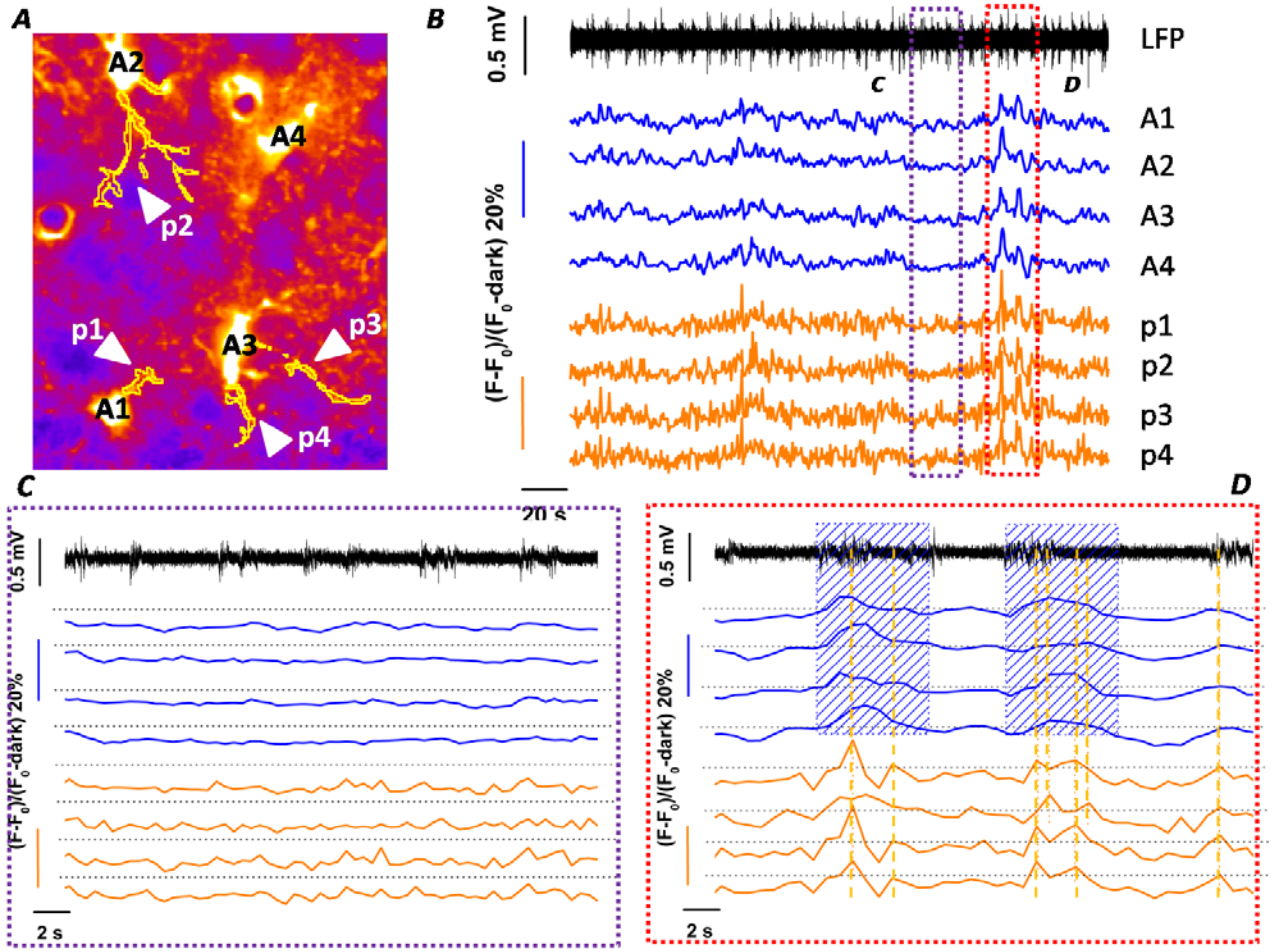

Figure 3.46: Intense astrocyte activity during micro-ictal events. A) Same field as in Figure 3.45. B) Astrocyte ΔF/F oscillates frequently under micro-ictal events. Transients are rounder and slower than neurons and neuroplie, yet the overall behavior are pretty much the same. Coincidence between Calcium oscillations and LFP events is maximum during microictal events although short epochs of LFP activity is not mirrored in ΔF/F tracks . 4 processes ΔF/F are also reported here. An intese activity resemble that of neurons with spiked transients and frequent oscillations. Processes appear to be in frame with astrocyte somata. C) Magnification of a period of ΔF/F silence boxed in B. astrocytes somata ΔF/F are completely flat, not even some subthreshole oscillations are to be observed. Precesses ΔF/F are also almost flat with some flickering oscillation. D) Magnification of a period of intense ΔF/F activity boxed in B. Two micro-ictal events are highlighted in blue shades, vertical orange dotted lines serve as temporal reference fot ΔF/F peaks and LFP. Astrocyte somata and processes show transients for each LFP event. ΔF/F. Multiple spikes overlaps between processes of different astrocytes and falls in time in different phase with respect to LFP events or somata ΔF/F oscillations. Difference alignment suggests a genuine astrocyte Calcium activity with little or none ROI contamination from neural or neuropil fluorescence.

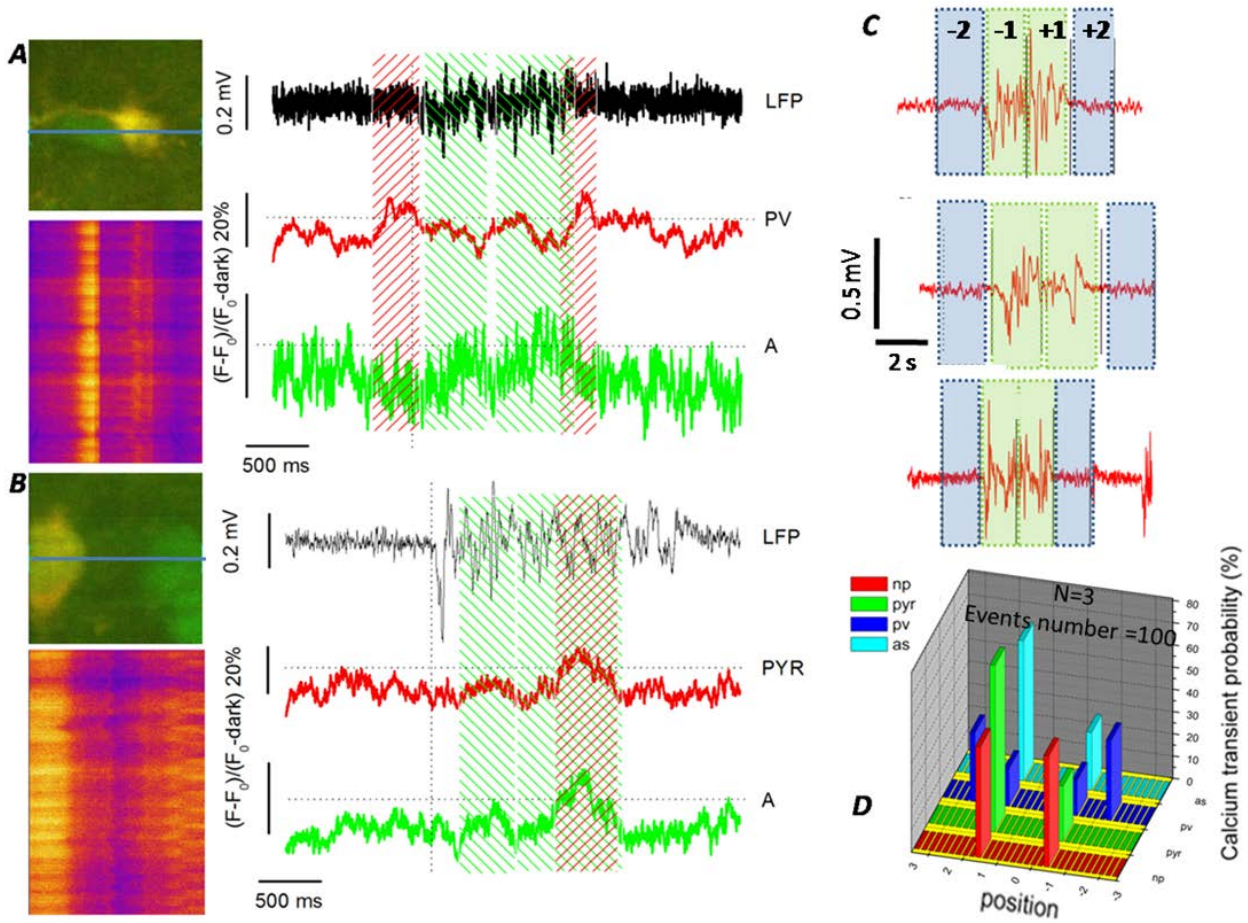

c

Figure 3.47: High speed line-scan of micro-ictal activity unmasks peculiar PV behavior. A) line scan reference frame showing a GFP+ PV neuron and an astrocyte. Below is the ΔF/F from the blue line across cells in the field. On the right black LFP track is compared with ΔF/F for PV (red) neuron and astrocyte (green). Green shades highlights two peaks in astrocyte fluorescence the first starting at micro-ictal onset, the second peaking at the termination of LFP event. Red shades underscores PV+ neurons ΔF/F behavior. Two sharp peaks flak LFP event. Secondary oscillations remains underthreshold inside micro-ictal LFP event. Flanking ΔF/F peaks starts and terminates just outside LFP transient. B) reference frame for a linescan (ΔF/F below) performed on GFP- neuron (putative pyramidal one) and astrocyte. On the right is displayed ΔF/F behavior below a LFP (black) microictal event. Onset of microictal event is marked by a vertical dotter black line. ΔF/F in putative pyramidal neuron (red) show a principal peak aligned toward the termination of micro-ictal event (red shade) and a couple of shallow ones (green shade) during the first part of LFP event. Astrocyte ΔF/F here behave just the same as pyramidal neuron, mirroring each peak although with slightly different kinetics. C) three representative micro-ictal events are shown. Usually a central symmetry is present. The whole duration is divided in two halves (green shades): -1, +1. Two other regions, each encompassing the same duration as a single green box, are defined as -2 and +2 (blue shades), these highlight LFP regions respectively one half of micro-ictal duration in advance and one half following. Green windows are defined as “inside microictal event” while blue ones are “outside microictal events”. Time windows are set in order to segregate ΔF/F oscillation in time for different ROI classes. A third region can be identified as neither blue nor green comprising LFP activity (region +3 and -3 in D). D) Histogram represents the probability with which a ΔF/F transient is observed in region -3, -2, -1, +1, +2, +3 for neuropile, GFP+/GFP- neurons and astrocytes. No ΔF/F are ever observed in regions +3 or -3. Neuropile (red) show an

equal chance to exhibit ΔF/F in region +1 or -1. Disproportional are, on the other hand, GFP- neurons and astrocytes preferring a ΔF/F peak in region -1 (green and cyan respectively). PV neurons show a preference for regions -2 and +2 instead. Being flanking regions, these are outside the LFP event.

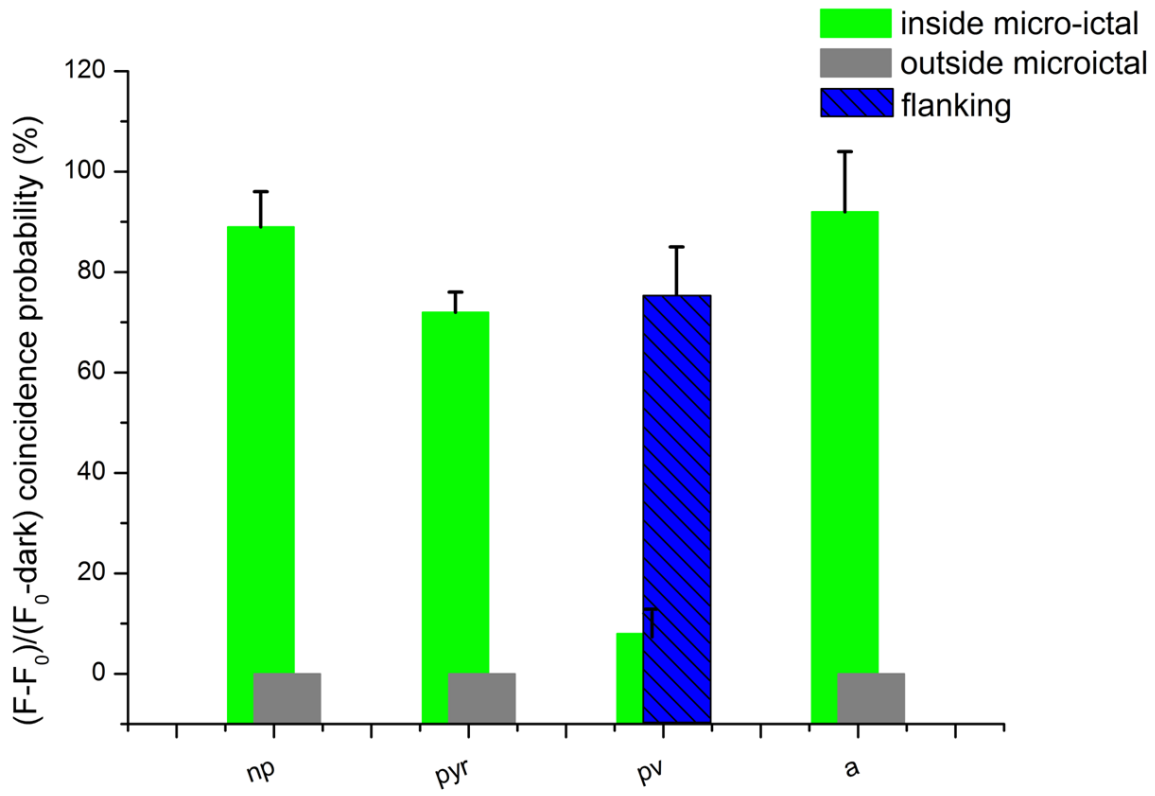

Figure 3.48: Microictal coincidence probability. Coincidence was estimated rejecting as "outsie microictall", every Calcium transient starting before the onset of an LFP event or after its termination (± 0.3 s confidence window). Green bars represent the chanche of coincidence between ΔF/F and LFP expressed as % of total LFP events (200 microictal events, 80 Pyramidal neurons, 10 astrocytes ,21 PV+, in atotal of 3 trials in 3 animals). Neuropile present an almost 100% probability of coincidence with 0 events falling outside microictals. Same is observed for pyramidal neurons although with slightly reduced coincidence. PV+ neurons show an inverted relation compared with the other cases. As depictad in Figure 3.47, PV ΔF/F falls in flanking regions beside each LFP. Coincidence for PV+ neurons is thus indicated in blue here. Low chance exist for PV+ neurons to exhibit a ΔF/F transient inside a microictal event. Astrocytes show a massive increase in coincidence probability exceeding PYR and going up to NP levels. Microictal events seem to be the best activator of astrocytes coincident Calcium events so far characterized.

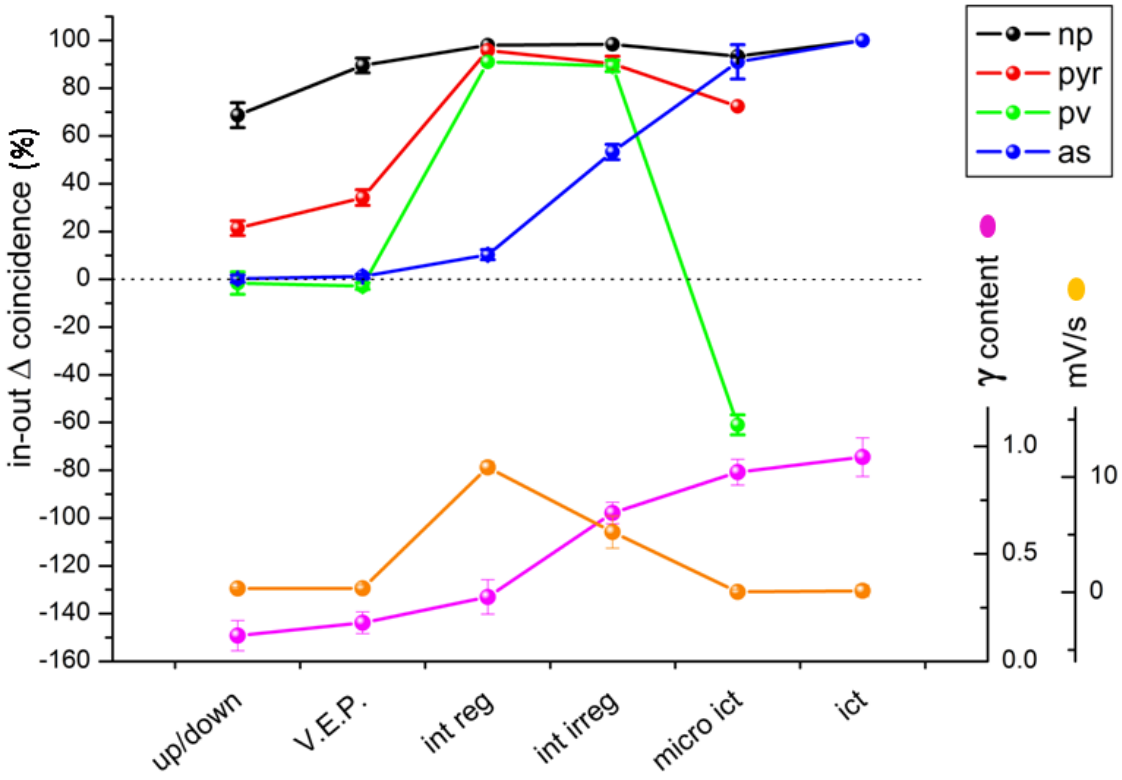

Figure 3.49: *Gamma power increase correlates with astrocyte activation. The plot summarizes coincidence probability of ΔF/F oscillations with LFP events, in different ROI classes and in different experimental conditions expressed as difference between "in" and "out" probability. Points above 0 (left Y axis) indicates a skewed propensity toward "in" coincidence since difference in probability equals to 0 is considered symmetric between "in" and "out". Black, red, blue and green lines refere to: neuropile, pyramidal neurons, astrocytes and PV+ neurons, respectively. Magenta dots indicates the gamma power contribution in different conditions. Differences are calculated from data presented above in the text. Gamma contribution was evaluated dividing 30-40 Hz STFT band powers by 10-20 Hz ones in different conditions. Each STFT was calculated using fixed parameters and average ratios is compared here. 3 representative STFT for each condition was chosen and 30'' STFT were produced from each LFP conditions, the average and s.d. is the plotted. Oange slope is calculated as the ratio between LFP amplitude and duration in seconds of evenst in each 30''field tracks chosen. Since greater amplitudes and shorter durations are interpreted as more synchronized events, orange slope is calculated in the attempt to evaluate changes in network coherence. Increase in orange track amplitude shall then be interpreted as increase in synchrony. Neuropile behave approximatively the same across all conditions, with an horizontal profile fixed on high coincidence level. No correlation appears with either synchronization degree or gamma content for neuropile. Pyramidal neurons and PV presents similar shapes with low coincidence for low synchronization degrees. PV profile is also exaggerated during micro-ictal events compared with principal cells. Astrocytes alone show a steady increase in coincidence with gamma content rises, with no apparent correlation with synchronization degree. Unfortunately, no data are avaible for neurons in ictal condition.*

Chapter4/Conclusions:

Results presented in this work are arranged on a chronological progression. We started describing Calcium dynamics in neurons and astrocytes in a convenient model of epileptiform activity where we succeeded in refining skills and begun to lay the foundations for a better understanding of the physiological role of astrocytes in shaping neural synchrony. Unfortunately the isolated guinea pig brain suffers from several limitations in this perspective. First of all homeostatic control of temperature, nutrients, extracellular fluids are inevitably altered limiting our intervention to a couple of hours in this preparation. Blood brain barrier and vasogenic responses are instead maintained (Librizzi et al., 2001, Gomez-Gonzalo et al., 2011) reducing the contribution of neuro inflammation and BBB breeching to Calcium oscillations in astrocytes. On the other hand, the extracorporeal circulation, where blood is replaced with hyperosmotic solution (in order to reduce brain edema) reduces astrocyte Potassium buffering capability interfering with neural activity and seizure generation itself (in a yet poorly characterized way, Breschi et al., 2013). Furthermore, 2 mM BMI perfusion triggers a generalized reduction in inhibitory tone with an estimated 20% of GABAa channels efficiently antagonized (de Curtis et al., 1996), which results in the generation of hippocampal-enthorhinal spontaneous seizures. The focus of ictal activity is questionable, with evidences favoring hippocampus or mEC or subicular areas (Jefferys et al., 2012). Calcium behavior in neurons and astrocytes in ictal focus or in regions where seizures propagate displays different dynamics and is associated with different physiological meanings (Trevelyan et al., 2006;2007; Trevelyan and Schevon, 2013). Nevertheless Calcium oscillations and LFP manifestations were utterly replicated at each seizure indicating a single mechanism of induction. Further drawback was the optical hindrance of myelinated structures around 300 μm deep in mEC, compromising signal quality from deeper regions, neuron somata were indeed seldom imaged. The interictal activity phase is also poorly represented in the isolated BMI-perfused brain which, on top of that, is considerably inactive in baseline periods and obviously, cannot be fed with sensorial inputs. Optical recordings *in vivo* of hippacampal region require invasive techniques (Levene et al., 2004; Jung et al., 2004; Dombeck et al 2010) altering cortical and BBB integrity, or three-photon imaging (Horton et al., 2013) unavailable in our set-up. Lack of transgenic *Cavia porcellum* models (and so far not described viral based transduction protocols in these animals) also prevented implementation of conditional expression of fluorescent tags or indicators. The isolated guinea pig brain preparation instead offered a reliable model of acute cortical ictal activity unavailable, to our knowledge, by other means. Several mouse chronic models of ictogenesis with recurrent seizures are notoriously available but issues related to glyosis, inflammation, rewiring, plasticity, neurotoxicity and impaired homeostasis discouraged us from taking into account such approaches, moreover, few manifest cortical phenomena accessible with the techniques in our disposal. Slice preparations suffer from similar limitations including the loss of circuitry integrity and disruption of blood-brain barrier. LFP ictal activity in the guinea pig brain is associated with a marked increase in gamma broad band (30-100 Hz) spectral power recorded from 250 μm deep in mEC. Gamma activity have been often associated with local cortical processing (Headley and Paré, 2013; Woźniak-Kwaśniewska et al., 2013; Igarashi et al., 2013; Roux et al., 2013) and fast spiking interneuron activation (Volman et al., 2011; Ahmed and Mehts, 2012; Pernía-Andrade and Jonas, 2013; McNally et al., 2013) together with gamma frequency entrinment (Lakatos et al., 2008; Schroeder and Lakatos, 2009; Scheffzük et al., 2011). These phenomena are all related with a peculiar increase in network coherence which could be read or could be primed by astrocytes. Calcium imaging in astrocytes revealed a massive (100% of astrocytes imaged) recruitment peaking shortly after ictal start (20 ± 5s in 20 seizures from 6 animals) when LFP is about to turn into after

discharge mode. Calcium elevation in astrocytes starts rising precisely at ictal start with a slow phase accelerating in a second peak aligned with ictal termination. All astrocytes observed are in phase in each ictal event. Neural Calcium starts rising together with astrocytes but reaches a first peak faster. A second peak in neurons is observed aligned with that in astrocytes at the termination of high frequency LFP phase. Comparing these dynamics with focal acute model in 0 Magnesium and double NMDA pulse (Gomez-Gonzalo et al., 2010) mEC appear to behave as an ictal focal region. A twin peak is described when ictal phase is started with NMDA pulse; here Calcium in neurons rises faster than in astrocytes and the second peak marks the termination of high frequency phase. If mEC was instead a region where seizure propagates different Calcium behavior would be expected: a single peak in neurons and astrocytes delayed by a transition period from ictal start (see figure 1.12). Since activation of somatic Calcium elevation in astrocytes was demonstrated to elicit pyramidal neuron SICs (Kang et al., 2005; Tian et al., 2005; Fellin et al., 2006) in a synchronized fashion (Fellin et al., 2004), such a large increase in Calcium during ictal, shall be responsible for a widespread astrocyte-to-neuron signaling. Large somatic Calcium elevations are believed to readily propagate into processes in a coordinated somatofugal trajectory, eventually filtering into adjacent cells at rest through CX43 or regenerating through an ADP paracrine mechanism (Bowser and Khakh, 2007; Zhang et al., 2007; Koizumi et al., 2010). Calcium elevation is processes shall be then responsible for gliosecretion. Sustained increase in process Calcium could also be the cause of transient NCX inversion (Rose and Kraus, 2013) leading to reversion of GAT-1,2 GABA transporters. Local increase in extracellular GABA due to impaired uptake through GAT transporters could also be responsible for a short lived tonic inhibition. E_{GAT} and E_{NCX} are indeed close to E_{Na} in astrocytes, thus hundredfold Calcium elevation transients might kick NCX and GAT into the reversal mode (Verkhratsky et al., 2013). On the other hand, glutamate clearance from synaptic space shall be operative during ictal until saturation E_{EAAT} being far more depolarized. Since neural firing appears sustained during ictal, large amounts of Glutamate would then be co-transported together with Sodium in astrocyte processes, contributing to GAT inversion. Co-localization of EAAT, NCX and GAT is reported in regions in close proximity with synapses (Blaustein et al., 2002; Minelli et al., 2007; Medina-Ceja et al., 2012) where incoming neuronal activity would have stronger effects on astrocytes local modulation. Both glutamatergic and GABA-ergic synchronized astrocyte output could help reverting ictal phase into a sparser and milder one, contributing to the termination of seizure. Given the fact that inhibition is often observed to break down at ictal onset in several models (Cossart et al., 2005; Lillis et al., 2012) GAT reversion could help restoring transiently excitation/inhibition balance while glutamatergic input might help re-synchronize neural pool bursting erratically during ictal phase. Principal targets of astrocyte GABA and Glutamate shall be also extrasynaptic ones where possibly GABA shunting effects might be shallower. During ictal activity, Magnesium and voltage NMDA blocks are relieved (Clasadonte et al., 2013) and an additional glutamatergic input from astrocytes might lead to a further increase in intracellular Calcium. This might be sufficient for triggering Calcium dependent Potassium currents which, combined with GABA, could serve as an hyperpolarizing restrain inducing synchrony and reducing firing rates (Wu et al., 2004). A Phase resetting event is actually observed together with the astrocyte Calcium peak: cross correlation of neural Calcium activity with LFP diminishes at this point while different cells or neuropile regions start displaying transients scattered one another. Peak in cross-correlation between astrocyte Calcium and LFP is observed at ictal start faster than for neurons or neuropile *i.e.* astrocytes Calcium behavior might suddenly change before all network is trapped in seizure. Yet Calcium peak in astrocytes is delayed with respect to that of neurons already firing at high frequency. This could indicate that astrocytes senses the transition in network activity but lags behind fast seizure development. If astrocyte Calcium increase leads toward ictal termination in a causative fashion, then triggering a faster Calcium increase in astrocytes would shorten ictal duration. Unfortunately the isolated BMI perfused guinea pig brain generates spontaneous seizures of short duration and prediction of next event is implausible. A tentative approach

was made with no results due to experimental constrains and we never managed to trigger Calcium elevation in time during ictal activity. Nonetheless TFLLR pulses were tested during baseline phases (lacking a more stringent technique such as intracellular Calcium uncaging). To our surprise, delivering TFLLR on a dishinibited mEC during interictal phases with low chance of spontaneous ictal events is enough to start seizures. Triggered events are shorter in duration (12.5 ± 5s in 7 trials on 3 animals) than spontaneous ones, yet LFP spectral signatures are indistinguishable. Calcium starts rising slowly in astrocytes following TFLLR pulse until a nonlinear acceleration is observed leading to a fast peak. Astrocytes appear de-synchronized during the slow onset with cells most proximal to injection pipette leading. Estimating diffusion front progression in time with SR 101 (M.W. similar to TFLLR) reveal a faster Calcium propagation in cells progressively more distant from the leading one. Recruitment of astrocytes appear radial regardless the anisotropic diffusion of the solution and magnitude of fluorescence increment result comparable across different cells (a "dilution" of Calcium front from proximal to distal cells is not observed). TFLLR thus might start a paracrine regenerative Calcium wave presenting propagation speed comparable with a ADP mediated mechanism (18.7 ±1.6μm/s compared with reported 15-20 μm/s, Haas et al. 2006). Calcium peaks synchronously for all responsive astrocytes as expected in case of a paracrine signaling involving increasing number of cells which in turn respond e reverberate the signal back and forth. A neuron to astrocyte feedback is also to be taken into account helping describing this synchronization. Although neuropile Calcium remains flat in this epoch, signs of increased neural activity are already building up as deducible from LFP. In about 10s from leading cell first Calcium rise, all responsive astrocytes display the peak. Since TFLLR administration, LFP shows augmented high frequency content associated with termination of interictal events but without ictal activity. At the peak of astrocyte Calcium elevation, LFP abruptly turns into ictal phase. Here, neuropile regions show a perfectly aligned Calcium peak. Calcium in neuropile decreases monotonically until ictal termination and oscillates into an afterdischarge pattern henceforth. Astrocytes show a plateau-like Calcium progression with an accessory small peak at ictal termination than fluorescence fades away into baseline silence while LFP is bursting ADs. The synchronization of neuropile Calcium with astrocyte peak reminds of the behavior observed in "Field B" receiving ictal activity from distal foci (Gomez-Gonzalo et al., 2010). Ictal threshold might thus be crossed away from imaged fields, most likely due to both ever greater astrocyte recruitment and concomitant increased neural activity. If this was the case we expected LFP signature of ictal activity to precede astrocyte Calcium peak instead. In our opinion the observed dynamic is indicative of the different ease with which neural and astrocyte activity contribute to ictal threshold crossing. When neurons are stimulated (NMDA pulses), astrocytes follow and reinforce in focal fields while receiving fields are bombarded with excitation and restrained by inhibition. As inhibition fades in fields B, a sudden increase in Calcium is observed in both astrocytes and neurons, a permissive event for seizure propagation. Here Calcium is slowly increased in astrocytes which need a time longer than NMDA to build up excitation in neurons. The peculiar feature in this experiment was the observation of neural phase resetting as a consequence of astrocyte activation. If astrocytes help ictal termination in response to increased firing rates, why should astrocyte activation trigger increased firing rates and de-synchronization in neural network? We speculated that astrocyte calcium increase ends always in the same output (gliosecretion and possibly inversion of Sodium-dependent transporters), producing different effects on neurons according to the state in which they reside. As depicted in figure 1.7, pro-epileptic networks could be represented as governed by two attractors: one forcing into seizure events the other collapsing into baseline activity. In dishinibited tissues, trajectories around these attractors become broader and even a relatively weak kick in a direction or in the other might well be enough to switch orbits.

As observed in TFLLR experiments, a first Calcium increase in astrocytes would be a driving force for phase resetting around seizure attractor while the accessory one at ictal termination could restore baseline orbits through ADs transition. In spontaneous ictal events, astrocytes sense the transition operated in neurons first and react on the network already entrained by seizure attractor. What is the signal astrocytes read as the telltale token for phase transition is not clear but the increment in gamma band content could be a candidate as discussed later. Epileptiform activity is not always populated with gamma activity; interictal phase is indeed a particularly poor one. Calcium activity in astrocytes during interictal events and inbetween consecutive ones is flat. Moving to the mouse model, we first described up-down state network behavior in order to explore astrocyte Calcium oscillations in a physiological low firing rate regimen. Here several limitation encountered in the guinea pig brain were easily compensated. In the face of silent LFP and Calcium signals from the baseline guinea pig, sleeping mouse cortex results particularly active. Up-down states are characterized by a spectral content rich in slow wave bands with little gamma contribution. Frequent low voltage incoherent LFP events correlate with scattered neural Calcium spikes. In this context astrocytes remain pretty inactive showing occasional Calcium transients with equal chance during up-states as well as during flat LFP periods. Overall the frequency of calcium oscillations in slow wave activity result higher for pyramidal cells and PV+ interneurons (smaller for the latter) compared with that of astrocytes. Calcium behavior in astrocyte processes appear much more active with fast sparkles appearing with chance similar to that of pyramidal cells. Although a good signal from processes was seldom available, spontaneous activity seems to be associated with low coherence in this district, with processes from the same astrocyte exhibiting calcium transients unrelated with “sister” ones and with no apparent relation to neural nor neuropile oscillations (consistent with what described in slice preparation in the context of spontaneous hippocampal activity, although with a lower spatial resolution Di Castro et al., 2011). Nevertheless when a somatic Calcium transient was observed, all processes emanating from that cell displayed Calcium oscillation in-synch. Cross correlation analysis confirm a low degree of coherence among neural Calcium oscillations and LFP, in this context, frequency of astrocyte Calcium transients and their correlation with electrical activity is the lowest across paradigms investigated here. Visual stimulation is classically described being sufficient in eliciting V1 intense Calcium oscillations correlated with increment in gamma band LFP power (Bonin et al., 2011; Li et al., 2012; Brunet et al., 2013; Betti et al., 2013; Matsuzaki et al., 2013). We tested different luminance contrast full field stimuli and chose parameters starting the highest LFP narrow band (30-50 Hz) gamma peak to be administered during imaging sessions. Stimuli presented no patterns and as expected together with V.E.P.s we observed substantial increase in the frequency and coincidence of neuronal Calcium oscillation. Surprisingly Pv+ neurons did not show any increment in Calcium transients frequency compared with baseline spontaneous activity nor did astrocytes in the face of a nearly doubled pyramidal and neuropile activity. Astrocyte processes, when correctly imaged, show instead a significant increase in Calcium activity consistent with visual stimuli presentation. Again each process available in the imaged field emanating from a same cell displaying stimulus-aligned Calcium oscillation in the soma, also presented Calcium transients. We then decided to explore hypersynchronous interictal activity in the anesthetized mouse. Hypersyncronization of neural activity would be expected to represent a strong signal for astrocytes believed to sniff and integrate neural output on vast spatial domains. Moreover, PDS manifestation in LFP, associated with interictal spikes were described to be mediated by astrocyte glutamatergic transmission in hippocampal slices (Kang et al., 2005). BMI intraparenchimal injection or superfusion equally started a sustained interictal activity. Scaling BMI concentrations, we observed a drastic alteration of spontaneous activity with the obliteration of up-down states oscillations at 0.15 mM. Frequency and amplitude of interictal events from sporadic and shallow, grow with increasing BMI concentration eventually stabilizing with 2 mV deflections presenting at 0.3 Hz for concentrations ≥ 1 mM. We proceeded with BMI 2 mM which was the same used in the isolated guinea pig brain. High as well as

lower doses of BMI never evolved into high frequency activity, not a single seizure-like event was ever observed in mouse V1. We never recorded from mEC in the mouse nor we did from V1 in the guinea pig, we cannot thus exclude a role of different connectivity between these regions as a possible explanation for this gross difference. Also the effect of anesthesia, oxygenation, pH or temperature could be taken into account, being necessarily strictly controlled in the isolated brain and obviously more variable *in vivo*. Being the control over these parameters loose, we expected a certain variability on the LFP pattern started by BMI administration which was never the case. Gamma content during interictal activity appears to be greater than that promoted by visual stimulation. Evaluation of gamma power was performed away from interictal LFP spikes the impulsive nature of which artefactually contaminates spectral analysis over a wide range of frequencies. High frequency-low power activity is actually detected after each interictal event fading away into a completely flat track. These intermittent gamma flickers are enough to increase normalized power spectra in 30-50 Hz band when compared with baseline or VEP activity. What already observed in the guinea pig isolated brain was confirmed in V1: astrocytes remain almost silent during hypersynchronous neural activity. Less than 20% of interictal LFP spikes presented coincident astrocyte Calcium fluctuations while no transients at all are observed between interictal events. Similar statistics emerge for VEPs and up-down states with a considerable increase in non-coincident Calcium transients. Overall, interictal activity is associated with nearly 100% coincidence for neuropile, pyramidal and PV+ neurons and no de-synchronized Calcium events, while astrocytes increase coincidence probability compared with VEPs and spontaneous activity, reducing total Calcium transients frequency. Each neuron displayed a single intense Calcium spike aligned with each peak in LFP interictal event although cross correlation analysis show some jittering with epochs of higher and lower coherence (the same is observed for astrocyte processes). Different cells behave similarly: either synchronization is high for the whole field or it is overall reduced. Interictal events are associated with a precocious increase in Calcium in pyramidal somata quickly followed by a faster one in PV+ neurons, as revealed by line scan acquisitions. A phase lock relation is observed between Calcium rise in pyramids and PV+ interneurons conserved across interictal events and in different animals (PV+ onset delayed by10 ±2ms, PV+ time to peak anticipated by 40 ±6ms compared with principal cells). In experiments protracted more than 2h sporadic “atypical” interictal events are detected. These were spotted because of more frequent astrocyte Calcium oscillations. LFP of these events present the hallmarks of diminished synchronization: lower amplitude and longer duration. FFT analysis on the tail border of these events, showed a substantial increase in gamma content compared with matched regions flanking “normal” hypersynchronous events. Neurons display no significant alteration in Calcium transients probability in coincidence of these events while astrocytes show a nearly threefold increment. Out of “atypical” interictal spikes Calcium oscillations probability drops to 0 for neurons and astrocytes as observed for “regular” ones. The shape of Calcium oscillations in astrocytes coincident with these events also is “atypical” with multiple peaks while single ones are always observed for “regular” interictals. Clusters of “atypical” events present with low frequency interspersed with regular ones. Only seldom the animal is allowed to survive more than 6h time at which both regular and atypical interictal events are sometimes replaced by normal spontaneous activity after a phase of diminished interictal frequency. In the attempt to increase excitatory tone in order to plausibly precipitate a seizure event, we combined visual stimulation during sustained interictal activity. To our surprise we were only able to trigger additional interictal events indistinguishable from spontaneous ones. Visual stimulation triggers a stereotyped interictal event given that no spontaneous one precedes ≤ 0.8s stimulus onset. Hypersynchronous network response is faithful to visual stimulation, nearly 100% of flashes distant ≥ 0.8s from a spontaneous interictal event trigger an evoked interictal. The next spontaneous

event falls in average after 2.8s preserving the intrinsic frequency of interictal events generation. No spectral differences are observed between spontaneous and evoked interictal events and neurons and astrocytes behave just the same in both conditions. From the mouse point of view, these hypersynchronous events might correspond to a relevant visual stimulation either spontaneous or triggered: the dishinibited visual cortex is no longer able to discriminate between light and darkness and generates delusional responses. Moreover when a "fake" input is generated (a spontaneous interictal event), no hypersynchronous events are allowed within 0.8s. The animal is either blinded by self generated "light" or falls into darkness rhythmically for periods of 0.8s. Interictal manifestations are common in different neurological conditions (Mickleborough et al., 2013; Malinowska et al., 2013; Enagstrom et al., 2013) and a pervasive feature in several types of epilepsies. The time a brain spends in interictal activity might well be much longer than seizures occurrence and some authors propose a much more detrimental role for recursive interictal events compare with sporadic seizures. Ictogenesis might be assisted by interictal activity, while others envisage a protective role (Avoli et al., 2013). This biphasic behavior of V1 reminds of anharmonic oscillators, building up energy and releasing it altogether in stereotyped cycles. During the accrual phase it is possible in these systems, to ectopically discharge the very same amount of energy (think about the dripping faucet) feeding an appropriate energy input. This would be analog to the visual stimulation during interictal activity. Interestingly, in the anharmonic oscillator as well as in the dishinibited cortex, a refractory period exists, during which inputs of arbitrarily large amount of energy are inefficient to discharge the system. But stereotyped hypersynchronous events do not appear all of a sudden in the LFP after BMI administration, a period of "interictal onset" marks the transition from spontaneous activity to interictal phase. During this epoch, neurons fire with increased rate although showing poor synchronization with LFP. Electrophysiological recordings display fast depolarized transients the duration of which decreases in time while the amplitude increases as the first clear interictal event appears. With the presentation of the first interictal events synchronization of neural Calcium oscillation reaches the top and Calcium transients assume the typical single peaked shape. LFP FFT analysis show a strong increase in gamma band power during this phase and astrocytes display a sustained Calcium activity. Frequent oscillations are associated with most of the LFP transients superimposed to secondary slow Calcium events of tens of seconds in duration. As the first interictal event manifests, Calcium in astrocytes falls back to inteictal behavior. Being the onset phase so volatile (less than 2 minutes), only few decent (3) experiments are so far collected. Most intriguing is the reversal of Calcium profile between neurons and astrocytes: scattered neural transients at high frequency correlate with intense astrocyte activity, never observed elsewhere in the mouse and reminiscent of ictal one. Note that in correspondence with highest Calcium peak in astrocyte, neural phase is re-setted into a synchronous one. This onset phase could be interpreted as a stretched ictal phase, with lower firing rates and extended duration, eventually triggering astrocyte recruitment. Possibly connectivity in V1 is not suitable for ictal generation as observed in mEC and an abortive ictal phase is transmutated into hypersynchronous one when astrocytes are activated. The longer duration of this high frequency epoch if compared with typical ictal ones, might represent the slow recruitment of astrocyte. Probably buffering calcium in astrocytes during this phase (photouncaging Calcium chelators in astrocytes) could results in a prologation of high frequency activity possibly developing into a seizure event. On the other hand, triggering Calcium elevation at will (photouncaging Calcium) in astrocytes during onset, might result in the anticipation of phase-reset and the appearance of interictal steady state. In this perspective, V1 atrractors of neural behavior shall be either baseline spontaneous activity, modulated by sensory inputs or hypersynchronous events in case of dishinibition. Border trajectories crosses a region of high frequency activity (the onset phase) which is sensed by astrocytes kicking the network toward synchronization as in the case of seizures. This time the hypersynchronous attractor would be so strong that the network would be trapped around it while astrocytes remain insensitive. Evidences although weak in this perspective are

the observations of spontaneous interictal events in the absence of dishinibition at least in human EEG (). Such a strong attractor would keep network behavior away from seizure generation at the cost of impaired cortical processing (interictal activity is associated with both reduced cognition development and acute impairment of lower and higher cognitive functions, Van Bogaert et al., 2012; Kleen et al., 2013). If this is proved true, interictal events might have a “protective” role against ictal generation and the fact that interictal events are poorly represented in models such as the guinea pig isolated/BMI perfused brain or in the hippocampal slice 0 Magnesium preparation, won’t be surprising at all. Local circuitry or molecular cues might be the basis for this difference. Hypesynchronous events are associated with massive increase in intracellular Calcium in neurons. Although intense these Calcium peaks are intermittent and between consecutive events several seconds elapse, leaving time to the cell for Calcium renormalization. Large Calcium oscillations might originate from the synchronization of firing in the network: at each interictal event every single neuron fire a short train of APs propagating and reverberating across all synaptic space, leading to massive EPSPs. Whole cell recordings confirm the presence of NMDA currents and vast Calcium conductances (probably via voltage gated calcium channels) during PDS (de Curtis et al., 1999). A chronic Calcium increment could lead to several cellular alteration ranging from cell death to subtle alterations of firing rates and plasticity (Alberi et al., 2013; Berridge, 2013; Bukalo et al., 2013; Mattews et al., 2013), yet interictal events are short lived and unlikely to be sufficient to alter Calcium homeostasis or induce functional plasticity. To evaluate Calcium levels in neurons during interictal phase, we measured fluorescence intensity between consecutive interictal spikes in flat epochs of LFP, avoiding the huge increment generated by PDS and compared it with periods of down states acquired in baseline. We assumed $[OGB]_i$ constant and kept laser power fixed imaging same neurons in baseline and during interictal activity. Also imaging sampling rate, PMT gain and imaging sessions duration was controlled and kept fixed in both conditions. OGB does not allow for a ratiometric measurement but relative increments would be a sign of actual $[Ca^{2+}]_i$ alterations. We found that “basal” Calcium between consecutive interictal events is threefold increased in neurons and neuropile compared with spontaneous activity epochs. Astrocytes instead present no significative increment in basal Calcium-dependent fluorescence (an indirect confirmation that other parameters affecting fluorescence intensity could be reasonably considered bypassed). Assuming a resting intracellular calcium concentration around 60 nM (Maravall et al., 2000) a threefold increment would set it in the hippocalcin regimen: 100-150 nM (Burgoyne et al., 2007). These levels are constant between consecutive interictal events pooled randomly during interictal phase and a threefold increment is observed in 3 mice. During LFP spike Calcium increase rises above tenfold the basal interevents value. Thus a biphasic oscillation in Calcium levels is present during interictal phase: a ceiling level of around 600 nM at the peak of interictal spike and a resting level around 180 nM. EC 50 for sIAHP channels is estimated to be around 300 nM (Andrande et al., 2007) thus each LFP spike shall be associated with a Calcium increase large enough to trigger Calcium activated Potassium currents. Three different currents are characterized: a fast one, an intermediate one and a slow one (Kim and McCormic, 1998; Lappin et al., 2005; Skov et al., 2009). Fast and intermediate ones are anthagonized by apamin and BMI and account for a short range hyperpolarization while the slow one (sIAHP) is BMI and apamin insentive and sustain a large, prolonged hyperpolarization for 0.6-1s. Ceiling Calcium increase in neurons might be the source for the slow hyperpolarization observed following each PDS associated with prolonged LFP silence. The duration of sIAHP is perfectly matched with the observed absolute refractory period or the “forbidden” phase of the cortical anharmonic oscillator. This current could set the lower limit of intrinsic periodism in interictal activity obliterating any response in 0.8s from an hypersynchronous event (Tzingounis et al., 2007).

Since every neuron seems to be synchronized at each interictal event and no Calcium oscillation are observed between events, another oscillator shall be responsible for the generation of spontaneous interictal phase. A Possibility could be that some neurons from the pool start oscillating over threshold and even a small noisy output could be enough to discharge the synchronized network. No signs of "out of pace" firing is although detected during interictal phase. Given the fact that the "natural" frequency of hypersynchronous events is around 0.3 Hz, thalamic CPG could be a suitable candidate. Up-down states also oscillate with similar frequency and the pace is imposed by thalamic intrinsic bursting neurons. resection of thalamo-cortical afferent fibers result in much slower cortical oscillation (Kandel and Buzsaki, 1997; Bonjean et al., 2011). Thus dishinibition builds up neural firing rate, astrocytes senses the transition and, somehow, reset the network toward an hypersyncronous firing, possibly via massive SICs and Calcium dependent GAT reversal. At this point sIAHP shall be activated by a first seed of hypersyncronicity as a consequence of massive Calcium entry and PDS. Long lasting hyperpolarization shall then further restrict the window of opportunity for AP generation contributing to synchronization. Thalamic input shall than be responsible for the generation of each interictal event, disseminating excitatory signals inside a synfire chain. The "basal" Calcium elevation observed between consecutive interictal events could be responsible for some drastic alteration in functional plasticity instead. If hippocalcin is activated constantly, LTD would be promoted (Isaac and Henley, 2005; Markova et al., 2008; Amici et al., 2009). This would produce dramatic effects on consolidation and possibly wiring during critical periods. At subcellular level, large EPSP inputs would compete with tonic LTD possibly resulting into alteration of spine motility and stabilization. If sIAHP contributes to neural synchronization, than blocking Calcium dependent potassium hyperpolarization shall result in a disruption of hypersynchronized events leading into high frequency neural firing, no longer restrained. Here neurons shall be constantly hyperexcited and maybe unleashed from thalamic drive. BMI and sIAHP blockade shall in fact result in an overall net increase in excitation with no absolute refractory periods. If astrocytes are sensitive to neural high frequency activity, Calcium shall then start oscillating in these cells unable to trigger a phase reset. UCL 2077 is potent selective antagonist of sIAHP (Shah et al., 2006). We tested the effect of UCL 2077 superfusion of V1 during steady interictal activity. In a matter of some 40 minutes, hypersynchronous LFP events start collapsing one closer to the next in bursts repeating rhythmically for few minutes. Eventually some interictal events falls within the absolute refractory period and the whole hypersynchronous activity is quickly lost in favour of an intermittent, low voltage long duration high frequency one. Until violation of absolute refractory period every LFP event under UCL 2077 is indistinguishable from those typical of interictal activity, also Calcium in neurons exhibits the same dynamic. Astrocytes remain silent so far. When refractory period falls apart, "micro ictal" events ensues, rich in gamma frequencies and lasting 3-4s attenuation of LFP amplitude and stretched durations are interpretable as loss of synchronization. Frequency of these events is close to that of interictal ones and of spontaneous oscillations of deep sleep: around 0.3 Hz. Calcium profile in neurons is completely changed compatred with interictal phase: shallower transients are coincident with LFP events in 60% of the cases in pyramidal neurons. PV+ cells display poor coincidence preferring flanking regions of LFP oscillation with good accuracy instead. Neuropile Calcium remains in phase as described for all the other contexts. Astrocytes show a dramatic increase of coincidence probability of Calcium transients with LFP events jumping up to values close of that of neuropile. Calcium oscillations in astrocytes start with a considerably constant delay from LFP start, peaking inside it and terminating often after "micro ictal" events. Neural Calcium oscillation instead peaks scattered inside the LFP event and most cells display multiple peaks. Astrocyte processes show peaked transients all in phase with the onset of somatic Calcium increase but are considerably shorter in duration. Having explored Calcium dynamics in several context of neural activity, we tentatively tried to find some feature correlating LFP "shape" with Calcium oscillation aiming to a plausible parameter defining a neuron-to-astrocyte transfer function. To allocate values to the "fidelity" of Calcium oscillation with

respect to LFP events, we calculated the difference in coincidence probability *i.e.* probability of a Calcium event coincident with LFP-probability of Calcium event falling outside LFP events, for all cell classes in all different network activity tested. Concerning LFP, we plotted gamma contents extracted from normalized FFTs of different events as the result of gamma narrow band (30-40 Hz) power divided by slow wave (10-20 Hz) power. This was intended in order to normalize for noise fluctuations, LFP pipette diameter variability and other poorly controllable parameters with the assumption that any broad band contamination in LFP will result in a broad frequency contamination of FFTs, hence the ratio "gamma over alpha" as an internal normalization. The average value of gamma content was plotted for all classes of LFP events (except for interictal onset of which too few replicas were available). We set the lowest value (up-down states) with the arbitrary value of 1 and reported relative increments for the other values. Average absolute amplitude over duration of each class of LFP events was also plotted as a measure of LFP synchronization. Amplitude of LFP is expected to increase with synchronization together with the reduction in duration, thus mV/s should be a monotonic function of synchronization in LFP. Ordering Coincidence probability difference in an increasing sequence for astrocyte we found that the LFP parameter that best correlate was, not surprisingly, gamma content. Obviously correlation does not imply causation….

5-Bibliography

- Abbott, N.J., and Pichon, Y. (1987). The glial blood-brain barrier of crustacea and cephalopods: a review. Journal de physiologie *82*, 304-313.
- Abeles, M. (1982). Role of the cortical neuron: integrator or coincidence detector? Israel journal of medical sciences *18*, 83-92.
- Abeles, M., Hayon, G., and Lehmann, D. (2004). Modeling compositionality by dynamic binding of synfire chains. Journal of computational neuroscience *17*, 179-201.
- Adelman, W.J., Jr., and Fitzhugh, R. (1975). Solutions of the Hodgkin-Huxley equations modified for potassium accumulation in a periaxonal space. Federation proceedings *34*, 1322-1329.
- Aguado, F., Espinosa-Parrilla, J.F., Carmona, M.A., and Soriano, E. (2002). Neuronal activity regulates correlated network properties of spontaneous calcium transients in astrocytes in situ. The Journal of neuroscience : the official journal of the Society for Neuroscience *22*, 9430-9444.
- Agulhon, C., Fiacco, T.A., and McCarthy, K.D. (2010). Hippocampal short- and long-term plasticity are not modulated by astrocyte Ca2+ signaling. Science *327*, 1250-1254.
- Agulhon, C., Petravicz, J., McMullen, A.B., Sweger, E.J., Minton, S.K., Taves, S.R., Casper, K.B., Fiacco, T.A., and McCarthy, K.D. (2008). What is the role of astrocyte calcium in neurophysiology? Neuron *59*, 932-946.
- Ahmed, O.J., and Mehta, M.R. (2012). Running speed alters the frequency of hippocampal gamma oscillations. The Journal of neuroscience : the official journal of the Society for Neuroscience *32*, 7373-7383.
- Akita, T., Fedorovich, S.V., and Okada, Y. (2011). Ca2+ nanodomain-mediated component of swelling-induced volume-sensitive outwardly rectifying anion current triggered by autocrine action of ATP in mouse astrocytes. Cellular physiology and biochemistry : international journal of experimental cellular physiology, biochemistry, and pharmacology *28*, 1181-1190.
- Alberi, L., Lintas, A., Kretz, R., Schwaller, B., and Villa, A.E. (2013). The calcium-binding protein parvalbumin modulates the firing 1 properties of the reticular thalamic nucleus bursting neurons. Journal of neurophysiology *109*, 2827-2841.
- Alger, B.E., and Nicoll, R.A. (1982). Feed-forward dendritic inhibition in rat hippocampal pyramidal cells studied in vitro. The Journal of physiology *328*, 105-123.
- Allman, J. M. (1999) Visual systems, organization. *Elsevier's Encyclopedia of Neuroscience* Elsevier, pp. 2141-2146.
- Allman, J., and Hasenstaub, A. (1999). Brains, maturation times, and parenting. Neurobiology of aging *20*, 447-454.
- Alvarez de Lorenzana, J.M., and Ward, L.M. (1987). On evolutionary systems. Behavioral science *32*, 19-33.
- Alvarez, V.A., and Sabatini, B.L. (2007). Anatomical and physiological plasticity of dendritic spines. Annual review of neuroscience *30*, 79-97.
- Amici, M., Doherty, A., Jo, J., Jane, D., Cho, K., Collingridge, G., and Dargan, S. (2009). Neuronal calcium sensors and synaptic plasticity. Biochemical Society transactions *37*, 1359-1363.
- Appaix, F., Girod, S., Boisseau, S., Romer, J., Vial, J.C., Albrieux, M., Maurin, M., Depaulis, A., Guillemain, I., and van der Sanden, B. (2012). Specific in vivo staining of astrocytes in the whole brain after intravenous injection of sulforhodamine dyes. PloS one *7*, e35169.
- Araque, A., Li, N., Doyle, R.T., and Haydon, P.G. (2000). SNARE protein-dependent glutamate release from astrocytes. The Journal of neuroscience : the official journal of the Society for Neuroscience *20*, 666-673.
- Araque, A., Sanzgiri, R.P., Parpura, V., and Haydon, P.G. (1998). Calcium elevation in astrocytes causes an NMDA receptor-dependent increase in the frequency of miniature synaptic currents in cultured hippocampal neurons. The Journal of neuroscience : the official journal of the Society for Neuroscience *18*, 6822-6829.
- Araya, R., Kudo, M., Kawano, M., Ishii, K., Hashikawa, T., Iwasato, T., Itohara, S., Terasaki, T., Oohira, A., Mishina, Y., *et al.* (2008). BMP signaling through BMPRIA in astrocytes is essential for proper cerebral angiogenesis and formation of the blood-brain-barrier. Molecular and cellular neurosciences *38*, 417-430.
- Aronica, E., Gorter, J.A., Ijlst-Keizers, H., Rozemuller, A.J., Yankaya, B., Leenstra, S., and Troost, D. (2003). Expression and functional role of mGluR3 and mGluR5 in human astrocytes and glioma cells: opposite regulation of glutamate transporter proteins. The European journal of neuroscience *17*, 2106-2118.
- Ashwood, T.J., Lancaster, B., and Wheal, H.V. (1986). Intracellular electrophysiology of CA1 pyramidal neurones in slices of the kainic acid lesioned hippocampus of the rat. Experimental brain research Experimentelle Hirnforschung Experimentation cerebrale *62*, 189-198.
- Avanzini, G. (2010). A sound conceptual framework for an epilepsy classification is still lacking. Epilepsia *51*, 720-722.

- Avoli, M., and de Curtis, M. (2011). GABAergic synchronization in the limbic system and its role in the generation of epileptiform activity. Progress in neurobiology *95*, 104-132.
- Avoli, M., and Williamson, A. (1996). Functional and pharmacological properties of human neocortical neurons maintained in vitro. Progress in neurobiology *48*, 519-554.
- Avoli, M., Panuccio, G., Herrington, R., D'Antuono, M., de Guzman, P., and Levesque, M. (2013). Two different interictal spike patterns anticipate ictal activity in vitro. Neurobiology of disease *52*, 168-176.
- Ayala, G.F., Dichter, M., Gumnit, R.J., Matsumoto, H., and Spencer, W.A. (1973). Genesis of epileptic interictal spikes. New knowledge of cortical feedback systems suggests a neurophysiological explanation of brief paroxysms. Brain research *52*, 1-17.
- Bak, P., and Paczuski, M. (1995). Complexity, contingency, and criticality. Proceedings of the National Academy of Sciences of the United States of America *92*, 6689-6696.
- Barclay, J.W., Morgan, A., and Burgoyne, R.D. (2005). Calcium-dependent regulation of exocytosis. Cell calcium *38*, 343-353.
- Barolet, A.W., and Morris, M.E. (1991). Changes in extracellular K+ evoked by GABA, THIP and baclofen in the guinea-pig hippocampal slice. Experimental brain research Experimentelle Hirnforschung Experimentation cerebrale *84*, 591-598.
- Barres, B.A. (2008). The mystery and magic of glia: a perspective on their roles in health and disease. Neuron *60*, 430-440.
- Bartho, P., Hirase, H., Monconduit, L., Zugaro, M., Harris, K.D., and Buzsaki, G. (2004). Characterization of neocortical principal cells and interneurons by network interactions and extracellular features. Journal of neurophysiology *92*, 600-608.
- Bear, D.M., and Fedio, P. (1977). Quantitative analysis of interictal behavior in temporal lobe epilepsy. Archives of neurology *34*, 454-467.
- Beggs, J.M., and Plenz, D. (2003). Neuronal avalanches in neocortical circuits. The Journal of neuroscience : the official journal of the Society for Neuroscience *23*, 11167-11177.
- Bekar, L.K., He, W., and Nedergaard, M. (2008). Locus coeruleus alpha-adrenergic-mediated activation of cortical astrocytes in vivo. Cerebral cortex *18*, 2789-2795.
- Bell, A.J., and Sejnowski, T.J. (1997). The "independent components" of natural scenes are edge filters. Vision research *37*, 3327-3338.
- Bell, W.L., Walczak, T.S., Shin, C., and Radtke, R.A. (1997). Painful generalised clonic and tonic-clonic seizures with retained consciousness. Journal of neurology, neurosurgery, and psychiatry *63*, 792-795.
- Ben-Ari, Y., Tremblay, E., and Ottersen, O.P. (1980). Injections of kainic acid into the amygdaloid complex of the rat: an electrographic, clinical and histological study in relation to the pathology of epilepsy. Neuroscience *5*, 515-528.
- Benediktsson, A.M., Schachtele, S.J., Green, S.H., and Dailey, M.E. (2005). Ballistic labeling and dynamic imaging of astrocytes in organotypic hippocampal slice cultures. Journal of neuroscience methods *141*, 41-53.
- Benfenati, V., Caprini, M., Dovizio, M., Mylonakou, M.N., Ferroni, S., Ottersen, O.P., and Amiry-Moghaddam, M. (2011). An aquaporin-4/transient receptor potential vanilloid 4 (AQP4/TRPV4) complex is essential for cell-volume control in astrocytes. Proceedings of the National Academy of Sciences of the United States of America *108*, 2563-2568.
- Berardi, N., Pizzorusso, T., and Maffei, L. (2004). Extracellular matrix and visual cortical plasticity: freeing the synapse. Neuron *44*, 905-908.
- Berridge, M.J. (2012). Calcium signalling remodelling and disease. Biochemical Society transactions *40*, 297-309.
- Berridge, M.J. (2013). Calcium regulation of neural rhythms, memory and Alzheimer's disease. The Journal of physiology.
- Berridge, M.J., and Irvine, R.F. (1989). Inositol phosphates and cell signalling. Nature *341*, 197-205.
- Berridge, M.J., Bootman, M.D., and Roderick, H.L. (2003). Calcium signalling: dynamics, homeostasis and remodelling. Nature reviews Molecular cell biology *4*, 517-529.
- Bertram, E.H., and Lothman, E.W. (1990). NMDA receptor antagonists and limbic status epilepticus: a comparison with standard anticonvulsants. Epilepsy research *5*, 177-184.
- Betti, V., Della Penna, S., de Pasquale, F., Mantini, D., Marzetti, L., Romani, G.L., and Corbetta, M. (2013). Natural scenes viewing alters the dynamics of functional connectivity in the human brain. Neuron *79*, 782-797.

- Bezprozvanny, I. (2005). The inositol 1,4,5-trisphosphate receptors. Cell calcium *38*, 261-272.
- Bezzi, P., Domercq, M., Vesce, S., and Volterra, A. (2001). Neuron-astrocyte cross-talk during synaptic transmission: physiological and neuropathological implications. Progress in brain research *132*, 255-265.
- Binder, D.K., Nagelhus, E.A., and Ottersen, O.P. (2012). Aquaporin-4 and epilepsy. Glia *60*, 1203-1214.
- Binder, D.K., Yao, X., Verkman, A.S., and Manley, G.T. (2006). Increased seizure duration in mice lacking aquaporin-4 water channels. Acta neurochirurgica Supplement *96*, 389-392.
- Binzegger, T., Douglas, R.J., and Martin, K.A. (2005). Axons in cat visual cortex are topologically self-similar. Cerebral cortex *15*, 152-165.
- Blaustein, M.P., Juhaszova, M., Golovina, V.A., Church, P.J., and Stanley, E.F. (2002). Na/Ca exchanger and PMCA localization in neurons and astrocytes: functional implications. Annals of the New York Academy of Sciences *976*, 356-366.
- Bock, D.D., Lee, W.C., Kerlin, A.M., Andermann, M.L., Hood, G., Wetzel, A.W., Yurgenson, S., Soucy, E.R., Kim, H.S., and Reid, R.C. (2011). Network anatomy and in vivo physiology of visual cortical neurons. Nature *471*, 177-182.
- Bockenhauer, D., Feather, S., Stanescu, H.C., Bandulik, S., Zdebik, A.A., Reichold, M., Tobin, J., Lieberer, E., Sterner, C., Landoure, G., *et al.* (2009). Epilepsy, ataxia, sensorineural deafness, tubulopathy, and KCNJ10 mutations. The New England journal of medicine *360*, 1960-1970.
- Bonanno, G., Raiteri, L., Milanese, M., Zappettini, S., Melloni, E., Pedrazzi, M., Passalacqua, M., Tacchetti, C., Usai, C., and Sparatore, B. (2007). The high-mobility group box 1 cytokine induces transporter-mediated release of glutamate from glial subcellular particles (gliosomes) prepared from in situ-matured astrocytes. International review of neurobiology *82*, 73-93.
- Bonfanti, L. (2006). PSA-NCAM in mammalian structural plasticity and neurogenesis. Progress in neurobiology *80*, 129-164.
- Bonin, V., Histed, M.H., Yurgenson, S., and Reid, R.C. (2011). Local diversity and fine-scale organization of receptive fields in mouse visual cortex. The Journal of neuroscience : the official journal of the Society for Neuroscience *31*, 18506-18521.
- Bonjean, M., Baker, T., Lemieux, M., Timofeev, I., Sejnowski, T., and Bazhenov, M. (2011). Corticothalamic feedback controls sleep spindle duration in vivo. The Journal of neuroscience : the official journal of the Society for Neuroscience *31*, 9124-9134.
- Bordey, A., and Sontheimer, H. (1998). Passive glial cells, fact or artifact? The Journal of membrane biology *166*, 213-222.
- Bordey, A., and Sontheimer, H. (2000). Ion channel expression by astrocytes in situ: comparison of different CNS regions. Glia *30*, 27-38.
- Borg-Graham, L.J., Monier, C., and Fregnac, Y. (1998). Visual input evokes transient and strong shunting inhibition in visual cortical neurons. Nature *393*, 369-373.
- Bortel, A., Levesque, M., Biagini, G., Gotman, J., and Avoli, M. (2010). Convulsive status epilepticus duration as determinant for epileptogenesis and interictal discharge generation in the rat limbic system. Neurobiology of disease *40*, 478-489.
- Bowser, D.N., and Khakh, B.S. (2007). Vesicular ATP is the predominant cause of intercellular calcium waves in astrocytes. The Journal of general physiology *129*, 485-491.
- Bragin, A.G., and Vinogradova, O.S. (1983). Comparison of neuronal activity in septal and hippocampal grafts developing in the anterior eye chamber of the rat. Brain research *312*, 279-286.
- Brain Res Bull. Jan 9;71(4):344-6. Epub 2006 Oct 27.

● Braitenberg V. (2001). Brain size and number of neurons: an exercise in synthetic neuroanatomy. J Comput Neurosci. 2001 Jan-Feb;10(1):71-7.

- Breschi, G.L., Cametti, M., Mastropietro, A., Librizzi, L., Baselli, G., Resnati, G., Metrangolo, P., and de Curtis, M. (2013). Different Permeability of Potassium Salts across the Blood-Brain Barrier Follows the Hofmeister Series. PloS one *8*, e78553.
- Bressler, S.L., and Kelso, J.A. (2001). Cortical coordination dynamics and cognition. Trends in cognitive sciences *5*, 26-36.
- Broer, S., Rahman, B., Pellegri, G., Pellerin, L., Martin, J.L., Verleysdonk, S., Hamprecht, B., and Magistretti, P.J. (1997). Comparison of lactate transport in astroglial cells and monocarboxylate transporter 1 (MCT 1) expressing Xenopus laevis oocytes. Expression of two different monocarboxylate transporters in astroglial cells and neurons. The Journal of biological chemistry *272*, 30096-30102.

- Brunet, N., Bosman, C.A., Roberts, M., Oostenveld, R., Womelsdorf, T., De Weerd, P., and Fries, P. (2013). Visual Cortical Gamma-Band Activity During Free Viewing of Natural Images. Cerebral cortex.
- Bukalo, O., Campanac, E., Hoffman, D.A., and Fields, R.D. (2013). Synaptic plasticity by antidromic firing during hippocampal network oscillations. Proceedings of the National Academy of Sciences of the United States of America *110*, 5175-5180.
- Bundgaard, M., and Abbott, N.J. (2008). All vertebrates started out with a glial blood-brain barrier 4-500 million years ago. Glia *56*, 699-708.
- Buracas, G.T., Zador, A.M., DeWeese, M.R., and Albright, T.D. (1998). Efficient discrimination of temporal patterns by motion-sensitive neurons in primate visual cortex. Neuron *20*, 959-969.
- Bushong, E.A., Martone, M.E., Jones, Y.Z., and Ellisman, M.H. (2002). Protoplasmic astrocytes in CA1 stratum radiatum occupy separate anatomical domains. The Journal of neuroscience : the official journal of the Society for Neuroscience *22*, 183-192.
- Butti, C., Santos, M., Uppal, N., and Hof, P.R. (2013). Von Economo neurons: clinical and evolutionary perspectives. Cortex; a journal devoted to the study of the nervous system and behavior *49*, 312-326.
- Buzsaki, G. (2004). Large-scale recording of neuronal ensembles. Nature neuroscience *7*, 446-451.
- Buzsaki, G., and Chrobak, J.J. (1995). Temporal structure in spatially organized neuronal ensembles: a role for interneuronal networks. Current opinion in neurobiology *5*, 504-510.
- Buzsaki, G., and Eidelberg, E. (1981). Commissural projection to the dentate gyrus of the rat: evidence for feed-forward inhibition. Brain research *230*, 346-350.
- Buzsaki, G., and Eidelberg, E. (1982). Convergence of associational and commissural pathways on CA1 pyramidal cells of the rat hippocampus. Brain research *237*, 283-295.
- Buzsaki, G., Leung, L.W., and Vanderwolf, C.H. (1983). Cellular bases of hippocampal EEG in the behaving rat. Brain research *287*, 139-171.
- Buzsaki, G., Logothetis, N., and Singer, W. (2013). Scaling brain size, keeping timing: evolutionary preservation of brain rhythms. Neuron *80*, 751-764.

- Buzsaki, G., Logothetis, N., and Singer, W. (2013). Scaling brain size, keeping timing: evolutionary preservation of brain rhythms. Neuron *80*, 751-764.

- Cacheaux, L.P., Ivens, S., David, Y., Lakhter, A.J., Bar-Klein, G., Shapira, M., Heinemann, U., Friedman, A., and Kaufer, D. (2009). Transcriptome profiling reveals TGF-beta signaling involvement in epileptogenesis. The Journal of neuroscience : the official journal of the Society for Neuroscience *29*, 8927-8935.
- Cakir, T., Alsan, S., Saybasili, H., Akin, A., and Ulgen, K.O. (2007). Reconstruction and flux analysis of coupling between metabolic pathways of astrocytes and neurons: application to cerebral hypoxia. Theoretical biology & medical modelling *4*, 48.
- Capogna, M., Volynski, K.E., Emptage, N.J., and Ushkaryov, Y.A. (2003). The alpha-latrotoxin mutant LTXN4C enhances spontaneous and evoked transmitter release in CA3 pyramidal neurons. The Journal of neuroscience : the official journal of the Society for Neuroscience *23*, 4044-4053.
- Carmignoto, G., and Gomez-Gonzalo, M. (2010). The contribution of astrocyte signalling to neurovascular coupling. Brain research reviews *63*, 138-148.
- Carmignoto, G., Pasti, L., and Pozzan, T. (1998). On the role of voltage-dependent calcium channels in calcium signaling of astrocytes in situ. The Journal of neuroscience : the official journal of the Society for Neuroscience *18*, 4637-4645.
- Carriero, G., Uva, L., Gnatkovsky, V., Avoli, M., and de Curtis, M. (2010). Independent epileptiform discharge patterns in the olfactory and limbic areas of the in vitro isolated Guinea pig brain during 4-aminopyridine treatment. Journal of neurophysiology *103*, 2728-2736.
- Cavalheiro, E.A., Riche, D.A., and Le Gal La Salle, G. (1982). Long-term effects of intrahippocampal kainic acid injection in rats: a method for inducing spontaneous recurrent seizures. Electroencephalography and clinical neurophysiology *53*, 581-589.
- Centemeri, C., Bolego, C., Abbracchio, M.P., Cattabeni, F., Puglisi, L., Burnstock, G., and Nicosia, S. (1997). Characterization of the Ca2+ responses evoked by ATP and other nucleotides in mammalian brain astrocytes. British journal of pharmacology *121*, 1700-1706.

- Chatrian, G.E., Lettich, E., Miller, L.H., Green, J.R., and Kupfer, C. (1970). Pattern-sensitive epilepsy. 2. Clinical changes, tests of responsiveness and motor output, alterations of evoked potenials and therapeutic measures. Epilepsia *11*, 151-162.
- Chen, X., Wang, L., Zhou, Y., Zheng, L.H., and Zhou, Z. (2005). "Kiss-and-run" glutamate secretion in cultured and freshly isolated rat hippocampal astrocytes. The Journal of neuroscience : the official journal of the Society for Neuroscience *25*, 9236-9243.
- Cherniak, C. (1995). Neural component placement. Trends in neurosciences *18*, 522-527.
- Chklovskii, D.B., and Koulakov, A.A. (2004). Maps in the brain: what can we learn from them? Annual review of neuroscience *27*, 369-392.
- Choi, S., and Friedman, W.J. (2009). Inflammatory cytokines IL-1beta and TNF-alpha regulate p75NTR expression in CNS neurons and astrocytes by distinct cell-type-specific signalling mechanisms. ASN neuro *1*.
- Chouchane, M., and Costa, M.R. (2012). Cell therapy for stroke: use of local astrocytes. Frontiers in cellular neuroscience *6*, 49.
- Christopherson, K.S., Ullian, E.M., Stokes, C.C., Mullowney, C.E., Hell, J.W., Agah, A., Lawler, J., Mosher, D.F., Bornstein, P., and Barres, B.A. (2005). Thrombospondins are astrocyte-secreted proteins that promote CNS synaptogenesis. Cell *120*, 421-433.
- Chuquet, J., Quilichini, P., Nimchinsky, E.A., and Buzsaki, G. (2010). Predominant enhancement of glucose uptake in astrocytes versus neurons during activation of the somatosensory cortex. The Journal of neuroscience : the official journal of the Society for Neuroscience *30*, 15298-15303.
- Clasadonte, J., Dong, J., Hines, D.J., and Haydon, P.G. (2013). Astrocyte control of synaptic NMDA receptors contributes to the progressive development of temporal lobe epilepsy. Proceedings of the National Academy of Sciences of the United States of America *110*, 17540-17545.
- Coco, S., Calegari, F., Pravettoni, E., Pozzi, D., Taverna, E., Rosa, P., Matteoli, M., and Verderio, C. (2003). Storage and release of ATP from astrocytes in culture. The Journal of biological chemistry *278*, 1354-1362.
- Cohen, I., and Miles, R. (2000). Contributions of intrinsic and synaptic activities to the generation of neuronal discharges in in vitro hippocampus. The Journal of physiology *524 Pt 2*, 485-502.
- Coles, J.A., and Abbott, N.J. (1996). Signalling from neurones to glial cells in invertebrates. Trends in neurosciences *19*, 358-362.
- Connors, B.W., and Long, M.A. (2004). Electrical synapses in the mammalian brain. Annual review of neuroscience *27*, 393-418.
- Connors, B.W., Gutnick, M.J., and Prince, D.A. (1982). Electrophysiological properties of neocortical neurons in vitro. Journal of neurophysiology *48*, 1302-1320.
- Cornell-Bell, A.H., Finkbeiner, S.M., Cooper, M.S., and Smith, S.J. (1990). Glutamate induces calcium waves in cultured astrocytes: long-range glial signaling. Science *247*, 470-473.
- Cossart, R., Bernard, C., and Ben-Ari, Y. (2005). Multiple facets of GABAergic neurons and synapses: multiple fates of GABA signalling in epilepsies. Trends in neurosciences *28*, 108-115.
- Cowey, A. (1979). Cortical maps and visual perception: the Grindley Memorial Lecture. The Quarterly journal of experimental psychology *31*, 1-17.
- Cracco, R.Q. (1972). The initial positive potential of the human scalp-recorded somatosensory evoked response. Electroencephalography and clinical neurophysiology *32*, 623-629.
- Crippa, D., Schenk, U., Francolini, M., Rosa, P., Verderio, C., Zonta, M., Pozzan, T., Matteoli, M., and Carmignoto, G. (2006). Synaptobrevin2-expressing vesicles in rat astrocytes: insights into molecular characterization, dynamics and exocytosis. The Journal of physiology *570*, 567-582.
- Csicsvari, J., Hirase, H., Czurko, A., and Buzsaki, G. (1998). Reliability and state dependence of pyramidal cell-interneuron synapses in the hippocampus: an ensemble approach in the behaving rat. Neuron *21*, 179-189.
- Csicsvari, J., Hirase, H., Czurko, A., and Buzsaki, G. (1998). Reliability and state dependence of pyramidal cell-interneuron synapses in the hippocampus: an ensemble approach in the behaving rat. Neuron *21*, 179-189.
- Csicsvari, J., Hirase, H., Czurko, A., Mamiya, A., and Buzsaki, G. (1999). Oscillatory coupling of hippocampal pyramidal cells and interneurons in the behaving Rat. The Journal of neuroscience : the official journal of the Society for Neuroscience *19*, 274-287.
- D'Ambrosio, R., Gordon, D.S., and Winn, H.R. (2002). Differential role of KIR channel and Na(+)/K(+)-pump in the regulation of extracellular K(+) in rat hippocampus. Journal of neurophysiology *87*, 87-102.
- D'Angelo, E., Nieus, T., Maffei, A., Armano, S., Rossi, P., Taglietti, V., Fontana, A., and Naldi, G. (2001). Theta-frequency bursting and resonance in cerebellar granule cells: experimental evidence and modeling of a slow k+-dependent mechanism. The Journal of neuroscience : the official journal of the Society for Neuroscience *21*, 759-770.

- D'Ascenzo, M., Fellin, T., Terunuma, M., Revilla-Sanchez, R., Meaney, D.F., Auberson, Y.P., Moss, S.J., and Haydon, P.G. (2007). mGluR5 stimulates gliotransmission in the nucleus accumbens. Proceedings of the National Academy of Sciences of the United States of America *104*, 1995-2000.
- Davis, G.W., and Bezprozvanny, I. (2001). Maintaining the stability of neural function: a homeostatic hypothesis. Annual review of physiology *63*, 847-869.
- de Curtis, M., Biella, G., and Forti, M. (1996). Epileptiform activity in the piriform cortex of the in vitro isolated guinea pig brain preparation. Epilepsy research *26*, 75-80.
- de Curtis, M., Radici, C., and Forti, M. (1999). Cellular mechanisms underlying spontaneous interictal spikes in an acute model of focal cortical epileptogenesis. Neuroscience *88*, 107-117.
- de Vivo, L., Landi, S., Panniello, M., Baroncelli, L., Chierzi, S., Mariotti, L., Spolidoro, M., Pizzorusso, T., Maffei, L., and Ratto, G.M. (2013). Extracellular matrix inhibits structural and functional plasticity of dendritic spines in the adult visual cortex. Nature communications *4*, 1484.
- Deller, T., Haas, C.A., Naumann, T., Joester, A., Faissner, A., and Frotscher, M. (1997). Up-regulation of astrocyte-derived tenascin-C correlates with neurite outgrowth in the rat dentate gyrus after unilateral entorhinal cortex lesion. Neuroscience *81*, 829-846.
- Destexhe, A., Rudolph, M., and Pare, D. (2003). The high-conductance state of neocortical neurons in vivo. Nature reviews Neuroscience *4*, 739-751.
- Devinsky, O., and Najjar, S. (1999). Evidence against the existence of a temporal lobe epilepsy personality syndrome. Neurology *53*, S13-25.
- Diba, K., Lester, H.A., and Koch, C. (2004). Intrinsic noise in cultured hippocampal neurons: experiment and modeling. The Journal of neuroscience : the official journal of the Society for Neuroscience *24*, 9723-9733.
- Dichter, M., and Spencer, W.A. (1969). Penicillin-induced interictal discharges from the cat hippocampus. II. Mechanisms underlying origin and restriction. Journal of neurophysiology *32*, 663-687.
- Dityatev, A., and Schachner, M. (2003). Extracellular matrix molecules and synaptic plasticity. Nature reviews Neuroscience *4*, 456-468.
- Djukic, B., Casper, K.B., Philpot, B.D., Chin, L.S., and McCarthy, K.D. (2007). Conditional knock-out of Kir4.1 leads to glial membrane depolarization, inhibition of potassium and glutamate uptake, and enhanced short-term synaptic potentiation. The Journal of neuroscience : the official journal of the Society for Neuroscience *27*, 11354-11365.
- Dombeck, D.A., Khabbaz, A.N., Collman, F., Adelman, T.L., and Tank, D.W. (2007). Imaging large-scale neural activity with cellular resolution in awake, mobile mice. Neuron *56*, 43-57.
- Duan, S., Anderson, C.M., Keung, E.C., Chen, Y., Chen, Y., and Swanson, R.A. (2003). P2X7 receptor-mediated release of excitatory amino acids from astrocytes. The Journal of neuroscience : the official journal of the Society for Neuroscience *23*, 1320-1328.
- Dunwiddie, T.V., and Masino, S.A. (2001). The role and regulation of adenosine in the central nervous system. Annual review of neuroscience *24*, 31-55.
- Echlin, F.A., and Battista, A. (1963). Epileptiform Seizures from Chronic Isolated Cortex. Archives of neurology *9*, 154-170.
- Eid, T., Lee, T.S., Thomas, M.J., Amiry-Moghaddam, M., Bjornsen, L.P., Spencer, D.D., Agre, P., Ottersen, O.P., and de Lanerolle, N.C. (2005). Loss of perivascular aquaporin 4 may underlie deficient water and K+ homeostasis in the human epileptogenic hippocampus. Proceedings of the National Academy of Sciences of the United States of America *102*, 1193-1198.
- Emptage, N.J., Reid, C.A., and Fine, A. (2001). Calcium stores in hippocampal synaptic boutons mediate short-term plasticity, store-operated Ca2+ entry, and spontaneous transmitter release. Neuron *29*, 197-208.
- Engel, A.K., Fries, P., and Singer, W. (2001). Dynamic predictions: oscillations and synchrony in top-down processing. Nature reviews Neuroscience *2*, 704-716.
- Engel, J., Jr. (2006). ILAE classification of epilepsy syndromes. Epilepsy research *70 Suppl 1*, S5-10.
- Engel, J., Jr. (2013). Progress in the field of epilepsy. Current opinion in neurology *26*, 160-162.
- Engstrom, M., Hagen, K., Bjork, M., Gravdahl, G.B., and Sand, T. (2013). Sleep-related and non-sleep-related migraine: interictal sleep quality, arousals and pain thresholds. The journal of headache and pain *14*, 68.
- Fedele, D.E., Gouder, N., Guttinger, M., Gabernet, L., Scheurer, L., Rulicke, T., Crestani, F., and Boison, D. (2005). Astrogliosis in epilepsy leads to overexpression of adenosine kinase, resulting in seizure aggravation. Brain : a journal of neurology *128*, 2383-2395.

- Fell, J., and Axmacher, N. (2011). The role of phase synchronization in memory processes. Nature reviews Neuroscience *12*, 105-118.
- Felleman, D.J., and Van Essen, D.C. (1991). Distributed hierarchical processing in the primate cerebral cortex. Cerebral cortex *1*, 1-47.
- Fellin, T., Gomez-Gonzalo, M., Gobbo, S., Carmignoto, G., and Haydon, P.G. (2006). Astrocytic glutamate is not necessary for the generation of epileptiform neuronal activity in hippocampal slices. The Journal of neuroscience : the official journal of the Society for Neuroscience *26*, 9312-9322.
- Fellin, T., Pascual, O., Gobbo, S., Pozzan, T., Haydon, P.G., and Carmignoto, G. (2004). Neuronal synchrony mediated by astrocytic glutamate through activation of extrasynaptic NMDA receptors. Neuron *43*, 729-743.
- Fellin, T., Pascual, O., Gobbo, S., Pozzan, T., Haydon, P.G., and Carmignoto, G. (2004). Neuronal synchrony mediated by astrocytic glutamate through activation of extrasynaptic NMDA receptors. Neuron *43*, 729-743.
- Fellin, T., Pozzan, T., and Carmignoto, G. (2006). Purinergic receptors mediate two distinct glutamate release pathways in hippocampal astrocytes. The Journal of biological chemistry *281*, 4274-4284.
- Fellous, J.M., Tiesinga, P.H., Thomas, P.J., and Sejnowski, T.J. (2004). Discovering spike patterns in neuronal responses. The Journal of neuroscience : the official journal of the Society for Neuroscience *24*, 2989-3001.
- Fiacco, T.A., and McCarthy, K.D. (2004). Intracellular astrocyte calcium waves in situ increase the frequency of spontaneous AMPA receptor currents in CA1 pyramidal neurons. The Journal of neuroscience : the official journal of the Society for Neuroscience *24*, 722-732.
- Filosa, J.A., Bonev, A.D., and Nelson, M.T. (2004). Calcium dynamics in cortical astrocytes and arterioles during neurovascular coupling. Circulation research *95*, e73-81.
- Fino, E., Packer, A.M., and Yuste, R. (2013). The logic of inhibitory connectivity in the neocortex. The Neuroscientist : a review journal bringing neurobiology, neurology and psychiatry *19*, 228-237.
- Fiser, J., Chiu, C., and Weliky, M. (2004). Small modulation of ongoing cortical dynamics by sensory input during natural vision. Nature *431*, 573-578.
- Fisher, R.S., van Emde Boas, W., Blume, W., Elger, C., Genton, P., Lee, P., and Engel, J., Jr. (2005). Epileptic seizures and epilepsy: definitions proposed by the International League Against Epilepsy (ILAE) and the International Bureau for Epilepsy (IBE). Epilepsia *46*, 470-472.
- Fletcher, D.A., and Mullins, R.D. (2010). Cell mechanics and the cytoskeleton. Nature *463*, 485-492.
- Fletcher, D.A., and Mullins, R.D. (2010). Cell mechanics and the cytoskeleton. Nature *463*, 485-492.
- Fonseca, C.G., Green, C.R., and Nicholson, L.F. (2002). Upregulation in astrocytic connexin 43 gap junction levels may exacerbate generalized seizures in mesial temporal lobe epilepsy. Brain research *929*, 105-116.
- Fountain, N.B., Kim, J.S., and Lee, S.I. (1998). Sleep deprivation activates epileptiform discharges independent of the activating effects of sleep. Journal of clinical neurophysiology : official publication of the American Electroencephalographic Society *15*, 69-75.
- Fox K (2002) Anatomical pathways and molecular mechanisms for plasticity in the barrel cortex.Neuroscience 111:799-814.
- Freund, T.F. (2003). Interneuron Diversity series: Rhythm and mood in perisomatic inhibition. Trends in neurosciences *26*, 489-495.
- Freund, T.F., and Gulyas, A.I. (1997). Inhibitory control of GABAergic interneurons in the hippocampus. Canadian journal of physiology and pharmacology *75*, 479-487.
- Friedman, E.J., and Landsberg, A.S. (2013). Hierarchical networks, power laws, and neuronal avalanches. Chaos *23*, 013135.
- Friston, K.J. (2000). The labile brain. I. Neuronal transients and nonlinear coupling. Philosophical transactions of the Royal Society of London Series B, Biological sciences *355*, 215-236.
- Friston, K.J. (2000). The labile brain. II. Transients, complexity and selection. Philosophical transactions of the Royal Society of London Series B, Biological sciences *355*, 237-252.
- Friston, K.J. (2000). The labile brain. II. Transients, complexity and selection. Philosophical transactions of the Royal Society of London Series B, Biological sciences *355*, 237-252.
- Front Cell Neurosci. Apr 10;7:38. doi: 10.3389/fncel.2013.00038. eCollection 2013.
- Fujiwara-Tsukamoto, Y., Isomura, Y., Imanishi, M., Ninomiya, T., Tsukada, M., Yanagawa, Y., Fukai, T., and Takada, M. (2010). Prototypic seizure activity driven by mature hippocampal fast-spiking interneurons. The Journal of neuroscience : the official journal of the Society for Neuroscience *30*, 13679-13689.
- Galione, A., and Ruas, M. (2005). NAADP receptors. Cell calcium *38*, 273-280.

- Garaschuk, O., and Konnerth, A. (2010). In vivo two-photon calcium imaging using multicell bolus loading. Cold Spring Harbor protocols *2010*, pdb prot5482.
- Garbelli, R., Frassoni, C., Condorelli, D.F., Trovato Salinaro, A., Musso, N., Medici, V., Tassi, L., Bentivoglio, M., and Spreafico, R. (2011). Expression of connexin 43 in the human epileptic and drug-resistant cerebral cortex. Neurology *76*, 895-902.
- Garber, S.S., and Miller, C. (1987). Single Na+ channels activated by veratridine and batrachotoxin. The Journal of general physiology *89*, 459-480.
- Genoud, C., Quairiaux, C., Steiner, P., Hirling, H., Welker, E., and Knott, G.W. (2006). Plasticity of astrocytic coverage and glutamate transporter expression in adult mouse cortex. PLoS biology *4*, e343.
- Giaume, C., Kirchhoff, F., Matute, C., Reichenbach, A., and Verkhratsky, A. (2007). Glia: the fulcrum of brain diseases. Cell death and differentiation *14*, 1324-1335.
- Gilbert, C.D., and Li, W. (2013). Top-down influences on visual processing. Nature reviews Neuroscience *14*, 350-363.
- Gilden, D.L. (2001). Cognitive emissions of 1/f noise. Psychological review *108*, 33-56.
- Glickfeld, L.L., Andermann, M.L., Bonin, V., and Reid, R.C. (2013). Cortico-cortical projections in mouse visual cortex are functionally target specific. Nature neuroscience *16*, 219-226.
- Gnatkovsky, V., Librizzi, L., Trombin, F., and de Curtis, M. (2008). Fast activity at seizure onset is mediated by inhibitory circuits in the entorhinal cortex in vitro. Annals of neurology *64*, 674-686.
- Gomez-Gonzalo, M., Losi, G., Brondi, M., Uva, L., Sato, S.S., de Curtis, M., Ratto, G.M., and Carmignoto, G. (2011). Ictal but not interictal epileptic discharges activate astrocyte endfeet and elicit cerebral arteriole responses. Frontiers in cellular neuroscience *5*, 8.
- Gomez-Gonzalo, M., Losi, G., Chiavegato, A., Zonta, M., Cammarota, M., Brondi, M., Vetri, F., Uva, L., Pozzan, T., de Curtis, M*., et al.* (2010). An excitatory loop with astrocytes contributes to drive neurons to seizure threshold. PLoS biology *8*, e1000352.
- Gomez-Gonzalo, M., Losi, G., Chiavegato, A., Zonta, M., Cammarota, M., Brondi, M., Vetri, F., Uva, L., Pozzan, T., de Curtis, M*., et al.* (2010). An excitatory loop with astrocytes contributes to drive neurons to seizure threshold. PLoS biology *8*, e1000352.
- Gonzalez-Burgos, G., Fish, K.N., and Lewis, D.A. (2011). GABA neuron alterations, cortical circuit dysfunction and cognitive deficits in schizophrenia. Neural plasticity *2011*, 723184.
- Gordon, G.R., Mulligan, S.J., and MacVicar, B.A. (2007). Astrocyte control of the cerebrovasculature. Glia *55*, 1214-1221.
- Grosche, A., Grosche, J., Tackenberg, M., Scheller, D., Gerstner, G., Gumprecht, A., Pannicke, T., Hirrlinger, P.G., Wilhelmsson, U., Huttmann, K*., et al.* (2013). Versatile and simple approach to determine astrocyte territories in mouse neocortex and hippocampus. PloS one *8*, e69143.
- Gulyas, A.I., Hajos, N., and Freund, T.F. (1996). Interneurons containing calretinin are specialized to control other interneurons in the rat hippocampus. The Journal of neuroscience : the official journal of the Society for Neuroscience *16*, 3397-3411.
- Gulyas, A.I., Miles, R., Sik, A., Toth, K., Tamamaki, N., and Freund, T.F. (1993). Hippocampal pyramidal cells excite inhibitory neurons through a single release site. Nature *366*, 683-687.
- Guthrie, P.B., Knappenberger, J., Segal, M., Bennett, M.V., Charles, A.C., and Kater, S.B. (1999). ATP released from astrocytes mediates glial calcium waves. The Journal of neuroscience : the official journal of the Society for Neuroscience *19*, 520-528.
- Haas, B., Schipke, C.G., Peters, O., Sohl, G., Willecke, K., and Kettenmann, H. (2006). Activity-dependent ATP-waves in the mouse neocortex are independent from astrocytic calcium waves. Cerebral cortex *16*, 237-246.
- Haas, H.L., and Jefferys, J.G. (1984). Low-calcium field burst discharges of CA1 pyramidal neurones in rat hippocampal slices. The Journal of physiology *354*, 185-201.
- Haber, M., Zhou, L., and Murai, K.K. (2006). Cooperative astrocyte and dendritic spine dynamics at hippocampal excitatory synapses. The Journal of neuroscience : the official journal of the Society for Neuroscience *26*, 8881-8891.
- Halassa, M.M., Dal Maschio, M., Beltramo, R., Haydon, P.G., Benfenati, F., and Fellin, T. (2010). Integrated brain circuits: neuron-astrocyte interaction in sleep-related rhythmogenesis. TheScientificWorldJournal *10*, 1634-1645.

- Halassa, M.M., Fellin, T., Takano, H., Dong, J.H., and Haydon, P.G. (2007). Synaptic islands defined by the territory of a single astrocyte. The Journal of neuroscience : the official journal of the Society for Neuroscience *27*, 6473-6477.
- Halassa, M.M., Fellin, T., Takano, H., Dong, J.H., and Haydon, P.G. (2007). Synaptic islands defined by the territory of a single astrocyte. The Journal of neuroscience : the official journal of the Society for Neuroscience *27*, 6473-6477.
- Hammer, J., Alvestad, S., Osen, K.K., Skare, O., Sonnewald, U., and Ottersen, O.P. (2008). Expression of glutamine synthetase and glutamate dehydrogenase in the latent phase and chronic phase in the kainate model of temporal lobe epilepsy. Glia *56*, 856-868.
- Harris, K.D., and Mrsic-Flogel, T.D. (2013). Cortical connectivity and sensory coding. Nature *503*, 51-58.
- Haseleu, J., Anlauf, E., Blaess, S., Endl, E., and Derouiche, A. (2013). Studying subcellular detail in fixed astrocytes: dissociation of morphologically intact glial cells (DIMIGs). Frontiers in cellular neuroscience *7*, 54.
- Hatton, G.I., Perlmutter, L.S., Salm, A.K., and Tweedle, C.D. (1984). Dynamic neuronal-glial interactions in hypothalamus and pituitary: implications for control of hormone synthesis and release. Peptides *5 Suppl 1*, 121-138.
- Haydon, P.G., and Carmignoto, G. (2006). Astrocyte control of synaptic transmission and neurovascular coupling. Physiological reviews *86*, 1009-1031.
- Haydon, P.G., and Carmignoto, G. (2006). Astrocyte control of synaptic transmission and neurovascular coupling. Physiological reviews *86*, 1009-1031.
- Headley, D.B., and Pare, D. (2013). In sync: gamma oscillations and emotional memory. Frontiers in behavioral neuroscience *7*, 170.
- Hebb DO. (1949) .The Organization of Behavior. New York: JohnWiley & Sons.
- Heimel, J.A., Saiepour, M.H., Chakravarthy, S., Hermans, J.M., and Levelt, C.N. (2010). Contrast gain control and cortical TrkB signaling shape visual acuity. Nature neuroscience *13*, 642-648.
- Heinrich, C., Gotz, M., and Berninger, B. (2012). Reprogramming of postnatal astroglia of the mouse neocortex into functional, synapse-forming neurons. Methods in molecular biology *814*, 485-498.
- Helmchen, F. (2011). Calibration protocols for fluorescent calcium indicators. Cold Spring Harbor protocols *2011*, 980-984.
- Henze, D.A., and Buzsaki, G. (2001). Action potential threshold of hippocampal pyramidal cells in vivo is increased by recent spiking activity. Neuroscience *105*, 121-130.
- Herculano-Houzel, S., Collins, C.E., Wong, P., Kaas, J.H., and Lent, R. (2008). The basic nonuniformity of the cerebral cortex. Proceedings of the National Academy of Sciences of the United States of America *105*, 12593-12598.
- Hesdorffer, D.C., Ishihara, L., Mynepalli, L., Webb, D.J., Weil, J., and Hauser, W.A. (2012). Epilepsy, suicidality, and psychiatric disorders: a bidirectional association. Annals of neurology *72*, 184-191.
- Hestrin, S., and Galarreta, M. (2005). Electrical synapses define networks of neocortical GABAergic neurons. Trends in neurosciences *28*, 304-309.
- Heuser, K., Nagelhus, E.A., Tauboll, E., Indahl, U., Berg, P.R., Lien, S., Nakken, S., Gjerstad, L., and Ottersen, O.P. (2010). Variants of the genes encoding AQP4 and Kir4.1 are associated with subgroups of patients with temporal lobe epilepsy. Epilepsy research *88*, 55-64.
- Higashi, K., Fujita, A., Inanobe, A., Tanemoto, M., Doi, K., Kubo, T., and Kurachi, Y. (2001). An inwardly rectifying K(+) channel, Kir4.1, expressed in astrocytes surrounds synapses and blood vessels in brain. American journal of physiology Cell physiology *281*, C922-931.
- Hinterkeuser, S., Schroder, W., Hager, G., Seifert, G., Blumcke, I., Elger, C.E., Schramm, J., and Steinhauser, C. (2000). Astrocytes in the hippocampus of patients with temporal lobe epilepsy display changes in potassium conductances. The European journal of neuroscience *12*, 2087-2096.
- Hirase, H., Qian, L., Bartho, P., and Buzsaki, G. (2004). Calcium dynamics of cortical astrocytic networks in vivo. PLoS biology *2*, E96.
- Hirrlinger, J., Hulsmann, S., and Kirchhoff, F. (2004). Astroglial processes show spontaneous motility at active synaptic terminals in situ. The European journal of neuroscience *20*, 2235-2239.
- Holland, E.C. (2001). Progenitor cells and glioma formation. Current opinion in neurology *14*, 683-688.
- Horton, N.G., Wang, K., Kobat, D., Clark, C.G., Wise, F.W., Schaffer, C.B., and Xu, C. (2013). three-photon microscopy of subcortical structures within an intact mouse brain. Nature photonics *7*.
- Houades, V., Rouach, N., Ezan, P., Kirchhoff, F., Koulakoff, A., and Giaume, C. (2006). Shapes of astrocyte networks in the juvenile brain. Neuron glia biology *2*, 3-14.

- Hsu, M.S., Lee, D.J., and Binder, D.K. (2007). Potential role of the glial water channel aquaporin-4 in epilepsy. Neuron glia biology *3*, 287-297.
- Iadecola, C., and Nedergaard, M. (2007). Glial regulation of the cerebral microvasculature. Nature neuroscience *10*, 1369-1376.
- Ida, T., Hara, M., Nakamura, Y., Kozaki, S., Tsunoda, S., and Ihara, H. (2008). Cytokine-induced enhancement of calcium-dependent glutamate release from astrocytes mediated by nitric oxide. Neuroscience letters *432*, 232-236.
- Igarashi, J., Isomura, Y., Arai, K., Harukuni, R., and Fukai, T. (2013). A theta-gamma Oscillation Code for Neuronal Coordination during Motor Behavior. The Journal of neuroscience : the official journal of the Society for Neuroscience *33*, 18515-18530.
- Jabs, R., Matthias, K., Grote, A., Grauer, M., Seifert, G., and Steinhauser, C. (2007). Lack of P2X receptor mediated currents in astrocytes and GluR type glial cells of the hippocampal CA1 region. Glia *55*, 1648-1655.
- Jefferys, J.G.R., Jiruska, P., de Curtis, M., and Avoli, M. (2012). Limbic Network Synchronization and Temporal Lobe Epilepsy. In Jasper's Basic Mechanisms of the Epilepsies, J.L. Noebels, M. Avoli, M.A. Rogawski, R.W. Olsen, and A.V. Delgado-Escueta, eds. (Bethesda (MD)).
- Joester, A., and Faissner, A. (2001). The structure and function of tenascins in the nervous system. Matrix biology : journal of the International Society for Matrix Biology *20*, 13-22.
- Johnston, D., and Brown, T.H. (1981). Giant synaptic potential hypothesis for epileptiform activity. Science *211*, 294-297.
- Jones, R.S., and Heinemann, U. (1988). Synaptic and intrinsic responses of medical entorhinal cortical cells in normal and magnesium-free medium in vitro. Journal of neurophysiology *59*, 1476-1496.
- Jones, T.A., and Greenough, W.T. (1996). Ultrastructural evidence for increased contact between astrocytes and synapses in rats reared in a complex environment. Neurobiology of learning and memory *65*, 48-56.
- Jones, T.A., Kleim, J.A., and Greenough, W.T. (1996). Synaptogenesis and dendritic growth in the cortex opposite unilateral sensorimotor cortex damage in adult rats: a quantitative electron microscopic examination. Brain research *733*, 142-148.
- Jorge, B.S., Campbell, C.M., Miller, A.R., Rutter, E.D., Gurnett, C.A., Vanoye, C.G., George, A.L., Jr., and Kearney, J.A. (2011). Voltage-gated potassium channel KCNV2 (Kv8.2) contributes to epilepsy susceptibility. Proceedings of the National Academy of Sciences of the United States of America *108*, 5443-5448.
- Jorge, B.S., Campbell, C.M., Miller, A.R., Rutter, E.D., Gurnett, C.A., Vanoye, C.G., George, A.L., Jr., and Kearney, J.A. (2011). Voltage-gated potassium channel KCNV2 (Kv8.2) contributes to epilepsy susceptibility. Proceedings of the National Academy of Sciences of the United States of America *108*, 5443-5448.
- Julesz, B., Dialogues on Perception, Cambridge: Bradford/MIT Press, (1995).
- Jung, J.C., Mehta, A.D., Aksay, E., Stepnoski, R., and Schnitzer, M.J. (2004). In vivo mammalian brain imaging using one- and two-photon fluorescence microendoscopy. Journal of neurophysiology *92*, 3121-3133.
- Kalisman, N., Silberberg, G., and Markram, H. (2005). The neocortical microcircuit as a tabula rasa. Proceedings of the National Academy of Sciences of the United States of America *102*, 880-885.
- Kamondi, A., Acsady, L., and Buzsaki, G. (1998). Dendritic spikes are enhanced by cooperative network activity in the intact hippocampus. The Journal of neuroscience : the official journal of the Society for Neuroscience *18*, 3919-3928.
- Kampa, B.M., Roth, M.M., Gobel, W., and Helmchen, F. (2011). Representation of visual scenes by local neuronal populations in layer 2/3 of mouse visual cortex. Frontiers in neural circuits *5*, 18.
- Kandel ER, Schwartz JH, Jessell TM 2000Principles of Neural Science, 4th Ed. McGraw-Hill
- Kandel, A., and Buzsaki, G. (1997). Cellular-synaptic generation of sleep spindles, spike-and-wave discharges, and evoked thalamocortical responses in the neocortex of the rat. The Journal of neuroscience : the official journal of the Society for Neuroscience *17*, 6783-6797.
- Kandel, E.R., and Spencer, W.A. (1961). The pyramidal cell during hippocampal seizure. Epilepsia *2*, 63-69.
- Kandel, E.R., and Squire, L.R. (2000). Neuroscience: breaking down scientific barriers to the study of brain and mind. Science *290*, 1113-1120.

- Kang, N., Xu, J., Xu, Q., Nedergaard, M., and Kang, J. (2005). Astrocytic glutamate release-induced transient depolarization and epileptiform discharges in hippocampal CA1 pyramidal neurons. Journal of neurophysiology *94*, 4121-4130.

- Kang, N., Xu, J., Xu, Q., Nedergaard, M., and Kang, J. (2005). Astrocytic glutamate release-induced transient depolarization and epileptiform discharges in hippocampal CA1 pyramidal neurons. Journal of neurophysiology *94*, 4121-4130.

- Katsumaru, H., Kosaka, T., Heizmann, C.W., and Hama, K. (1988). Gap junctions on GABAergic neurons containing the calcium-binding protein parvalbumin in the rat hippocampus (CA1 region). Experimental brain research Experimentelle Hirnforschung Experimentation cerebrale *72*, 363-370.
- Keegan, B.M., and Noseworthy, J.H. (2002). Multiple sclerosis. Annual review of medicine *53*, 285-302.
- Kelso, J.A., and Fuchs, A. (1995). Self-organizing dynamics of the human brain: Critical instabilities and Sil'nikov chaos. Chaos *5*, 64-69.
- Kimelberg, H.K., and Nedergaard, M. (2010). Functions of astrocytes and their potential as therapeutic targets. Neurotherapeutics : the journal of the American Society for Experimental NeuroTherapeutics *7*, 338-353.
- Kleen, J.K., Scott, R.C., Holmes, G.L., Roberts, D.W., Rundle, M.M., Testorf, M., Lenck-Santini, P.P., and Jobst, B.C. (2013). Hippocampal interictal epileptiform activity disrupts cognition in humans. Neurology *81*, 18-24.
- Kleene, R., and Schachner, M. (2004). Glycans and neural cell interactions. Nature reviews Neuroscience *5*, 195-208.
- Ko, H., Cossell, L., Baragli, C., Antolik, J., Clopath, C., Hofer, S.B., and Mrsic-Flogel, T.D. (2013). The emergence of functional microcircuits in visual cortex. Nature *496*, 96-100.
- Kofuji, P., and Connors, N.C. (2003). Molecular substrates of potassium spatial buffering in glial cells. Molecular neurobiology *28*, 195-208.
- Kofuji, P., and Newman, E.A. (2004). Potassium buffering in the central nervous system. Neuroscience *129*, 1045-1056.
- Kohling, R., Vreugdenhil, M., Bracci, E., and Jefferys, J.G. (2000). Ictal epileptiform activity is facilitated by hippocampal GABAA receptor-mediated oscillations. The Journal of neuroscience : the official journal of the Society for Neuroscience *20*, 6820-6829.
- Koizumi, S. (2010). Synchronization of Ca2+ oscillations: involvement of ATP release in astrocytes. The FEBS journal *277*, 286-292.
- Komisaruk BR. (1970) Synchrony between limbic system theta activity and rhythmical behavior in rats. J Comp Physiol Psychol. .70(3):482-92

- Kosaka, T., and Hama, K. (1986). Three-dimensional structure of astrocytes in the rat dentate gyrus. The Journal of comparative neurology *249*, 242-260.
- Kubota, Y., Karube, F., Nomura, M., Gulledge, A.T., Mochizuki, A., Schertel, A., and Kawaguchi, Y. (2011). Conserved properties of dendritic trees in four cortical interneuron subtypes. Scientific reports *1*, 89.
- Lakatos, P., Karmos, G., Mehta, A.D., Ulbert, I., and Schroeder, C.E. (2008). Entrainment of neuronal oscillations as a mechanism of attentional selection. Science *320*, 110-113.
- Lappin, S.C., Dale, T.J., Brown, J.T., Trezise, D.J., and Davies, C.H. (2005). Activation of SK channels inhibits epileptiform bursting in hippocampal CA3 neurons. Brain research *1065*, 37-46.
- Laughlin, S.B., and Sejnowski, T.J. (2003). Communication in neuronal networks. Science *301*, 1870-1874.
- Le Meur, K., Mendizabal-Zubiaga, J., Grandes, P., and Audinat, E. (2012). GABA release by hippocampal astrocytes. Frontiers in computational neuroscience *6*, 59.
- Le Van Quyen, M., Chavez, M., Rudrauf, D., and Martinerie, J. (2003). Exploring the nonlinear dynamics of the brain. Journal of physiology, Paris *97*, 629-639.
- Lee, S.H., Kwan, A.C., Zhang, S., Phoumthipphavong, V., Flannery, J.G., Masmanidis, S.C., Taniguchi, H., Huang, Z.J., Zhang, F., Boyden, E.S., *et al.* (2012). Activation of specific interneurons improves V1 feature selectivity and visual perception. Nature *488*, 379-383.
- Lenzen, K.P., Heils, A., Lorenz, S., Hempelmann, A., Hofels, S., Lohoff, F.W., Schmitz, B., and Sander, T. (2005). Supportive evidence for an allelic association of the human KCNJ10 potassium channel gene with idiopathic generalized epilepsy. Epilepsy research *63*, 113-118.
- Levene, M.J., Dombeck, D.A., Kasischke, K.A., Molloy, R.P., and Webb, W.W. (2004). In vivo multiphoton microscopy of deep brain tissue. Journal of neurophysiology *91*, 1908-1912.
- Levy, W.B., and Baxter, R.A. (1996). Energy efficient neural codes. Neural computation *8*, 531-543.

- Libet, B. (1993). The neural time factor in conscious and unconscious events. Ciba Foundation symposium *174*, 123-137; discussion 137-146.
- Lillis, K.P., Kramer, M.A., Mertz, J., Staley, K.J., and White, J.A. (2012). Pyramidal cells accumulate chloride at seizure onset. Neurobiology of disease *47*, 358-366.
- Linkenkaer-Hansen, K., Nikouline, V.V., Palva, J.M., and Ilmoniemi, R.J. (2001). Long-range temporal correlations and scaling behavior in human brain oscillations. The Journal of neuroscience : the official journal of the Society for Neuroscience *21*, 1370-1377.
- Liu, H.T., Akita, T., Shimizu, T., Sabirov, R.Z., and Okada, Y. (2009). Bradykinin-induced astrocyte-neuron signalling: glutamate release is mediated by ROS-activated volume-sensitive outwardly rectifying anion channels. The Journal of physiology *587*, 2197-2209.
- Llinas, R., and Sugimori, M. (1980). Electrophysiological properties of in vitro Purkinje cell somata in mammalian cerebellar slices. The Journal of physiology *305*, 171-195.
- Lopantsev, V., and Avoli, M. (1998). Laminar organization of epileptiform discharges in the rat entorhinal cortex in vitro. The Journal of physiology *509 (Pt 3)*, 785-796.
- Lothman, E.W., and Bertram, E.H., 3rd (1993). Epileptogenic effects of status epilepticus. Epilepsia *34 Suppl 1*, S59-70.
- Lytton, W.W. (2008). Computer modelling of epilepsy. Nature reviews Neuroscience *9*, 626-637.
- Mackey, M.C., and Glass, L. (1977). Oscillation and chaos in physiological control systems. Science *197*, 287-289.
- Magistretti, J., and Alonso, A. (1999). Slow voltage-dependent inactivation of a sustained sodium current in stellate cells of rat entorhinal cortex layer II. Annals of the New York Academy of Sciences *868*, 84-87.
- Magistretti, J., and de Curtis, M. (1998). Low-voltage activated T-type calcium currents are differently expressed in superficial and deep layers of guinea pig piriform cortex. Journal of neurophysiology *79*, 808-816.
- Magistretti, J., Brevi, S., and de Curtis, M. (2000). A blocker-resistant, fast-decaying, intermediate-threshold calcium current in palaeocortical pyramidal neurons. The European journal of neuroscience *12*, 2376-2386.
- Magistretti, P.J. (2006). Neuron-glia metabolic coupling and plasticity. The Journal of experimental biology *209*, 2304-2311.
- Maier, A., Adams, G.K., Aura, C., and Leopold, D.A. (2010). Distinct superficial and deep laminar domains of activity in the visual cortex during rest and stimulation. Frontiers in systems neuroscience *4*.
- Mainen, Z.F., and Sejnowski, T.J. (1995). Reliability of spike timing in neocortical neurons. Science *268*, 1503-1506.
- Mainen, Z.F., and Sejnowski, T.J. (1996). Influence of dendritic structure on firing pattern in model neocortical neurons. Nature *382*, 363-366.
- Malinowska, U., Badier, J.M., Gavaret, M., Bartolomei, F., Chauvel, P., and Benar, C.G. (2013). Interictal networks in Magnetoencephalography. Human brain mapping.
- Mantegazza, M., Franceschetti, S., and Avanzini, G. (1998). Anemone toxin (ATX II)-induced increase in persistent sodium current: effects on the firing properties of rat neocortical pyramidal neurones. The Journal of physiology *507 (Pt 1)*, 105-116.
- Maragakis, N.J., and Rothstein, J.D. (2006). Mechanisms of Disease: astrocytes in neurodegenerative disease. Nature clinical practice Neurology *2*, 679-689.
- Marchi, N., Angelov, L., Masaryk, T., Fazio, V., Granata, T., Hernandez, N., Hallene, K., Diglaw, T., Franic, L., Najm, I.*, et al.* (2007). Seizure-promoting effect of blood-brain barrier disruption. Epilepsia *48*, 732-742.
- Markova, O., Fitzgerald, D., Stepanyuk, A., Dovgan, A., Cherkas, V., Tepikin, A., Burgoyne, R.D., and Belan, P. (2008). Hippocalcin signaling via site-specific translocation in hippocampal neurons. Neuroscience letters *442*, 152-157.
- Markram, H. (1997). A network of tufted layer 5 pyramidal neurons. Cerebral cortex *7*, 523-533.
- Markram, H., Toledo-Rodriguez, M., Wang, Y., Gupta, A., Silberberg, G., and Wu, C. (2004). Interneurons of the neocortical inhibitory system. Nature reviews Neuroscience *5*, 793-807.
- Matsumoto, H., and Ajmonemarsan, C. (1964). Cellular Mechanisms in Experimental Epileptic Seizures. Science *144*, 193-194.

- Matsuzaki, N., Juhasz, C., and Asano, E. (2013). Cortico-cortical evoked potentials and stimulation-elicited gamma activity preferentially propagate from lower- to higher-order visual areas. Clinical neurophysiology : official journal of the International Federation of Clinical Neurophysiology *124*, 1290-1296.
- Matthews, E.A., Schoch, S., and Dietrich, D. (2013). Tuning local calcium availability: cell-type-specific immobile calcium buffer capacity in hippocampal neurons. The Journal of neuroscience : the official journal of the Society for Neuroscience *33*, 14431-14445.
- Matthias, K., Kirchhoff, F., Seifert, G., Huttmann, K., Matyash, M., Kettenmann, H., and Steinhauser, C. (2003). Segregated expression of AMPA-type glutamate receptors and glutamate transporters defines distinct astrocyte populations in the mouse hippocampus. The Journal of neuroscience : the official journal of the Society for Neuroscience *23*, 1750-1758.
- Matyash, M., Matyash, V., Nolte, C., Sorrentino, V., and Kettenmann, H. (2002). Requirement of functional ryanodine receptor type 3 for astrocyte migration. FASEB journal : official publication of the Federation of American Societies for Experimental Biology *16*, 84-86.
- Mazzarello P. (2007). Net without nodes and vice versa, the paradoxical Golgi-Cajal story: a reconciliation?
- McClelland, J.L., McNaughton, B.L., and O'Reilly, R.C. (1995). Why there are complementary learning systems in the hippocampus and neocortex: insights from the successes and failures of connectionist models of learning and memory. Psychological review *102*, 419-457.
- McCormick, D.A., Wang, Z., and Huguenard, J. (1993). Neurotransmitter control of neocortical neuronal activity and excitability. Cerebral cortex *3*, 387-398.
- McDonald, C.T., and Burkhalter, A. (1993). Organization of long-range inhibitory connections with rat visual cortex. The Journal of neuroscience : the official journal of the Society for Neuroscience *13*, 768-781.
- McIntyre, D.C., and Racine, R.J. (1986). Kindling mechanisms: current progress on an experimental epilepsy model. Progress in neurobiology *27*, 1-12.
- McNally, J.M., McCarley, R.W., and Brown, R.E. (2013). Impaired GABAergic neurotransmission in schizophrenia underlies impairments in cortical gamma band oscillations. Current psychiatry reports *15*, 346.
- Medici, V., Frassoni, C., Tassi, L., Spreafico, R., and Garbelli, R. (2011). Aquaporin 4 expression in control and epileptic human cerebral cortex. Brain research *1367*, 330-339.
- Medina-Ceja, L., Sandoval-Garcia, F., Morales-Villagran, A., and Lopez-Perez, S.J. (2012). Rapid compensatory changes in the expression of EAAT-3 and GAT-1 transporters during seizures in cells of the CA1 and dentate gyrus. Journal of biomedical science *19*, 78.
- Menendez de la Prida, L., and Trevelyan, A.J. (2011). Cellular mechanisms of high frequency oscillations in epilepsy: on the diverse sources of pathological activities. Epilepsy research *97*, 308-317.
- Metea, M.R., and Newman, E.A. (2006). Glial cells dilate and constrict blood vessels: a mechanism of neurovascular coupling. The Journal of neuroscience : the official journal of the Society for Neuroscience *26*, 2862-2870.
- Mickleborough, M.J., Chapman, C.M., Toma, A.S., Chan, J.H., Truong, G., and Handy, T.C. (2013). Interictal neurocognitive processing of visual stimuli in migraine: evidence from event-related potentials. PloS one *8*, e80920.
- Miles, R., and Wong, R.K. (1983). Single neurones can initiate synchronized population discharge in the hippocampus. Nature *306*, 371-373.
- Miller, G. (2005). Neuroscience. The dark side of glia. Science *308*, 778-781.
- Min, R., and Nevian, T. (2012). Astrocyte signaling controls spike timing-dependent depression at neocortical synapses. Nature neuroscience *15*, 746-753.
- Minelli, A., Castaldo, P., Gobbi, P., Salucci, S., Magi, S., and Amoroso, S. (2007). Cellular and subcellular localization of Na+-Ca2+ exchanger protein isoforms, NCX1, NCX2, and NCX3 in cerebral cortex and hippocampus of adult rat. Cell calcium *41*, 221-234.
- Miyakawa, T., Mizushima, A., Hirose, K., Yamazawa, T., Bezprozvanny, I., Kurosaki, T., and Iino, M. (2001). Ca(2+)-sensor region of IP(3) receptor controls intracellular Ca(2+) signaling. The EMBO journal *20*, 1674-1680.
- Mody, I., and Heinemann, U. (1987). NMDA receptors of dentate gyrus granule cells participate in synaptic transmission following kindling. Nature *326*, 701-704.
- Mody, I., and Pearce, R.A. (2004). Diversity of inhibitory neurotransmission through GABA(A) receptors. Trends in neurosciences *27*, 569-575.
- Montana, V., Ni, Y., Sunjara, V., Hua, X., and Parpura, V. (2004). Vesicular glutamate transporter-dependent glutamate release from astrocytes. The Journal of neuroscience : the official journal of the Society for Neuroscience *24*, 2633-2642.

- Morita, M., Higuchi, C., Moto, T., Kozuka, N., Susuki, J., Itofusa, R., Yamashita, J., and Kudo, Y. (2003). Dual regulation of calcium oscillation in astrocytes by growth factors and pro-inflammatory cytokines via the mitogen-activated protein kinase cascade. The Journal of neuroscience : the official journal of the Society for Neuroscience *23*, 10944-10952.
- Mota, B., and Herculano-Houzel, S. (2012). How the cortex gets its folds: an inside-out, connectivity-driven model for the scaling of Mammalian cortical folding. Frontiers in neuroanatomy *6*, 3.
- Moutoussis, K., and Zeki, S. (1997). Functional segregation and temporal hierarchy of the visual perceptive systems. Proceedings Biological sciences / The Royal Society *264*, 1407-1414.
- Muller, C.M. (1990). Dark-rearing retards the maturation of astrocytes in restricted layers of cat visual cortex. Glia *3*, 487-494.
- Muller, D., Wang, C., Skibo, G., Toni, N., Cremer, H., Calaora, V., Rougon, G., and Kiss, J.Z. (1996). PSA-NCAM is required for activity-induced synaptic plasticity. Neuron *17*, 413-422.
- Mulligan, S.J., and MacVicar, B.A. (2004). Calcium transients in astrocyte endfeet cause cerebrovascular constrictions. Nature *431*, 195-199.
- Murai, K.K., and Pasquale, E.B. (2011). Eph receptors and ephrins in neuron-astrocyte communication at synapses. Glia *59*, 1567-1578.
- Mylvaganam, S., Zhang, L., Wu, C., Zhang, Z.J., Samoilova, M., Eubanks, J., Carlen, P.L., and Poulter, M.O. (2010). Hippocampal seizures alter the expression of the pannexin and connexin transcriptome. Journal of neurochemistry *112*, 92-102.
- Naude, J., Cessac, B., Berry, H., and Delord, B. (2013). Effects of cellular homeostatic intrinsic plasticity on dynamical and computational properties of biological recurrent neural networks. The Journal of neuroscience : the official journal of the Society for Neuroscience *33*, 15032-15043.
- Naus, C.C., and Laird, D.W. (2010). Implications and challenges of connexin connections to cancer. Nature reviews Cancer *10*, 435-441.
- Navarrete, M., and Araque, A. (2011). Basal synaptic transmission: astrocytes rule! Cell *146*, 675-677.
- Nedergaard, M., Ransom, B., and Goldman, S.A. (2003). New roles for astrocytes: redefining the functional architecture of the brain. Trends in neurosciences *26*, 523-530.
- Nedergaard, M., Ransom, B., and Goldman, S.A. (2003). New roles for astrocytes: redefining the functional architecture of the brain. Trends in neurosciences *26*, 523-530.
- Nestor, M.W., Mok, L.P., Tulapurkar, M.E., and Thompson, S.M. (2007). Plasticity of neuron-glial interactions mediated by astrocytic EphARs. The Journal of neuroscience : the official journal of the Society for Neuroscience *27*, 12817-12828.
- Nett, W.J., Oloff, S.H., and McCarthy, K.D. (2002). Hippocampal astrocytes in situ exhibit calcium oscillations that occur independent of neuronal activity. Journal of neurophysiology *87*, 528-537.
- Newman, E., and Reichenbach, A. (1996). The Muller cell: a functional element of the retina. Trends in neurosciences *19*, 307-312.
- Newman, E.A. (2001). Propagation of intercellular calcium waves in retinal astrocytes and Muller cells. The Journal of neuroscience : the official journal of the Society for Neuroscience *21*, 2215-2223.
- Ngomba, R.T., Santolini, I., Biagioni, F., Molinaro, G., Simonyi, A., van Rijn, C.M., D'Amore, V., Mastroiacovo, F., Olivieri, G., Gradini, R., *et al.* (2011). Protective role for type-1 metabotropic glutamate receptors against spike and wave discharges in the WAG/Rij rat model of absence epilepsy. Neuropharmacology *60*, 1281-1291.
- Nicholson, C., and Sykova, E. (1998). Extracellular space structure revealed by diffusion analysis. Trends in neurosciences *21*, 207-215.
- Nishida, H., and Okabe, S. (2007). Direct astrocytic contacts regulate local maturation of dendritic spines. The Journal of neuroscience : the official journal of the Society for Neuroscience *27*, 331-340.
- Noorbakhsh, F., Vergnolle, N., Hollenberg, M.D., and Power, C. (2003). Proteinase-activated receptors in the nervous system. Nature reviews Neuroscience *4*, 981-990.
- Norenberg, M.D. (1979). Distribution of glutamine synthetase in the rat central nervous system. The journal of histochemistry and cytochemistry : official journal of the Histochemistry Society *27*, 756-762.
- Nusser, Z., and Mody, I. (2002). Selective modulation of tonic and phasic inhibitions in dentate gyrus granule cells. Journal of neurophysiology *87*, 2624-2628.

- Nyitrai, G., Lasztoczi, B., and Kardos, J. (2010). Glutamate uptake shapes low-[Mg2+] induced epileptiform activity in juvenile rat hippocampal slices. Brain research *1309*, 172-178.
- Oberheim, N.A., Wang, X., Goldman, S., and Nedergaard, M. (2006). Astrocytic complexity distinguishes the human brain. Trends in neurosciences *29*, 547-553.
- Ogata, K., and Kosaka, T. (2002). Structural and quantitative analysis of astrocytes in the mouse hippocampus. Neuroscience *113*, 221-233.
- Oliet, S.H., Piet, R., Poulain, D.A., and Theodosis, D.T. (2004). Glial modulation of synaptic transmission: Insights from the supraoptic nucleus of the hypothalamus. Glia *47*, 258-267.
- Olson, J.E., and Li, G.Z. (1997). Increased potassium, chloride, and taurine conductances in astrocytes during hypoosmotic swelling. Glia *20*, 254-261.
- Ortinski, P.I., Dong, J., Mungenast, A., Yue, C., Takano, H., Watson, D.J., Haydon, P.G., and Coulter, D.A. (2010). Selective induction of astrocytic gliosis generates deficits in neuronal inhibition. Nature neuroscience *13*, 584-591.
- Ortinski, P.I., Dong, J., Mungenast, A., Yue, C., Takano, H., Watson, D.J., Haydon, P.G., and Coulter, D.A. (2010). Selective induction of astrocytic gliosis generates deficits in neuronal inhibition. Nature neuroscience *13*, 584-591.
- Otoom, S., Tian, L.M., and Alkadhi, K.A. (1998). Veratridine-treated brain slices: a cellular model for epileptiform activity. Brain research *789*, 150-156.
- Palmer, C.L., Lim, W., Hastie, P.G., Toward, M., Korolchuk, V.I., Burbidge, S.A., Banting, G., Collingridge, G.L., Isaac, J.T., and Henley, J.M. (2005). Hippocalcin functions as a calcium sensor in hippocampal LTD. Neuron *47*, 487-494.
- Panatier, A., Vallee, J., Haber, M., Murai, K.K., Lacaille, J.C., and Robitaille, R. (2011). Astrocytes are endogenous regulators of basal transmission at central synapses. Cell *146*, 785-798.
- Park, H.J., and Friston, K. (2013). Structural and functional brain networks: from connections to cognition. Science *342*, 1238411.
- Parker, R.J., and Auld, V.J. (2006). Roles of glia in the Drosophila nervous system. Seminars in cell & developmental biology *17*, 66-77.
- Parpura, V., Basarsky, T.A., Liu, F., Jeftinija, K., Jeftinija, S., and Haydon, P.G. (1994). Glutamate-mediated astrocyte-neuron signalling. Nature *369*, 744-747.
- Parpura, V., Scemes, E., and Spray, D.C. (2004). Mechanisms of glutamate release from astrocytes: gap junction "hemichannels", purinergic receptors and exocytotic release. Neurochemistry international *45*, 259-264.
- Parri, H.R., and Crunelli, V. (2003). The role of Ca2+ in the generation of spontaneous astrocytic Ca2+ oscillations. Neuroscience *120*, 979-992.
- Parri, H.R., and Crunelli, V. (2003). The role of Ca2+ in the generation of spontaneous astrocytic Ca2+ oscillations. Neuroscience *120*, 979-992.
- Pekny, M., and Pekna, M. (2004). Astrocyte intermediate filaments in CNS pathologies and regeneration. The Journal of pathology *204*, 428-437.
- Pekny, M., Leveen, P., Pekna, M., Eliasson, C., Berthold, C.H., Westermark, B., and Betsholtz, C. (1995). Mice lacking glial fibrillary acidic protein display astrocytes devoid of intermediate filaments but develop and reproduce normally. The EMBO journal *14*, 1590-1598.
- Pellerin, L., and Magistretti, P.J. (1994). Glutamate uptake into astrocytes stimulates aerobic glycolysis: a mechanism coupling neuronal activity to glucose utilization. Proceedings of the National Academy of Sciences of the United States of America *91*, 10625-10629.
- Pellerin, L., Pellegri, G., Martin, J.L., and Magistretti, P.J. (1998). Expression of monocarboxylate transporter mRNAs in mouse brain: support for a distinct role of lactate as an energy substrate for the neonatal vs. adult brain. Proceedings of the National Academy of Sciences of the United States of America *95*, 3990-3995.
- Penttonen, M., Kamondi, A., Acsady, L., and Buzsaki, G. (1998). Gamma frequency oscillation in the hippocampus of the rat: intracellular analysis in vivo. The European journal of neuroscience *10*, 718-728.
- Pernia-Andrade, A.J., and Jonas, P. (2013). Theta-Gamma-Modulated Synaptic Currents in Hippocampal Granule Cells In Vivo Define a Mechanism for Network Oscillations. Neuron.
- Peters, A., Sethares, C., and Harriman, K.M. (1990). Different kinds of axon terminals forming symmetric synapses with the cell bodies and initial axon segments of layer II/III pyramidal cells. II. Synaptic junctions. Journal of neurocytology *19*, 584-600.
- Peters, A.C., and Callenbach, P.M. (2003). Death in children with epilepsy: a population-based study. The Journal of pediatrics *142*, 87.

- Petilla Interneuron Nomenclature, G., Ascoli, G.A., Alonso-Nanclares, L., Anderson, S.A., Barrionuevo, G., Benavides-Piccione, R., Burkhalter, A., Buzsaki, G., Cauli, B., Defelipe, J., *et al.* (2008). Petilla terminology: nomenclature of features of GABAergic interneurons of the cerebral cortex. Nature reviews Neuroscience *9*, 557-568.
- Petravicz, J., Fiacco, T.A., and McCarthy, K.D. (2008). Loss of IP3 receptor-dependent Ca2+ increases in hippocampal astrocytes does not affect baseline CA1 pyramidal neuron synaptic activity. The Journal of neuroscience : the official journal of the Society for Neuroscience *28*, 4967-4973.
- Pike, F.G., Goddard, R.S., Suckling, J.M., Ganter, P., Kasthuri, N., and Paulsen, O. (2000). Distinct frequency preferences of different types of rat hippocampal neurones in response to oscillatory input currents. The Journal of physiology *529 Pt 1*, 205-213.
- Plenz, D., and Thiagarajan, T.C. (2007). The organizing principles of neuronal avalanches: cell assemblies in the cortex? Trends in neurosciences *30*, 101-110.
- Pocock, J.M., and Kettenmann, H. (2007). Neurotransmitter receptors on microglia. Trends in neurosciences *30*, 527-535.
- Poduri, A., Evrony, G.D., Cai, X., and Walsh, C.A. (2013). Somatic mutation, genomic variation, and neurological disease. Science *341*, 1237758.
- Poil, S.S., Hardstone, R., Mansvelder, H.D., and Linkenkaer-Hansen, K. (2012). Critical-state dynamics of avalanches and oscillations jointly emerge from balanced excitation/inhibition in neuronal networks. The Journal of neuroscience : the official journal of the Society for Neuroscience *32*, 9817-9823.
- Porter, J.T., and McCarthy, K.D. (1995). GFAP-positive hippocampal astrocytes in situ respond to glutamatergic neuroligands with increases in [Ca2+]i. Glia *13*, 101-112.
- Porter, J.T., and McCarthy, K.D. (1996). Hippocampal astrocytes in situ respond to glutamate released from synaptic terminals. The Journal of neuroscience : the official journal of the Society for Neuroscience *16*, 5073-5081.
- Pouille, F., and Scanziani, M. (2001). Enforcement of temporal fidelity in pyramidal cells by somatic feed-forward inhibition. Science *293*, 1159-1163.
- Pryazhnikov, E., and Khiroug, L. (2008). Sub-micromolar increase in [Ca(2+)](i) triggers delayed exocytosis of ATP in cultured astrocytes. Glia *56*, 38-49.
- Pu, J., Gong, H., Li, X., and Luo, Q. (2013). Developing neuronal networks: self-organized criticality predicts the future. Scientific reports *3*, 1081.
- Rabert, D.K., Koch, B.D., Ilnicka, M., Obernolte, R.A., Naylor, S.L., Herman, R.C., Eglen, R.M., Hunter, J.C., and Sangameswaran, L. (1998). A tetrodotoxin-resistant voltage-gated sodium channel from human dorsal root ganglia, hPN3/SCN10A. Pain *78*, 107-114.
- Ragsdale, D.S., and Avoli, M. (1998). Sodium channels as molecular targets for antiepileptic drugs. Brain research Brain research reviews *26*, 16-28.
- Ramirez-Munguia, N., Vera, G., and Tapia, R. (2003). Epilepsy, neurodegeneration, and extracellular glutamate in the hippocampus of awake and anesthetized rats treated with okadaic acid. Neurochemical research *28*, 1517-1524.
- Ransom, B., Behar, T., and Nedergaard, M. (2003). New roles for astrocytes (stars at last). Trends in neurosciences *26*, 520-522.
- Ransom, B.R., and Sontheimer, H. (1992). The neurophysiology of glial cells. Journal of clinical neurophysiology : official publication of the American Electroencephalographic Society *9*, 224-251.
- Rockel, A.J., Hiorns, R.W., and Powell, T.P. (1980). The basic uniformity in structure of the neocortex. Brain : a journal of neurology *103*, 221-244.
- Rose, C.R., and Karus, C. (2013). Two sides of the same coin: sodium homeostasis and signaling in astrocytes under physiological and pathophysiological conditions. Glia *61*, 1191-1205.
- Roux, F., Wibral, M., Singer, W., Aru, J., and Uhlhaas, P.J. (2013). The phase of thalamic alpha activity modulates cortical gamma-band activity: evidence from resting-state MEG recordings. The Journal of neuroscience : the official journal of the Society for Neuroscience *33*, 17827-17835.
- Rutecki, P.A., Lebeda, F.J., and Johnston, D. (1985). Epileptiform activity induced by changes in extracellular potassium in hippocampus. Journal of neurophysiology *54*, 1363-1374.
- Salthe, S.N. (2008). Natural selection in relation to complexity. Artificial life *14*, 363-374.
- Sander, J.W. (2003). The epidemiology of epilepsy revisited. Current opinion in neurology *16*, 165-170.

- Sarnthein, J., Petsche, H., Rappelsberger, P., Shaw, G.L., and von Stein, A. (1998). Synchronization between prefrontal and posterior association cortex during human working memory. Proceedings of the National Academy of Sciences of the United States of America *95*, 7092-7096.
- Savidge, T.C., Sofroniew, M.V., and Neunlist, M. (2007). Starring roles for astroglia in barrier pathologies of gut and brain. Laboratory investigation; a journal of technical methods and pathology *87*, 731-736.
- Scheffzuk, C., Kukushka, V.I., Vyssotski, A.L., Draguhn, A., Tort, A.B., and Brankack, J. (2011). Selective coupling between theta phase and neocortical fast gamma oscillations during REM-sleep in mice. PloS one *6*, e28489.
- Schevon, C.A., Weiss, S.A., McKhann, G., Jr., Goodman, R.R., Yuste, R., Emerson, R.G., and Trevelyan, A.J. (2012). Evidence of an inhibitory restraint of seizure activity in humans. Nature communications *3*, 1060.
- Schroeder, C.E., and Lakatos, P. (2009). The gamma oscillation: master or slave? Brain topography *22*, 24-26.
- Schroeter, M., and Jander, S. (2005). T-cell cytokines in injury-induced neural damage and repair. Neuromolecular medicine *7*, 183-195.
- Schummers, J., Yu, H., and Sur, M. (2008). Tuned responses of astrocytes and their influence on hemodynamic signals in the visual cortex. Science *320*, 1638-1643.
- Segal, M.M., and Douglas, A.F. (1997). Late sodium channel openings underlying epileptiform activity are preferentially diminished by the anticonvulsant phenytoin. Journal of neurophysiology *77*, 3021-3034.
- Seifert, G., Carmignoto, G., and Steinhauser, C. (2010). Astrocyte dysfunction in epilepsy. Brain research reviews *63*, 212-221.
- Seifert, G., Schilling, K., and Steinhauser, C. (2006). Astrocyte dysfunction in neurological disorders: a molecular perspective. Nature reviews Neuroscience *7*, 194-206.
- Shadlen, M.N., and Movshon, J.A. (1999). Synchrony unbound: a critical evaluation of the temporal binding hypothesis. Neuron *24*, 67-77, 111-125.
- Shah, M.M., Javadzadeh-Tabatabaie, M., Benton, D.C., Ganellin, C.R., and Haylett, D.G. (2006). Enhancement of hippocampal pyramidal cell excitability by the novel selective slow-afterhyperpolarization channel blocker 3-(triphenylmethylaminomethyl)pyridine (UCL2077). Molecular pharmacology *70*, 1494-1502.
- Sheen, S.H., Kim, J.E., Ryu, H.J., Yang, Y., Choi, K.C., and Kang, T.C. (2011). Decrease in dystrophin expression prior to disruption of brain-blood barrier within the rat piriform cortex following status epilepticus. Brain research *1369*, 173-183.
- Sik, A., Ylinen, A., Penttonen, M., and Buzsaki, G. (1994). Inhibitory CA1-CA3-hilar region feedback in the hippocampus. Science *265*, 1722-1724.
- Silberberg, G., Wu, C., and Markram, H. (2004). Synaptic dynamics control the timing of neuronal excitation in the activated neocortical microcircuit. The Journal of physiology *556*, 19-27.
- Silva-Barrat, C., Araneda, S., Menini, C., Champagnat, J., and Naquet, R. (1992). Burst generation in neocortical neurons after GABA withdrawal in the rat. Journal of neurophysiology *67*, 715-727.
- Simard, M., and Nedergaard, M. (2004). The neurobiology of glia in the context of water and ion homeostasis. Neuroscience *129*, 877-896.
- Singer, W. (1999). Neuronal synchrony: a versatile code for the definition of relations? Neuron *24*, 49-65, 111-125.
- Skov, J., Nedergaard, S., and Andreasen, M. (2009). The slow Ca2+ -dependent K+ -current facilitates synchronization of hyperexcitable pyramidal neurons. Brain research *1252*, 76-86.
- Softky, W.R., and Koch, C. (1993). The highly irregular firing of cortical cells is inconsistent with temporal integration of random EPSPs. The Journal of neuroscience : the official journal of the Society for Neuroscience *13*, 334-350.
- Sohal, V.S., Zhang, F., Yizhar, O., and Deisseroth, K. (2009). Parvalbumin neurons and gamma rhythms enhance cortical circuit performance. Nature *459*, 698-702.
- Solovyova, N., Veselovsky, N., Toescu, E.C., and Verkhratsky, A. (2002). Ca(2+) dynamics in the lumen of the endoplasmic reticulum in sensory neurons: direct visualization of Ca(2+)-induced Ca(2+) release triggered by physiological Ca(2+) entry. The EMBO journal *21*, 622-630.
- Sporns, O., Chialvo, D.R., Kaiser, M., and Hilgetag, C.C. (2004). Organization, development and function of complex brain networks. Trends in cognitive sciences *8*, 418-425.
- Sporns, O., Tononi, G., and Edelman, G.M. (2000). Connectivity and complexity: the relationship between neuroanatomy and brain dynamics. Neural networks : the official journal of the International Neural Network Society *13*, 909-922.

- Sporns, O., Tononi, G., and Edelman, G.M. (2000). Connectivity and complexity: the relationship between neuroanatomy and brain dynamics. Neural networks : the official journal of the International Neural Network Society *13*, 909-922.
- Sporns, O., Tononi, G., and Edelman, G.M. (2002). Theoretical neuroanatomy and the connectivity of the cerebral cortex. Behavioural brain research *135*, 69-74.
- Stam, C.J., and de Bruin, E.A. (2004). Scale-free dynamics of global functional connectivity in the human brain. Human brain mapping *22*, 97-109.
- Stellwagen, D., and Malenka, R.C. (2006). Synaptic scaling mediated by glial TNF-alpha. Nature *440*, 1054-1059.
- Steriade, M. (2004). Neocortical cell classes are flexible entities. Nature reviews Neuroscience *5*, 121-134.
- Steriade, M., and Timofeev, I. (2003). Neuronal plasticity in thalamocortical networks during sleep and waking oscillations. Neuron *37*, 563-576.
- Steriade, M., Datta, S., Pare, D., Oakson, G., and Curro Dossi, R.C. (1990). Neuronal activities in brain-stem cholinergic nuclei related to tonic activation processes in thalamocortical systems. The Journal of neuroscience : the official journal of the Society for Neuroscience *10*, 2541-2559.
- Stevens, B. (2003). Glia: much more than the neuron's side-kick. Current biology : CB *13*, R469-472.
- Stevens, E.R., Esguerra, M., Kim, P.M., Newman, E.A., Snyder, S.H., Zahs, K.R., and Miller, R.F. (2003). D-serine and serine racemase are present in the vertebrate retina and contribute to the physiological activation of NMDA receptors. Proceedings of the National Academy of Sciences of the United States of America *100*, 6789-6794.
- Stobart JL, Anderson CM. (2013). Multifunctional role of astrocytes as gatekeepers of neuronal energy supply.
- Stopfer, M., and Laurent, G. (1999). Short-term memory in olfactory network dynamics. Nature *402*, 664-668.
- Stosiek, C., Garaschuk, O., Holthoff, K., and Konnerth, A. (2003). In vivo two-photon calcium imaging of neuronal networks. Proceedings of the National Academy of Sciences of the United States of America *100*, 7319-7324.
- Stringer, J.L., and Lothman, E.W. (1989). Model of spontaneous hippocampal epilepsy in the anesthetized rat: electrographic, [K+]0, and [Ca2+]0 response patterns. Epilepsy research *4*, 177-186.
- Strohschein, S., Huttmann, K., Gabriel, S., Binder, D.K., Heinemann, U., and Steinhauser, C. (2011). Impact of aquaporin-4 channels on K+ buffering and gap junction coupling in the hippocampus. Glia *59*, 973-980.
- Suadicani, S.O., Brosnan, C.F., and Scemes, E. (2006). P2X7 receptors mediate ATP release and amplification of astrocytic intercellular Ca2+ signaling. The Journal of neuroscience : the official journal of the Society for Neuroscience *26*, 1378-1385.
- Sullivan, D., Csicsvari, J., Mizuseki, K., Montgomery, S., Diba, K., and Buzsaki, G. (2011). Relationships between hippocampal sharp waves, ripples, and fast gamma oscillation: influence of dentate and entorhinal cortical activity. The Journal of neuroscience : the official journal of the Society for Neuroscience *31*, 8605-8616.
- Surges, R., Kukley, M., Brewster, A., Ruschenschmidt, C., Schramm, J., Baram, T.Z., Beck, H., and Dietrich, D. (2012). Hyperpolarization-activated cation current Ih of dentate gyrus granule cells is upregulated in human and rat temporal lobe epilepsy. Biochemical and biophysical research communications *420*, 156-160.
- Swadlow, H.A. (2000). Descending corticofugal neurons in layer 5 of rabbit S1: evidence for potent corticocortical, but not thalamocortical, input. Experimental brain research Experimentelle Hirnforschung Experimentation cerebrale *130*, 188-194.
- Swadlow, H.A. (2002). Thalamocortical control of feed-forward inhibition in awake somatosensory 'barrel' cortex. Philosophical transactions of the Royal Society of London Series B, Biological sciences *357*, 1717-1727.
- Swartzwelder, H.S., Lewis, D.V., Anderson, W.W., and Wilson, W.A. (1987). Seizure-like events in brain slices: suppression by interictal activity. Brain research *410*, 362-366.
- Syed, N., Martens, C.A., and Hsu, W.H. (2007). Arginine vasopressin increases glutamate release and intracellular Ca2+ concentration in hippocampal and cortical astrocytes through two distinct receptors. Journal of neurochemistry *103*, 229-237.
- Szabadics, J., Varga, C., Molnar, G., Olah, S., Barzo, P., and Tamas, G. (2006). Excitatory effect of GABAergic axo-axonic cells in cortical microcircuits. Science *311*, 233-235.

- Szentagothai, J. (1978). The Ferrier Lecture, 1977. The neuron network of the cerebral cortex: a functional interpretation. Proceedings of the Royal Society of London Series B, Containing papers of a Biological character Royal Society *201*, 219-248.
- Szente, M., and Baranyi, A. (1987). Mechanism of aminopyridine-induced ictal seizure activity in the cat neocortex. Brain research *413*, 368-373.
- Takano, T., Kang, J., Jaiswal, J.K., Simon, S.M., Lin, J.H., Yu, Y., Li, Y., Yang, J., Dienel, G., Zielke, H.R., *et al.* (2005). Receptor-mediated glutamate release from volume sensitive channels in astrocytes. Proceedings of the National Academy of Sciences of the United States of America *102*, 16466-16471.
- Takano, T., Tian, G.F., Peng, W., Lou, N., Libionka, W., Han, X., and Nedergaard, M. (2006). Astrocyte-mediated control of cerebral blood flow. Nature neuroscience *9*, 260-267.
- Tanskanen, J.M., Mikkonen, J.E., Hyttinen, J.A., and Penttonen, M. (2006). Observing frequency content time evolution of independent hippocampal signals. Conference proceedings : Annual International Conference of the IEEE Engineering in Medicine and Biology Society IEEE Engineering in Medicine and Biology Society Conference *1*, 727-730.
- Taverna, S., Mantegazza, M., Franceschetti, S., and Avanzini, G. (1998). Valproate selectively reduces the persistent fraction of Na+ current in neocortical neurons. Epilepsy research *32*, 304-308.
- Tergau, F., Naumann, U., Paulus, W., and Steinhoff, B.J. (1999). Low-frequency repetitive transcranial magnetic stimulation improves intractable epilepsy. Lancet *353*, 2209.
- Theodosis, D.T., and MacVicar, B. (1996). Neurone-glia interactions in the hypothalamus and pituitary. Trends in neurosciences *19*, 363-367.
- Theodosis, D.T., and Poulain, D.A. (1993). Activity-dependent neuronal-glial and synaptic plasticity in the adult mammalian hypothalamus. Neuroscience *57*, 501-535.
- Theodosis, D.T., Piet, R., Poulain, D.A., and Oliet, S.H. (2004). Neuronal, glial and synaptic remodeling in the adult hypothalamus: functional consequences and role of cell surface and extracellular matrix adhesion molecules. Neurochemistry international *45*, 491-501.
- Theodosis, D.T., Poulain, D.A., and Vincent, J.D. (1981). Possible morphological bases for synchronisation of neuronal firing in the rat supraoptic nucleus during lactation. Neuroscience *6*, 919-929.
- Thomas, W.B. (2010). Idiopathic epilepsy in dogs and cats. The Veterinary clinics of North America Small animal practice *40*, 161-179.
- Thomson, A.M., and Bannister, A.P. (2003). Interlaminar connections in the neocortex. Cerebral cortex *13*, 5-14.
- Tian, G.F., Azmi, H., Takano, T., Xu, Q., Peng, W., Lin, J., Oberheim, N., Lou, N., Wang, X., Zielke, H.R., *et al.* (2005). An astrocytic basis of epilepsy. Nature medicine *11*, 973-981.
- Timofeev, I., Bazhenov, M., Sejnowski, T., and Steriade, M. (2002). Cortical hyperpolarization-activated depolarizing current takes part in the generation of focal paroxysmal activities. Proceedings of the National Academy of Sciences of the United States of America *99*, 9533-9537.
- Tononi, G., Sporns, O., and Edelman, G.M. (1994). A measure for brain complexity: relating functional segregation and integration in the nervous system. Proceedings of the National Academy of Sciences of the United States of America *91*, 5033-5037.
- Tononi, G., Sporns, O., and Edelman, G.M. (1996). A complexity measure for selective matching of signals by the brain. Proceedings of the National Academy of Sciences of the United States of America *93*, 3422-3427.
- Traub, R.D., and Wong, R.K. (1982). Cellular mechanism of neuronal synchronization in epilepsy. Science *216*, 745-747.
- Traub, R.D., and Wong, R.K. (1982). Cellular mechanism of neuronal synchronization in epilepsy. Science *216*, 745-747.
- Trevelyan, A. (2013). Why do some brains seize? Molecular, cellular and network mechanisms. The Journal of physiology *591*, 751-752.
- Trevelyan, A.J. (2009). The direct relationship between inhibitory currents and local field potentials. The Journal of neuroscience : the official journal of the Society for Neuroscience *29*, 15299-15307.
- Trevelyan, A.J., and Schevon, C.A. (2013). How inhibition influences seizure propagation. Neuropharmacology *69*, 45-54.
- Trevelyan, A.J., Sussillo, D., Watson, B.O., and Yuste, R. (2006). Modular propagation of epileptiform activity: evidence for an inhibitory veto in neocortex. The Journal of neuroscience : the official journal of the Society for Neuroscience *26*, 12447-12455.

- Trevelyan, A.J., Sussillo, D., Watson, B.O., and Yuste, R. (2006). Modular propagation of epileptiform activity: evidence for an inhibitory veto in neocortex. The Journal of neuroscience : the official journal of the Society for Neuroscience *26*, 12447-12455.

- Trevelyan, A.J., Sussillo, D., Watson, B.O., and Yuste, R. (2006). Modular propagation of epileptiform activity: evidence for an inhibitory veto in neocortex. The Journal of neuroscience : the official journal of the Society for Neuroscience *26*, 12447-12455.

- Tseng, G.F., and Haberly, L.B. (1989). Deep neurons in piriform cortex. II. Membrane properties that underlie unusual synaptic responses. Journal of neurophysiology *62*, 386-400.
- Tu, H., Wang, Z., and Bezprozvanny, I. (2005). Modulation of mammalian inositol 1,4,5-trisphosphate receptor isoforms by calcium: a role of calcium sensor region. Biophysical journal *88*, 1056-1069.
- Tweedle, C.D., and Hatton, G.I. (1980). Evidence for dynamic interactions between pituicytes and neurosecretory axons in the rat. Neuroscience *5*, 661-671.
- Tzingounis, A.V., Kobayashi, M., Takamatsu, K., and Nicoll, R.A. (2007). Hippocalcin gates the calcium activation of the slow afterhyperpolarization in hippocampal pyramidal cells. Neuron *53*, 487-493.
- Ullian, E.M., Sapperstein, S.K., Christopherson, K.S., and Barres, B.A. (2001). Control of synapse number by glia. Science *291*, 657-661.
- Uva, L., Avoli, M., and de Curtis, M. (2009). Synchronous GABA-receptor-dependent potentials in limbic areas of the in-vitro isolated adult guinea pig brain. The European journal of neuroscience *29*, 911-920.
- Uva, L., Librizzi, L., Wendling, F., and de Curtis, M. (2005). Propagation dynamics of epileptiform activity acutely induced by bicuculline in the hippocampal-parahippocampal region of the isolated Guinea pig brain. Epilepsia *46*, 1914-1925.
- Vaadia, E., Aertsen, A., and Nelken, I. (1995). 'Dynamics of neuronal interactions' cannot be explained by 'neuronal transients'. Proceedings Biological sciences / The Royal Society *261*, 407-410.
- Van Bogaert, P., Urbain, C., Galer, S., Ligot, N., Peigneux, P., and De Tiege, X. (2012). Impact of focal interictal epileptiform discharges on behaviour and cognition in children. Neurophysiologie clinique = Clinical neurophysiology *42*, 53-58.
- Van Essen, D.C., and Drury, H.A. (1997). Structural and functional analyses of human cerebral cortex using a surface-based atlas. The Journal of neuroscience : the official journal of the Society for Neuroscience *17*, 7079-7102.
- van Vliet, E.A., da Costa Araujo, S., Redeker, S., van Schaik, R., Aronica, E., and Gorter, J.A. (2007). Blood-brain barrier leakage may lead to progression of temporal lobe epilepsy. Brain : a journal of neurology *130*, 521-534.
- Ventura, R., and Harris, K.M. (1999). Three-dimensional relationships between hippocampal synapses and astrocytes. The Journal of neuroscience : the official journal of the Society for Neuroscience *19*, 6897-6906.
- Ventura-Antunes, L., Mota, B., and Herculano-Houzel, S. (2013). Different scaling of white matter volume, cortical connectivity, and gyrification across rodent and primate brains. Frontiers in neuroanatomy *7*, 3.
- Verkhratsky, A., and Kirchhoff, F. (2007). Glutamate-mediated neuronal-glial transmission. Journal of anatomy *210*, 651-660.
- Verkhratsky, A., and Toescu, E.C. (2006). Neuronal-glial networks as substrate for CNS integration. Journal of cellular and molecular medicine *10*, 826-836.
- Verkhratsky, A., Noda, M., Parpura, V., and Kirischuk, S. (2013). Sodium fluxes and astroglial function. Advances in experimental medicine and biology *961*, 295-305.
- Vogels, T.P., and Abbott, L.F. (2005). Signal propagation and logic gating in networks of integrate-and-fire neurons. The Journal of neuroscience : the official journal of the Society for Neuroscience *25*, 10786-10795.
- Vogels, T.P., Rajan, K., and Abbott, L.F. (2005). Neural network dynamics. Annual review of neuroscience *28*, 357-376.
- Volman, V., Behrens, M.M., and Sejnowski, T.J. (2011). Downregulation of parvalbumin at cortical GABA synapses reduces network gamma oscillatory activity. The Journal of neuroscience : the official journal of the Society for Neuroscience *31*, 18137-18148.
- Volterra, A., and Meldolesi, J. (2005). Astrocytes, from brain glue to communication elements: the revolution continues. Nature reviews Neuroscience *6*, 626-640.
- von Stein, A., Rappelsberger, P., Sarnthein, J., and Petsche, H. (1999). Synchronization between temporal and parietal cortex during multimodal object processing in man. Cerebral cortex *9*, 137-150.

- Vorisek, I., and Sykova, E. (2009). Measuring diffusion parameters in the brain: comparing the real-time iontophoretic method and diffusion-weighted magnetic resonance. Acta physiologica *195*, 101-110.
- Vutskits, L., Djebbara-Hannas, Z., Zhang, H., Paccaud, J.P., Durbec, P., Rougon, G., Muller, D., and Kiss, J.Z. (2001). PSA-NCAM modulates BDNF-dependent survival and differentiation of cortical neurons. The European journal of neuroscience *13*, 1391-1402.
- Wada, J.A., Sato, M., and Corcoran, M.E. (1974). Persistent seizure susceptibility and recurrent spontaneous seizures in kindled cats. Epilepsia *15*, 465-478.
- Wallraff, A., Kohling, R., Heinemann, U., Theis, M., Willecke, K., and Steinhauser, C. (2006). The impact of astrocytic gap junctional coupling on potassium buffering in the hippocampus. The Journal of neuroscience : the official journal of the Society for Neuroscience *26*, 5438-5447.
- Wallraff, A., Kohling, R., Heinemann, U., Theis, M., Willecke, K., and Steinhauser, C. (2006). The impact of astrocytic gap junctional coupling on potassium buffering in the hippocampus. The Journal of neuroscience : the official journal of the Society for Neuroscience *26*, 5438-5447.
- Wallraff, A., Odermatt, B., Willecke, K., and Steinhauser, C. (2004). Distinct types of astroglial cells in the hippocampus differ in gap junction coupling. Glia *48*, 36-43.
- Walter W.G., Cooper R., Aldridge V.J., McCallum W.C., Winter A.L**.,** (1964) CONTINGENT NEGATIVE VARIATION: AN ELECTRIC SIGN OF SENSORIMOTOR ASSOCIATION AND EXPECTANCY IN THE HUMAN BRAIN. Nature. Jul 25;203:380-4.
- Walz, W. (1987). Swelling and potassium uptake in cultured astrocytes. Canadian journal of physiology and pharmacology *65*, 1051-1057.
- Wang, D.D., and Bordey, A. (2008). The astrocyte odyssey. Progress in neurobiology *86*, 342-367.
- Wang, Y.F., and Hamilton, K. (2009). Chronic vs. acute interactions between supraoptic oxytocin neurons and astrocytes during lactation: role of glial fibrillary acidic protein plasticity. TheScientificWorldJournal *9*, 1308-1320.
- Watanabe, E., Hiyama, T.Y., Shimizu, H., Kodama, R., Hayashi, N., Miyata, S., Yanagawa, Y., Obata, K., and Noda, M. (2006). Sodium-level-sensitive sodium channel Na(x) is expressed in glial laminate processes in the sensory circumventricular organs. American journal of physiology Regulatory, integrative and comparative physiology *290*, R568-576.
- Waxman, S.G., and Geschwind, N. (1975). The interictal behavior syndrome of temporal lobe epilepsy. Archives of general psychiatry *32*, 1580-1586.
- Wehr, M., and Zador, A.M. (2003). Balanced inhibition underlies tuning and sharpens spike timing in auditory cortex. Nature *426*, 442-446.
- Weliky, M., Fiser, J., Hunt, R.H., and Wagner, D.N. (2003). Coding of natural scenes in primary visual cortex. Neuron *37*, 703-718.
- Wenzel, J., Lammert, G., Meyer, U., and Krug, M. (1991). The influence of long-term potentiation on the spatial relationship between astrocyte processes and potentiated synapses in the dentate gyrus neuropil of rat brain. Brain research *560*, 122-131.
- Wolf, F., and Kirchhoff, F. (2008). Neuroscience. Imaging astrocyte activity. Science *320*, 1597-1599.
- Wong, R.K., and Traub, R.D. (1983). Synchronized burst discharge in disinhibited hippocampal slice. I. Initiation in CA2-CA3 region. Journal of neurophysiology *49*, 442-458.
- Wozniak-Kwasniewska, A., Szekely, D., Aussedat, P., Bougerol, T., and David, O. (2013). Changes of oscillatory brain activity induced by repetitive transcranial magnetic stimulation of the left dorsolateral prefrontal cortex in healthy subjects. NeuroImage.
- Wu, W.W., Chan, C.S., and Disterhoft, J.F. (2004). Slow afterhyperpolarization governs the development of NMDA receptor-dependent afterdepolarization in CA1 pyramidal neurons during synaptic stimulation. Journal of neurophysiology *92*, 2346-2356.
- Yang, J.W., Czech, T., Gelpi, E., and Lubec, G. (2005). Extravasation of plasma proteins can confound interpretation of proteomic studies of brain: a lesson from apo A-I in mesial temporal lobe epilepsy. Brain research Molecular brain research *139*, 348-356.
- Yang, Y., Ge, W., Chen, Y., Zhang, Z., Shen, W., Wu, C., Poo, M., and Duan, S. (2003). Contribution of astrocytes to hippocampal long-term potentiation through release of D-serine. Proceedings of the National Academy of Sciences of the United States of America *100*, 15194-15199.
- Ylinen, A., Bragin, A., Nadasdy, Z., Jando, G., Szabo, I., Sik, A., and Buzsaki, G. (1995). Sharp wave-associated high-frequency oscillation (200 Hz) in the intact hippocampus: network and intracellular mechanisms. The Journal of neuroscience : the official journal of the Society for Neuroscience *15*, 30-46.

- Yoon, B.E., Woo, J., and Lee, C.J. (2012). Astrocytes as GABA-ergic and GABA-ceptive cells. Neurochemical research *37*, 2474-2479.
- Yoshimura, H. (2005). The potential of caffeine for functional modification from cortical synapses to neuron networks in the brain. Current neuropharmacology *3*, 309-316.
- Yu Y, Lee TS (2005) Adaptive contrast gain control and information maximization. Neurocomputing 65–66: 111–116.
- Zador, Z., Stiver, S., Wang, V., and Manley, G.T. (2009). Role of aquaporin-4 in cerebral edema and stroke. Handbook of experimental pharmacology, 159-170.
- Zhang, J.M., Wang, H.K., Ye, C.Q., Ge, W., Chen, Y., Jiang, Z.L., Wu, C.P., Poo, M.M., and Duan, S. (2003). ATP released by astrocytes mediates glutamatergic activity-dependent heterosynaptic suppression. Neuron *40*, 971-982.

- Zhang, J.M., Wang, H.K., Ye, C.Q., Ge, W., Chen, Y., Jiang, Z.L., Wu, C.P., Poo, M.M., and Duan, S. (2003). ATP released by astrocytes mediates glutamatergic activity-dependent heterosynaptic suppression. Neuron *40*, 971-982.

- Zonta, M., Angulo, M.C., Gobbo, S., Rosengarten, B., Hossmann, K.A., Pozzan, T., and Carmignoto, G. (2003). Neuron-to-astrocyte signaling is central to the dynamic control of brain microcirculation. Nature neuroscience *6*, 43-50.
- Zuckermann, E.C., and Glaser, G.H. (1970). Activation of experimental epileptogenic foci. Action of increased K+ in extracellular spaces of the brain. Archives of neurology *23*, 358-364.